博士論文

Thermodynamics of Calcium Phosphate-based Solid Solution for Steelmaking

（鉄鋼精錬プロセスにおけるりん酸カルシウム系固溶体の熱力学）

鍾　明

Contents

Chapter 1 Introduction

1.1 Introduction

The iron and steel industry spends a large amount of natural resources and energy resources, and produces a large amount of greenhouse gas and dust. In current view, developing the technology not only for promoting the quality of product but also for achieving the eco-friendly manufacturing technique is instant.

Since impurities in steel decrease the usability, the impurities should be removed during the smelting process. Especially, phosphorus should be removed as much as possible for most of the steel products. For the current method of dephosphorization, it consumes much lime and the slag amount is huge. At the same time, due to CaO which remains unreacted or precipitates during solidification of dephosphorization slag, the slag is difficult to be reused. In consequence of the harm for environment and human, fluorite is strictly used although it can enhance the dissolution of CaO into slag. Under this condition, the concept of multi-phase flux for dephosphorization was considered.

In multi-phase flux, the solid solution between di-calcium silicate ($2CaO \cdot SiO_2$) and tri-calcium phosphate ($3CaO \cdot P_2O_5$) is considered as the solid phase. In order to deeply understand and well apply the multi-phase flux for dephosphorization, not only the thermodynamics but also the kinetics about the calcium phosphate-based solid solution has been studied. Despite all that, the thermodynamic data about the calcium phosphate-based solid solution are still scarce. In current research, in order to offer the thermodynamic data not only for the scientific research but also for the industrial manufacture, the activity and activity coefficient of P_2O_5 in the calcium phosphate-based solid solution have been measured at 1823 and 1873 K which is considered as the steelmaking temperature. In addition, the other thermodynamic data about this system have been discussed.

1.2 Research background

1.2.1 Introduction of steelmaking and source of phosphorus in steel

There are three processes for steelmaking. The process of iron ore → blast furnace → basic oxygen furnace → continuous casting is the main stream of steel production. The process of steel scrap → refining → continuous casting is getting popular recently. In addition, non-blast furnace ironmaking also has been adopted by a part of plants. **Figure 1.1** shows the steelmaking process which is the main stream process all over the world. The raw materials such as the iron ore, coke and lime are charged into a blast furnace, and iron ore is reduced into pig iron in the reducing atmosphere in a blast furnace. Then the pig iron is transferred by a torpedo car or ladle to basic oxygen furnace, and a part of impurities are removed by various methods. Finally the molten steel is cast, rolled and made products for different applications.

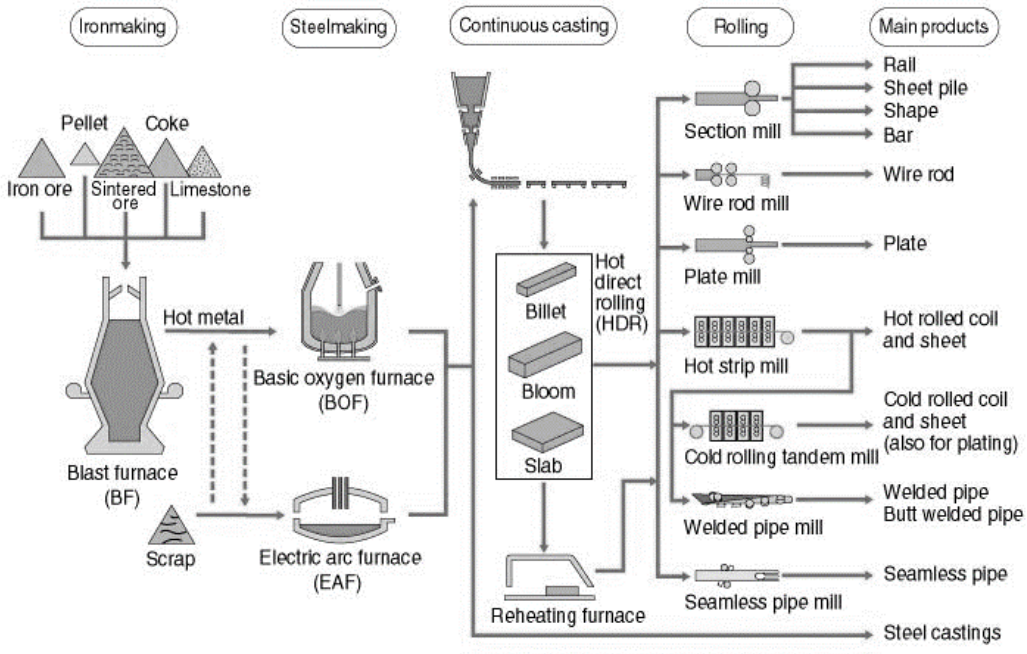

Fig. 1.1 Steelmaking process. Copy right by 1997-2002 KAWASAKI STEEL 21st Century Foundation and by 2003 JFE 21st Century Foundation.[1]

The phosphorus in steel is mainly brought by iron ore. The P_2O_5 is reduced to phosphorus in blast furnace and the phosphorus dissolves in liquid iron as Eq. (1.1).

$$P_2O_5(s) + 5C(s) = 2\underline{P}(mass\%) + 5CO(g) \ldots\ldots (1.1)$$

In another words, the phosphorus cannot be removed at blast furnace and almost all the phosphorus dissolves in molten iron in which the concentration of phosphorus is about 0.1 mass%. During the molten iron is transferred from blast furnace to basic oxygen furnace by a torpedo car or ladle even in the basic oxygen furnace itself, the phosphorus is removed.

1.2.2 Disadvantage of phosphorus for steel

Usually, the phosphorus is considered as a harmful element in steel since it causes embrittlement for steel to decrease the plasticity and toughness of steel.[2-6] From Fe-P phase diagram as shown in **Figure 1.2**, phosphorus has the biggest solubility in α-Fe at 1048 ˚C. With the decrease of the temperature the solubility decreases and then the redundant P segregates at the grain boundary of Fe as Fe_3P or Fe_2P, and the segregation cannot disappear by heat treatment due to the diffusion of P in Fe is slow.

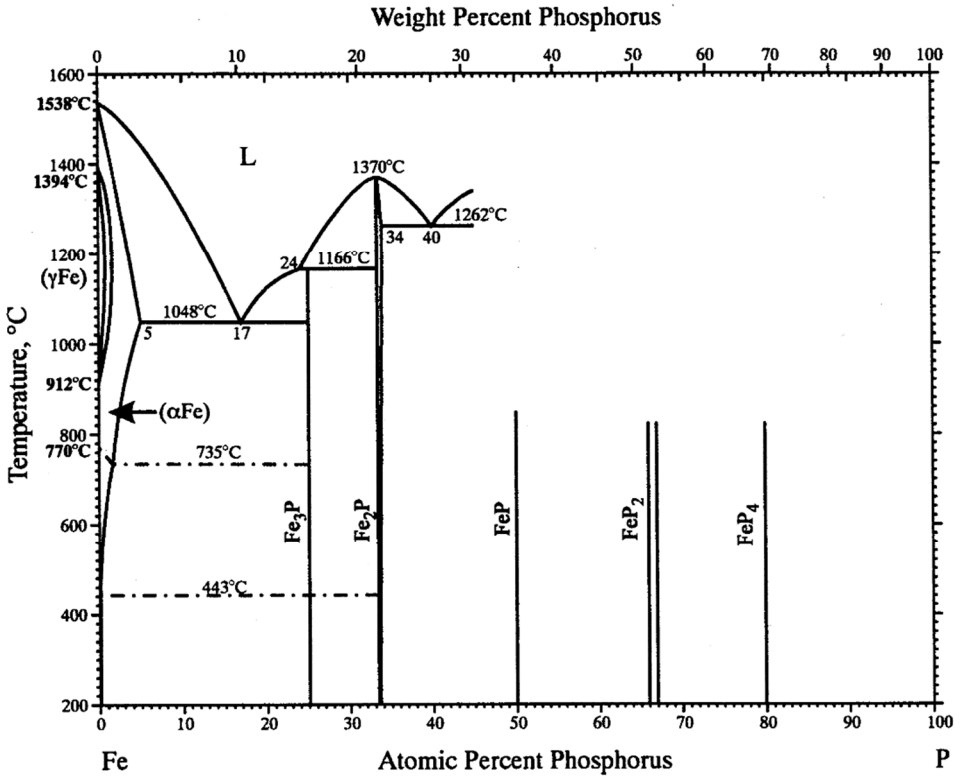

Fig. 1.2 Binary phase diagram for the Fe-P system.[7]

Viswanathan confirmed the phosphorus segregation in austenite grain boundary which increased the fracture appearance transition temperature of steel by experiments.[2] **Figure 1.3** shows the SEM image of auger specimens of Ni-Cr-C-0.02mass%P steel and Ni-Cr-C-0.0005mass%P steel. Comparing with the two samples, the typical intergranular fracture surface was clear in the Ni-Cr-C-0.02mass%P steel.

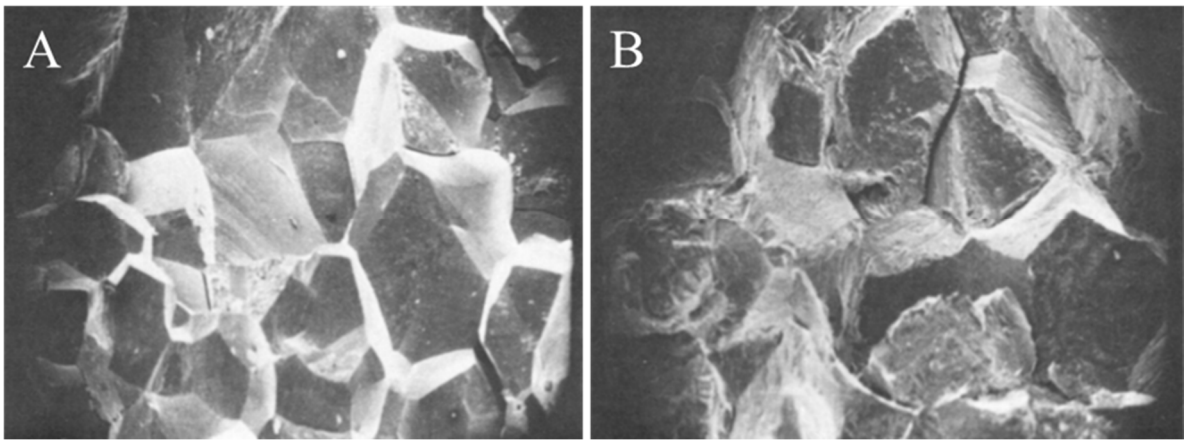

Fig. 1.3 SEM image of auger specimens. A: Ni-Cr-C-P-0.02mass%P steel. B: Ni-Cr-C-0.0005mass%P steel. The samples were treated to embrittle and fractured at -112.2 ˚C.[2]

Viswanathan also studied the relationship between the phosphorous concentration at prior anstenite grain boundaries and the fracture appearance transition temperature as shown in **Figure 1.4**.[2] It was obvious that the fracture appearance transition temperature increased with the increase of the phosphorous concentration at prior anstenite grain boundaries.

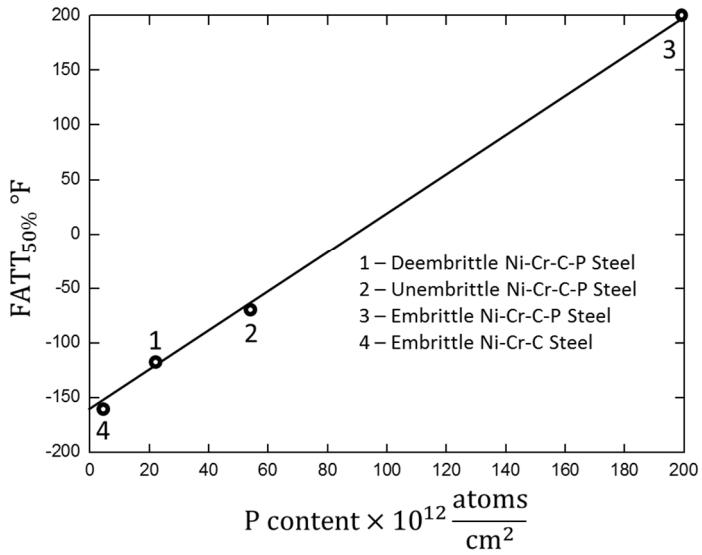

Fig. 1.4 Relationship between the phosphorous concentration at prior austenite grain boundaries and the fracture appearance transition temperature.[2]

1.2.3 Conventional methods of dephosphorization

Momokawa *et al.*[8] studied the relationship between the content of P in 41mass%CaO-59mass%Al_2O_5 slag and the oxygen partial pressure under a constant temperature and P_2 partial pressure as shown in **Figure 1.5**. From the results, the content of P in the 41mass%CaO-59mass%Al_2O_5 slag at 1550 ˚C at first decreased and then increased with the increase of oxygen partial pressure. For different oxygen partial pressures, the stable forms of P in slag were different. In the condition of Momokawa *et al.*'s experiments, when the oxygen partial pressure was smaller than 2.2×10^{-18} atm, the phosphide was predominant and when the oxygen partial pressure was larger than 2.2×10^{-18} atm, the phosphate was predominant.

In normal condition of steelmaking, the oxygen partial pressure is relatively high and the P in molten steel is removed by basic slag according to Reaction (1.2).

$$\underline{\mathrm{P}}(\mathrm{mass\%}) + 5/4\,\mathrm{O_2(g)} + 3/2\,\mathrm{O^{2-}} = (\mathrm{PO_4^{3-}}) \ldots\ldots (1.2)$$

As this reaction is exothermic reaction, the referable conditions for dephosphorization are higher oxygen partial pressure, higher basicity and lower temperature.

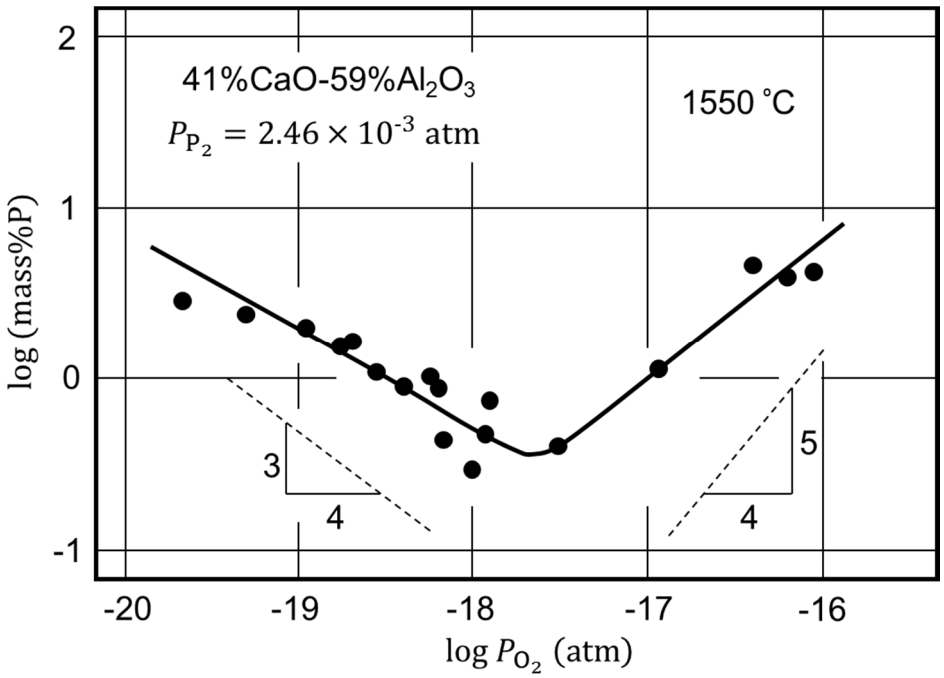

Fig. 1.5 Variation of P content in the 41mass%CaO-59mass%Al_2O_5 melt with various oxygen partial pressure of oxygen.[8]

For dephosphorization by oxidation, the phosphorus capacity is defined as Eq. (1.3) by Wagner.[9] The phosphorus partition ratio (L_P) is expressed as Eq. (1.4). These two parameters represent the ability of dephosphorization for slag. For achieving good effect of dephosphorization, the large phosphorus capacity and phosphorus partition ratio are expected in the process of dephosphorization. **Figure 1.6** shows the phosphate capacity for various systems.

$$C_{PO_4^{3-}} = \frac{(\text{mass\%}PO_4^{3-})}{{P_{P_2}}^{1/2}{P_{O_2}}^{5/4}} = \frac{K_{1.2}a_{O^{2-}}^{3/2}}{f_{PO_4^{3-}}} \ldots\ldots (1.3)$$

$$L_P = \frac{(\text{mass\%P})}{[\text{mass\%P}]} \ldots\ldots (1.4)$$

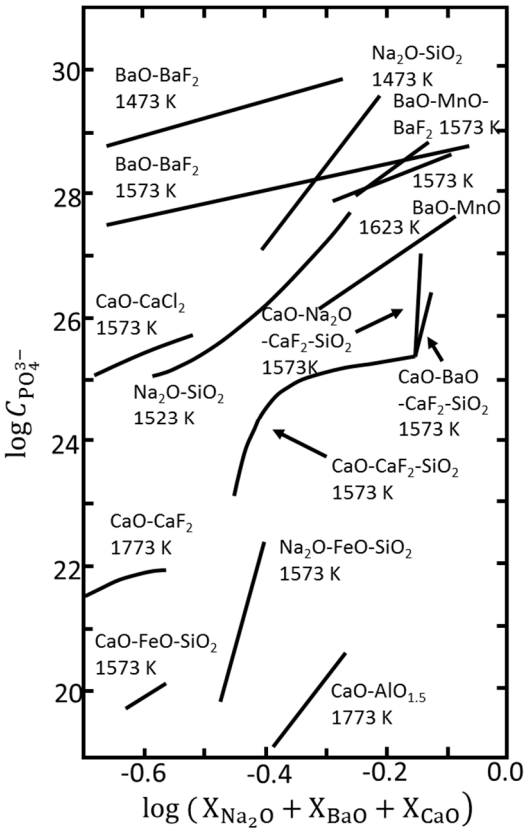

Fig. 1.6 Phosphorus capacity for various systems.[10]

For the traditional method of dephosphorization, CaO is commonly adopted as a cheap and efficient dephosphorization agent. In order to achieve better effect of dephosphorization, the excess CaO is added and then the BOF slag is difficult to be reused due to CaO remains

unreacted or precipitates during solidification of dephosphorization slag. Meanwhile the consumption of lime and the amount of slag increase. Besides, the fluorite is strictly regulated used due to the harm for environment and human although it could enhance the dissolution of CaO into slag. In current steel industry, what the metallurgists are chasing is not only the top quality product but also how to achieve the eco-friendly technique. Under this condition, the use of multi-phase flux as a refining reagent was considered.

1.2.4 Dephosphorization by multi-phase flux

When the CaO tablet was dipped into the CaO-SiO_2-FeO-P_2O_5 slag, the existence of $2CaO{\cdot}SiO_2$-$3CaO{\cdot}P_2O_5$ solid solution was confirmed by Suito *et al*.[11] as shown in **Figure 1.7**. After dipping the CaO tablet into the CaO-SiO_2-FeO-P_2O_5 slag for 30 seconds, the layer of $2CaO{\cdot}SiO_2$-$3CaO{\cdot}P_2O_5$ solid solution was found on the surface of the block CaO and after 5 minutes the layer of $2CaO{\cdot}SiO_2$-$3CaO{\cdot}P_2O_5$ solid solution was still there meanwhile the layer of CaO-Fe_tO was found between the block CaO and the layer of $2CaO{\cdot}SiO_2$-$3CaO{\cdot}P_2O_5$ solid solution. Besides, it was also confirmed that the di-calcium silicate formed a pseudo-binary solid solution with tri-calcium phosphate over a wide range of compositions at the steelmaking temperature by Fix *et al*.[12] as shown in **Figure 1.8**. These provided the possibility for utilizing the formed solid phase in the process of dephosphorization to decrease the consumption of CaO and the amount of slag.

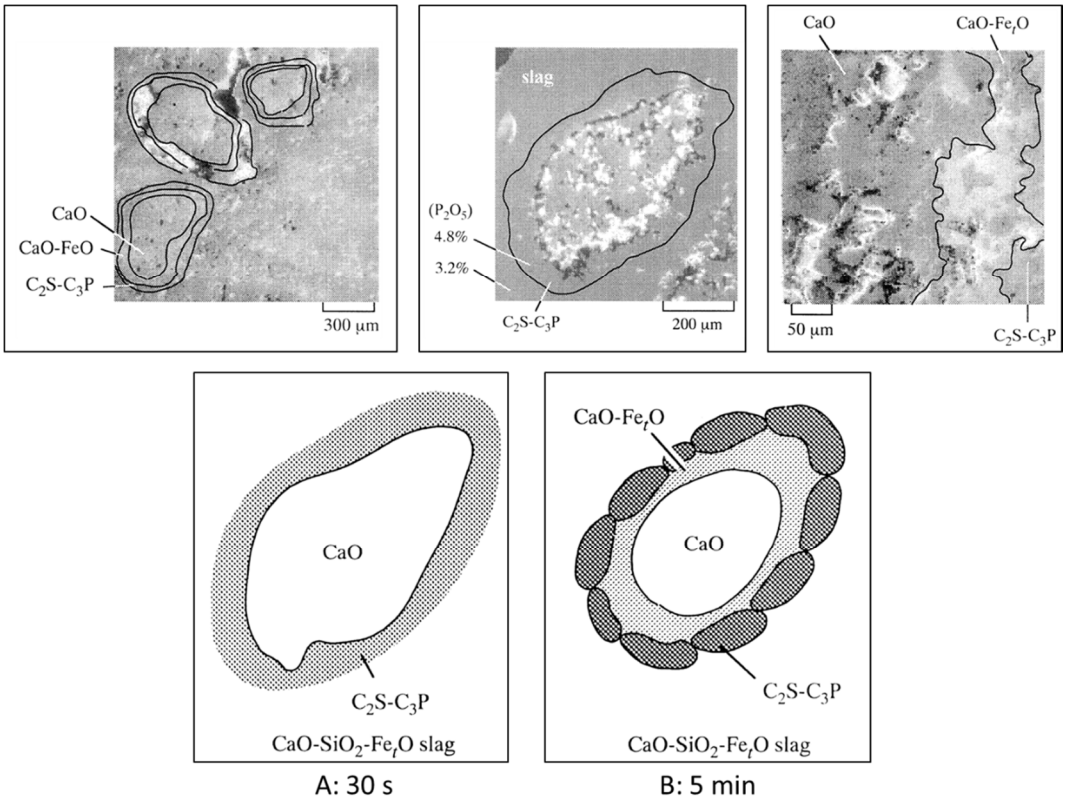

Fig. 1.7 SEM image and schematic illustration of reaction between CaO particle and the CaO-SiO_2-Fe_tO-5mass%P_2O_5 system.[11]

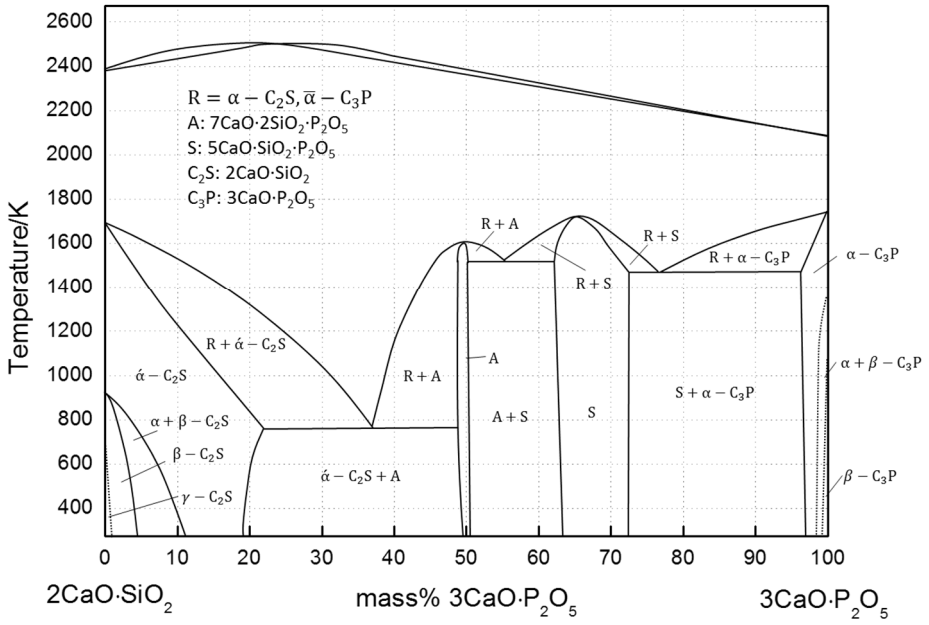

Fig. 1.8 Phase diagram for the $2CaO \cdot SiO_2$-$3CaO \cdot P_2O_5$ pseudo-binary system.[12]

Hasegawa *et al.*[13] reported the advantage of multi-phase flux in the process of dephosphorization comparing with the conventional method as shown in **Figure 1.9**. In conventional method of dephosphorization, the activity of FeO decreases and the activity of P_2O_5 increases with the reaction due to the reduction of FeO and the generating P_2O_5 in slag. In order to obtain better effect of dephosphorization, the extra FeO and CaO are added into slag during reaction. In the process of dephosphorization by multi-phase flux, the activity of FeO and P_2O_5 could be maintained stable which means it is not necessary to add extra FeO and CaO during reaction. **Figure 1.10** shows the theoretical consumption of CaO for producing one ton steel comparing with the current value without fluoride, if all the phosphorus could be concentrated into $3CaO \cdot P_2O_5$, $4CaO \cdot P_2O_5$, $5CaO \cdot SiO_2 \cdot P_2O_5$ or $7CaO \cdot 2SiO_2 \cdot P_2O_5$ when the phosphorus concentration decreased from 0.1 mass% to 0.01 mass%. From this estimation, the use of multi-phase flux is considered to be effective for dephosphorization of steel.

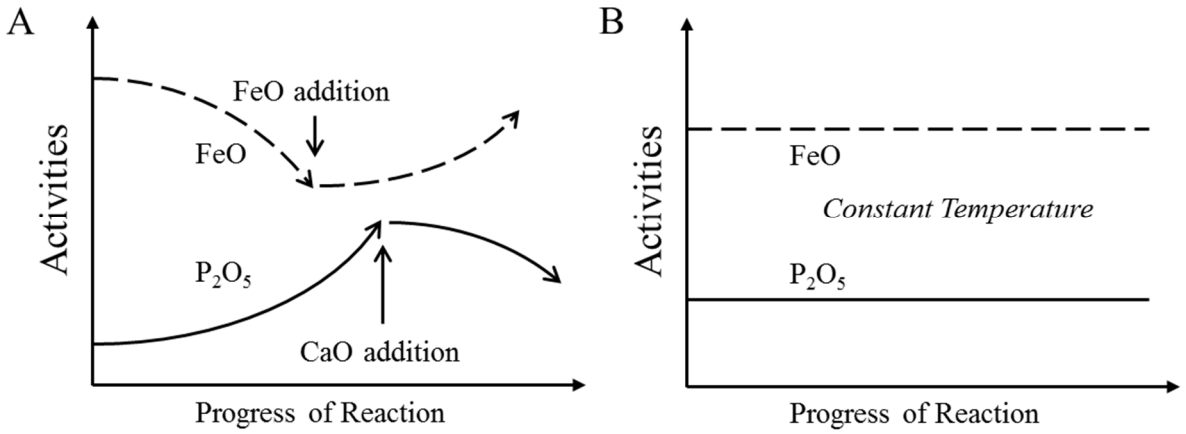

Fig. 1.9 Schematic illustration showing the variations of the activities of FeO and P_2O_5 within slag phase during the removal of phosphorous from molten iron.[13] A: With homogeneous liquid slags. B: with heterogeneous slags of unit freedom degree.

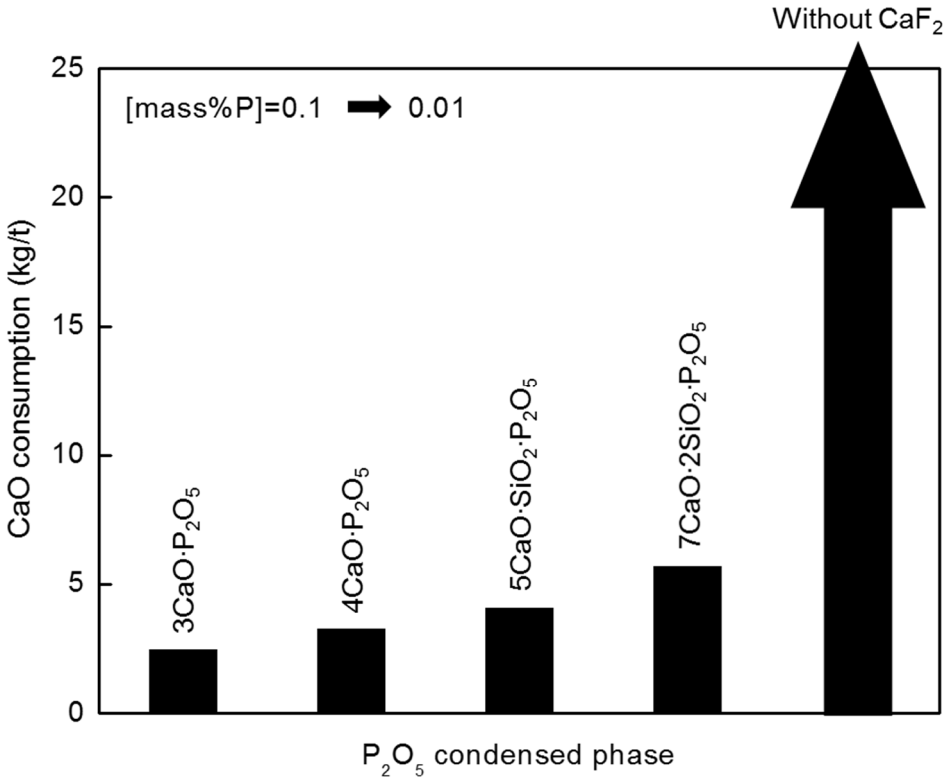

Fig. 1.10 Consumption of CaO for different P_2O_5 condensed phase in the process of dephosphorization. After K. Ito, Waseda University.[14]

1.3 Previous research

1.3.1 Reaction between solid CaO and liquid slag

Suito *et al.*[11] confirmed the existence of $2CaO \cdot SiO_2$-$3CaO \cdot P_2O_5$ solid solution as shown in Figure 1.7. The similar phenomenon was observed by Kami *et al*.[15] and Hamano *et al*.[16] as shown in **Figures 1.11** and **1.12**.

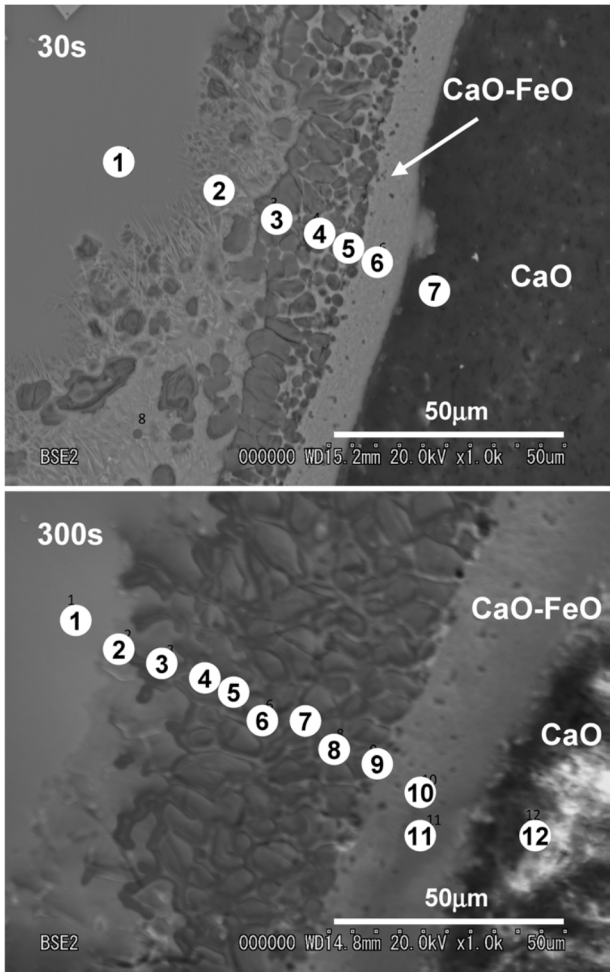

Fig. 1.11 SEM images of the interface between solid CaO and the CaO-SiO_2-FeO-P_2O_5 slag.[15]

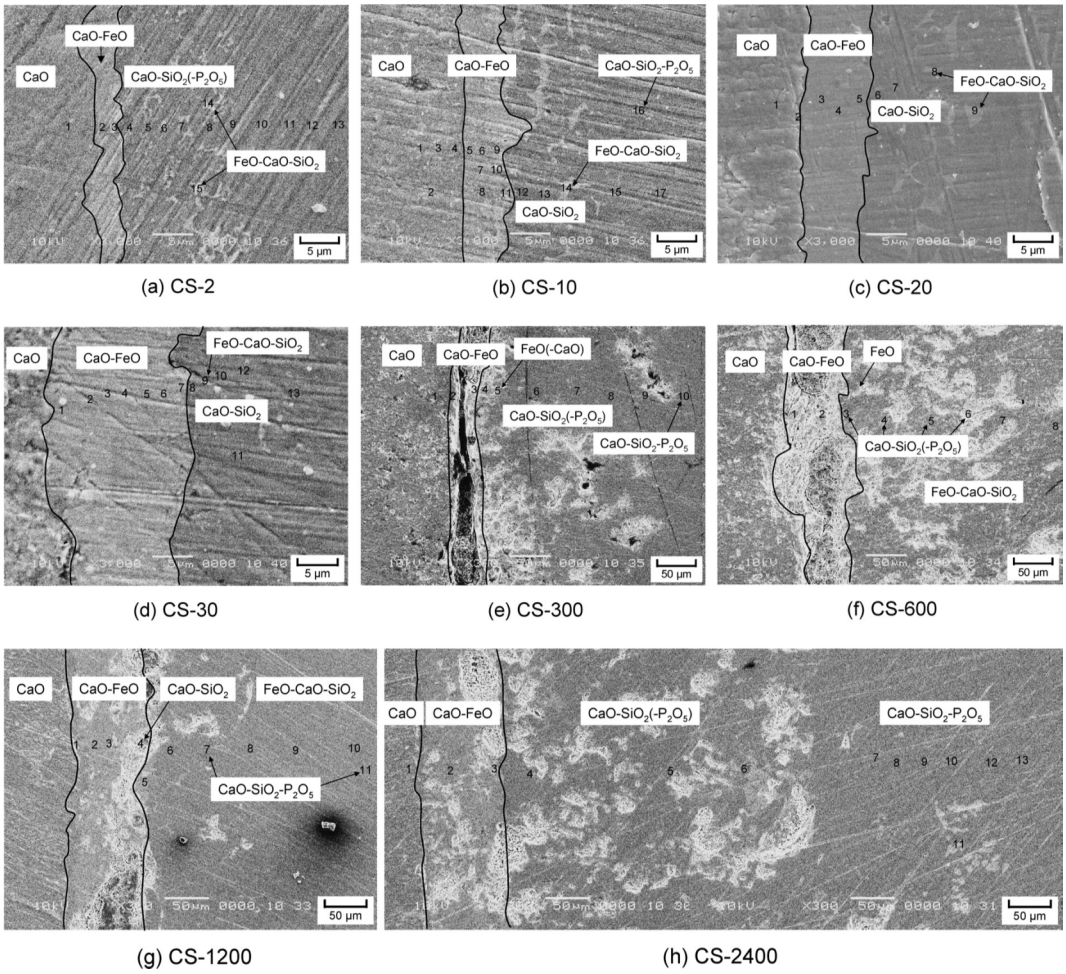

Fig. 1.12 SEM images of the interface between solid CaO and the FeO_x-CaO-SiO_2-P_2O_5 slag.[16]

The relationship between the thickness of CaO-FeO layer and the reaction time has been studied by Kami *et al*. and Hamano *et al*., respectively. The thickness of CaO-FeO layer increased with the squire root of reaction time with an approximate liner relationship reported by Kami *et al*. as shown in **Figure 1.13**. Similarly, Hamano *et al*. reported that the thickness of CaO-FeO layer increased with the squire root of reaction time at 1573 K as shown in **Figure 1.14**.

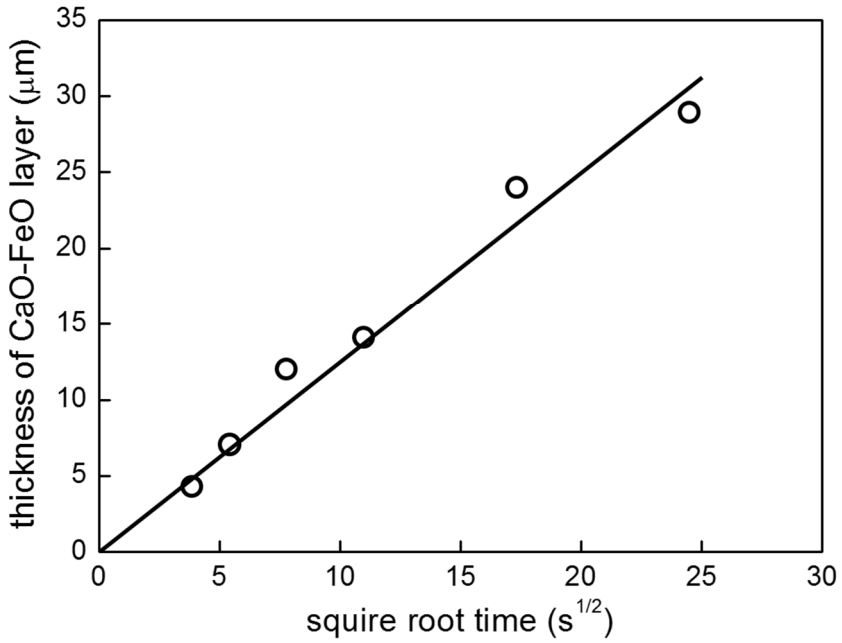

Fig. 1.13 Relationship between the thickness of CaO-FeO layer and the reaction time at 1673 K reported by Kami *et al*.[15]

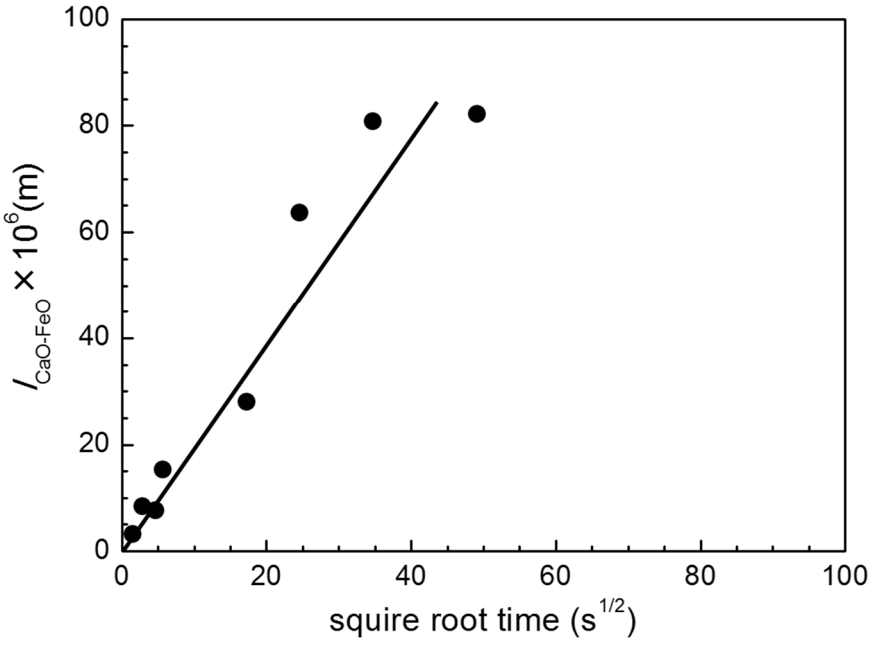

Fig. 1.14 Relationship between the thickness of CaO-FeO layer and the reaction time at 1573 K reported by Hamano *et al*.[16]

In addition, Hamano *et al*. summarized the reaction mechanism between solid CaO and the FeO_x-CaO-SiO_2-P_2O_5 slag at 1573 K as shown in **Figure 1.15**. As the solid CaO contacted with the FeO_x-CaO-SiO_2-P_2O_5 slag, the CaO dissolved into slag because the initial composition of slag was unsaturated with CaO. With the dissolution of CaO, at the interface between CaO and slag the concentration of CaO increased which caused the increase of the CaO activity. Due to the increase of CaO activity, the $2CaO{\cdot}SiO_2$ formed and the concentration of FeO increased. Then the Fe^{2+} began to diffuse to both sides. The CaO-FeO layer formed at the CaO boundary. With reaction, the CaO continuously diffused into slag through the CaO-FeO layer, and meanwhile the thickness of CaO-FeO layer increased.

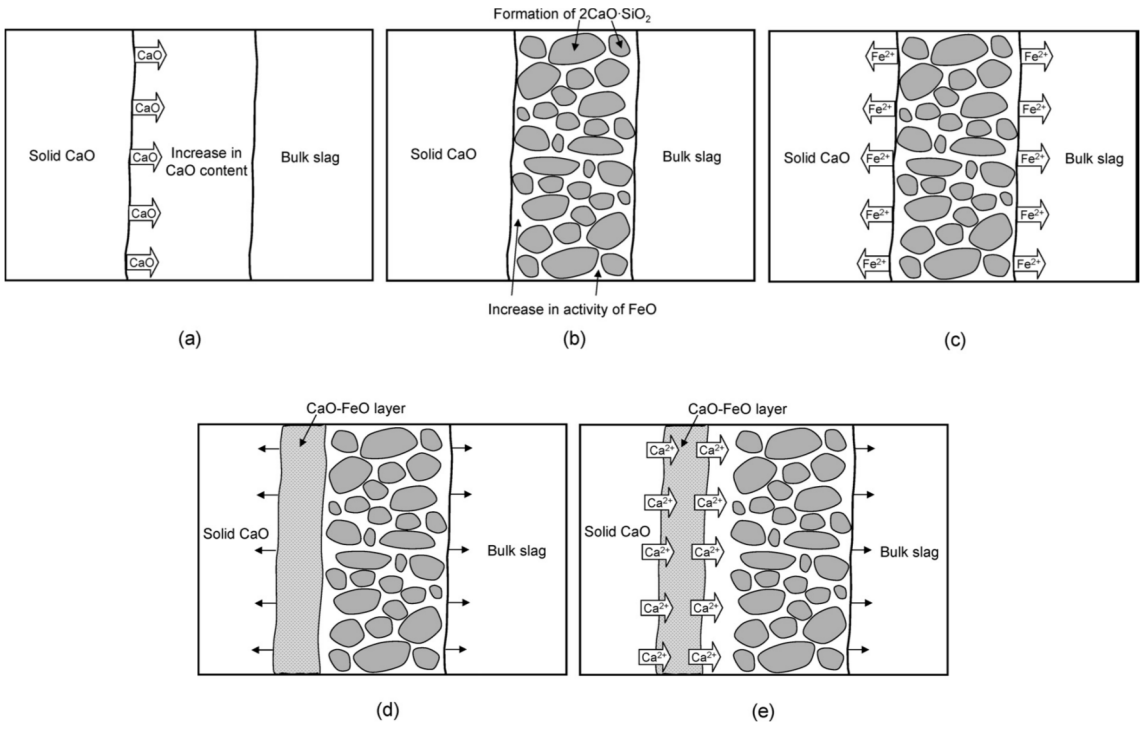

Fig. 1.15 Schematic of reaction mechanism between solid CaO and the FeO_x-CaO-SiO_2-P_2O_5 slag.[16]

1.3.2 Reaction between solid $2CaO \cdot SiO_2$ and liquid slag

Yang *et al.*[17-20] studied the reaction mechanism between solid $2CaO \cdot SiO_2$ and the homogeneous $CaO\text{-}SiO_2\text{-}FeO_x\text{-}P_2O_5$ slag or the heterogeneous $CaO\text{-}SiO_2\text{-}FeO_x\text{-}P_2O_5$ slag. After dipping the $2CaO \cdot SiO_2$ tablet into the $CaO\text{-}SiO_2\text{-}FeO_x\text{-}P_2O_5$ slag, the multi-phase area was found between solid $2CaO \cdot SiO_2$ and $CaO\text{-}SiO_2\text{-}FeO_x\text{-}P_2O_5$ slag as shown in **Figure 1.16**.

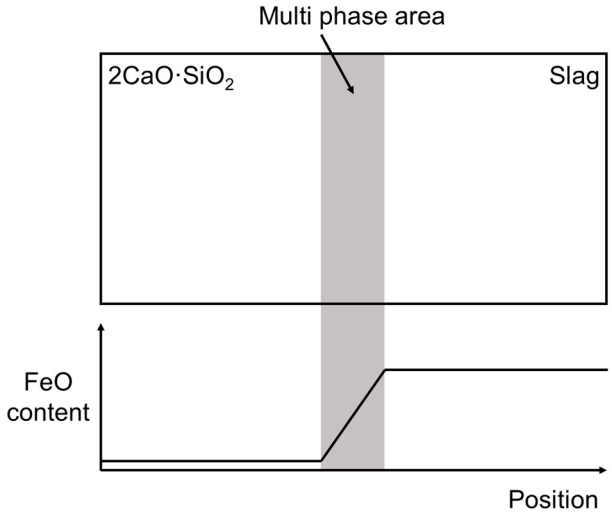

Fig. 1.16 Partition of the area near the interface between solid $2CaO \cdot SiO_2$ and the $CaO\text{-}SiO_2\text{-}FeO_x\text{-}P_2O_5$ slag.[17]

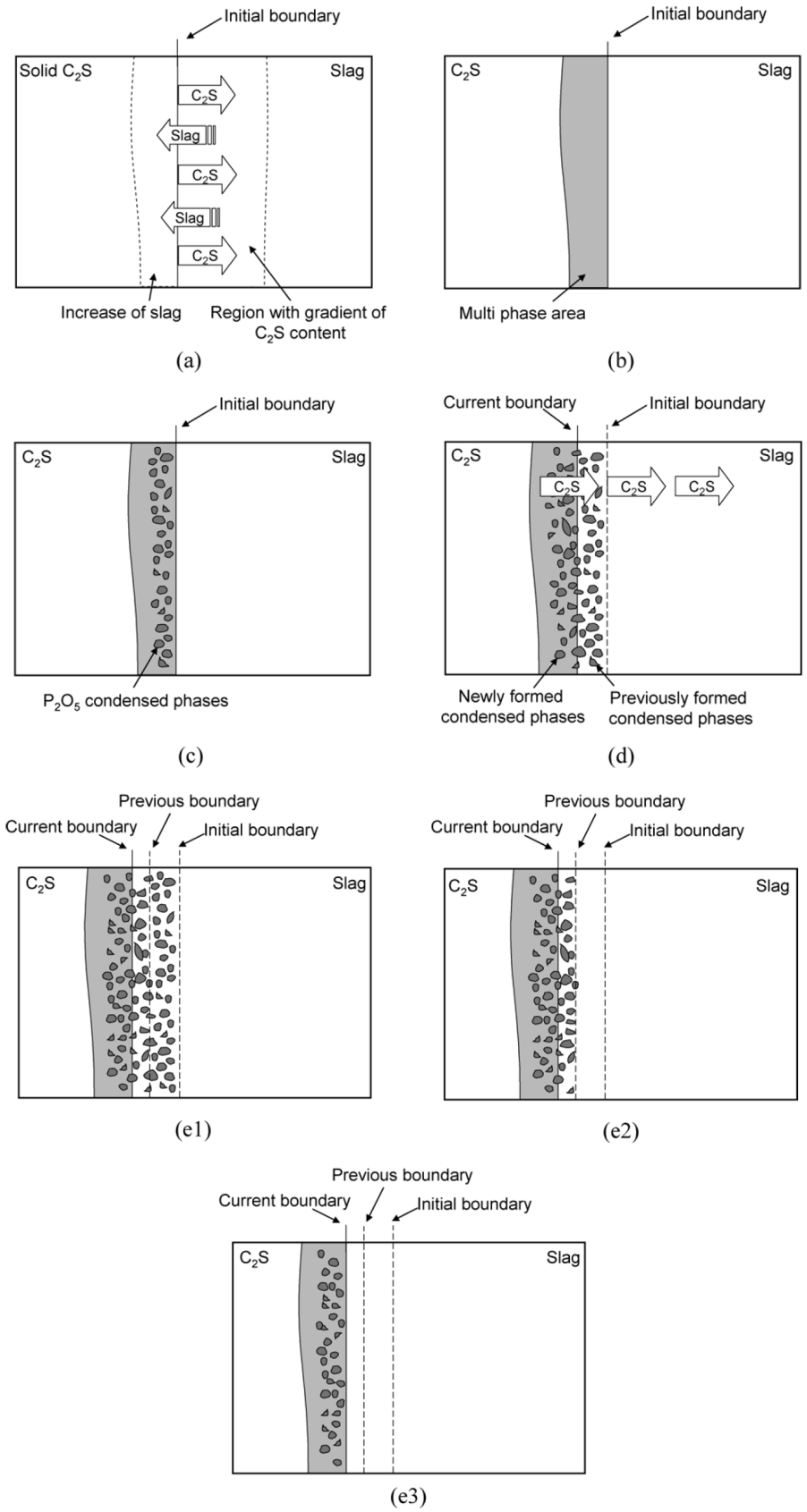

Fig. 1.17 Phosphorous behavior at interface between $2CaO \cdot SiO_2$ and the $CaO\text{-}SiO_2\text{-}FeO_x\text{-}P_2O_5$ slag. "C_2S" is short for $2CaO \cdot SiO_2$.[17]

Yang *et al*. summarized the reaction mechanism between solid $2CaO \cdot SiO_2$ and the homogeneous $CaO\text{-}SiO_2\text{-}FeO_x\text{-}P_2O_5$ slag as shown in **Figure 1.17**. At first the solid $2CaO \cdot SiO_2$ dissolved into slag and at the same time the slag penetrated into solid $2CaO \cdot SiO_2$. Then at the interface between solid $2CaO \cdot SiO_2$ and the homogeneous $CaO\text{-}SiO_2\text{-}FeO_x\text{-}P_2O_5$ slag, the multi-phase area of the solid $2CaO \cdot SiO_2$ in liquid slag formed. And the concentration gradient of solid $2CaO \cdot SiO_2$ near the interface formed. In the multi-phase area the CaO and P_2O_5 reacted with $2CaO \cdot SiO_2$ to form P_2O_5 condensed phase. At this time, the multi-phase area was the mixture of P_2O_5 condensed phase and liquid slag phase. With proceeding the reaction, the solid $2CaO \cdot SiO_2$ continuously dissolved into slag and the multi-phase area shifted to the side of solid $2CaO \cdot SiO_2$ to form the new P_2O_5 condensed phase.

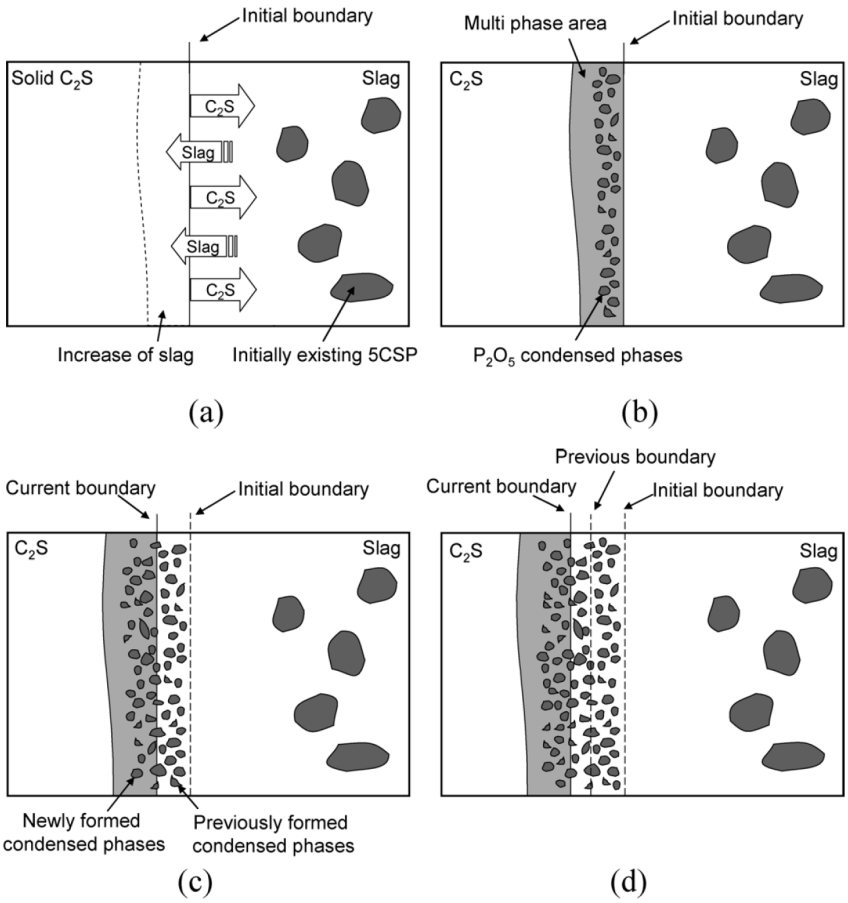

Fig. 1.18 Reaction behavior of phosphorus at the interface between $2CaO \cdot SiO_2$ and the heterogeneous $CaO\text{-}SiO_2\text{-}FeO_x\text{-}P_2O_5$ slag. "C_2S" and "5CSP" are short for $2CaO \cdot SiO_2$ and $5CaO \cdot SiO_2 \cdot P_2O_5$, respectively.[18]

Figure 1.18 shows the reaction mechanism between solid $2CaO \cdot SiO_2$ and the heterogeneous $CaO\text{-}SiO_2\text{-}FeO_x\text{-}P_2O_5$ slag which was initially saturated with $5CaO \cdot SiO_2 \cdot P_2O_5$. At the beginning the solid $2CaO \cdot SiO_2$ dissolved into slag and the slag penetrated into solid $2CaO \cdot SiO_2$. Then the multi-phase area formed and the P_2O_5 condensed phase formed in the multi-phase area. As the initial slag was saturated with $5CaO \cdot SiO_2 \cdot P_2O_5$, the previously formed P_2O_5 condensed phase was remained and the multi-phase area shifted to the side of solid $2CaO \cdot SiO_2$ to form the new P_2O_5 condensed phase.

Kitamura *et al.*[21] studied the mass transfer of P_2O_5 between liquid slag and $2CaO \cdot SiO_2\text{-}3CaO \cdot P_2O_5$ solid solution. The preheated $2CaO \cdot SiO_2$ rod was immersed into different compositions of slags with different reaction periods. Then the rod was quenched and the interface between the rod and slag was observed by electron probe micro-analyzer (EPMA).

In the first case, when P_2O_5 was transferred from slag to $2CaO \cdot SiO_2\text{-}3CaO \cdot P_2O_5$ solid solution, a certain amount of CaO was consumed to form $2CaO \cdot SiO_2\text{-}3CaO \cdot P_2O_5$ solid solution. The content of CaO in slag decreased and the content of SiO_2 increased then the liquidus composition changed to a larger CaO/SiO_2 ratio according to Shimauchi *et al.*'s research[22] as shown in **Figure 1.19 A**. In this case, the $2CaO \cdot SiO_2\text{-}3CaO \cdot P_2O_5$ solid solution dissolved in slag near the interface and the reaction layer formed between $2CaO \cdot SiO_2\text{-}3CaO \cdot P_2O_5$ solid solution and slag as shown in **Figure 1.20 A**. On the contrary, when P_2O_5 is transferred from $2CaO \cdot SiO_2\text{-}3CaO \cdot P_2O_5$ solid solution to slag, the activity of P_2O_5 in the solid solution was larger than that in slag. The content of CaO in slag increased and the content of SiO_2 decreased then the liquidus composition changed to a smaller CaO/SiO_2 ratio as shown in **Figure 1.19 B**. In this case, no dissolved part was observed at the side of $2CaO \cdot SiO_2\text{-}3CaO \cdot P_2O_5$ solid solution as shown in **Figure 1.20 B**.

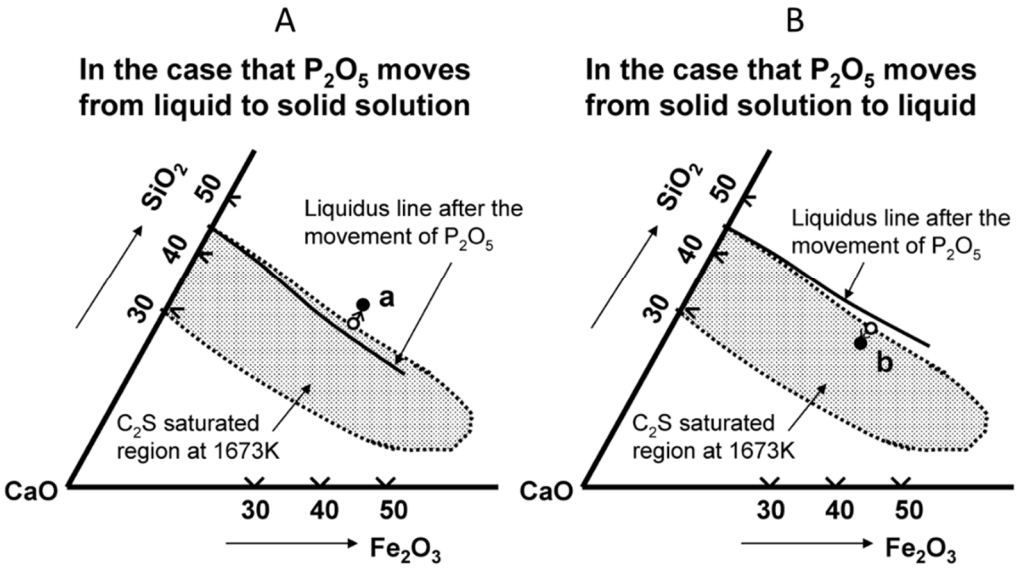

Fig. 1.19 Schematic change in liquid composition and liquidus line position after transfer of P_2O_5 between $2CaO{\cdot}SiO_2$-$3CaO{\cdot}P_2O_5$ solid solution and slag.[21]

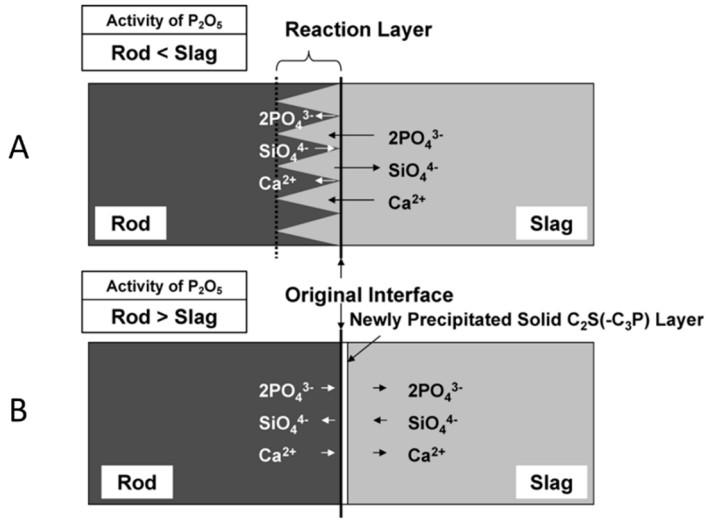

Fig. 1.20 Schematic of the phenomena at the interface between $2CaO{\cdot}SiO_2$-$3CaO{\cdot}P_2O_5$ solid solution and slag.[21]

1.3.3 Phosphorus distribution ratio between liquid slag and metal and P_2O_5 distribution ratio between solid solution and liquid slag

Not only the phosphorus distribution ratio between the homogeneous slag and molten iron but also the phosphorus distribution ratio between the heterogeneous slag and molten iron has been studied by Suito *et al*.[11] About 20 g of Fe-0.5mass%P alloy was dephosphorized at 1833 K for 30 minutes in an MgO crucible by the heterogeneous slag. The compositions were projected on the CaO-SiO_2-Fe_tO system as shown in **Figure 1.21** with the values of phosphorus distribution ratio.

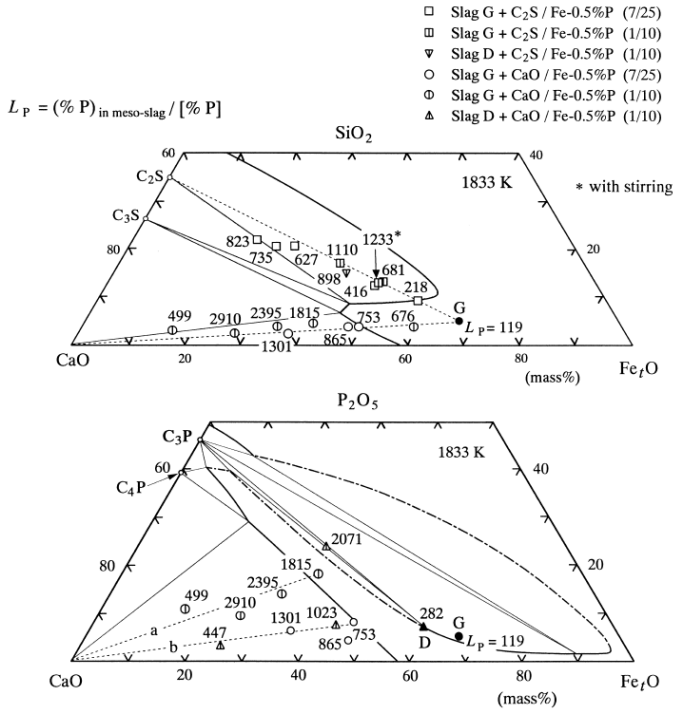

Fig. 1.21 Phosphorus distribution ratio between various heterogeneous slag and molten iron.[11]

Inoue *et al*.[23] measured the phosphorous distribution ratio between $2CaO{\cdot}SiO_2$-$3CaO{\cdot}P_2O_5$ solid solution and slag. The phosphorous distribution ratio between $2CaO{\cdot}SiO_2$-$3CaO{\cdot}P_2O_5$ solid solution and slag was shown in **Figure 1.22** with the phosphorous distribution ratio between the slag and molten iron expressed by Eq. (1.5).

$$\log L'_{\mathrm{P}} = 0.072\{(\mathrm{mass\%CaO}) + 0.3(\mathrm{mass\%MgO})\} + 2.5\log(\mathrm{mass\%T.Fe}) + 11570/T - 10.52 \ldots\ldots (1.5)^{[24]}$$

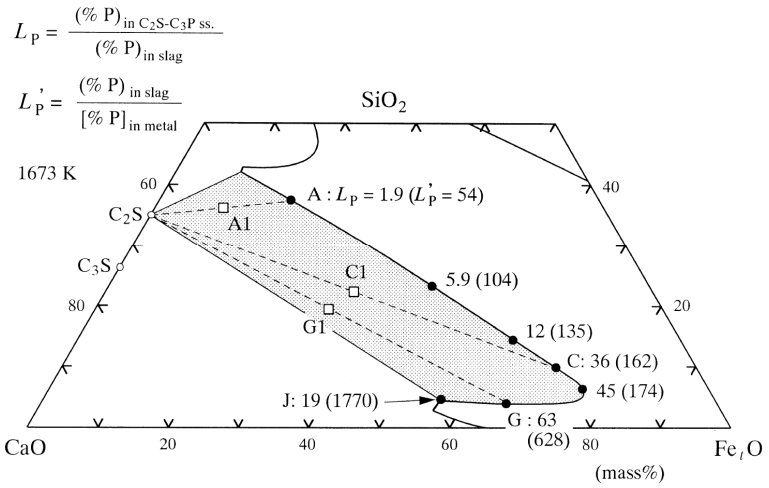

Fig 1.22 Phosphorous distribution ratio between $2CaO{\cdot}SiO_2$-$3CaO{\cdot}P_2O_5$ solid solution and slag.[23]

Shimauchi *et al.*[22] applied the chemical equilibration method to study the P_2O_5 distribution ratio between solid solution and liquid slag. The slag was melted at 1873 K completely, then cooling down slowly to 1673 K to achieve the equilibrium between solid solution and liquid slag. **Figure 1.23 A** shows the observed slag compositions in the CaO-SiO_2-Fe_2O_3 system. **Figure 1.23 B** shows the observed compositions of $2CaO{\cdot}SiO_2$-$3CaO{\cdot}P_2O_5$ solid solution. **Figure 1.23 C** shows the relationship between the P_2O_5 distribution ratio between $2CaO{\cdot}SiO_2$-$3CaO{\cdot}P_2O_5$ solid solution and slag and the T.Fe content. The linear relationship was observed and it was independent of the lime/silica ratio and P_2O_5 content. **Figure 1.23 D** indicated no clear influence of the 10mass% MgO or MnO addition on the P_2O_5 distribution ratio between $2CaO{\cdot}SiO_2$-$3CaO{\cdot}P_2O_5$ solid solution and slag.

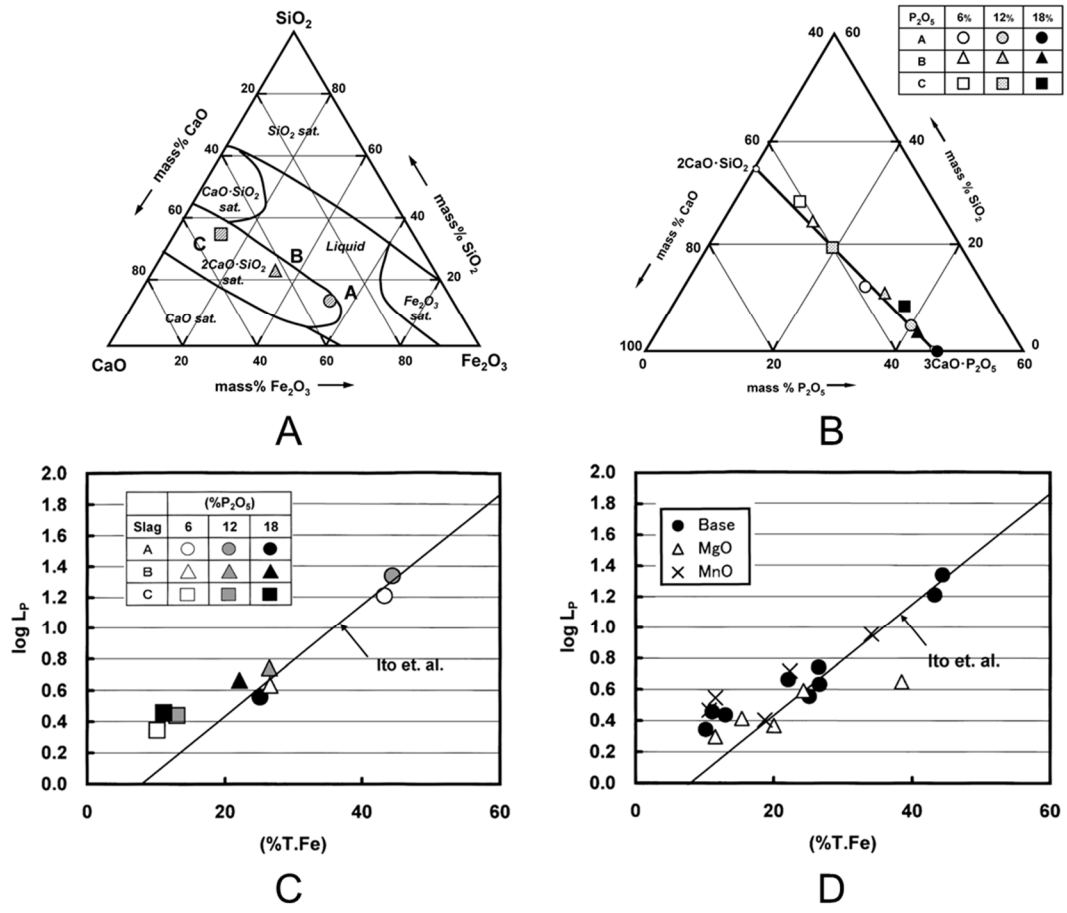

Fig. 1.23 A: Observed slag compositions in the $CaO-SiO_2-Fe_2O_3$ system. B: Composition of solid solution for each slag with various P_2O_5 contents in $CaO-SiO_2-P_2O_5$ system. C: Relationship of P_2O_5 distribution ratio between solid solution and liquid slag with the T.Fe content. D: Influence of MgO and MnO addition on the P_2O_5 distribution ratio between solid solution and liquid slag. In C and D the solid line was reported by Ito *et. al.*[25]

Pahlevani *et al.*[26] investigated the P_2O_5 distribution ratio between solid solution and liquid slag as shown in **Figure 1.24**. Figure 1.24 A shows the relationship between the P_2O_5 distribution ratio between solid solution and the $CaO-SiO_2-P_2O_5-Fe_2O_3$ slag and the T.Fe content. The P_2O_5 distribution ratio increased with the increase of the T.Fe content in slag, and in a low T.Fe content, the addition of Al_2O_3 increased P_2O_5 distribution ratio comparing with the effect of adding MgO or MnO measured by Shimauchi *et al*. as shown in Figure 1.24 B. In the case of adding MgO or MnO, the P_2O_5 distribution ratio decreased with the increase of CaO content in slag, but with the addition of Al_2O_3, the P_2O_5 distribution ratio barely changed.

Figures 1.24 C and D showed the influence of different slags on the P_2O_5 distribution ratio. The P_2O_5 distribution ratio in the CaO-SiO_2-P_2O_5-Fe_2O_3 slag was larger than that in the CaO-SiO_2-P_2O_5-FeO slag at different T.Fe contents in liquid phase as shown in Figure 1.24 C, and this tendency was more clear at different CaO contents in liquid phase as shown in Figure 1.24 D. Figure 1.24 E shows the effect of various added oxides on the P_2O_5 distribution ratio in the CaO-SiO_2-P_2O_5-FeO slag. It was found that the effect of adding MgO, MnO or Al_2O_3 on the P_2O_5 distribution ratio in the CaO-SiO_2-P_2O_5-FeO slag was smaller than that in the CaO-SiO_2-P_2O_5-Fe_2O_3 slag.

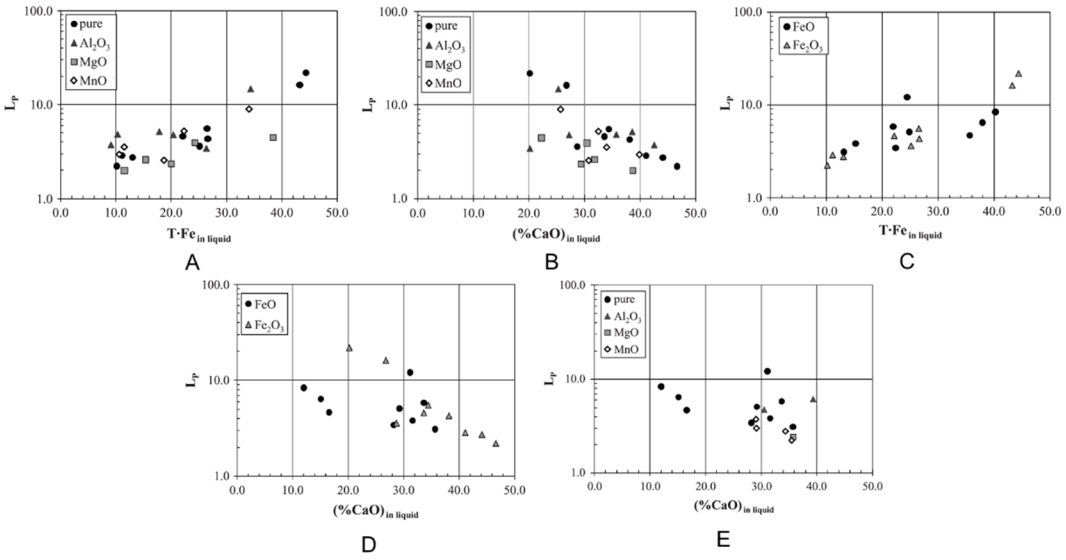

Fig.1.24 Influence of various additions on the P_2O_5 distribution ratio between solid solution and liquid slag at different T.Fe contents or CaO contents in liquid phase.[26] In A and B, the CaO-SiO_2-P_2O_5-Fe_2O_3 system was adopted and the values of L_P with adding MgO and MnO were measured by Shimauchi *et al*.[22] In C and D both the CaO-SiO_2-P_2O_5-Fe_2O_3 system and the CaO-SiO_2-P_2O_5-FeO system were adopted. In E the CaO-SiO_2-P_2O_5-FeO system was adopted.

1.3.4 Activity and activity coefficient of P_2O_5 in the $2CaO{\cdot}SiO_2$-$3CaO{\cdot}P_2O_5$ solid solution

According to the activity of P_2O_5 in slag estimated by applying the regular solution model reported by Ban-ya *et al*.,[27] the activity coefficient of P_2O_5 with the P_2O_5 content in the $2CaO{\cdot}SiO_2$-$3CaO{\cdot}P_2O_5$ solid solution was shown in **Figure 1.25**. The compositions of slag were shown in Figure 1.23 A.[22]

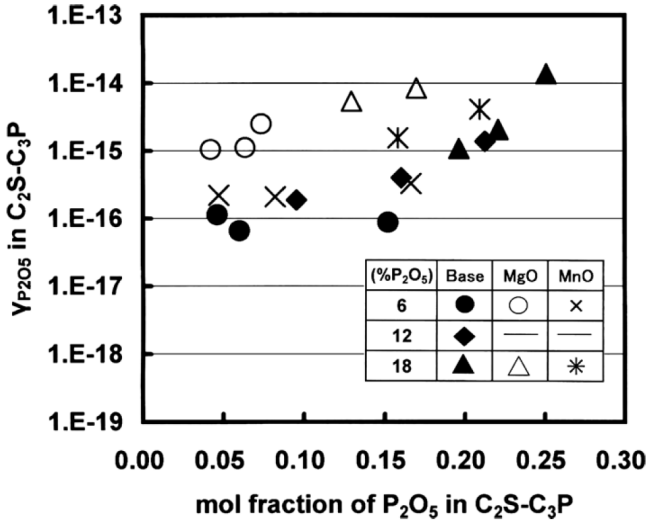

Fig. 1.25 Relationship between the activity coefficient of P_2O_5 and the content of P_2O_5 in the $2CaO{\cdot}SiO_2$-$3CaO{\cdot}P_2O_5$ solid solution.[22]

Figure 1.26 shows the activity coefficient of P_2O_5 in the $2CaO{\cdot}SiO_2$-$3CaO{\cdot}P_2O_5$ solid solution with different additions in the CaO-SiO_2-P_2O_5-Fe_2O_3 system or the CaO-SiO_2-P_2O_5-FeO system.[26] The activity coefficient with the addition of MgO or MnO was larger than that without addition, and the addition of Al_2O_3 decreased the activity coefficient of P_2O_5 both in the CaO-SiO_2-P_2O_5-Fe_2O_3 system and the CaO-SiO_2-P_2O_5-FeO system.

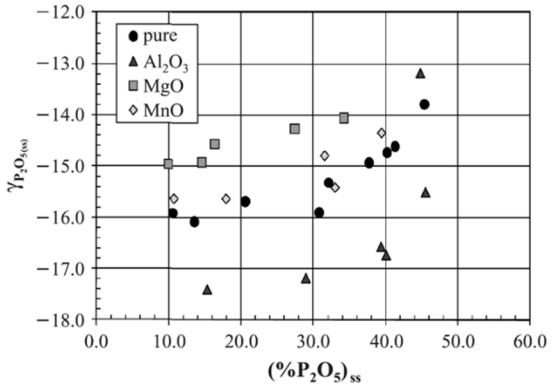

A

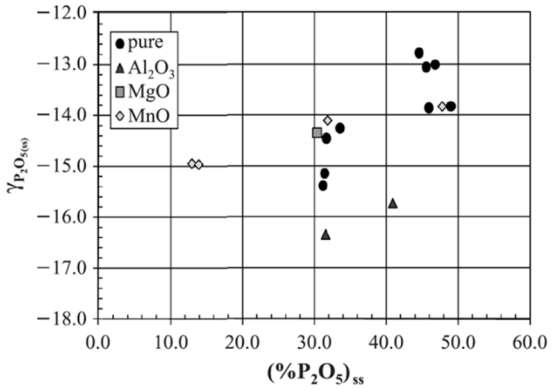

B

Fig. 1.26 Activity coefficient of P_2O_5 in the $2CaO{\cdot}SiO_2$-$3CaO{\cdot}P_2O_5$ solid solution. A: the $2CaO{\cdot}SiO_2$-$3CaO{\cdot}P_2O_5$ solid solution was equilibrated with CaO-SiO_2-P_2O_5-Fe_2O_3 system. B: the $2CaO{\cdot}SiO_2$-$3CaO{\cdot}P_2O_5$ solid solution was equilibrated with CaO-SiO_2-P_2O_5-FeO system.[26]

Hasegawa *et al*.[28] estimated the activity of P_2O_5, CaO, SiO_2, $2CaO{\cdot}SiO_2$ and $3CaO{\cdot}P_2O_5$ in the $2CaO{\cdot}SiO_2$-$3CaO{\cdot}P_2O_5$ solid solution by applying the regular solution model and the phase relationship. The equilibrium between molten Cu and $2CaO{\cdot}SiO_2$-$3CaO{\cdot}P_2O_5$ solid solution was investigated. The regular solution model is expressed by Eqs. (1.6), (1.7) and (1.8), where R is the gas constant, $\Delta G_t^{\circ}(Ca_2SiO_4)$ and $\Delta G_t^{\circ}(Ca_3P_2O_8)$ are the Gibbs free energy changes of the phase transformations and Ω is the interaction parameter. **Figure 1.27** shows the activity of $2CaO{\cdot}SiO_2$ and $3CaO{\cdot}P_2O_5$ estimated by applying the ideal solution model by dot line and the regular solution model by solid line. **Figure 1.28** shows the activity of CaO by solid line, the activity of SiO_2 by dashed line and the activity of P_2O_5 by dashed dot line in the $2CaO{\cdot}SiO_2$-

$3CaO{\cdot}P_2O_5$ solid solution.

$$R\mathit{T}\ln a_{Ca_2SiO_4} = \Delta G_t^{\circ}(Ca_2SiO_4) + R\mathit{T}\ln(1-Y) + \Omega Y^2 \quad \ldots\ldots (1.6)$$

$$R\mathit{T}\ln a_{Ca_3P_2O_8} = 2R\mathit{T}\ln a_{(1/2)Ca_3P_2O_8} = \Delta G_t^{\circ}(Ca_3P_2O_8) + 2R\mathit{T}\ln Y + 2\Omega(1-Y)^2 \quad \ldots\ldots (1.7)$$

$$Y \equiv n_{(1/2)Ca_3P_2O_8}/\left(n_{Ca_2SiO_4} + n_{(1/2)Ca_3P_2O_8}\right)$$

$$= 2n_{Ca_3P_2O_8}/\left(n_{Ca_2SiO_4} + 2n_{Ca_3P_2O_8}\right) \quad \ldots\ldots (1.8)$$

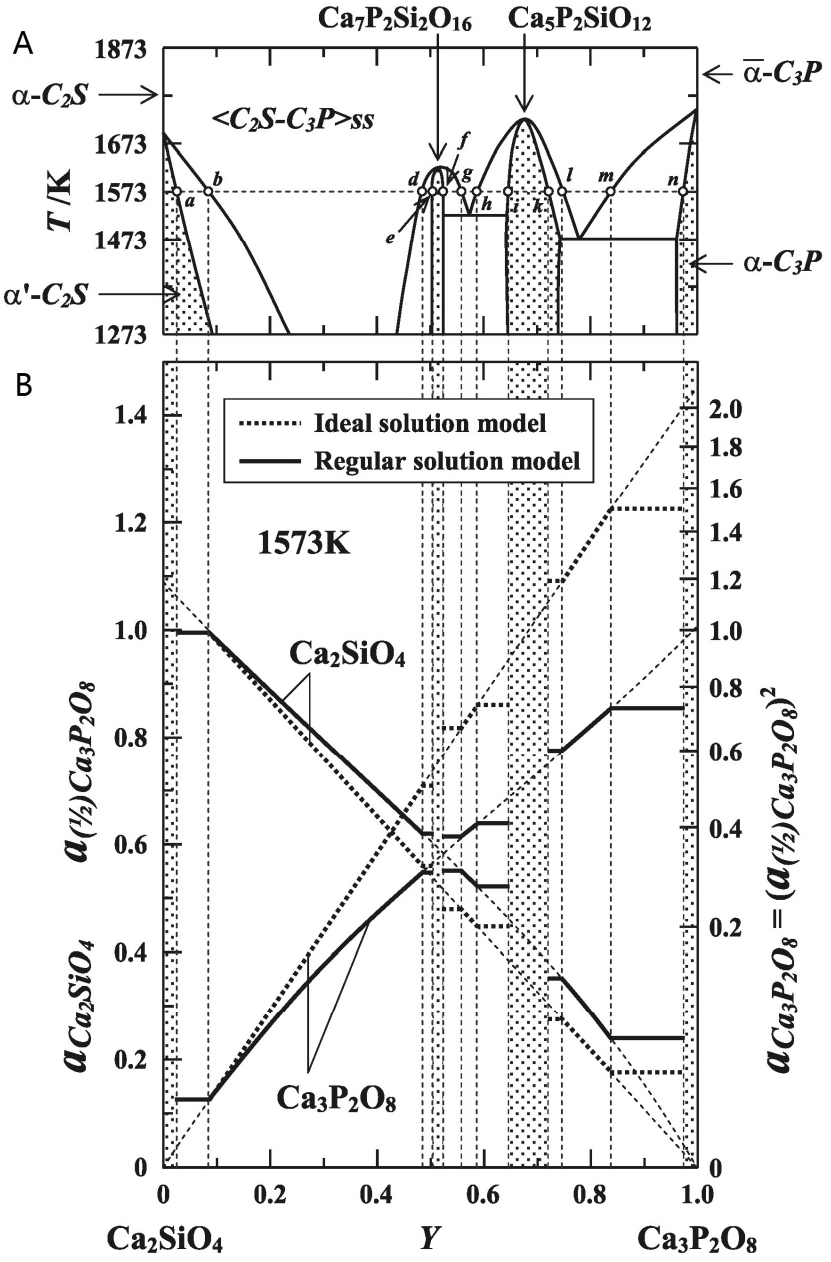

Fig. 1.27 A: Phase diagram of the Ca_2SiO_4-$Ca_3P_2O_8$ pseudo-binary system. B: Activities of Ca_2SiO_4 and $Ca_3P_2O_8$ as functions of the substitution ratio Y.[28]

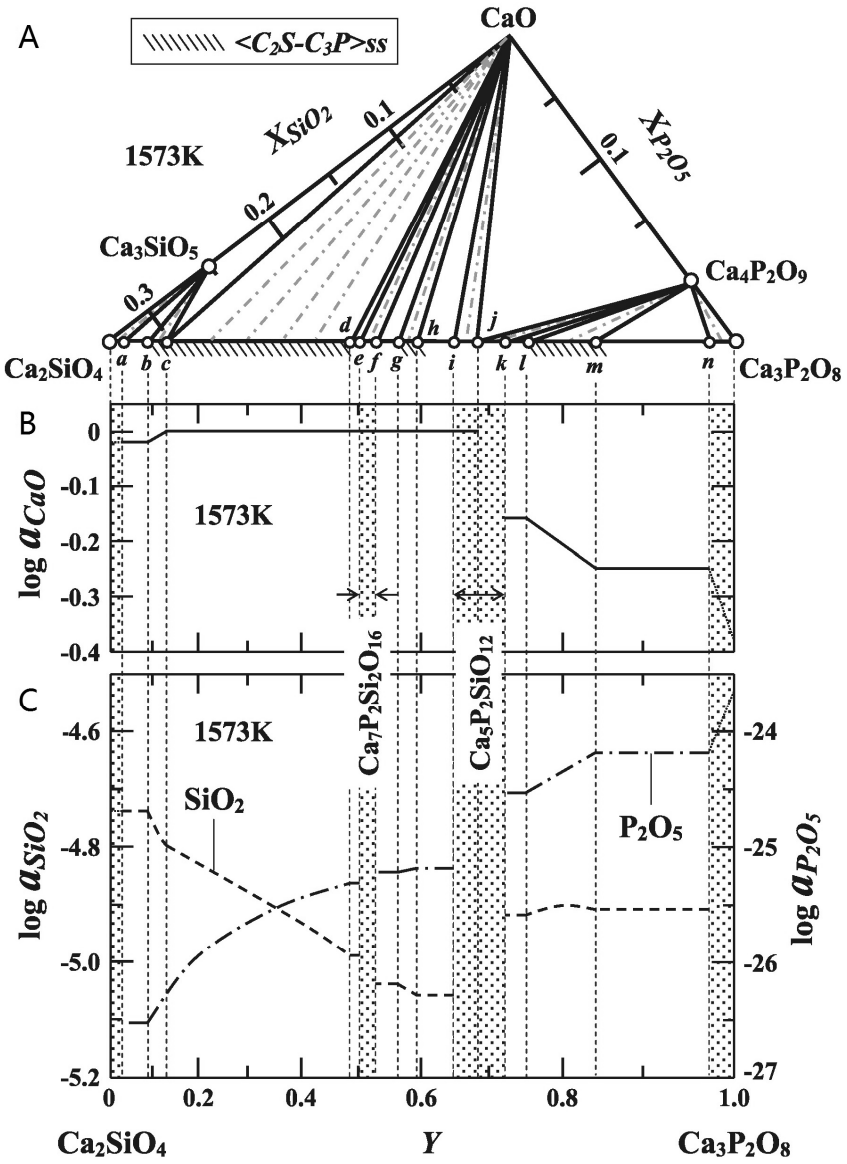

Fig. 1.28 A: Iso-thermal section of the ternary system CaO-SiO_2-P_2O_5 near the CaO apex at 1573 K. B: Activity of CaO at 1573 K. C: Activities of SiO_2 and P_2O_5 at 1573 K.[28]

1.3.5 Phase relationship of CaO-SiO_2-FeO-5mass%P_2O_5(-5mass%Al_2O_3) system

Gao *et al*. studied the phase relationship of CaO-SiO_2-FeO-5mass%P_2O_5(-5mass%Al_2O_3) system at various temperatures and oxygen partial pressures.[29-31]

The phase relationship of CaO-SiO_2-FeO-5mass%P_2O_5 system with the oxygen partial pressure of 9.24×10^{-11} atm at 1673 K was shown in **Figures 1.29** and **1.30**. Figure 1.29 A shows the initial compositions. At first the mixture was completely melted at 1923 K and then cooling down slowly to achieve the equilibrium between solid phase and liquid phase. After keeping the sample for a long enough time, the sample was quenched and the morphology was analyzed by SEM and EDS. The observed solid phase was projected onto the CaO-SiO_2-P_2O_5 system as shown in Figure 1.29 B. All compositions were located close to the tie line between $2CaO\cdot SiO_2$ and $3CaO\cdot P_2O_5$. Figures 1.29 C and D show the projections of observed phases onto the CaO-SiO_2-FeO system. The solid solution containing with FeO was located around the area between $2CaO\cdot SiO_2$ and $3CaO\cdot SiO_2$. Comparing with the liquidus at 1673 K equilibrated with the metallic iron as solid curve shown in Figure 1.29 C, the liquidus conducted by Gao *et al*. moved toward to the corner of FeO. Figure 1.29 D shows the equilibrium phase sections according to the projections of the various observed phases and Figure 1.30 shows the phase relationship of CaO-SiO_2-FeO-5mass%P_2O_5 system with the oxygen partial pressure of 9.24×10^{-11} atm at 1673 K.

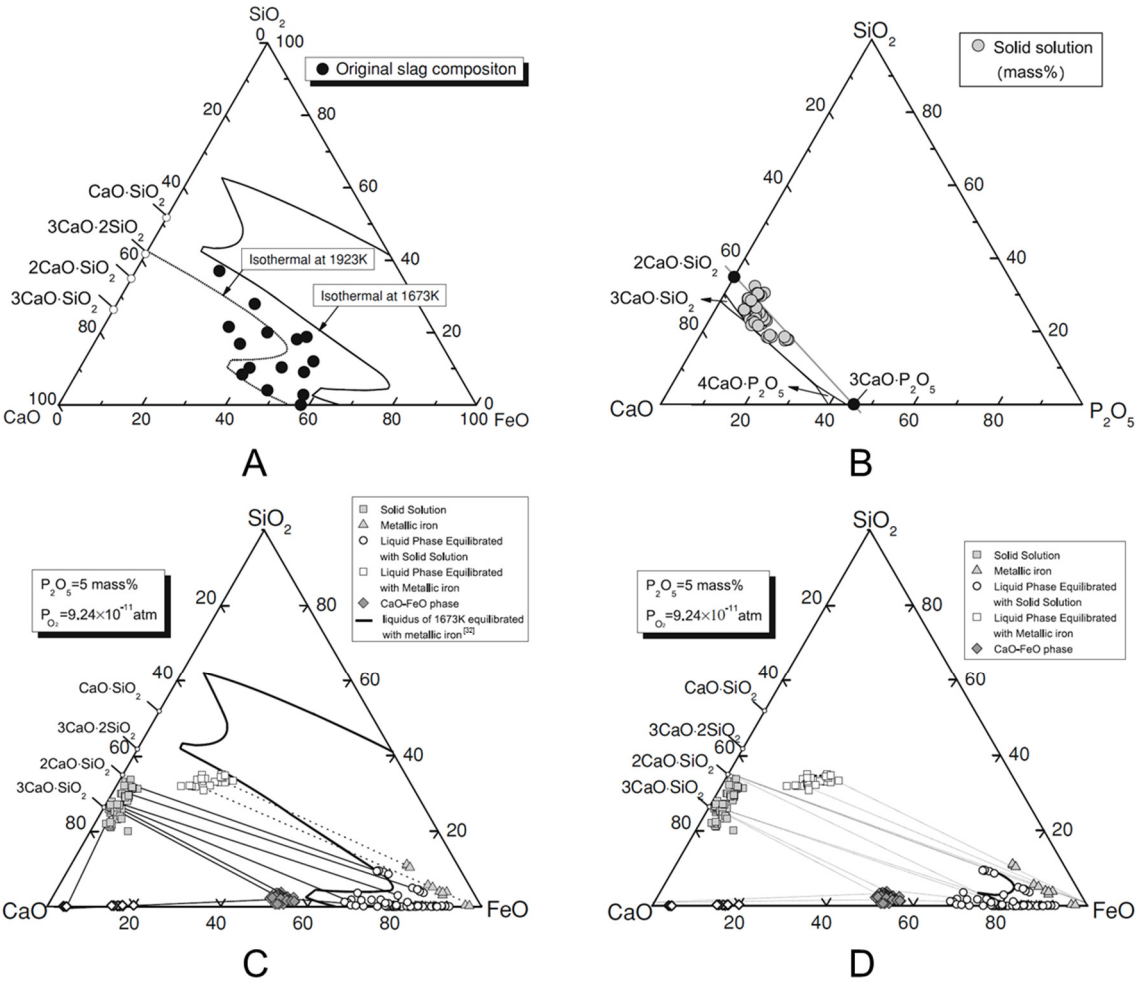

Fig. 1.29 A: Initial compositions of slag (mass%) in CaO-SiO_2-FeO system. B: Projections of compositions onto the CaO-SiO_2-P_2O_5 system (mass%). C: Projections of compositions onto the CaO-SiO_2-FeO system comparing with the liquidus equilibrated with metallic iron at 1673 K (mass%).[32] D: Projections of compositions onto the CaO-SiO_2-FeO system with the phase sections (mass%).[29]

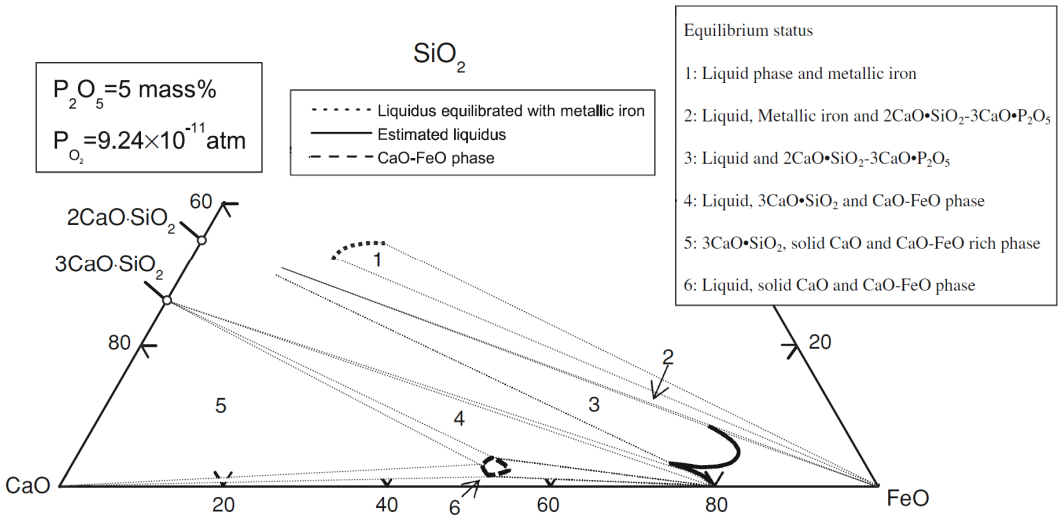

Fig. 1.30 Phase relationship of CaO-SiO_2-FeO-5mass%P_2O_5 system with the oxygen partial pressure of 9.24×10^{-11} atm at 1673 K (mass%).[29]

Gao *et al*. also investigated the phase relationship of CaO-SiO_2-FeO-5mass%P_2O_5 system with oxygen partial pressure of 1.08×10^{-10} atm at 1623 and 1673 K.[30] **Figure 1.31** shows the liquidus and the phase sections of CaO-SiO_2-FeO-P_2O_5 system at 1623 and 1673 K with the oxygen partial pressures of 1.08×10^{-10} and 9.24×10^{-9} atm. Since the compositions of $2CaO\cdot SiO_2$-$3CaO\cdot P_2O_5$ solid solution changed with the composition of slag, the projections of the compositions of solid solution were focused around an area rather than a point. Because the $3CaO\cdot SiO_2$ was not detected, only one three-phase equilibrium region was found as CaO-($2CaO\cdot SiO_2$-$3CaO\cdot P_2O_5$)-slag. Comparing with the liquidus with the oxygen partial pressure of 9.24×10^{-9} atm at 1673 K, the liquidus with the oxygen partial pressure of 1.08×10^{-10} atm at 1623 K shrunk to the corner of FeO. **Figure 1.32** shows the projection of phase relationship onto the three-dimensional space. The solid solution was closed to the CaO-SiO_2-P_2O_5 plane and the liquid phase equilibrated with the solid solution was closed to the CaO-SiO_2-FeO plane. Besides, the liquid phase equilibrated with the solid CaO was closed to the CaO-P_2O_5-FeO plane.

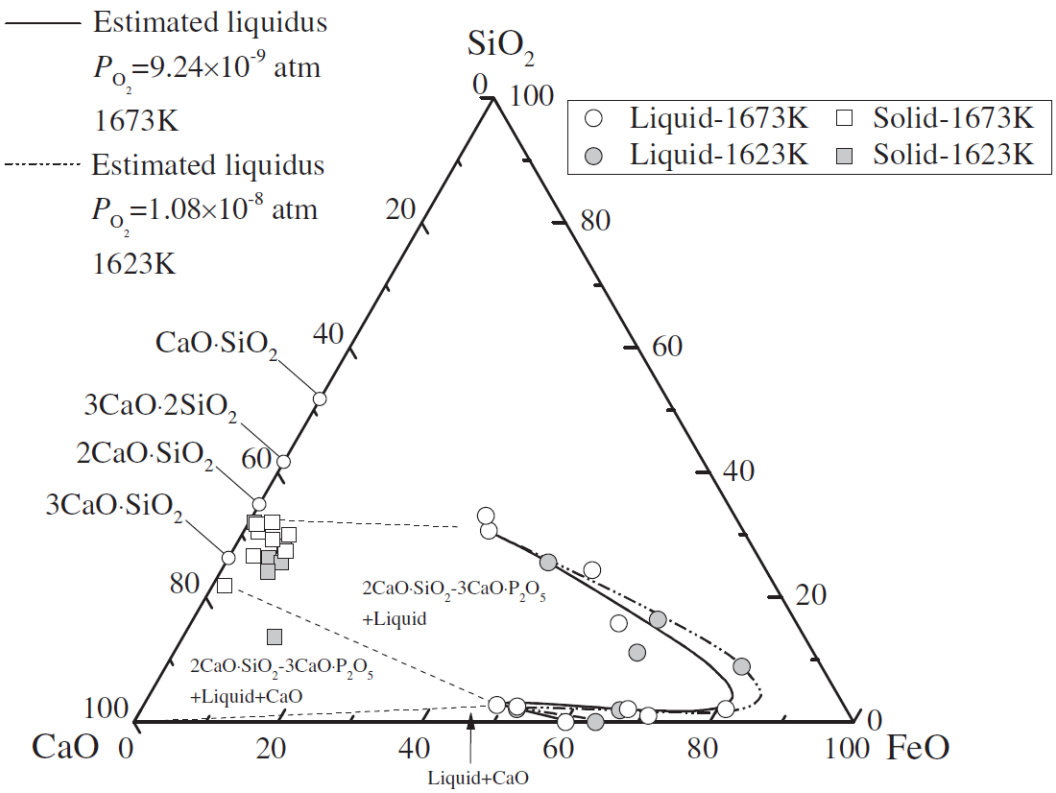

Fig. 1.31 Liquidus and phase sections of CaO-SiO_2-FeO-P_2O_5 system (mass%).[30]

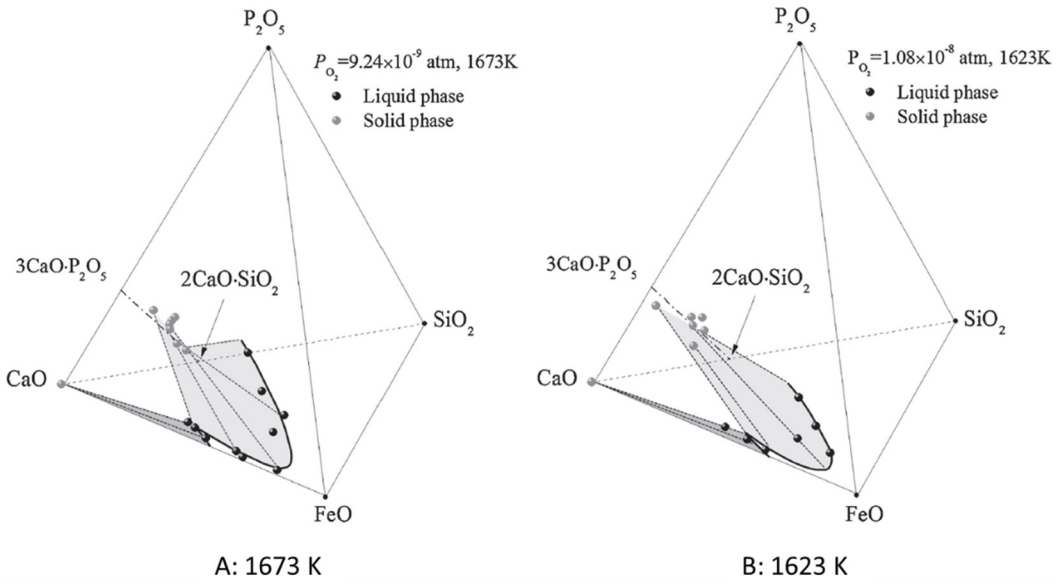

Fig. 1.32 Phase relationship of CaO-SiO_2-FeO-P_2O_5 system (mass%) in the tetrahedra.[30]

Furthermore, the phase relationship of CaO-SiO_2-FeO-5mass%P_2O_5-5mass%Al_2O_3 system with the oxygen partial pressure of 9.24×10^{-11} atm at 1673 K was also studied by Gao *et al*.[31]

Ignoring the variation in Al_2O_3 content, the liquidus of CaO-SiO_2-FeO-P_2O_5-10mass%Al_2O_3 was summarized as shown in **Figure 1.33**. The liquid phase area enlarged comparing with that of the CaO-SiO_2-FeO_x system equilibrated with metallic iron.[33] Comparing with the liquid phase area of CaO-SiO_2-FeO-Fe_2O_3-5mass%Al_2O_3 system with the oxygen partial pressure of 10^{-8} atm at 1573 K,[34] the current liquid phase area also enlarged. Comparing with the CaO-SiO_2-FeO_x system equilibrated with metallic iron, the current CaO primary region shrunk a lot. **Figure 1.34** shows the effect of Al_2O_3 on the liquidus of CaO-SiO_2-FeO-5mass%P_2O_5 system. The liquid phase area of CaO-SiO_2-FeO-5mass%P_2O_5-10mass%Al_2O_3 system enlarged significantly at larger FeO content region comparing with the CaO-SiO_2-FeO-5mass%P_2O_5 system with the oxygen partial pressure of 9.24×10^{-11} atm at 1673 K.

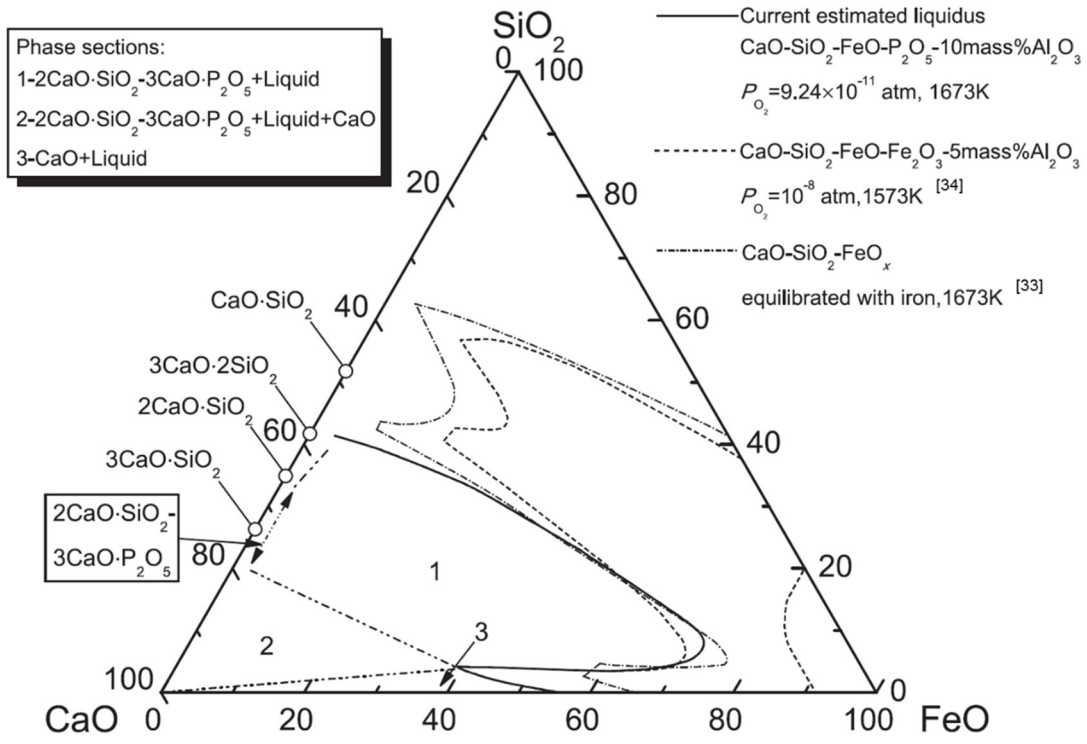

Fig. 1.33 Phase sections for CaO-SiO_2-FeO-5mass%P_2O_5-5mass%Al_2O_3 system with the oxygen partial pressure of 9.24×10^{-11} atm at 1673 K on the CaO-SiO_2-FeO ternary section.[31]

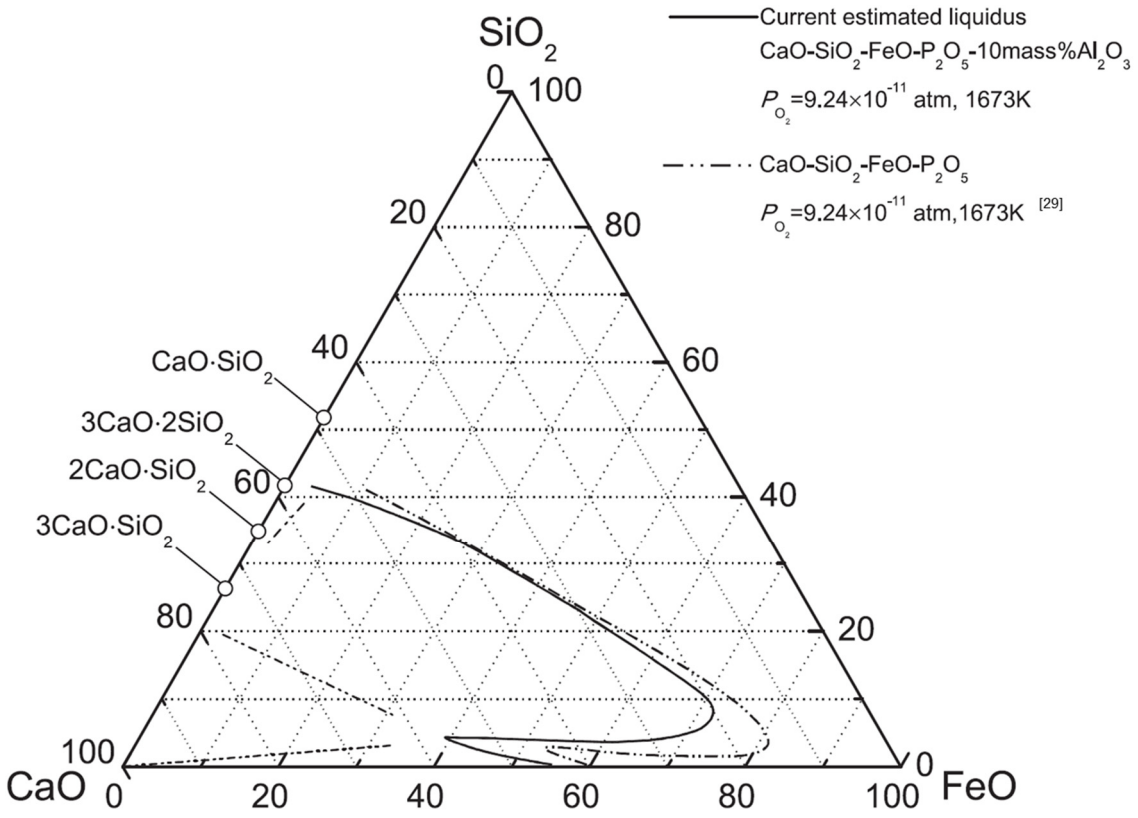

Fig. 1.34 Effect of Al_2O_3 addition on the liquidus with the oxygen partial pressure of 9.24×10^{-11} atm at 1673 K.[31]

1.3.6 Formation free energies of solid solution between di-calcium silicate and tri-calcium phosphate

Takeshita *et al*.[35] studied the formation free energies of solid solution between di-calcium silicate and tri-calcium phosphate by applying the chemical equilibration method. **Figure 1.35** shows the phase diagram of pseudo-ternary CaO-SiO_2-P_2O_5 system and the pseudo-binary $2CaO\cdot SiO_2$-$3CaO\cdot P_2O_5$ system. In Figure 1.35 A, there were several three-phase assemblages, and the three-phase assemblage with the lowest activity of P_2O_5 in the solid solution was $3CaO\cdot SiO_2$+$2CaO\cdot SiO_2$+$2CaO\cdot SiO_2$-$3CaO\cdot P_2O_5$ in which the activity of P_2O_5 was fixed as expressed by Eq. (1.9).

$$3\langle Ca_3SiO_3\rangle + \frac{4y-3}{1-y}\langle Ca_2SiO_4\rangle + \{P_2O_5\} = \frac{1}{1-y}\langle Ca_{(3-y)}Si_yP_{(2-2y)}O_{(8-4y)}\rangle \quad \ldots\ldots (1.9)$$

y is the mole fraction of $2CaO\cdot SiO_2$ corresponding to the composition of point 3 in Figure 1.35. The molten copper was equilibrated with the mixture of $3CaO\cdot SiO_2$+$2CaO\cdot SiO_2$+$2CaO\cdot SiO_2$-$3CaO\cdot P_2O_5$ in the mixture of Ar, H_2 and H_2O gases and the reaction was expressed as Eq. (1.10) where $[mass\%P]_{Cu}$ denotes phosphorus in liquid copper.

$$3Ca_3SiO_3(s) + \frac{4y-3}{1-y}Ca_3SiO_3(s) + 2[mass\%P]_{Cu} + 5H_2O(g) = \frac{1}{1-y}Ca_{(3-y)}Si_yP_{(2-2y)}O_{(8-4y)}(s) + 5H_2(g) \quad \ldots\ldots (1.10)$$

The equilibrium constant was expressed as Eq. (1.11) assuming Henry's low.

$$\log K_{1.10} = 5\log\left(P_{H_2}/P_{H_2O}\right) - 2\log[mass\%P]_{Cu} \quad \ldots\ldots (1.11)$$

From Eq. (1.11) the slope of $\log\left(P_{H_2}/P_{H_2O}\right)$ and $\log[mass\%P]_{Cu}$ should be 2/5 which was confirmed by **Figure 1.36 A**. From the results shown in **Figure 1.36 B**, the Eqs. (1.12) and (1.13) were obtained by least squares method.

$$\log K_{1.10} = -22.23 + \frac{60600}{(T/K)} \pm 0.3 \quad \ldots\ldots (1.12)$$

$$\Delta G^{\circ}_{1.10} = -1160000 + 425.7T \pm 9000\ J/mol \quad \ldots\ldots (1.13)$$

The Gibbs free energy for the following reactions are available in the literatures.

$$(1/2)P_2(g) = [mass\%P]_{Cu}$$

$$\Delta G_{1.14}^{\circ} = -125000 + 0.54T \pm 5500\,\mathrm{J/mol} \ldots\ldots (1.14)^{[36]}$$

$$\mathrm{P_2(g) + 5/2\,O_2(g) = P_2O_5(l)}$$

$$\Delta G_{1.15}^{\circ} = -1534500 + 506.3T\,\mathrm{J/mol} \ldots\ldots (1.15)^{[37]}$$

$$\mathrm{H_2(g) + 1/2\,O_2(g) = H_2O(g)}$$

$$\Delta G_{1.16}^{\circ} = -246000 + 54.8T\,\mathrm{J/mol} \ldots\ldots (1.16)^{[38]}$$

By referring the Eqs. (1.13), (1.14), (1.15) and (1.16), the Gibbs free energy for the reaction (1.9) is expressed as Eq. (1.17).

$$\Delta G_{1.9}^{\circ} = RT\ln a_{P_2O_5} = -1106000 + 194.7T \pm 20000\,\mathrm{J/mol} \ldots\ldots (1.17)$$

Where the activity of P_2O_5 is relative to hypothetical pure liquid P_2O_5 from 1528 K to 1598 K.

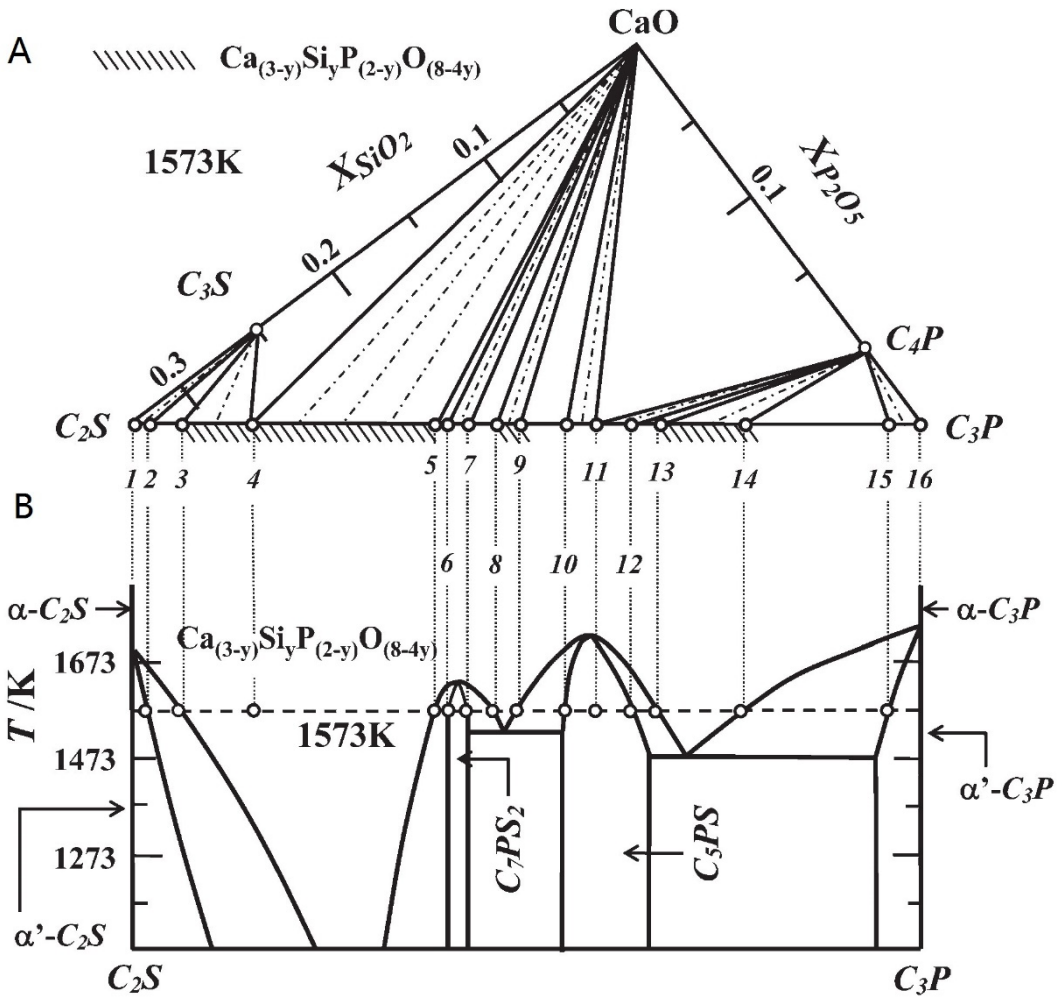

Fig. 1.35 A: Iso-thermal section of the ternary CaO-SiO_2-P_2O_5 system at 1573 K. B: Phase diagram of the pseudo-binary $2CaO{\cdot}SiO_2$-$3CaO{\cdot}P_2O_5$ system.[35]

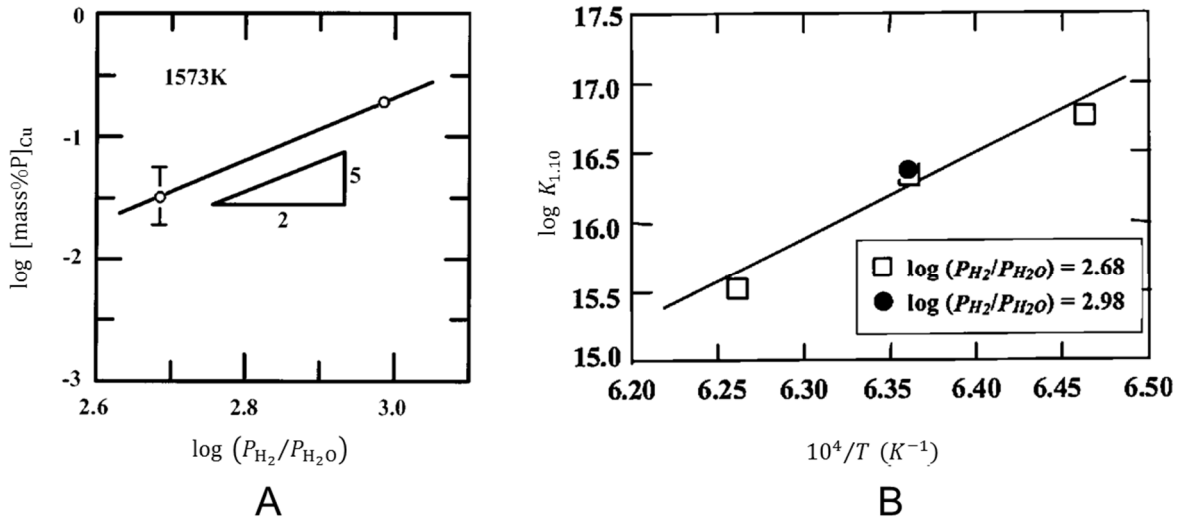

Fig. 1.36 A: Relationship between the logarithm of P concentration in Cu and the ratio between H_2 and H_2O at 1573 K. B: Relationship between the logarithm of $K_{1.10}$ and the reciprocal of T.[35]

1.4 Research objective and significance

As introduced in previous sections, the phosphorus should be removed from molten iron and steel to avoid the embrittlement. In order to utilize the CaO efficiently, the concept of multi-phase flux was considered. For deeper understanding and better application of the multi-phase flux to commercial operation, it is necessary to clarify the thermodynamic properties about the calcium phosphate-based solid solution.

As the thermodynamic properties about the calcium phosphate-based solid solution are clear, the degree of dephosphorization for various compositions of the calcium phosphate-based solid solution can be estimated with various oxygen partial pressures and temperatures. Meanwhile combining with the previous researches, how to choose the corresponding composition of slag and how to control the slag operation are getting clear. For these reasons, it is urgent to obtain the thermodynamic properties especial the activity and activity coefficient of P_2O_5 for optimizing the dephosphorization by multi-phase flux.

About the activity and activity coefficient of P_2O_5 in the $2CaO{\cdot}SiO_2$-$3CaO{\cdot}P_2O_5$ solid solution, the regular solution model and the phase relationship were adopted for estimating the values although they have been measured so far. In order to eliminate the deviation of the regular solution model and the phase relationship, it is necessary to measure the activity and activity coefficient of P_2O_5 directly by chemical equilibration method. Since in practical manufacture, the excess CaO is added and the slag is containing a certain amount of MgO, not only the thermodynamic properties about the $2CaO{\cdot}SiO_2$-$3CaO{\cdot}P_2O_5$ solid solution but also the $2CaO{\cdot}SiO_2$-$3CaO{\cdot}P_2O_5$ solid solution containing with CaO or MgO should be studied. In current researches, the activity and activity coefficient of P_2O_5 in the $2CaO{\cdot}SiO_2$-$3CaO{\cdot}P_2O_5$ solid solution or containing with CaO or MgO and other related thermodynamic properties have been well studied.

1.5 Outline of the thesis

In **Chapter 1**, the overview about steelmaking, dephosphorization and multi-phase flux were introduced. Also the previous researches about the multi-phase flux and correlational researches about this topic were summarized. Meanwhile the research objective and significance about current research were proposed.

In **Chapter 2**, the experimental principle, method and parameters were explained in detail. Also the method of making tablet and the method of chemical analyses were presented particularly.

In **Chapters 3, 4** and **5**, the results and discussion of the thermodynamics about the $2CaO{\cdot}SiO_2$-$3CaO{\cdot}P_2O_5$ solid solution, the mixture of $2CaO{\cdot}SiO_2$-$3CaO{\cdot}P_2O_5$ solid solution and CaO and the mixture of $2CaO{\cdot}SiO_2$-$3CaO{\cdot}P_2O_5$ solid solution and MgO were presented, respectively. In each chapter, the activity coefficient of FeO in the tablet after reaction, the equilibrium concentration of P in Fe, phosphorus partition ratio between the tablet and molten iron and the activity and activity coefficient of P_2O_5 were investigated, respectively. In Chapter 4, the activity of $3CaO{\cdot}P_2O_5$ in the $2CaO{\cdot}SiO_2$-$3CaO{\cdot}P_2O_5$ solid solution saturated with CaO was estimated and in Chapter 5, the activity of $3MgO{\cdot}P_2O_5$ in the $2CaO{\cdot}SiO_2$-$3CaO{\cdot}P_2O_5$ solid solution saturated with MgO was estimated.

In **Chapter 6**, the thermodynamic data introduced in Chapters 3, 4 and 5 were summarized and the effect of MgO on the activity of P_2O_5 in the calcium phosphate-based solid solution was discussed. Based on the thermodynamic data investigated in current research together with the previous researches, the application of multi-phase flux for the dephosphorization process was proposed and discussed.

The conclusions were presented as **Chapter 7** by summarizing the previous chapters.

References

1. http://www.jfe-21st-cf.or.jp/chapter_2/2a_1_img.html
2. R. Viswanathan: *Metall. Trans.*, **2** (1971), 809-815.
3. C.L. Briant and R.P. Messmer: *Acta Metall.*, **30** (1982), 1811-1818.
4. C. L. Briant and S. K. Banerji: *Metall. Trans. A*, **10A** (1979), 123-126.
5. C. L. Briant and S. K. Banerji: *Metall. Trans. A*, **10A** (1979), 1729-1737.
6. R. A. Mulford, C. J. Mcmahon, D. P. Pope and H. C. Feng: *Metall. Trans. A*, **7A** (1976), 1183-1195.
7. H. Okamoto: *Bull. Alloy Phase Diagrams*, **4** (1990), 404-412.
8. H. Momokawa and N. Sano: *Metall. Trans. B*, **13B** (1982), 643-644.
9. C. Wagner: *Metall. Trans. B*, **6B** (1975), 405.
10. F. Tsukihashi and H. Sano: International conference 21st century steel industry of Russia and CIS, Moscow, (1994), 3, 14-18.
11. H. Suito and R. Inoue: *ISIJ Int.*, **46** (2006), 180-187.
12. W. Fix, H. Heymann and R. S. Heinke: *J. Am. Ceram. Soc.*, **52** (1969), 346.
13. M. Hasegawa and M. Iwase: *Tetsu-to-Hagané*, **95** (2009), 222.
14. F. Tsukihashi: Final report on innovative development of refining processes in steelmaking by multi phase flux, *ISIJ*, (2009), 2.
15. M. Kami, M. Terasawa, A. Matsumoto and K. Ito: *Tetsu-to-Hagané*, **95** (2009), 236-240.
16. T. Hamano, S. Fukagai and F. Tsukihashi: *ISIJ Int.*, **46** (2006), 490-495.
17. X. Yang, H. Matsuura and F. Tsukihashi: *ISIJ Int.*, **49** (2009), 1298-1307.
18. X. Yang, H. Matsuura and F. Tsukihashi: *ISIJ Int.*, **50** (2010), 702-711.
19. X. Yang, H. Matsuura and F. Tsukihashi: *Mater. Trans.*, **51** (2010), 1094-1101.
20. X. Yang, H. Matsuura and F. Tsukihashi: *Tetsu-to-Hagané*, **95** (2009), 268-274.
21. S. Kitamura, S. Saito, K. Utagawa, H. Shibata and D. G. C. Robertson: *ISIJ Int.*, **49** (2009), 1838-1844.
22. K. Shimauchi, S. Kitamura, K. and H. Shibata: *ISIJ Int.*, **49** (2009), 505-511.
23. R. Inoue and H. Suito: *ISIJ Int.*, **46** (2006), 188-194.

24. R. Inoue and H. Suito: *ISIJ Int*., **46** (2006), 174-179.
25. K. Ito, M. Yanagisawa and N. Sano: *Tetsu-to-Hagané*, **68** (1982), 342.
26. F. Pahlevani, S. Kitamura, H. Shibata and N. Maruoka: *ISIJ Int.*, **50** (2010), 822-829.
27. S. Ban-ya: *ISIJ Int.*, **33** (1993), 2.
28. M. Hasegawa, Y. Kashiwaya and M. Iwase: *High Temp. Mater. Proc.*, **31** (2012), 421-430.
29. X. Gao, H. Matsuura, I. Sohn, W. Wang, D. Min and F. Tsukihashi: *Metall. Mater. Trans. B*, **43B** (2012), 694-702.
30. X. Gao, H. Matsuura, I. Sohn, W. Wang, D. Min and F. Tsukihashi: *Mater. Trans.*, **54** (2013), 544-552.
31. X. Gao, H. Matsuura, M. Miyata and F. Tsukihashi: *ISIJ Int.*, **53** (2013), 1381-1385.
32. M. Allibert *et al.*: SLAG ATLAS 2nd Edition, Verein Deutscher Eisenhüttenleute, Germany, (1995), 57, 126.
33. M. Allibert *et al.*: SLAG ATLAS 2nd Edition, Verein Deutscher Eisenhüttenleute, Germany, (1995), 126, 138.
34. H. Kimura, T. Ogawa, M. Kakiki, A. Matsumoto and F. Tsukihashi: *ISIJ Int.*, **45** (2005), 506.
35. H. Takeshita, M. Hasegawa, Y. Kashiwaya, and M. Iwase: *Steel Research Int.*, **81** (2010), 100-104.
36. M. Iwase, E. Ichise and N. Yamada: *Steel Research*, **56** (1985), 319-326.
37. E. T. Turkdogan and J. Pearson: *J. Iron Steel Inst.*, **175** (1953), 393-401.
38. O. Kubaschewski and C. B. Alcock: Metallurgical Thermochemistry, 5th edition, Pergamon Press, Oxford.

Chapter 2 Experimental Method

2.1 Introduction

The current research focuses on the thermodynamic properties about the calcium phosphate-based solid solution. The chemical equilibration method was applied which was commonly adopted for obtaining the thermodynamic data like the equilibrium constant, the Gibbs free energy, the activity, the interaction coefficient and so on. This method has been applied for decades in the field of physical chemistry as a very mature method.

In the field of metallurgy, the chemical equilibration method has been applied on the study of the equilibrium at the interface between slag and molten metal,[1,2] the phase equilibrium,[3] the equilibrium between molten metal and solid solution.[4] In current experiments, the electrolytic iron was equilibrium with the tablet of the calcium phosphate-based solid solution, then the sample was quenched and finally the concentration of P in Fe and the compositions of tablet were analyzed by chemical analysis.

2.2 Experimental

The equilibrium between molten iron and the calcium phosphate-based solid solution is expressed in term of phosphorus as Eq. (2.1). In the case of the atmosphere is controlled by the mixture of CO and CO_2 gases, the equilibrium between molten iron and the calcium phosphate-based solid solution in term of phosphorus is expressed as Eq. (2.3) by Eqs. (2.1) and (2.2).

$$\mathrm{P_2O_5(l)} = 2\underline{\mathrm{P}}(\mathrm{mass\%}) + 5\underline{\mathrm{O}}(\mathrm{mass\%})$$

$$\Delta G^{\circ}_{2.1} = 832384 - 632.65T \ \mathrm{J/mol} \ldots\ldots (2.1)^{[5]}$$

$$\underline{\mathrm{O}}(\mathrm{mass\%}) + \mathrm{CO(g)} = \mathrm{CO_2(g)}$$

$$\Delta G^{\circ}_{2.2} = -166900 + 91.16T \ \mathrm{J/mol} \ldots\ldots (2.2)^{[6]}$$

$$\mathrm{P_2O_5(l)} + 5\mathrm{CO(g)} = 2\underline{\mathrm{P}}(\mathrm{mass\%}) + 5\mathrm{CO_2(g)}$$

$$\Delta G^{\circ}_{2.3} = -2116 - 177.0T \ \mathrm{J/mol} \ldots\ldots (2.3)^{[5,\ 6]}$$

$$K_{2.3} = \frac{(f_{\mathrm{P}}[\mathrm{mass\%P}])^2}{a_{\mathrm{P_2O_5}}}\left(\frac{P_{\mathrm{CO_2}}}{P_{\mathrm{CO}}}\right)^5 \ldots\ldots (2.4)$$

Eq. (2.4) was used to obtain the activity of P_2O_5. f_P is the activity coefficients of phosphorus in liquid iron relative to 1 mass% expressed as Eq. (2.5), and $a_{P_2O_5}$ is the activity of P_2O_5 relative to hypothetical pure liquid P_2O_5. The values of f_P could be estimated by Eqs. (2.2) and (2.6) and the reported interaction parameters in molten iron shown in **Table 2.1** after measuring the concentration of P in Fe. The oxygen partial pressure was controlled by the mixture of CO and CO_2 gases according to Eq. (2.7) with the corresponding flow rate shown in **Table 2.2**.

$$\log f_P = e_P^P[\text{mass\%P}] + e_P^O[\text{mass\%O}] + e_P^C[\text{mass\%C}] \ldots\ldots (2.5)$$

$$\underline{C}(\text{mass\%}) + CO_2(g) = 2CO(g)$$

$$\Delta G_{2.6}^{\circ} = 144700 - 129.5T \text{ J/mol} \ldots\ldots (2.6)^{[6]}$$

$$CO(g) + 1/2\, O_2(g) = CO_2(g)$$

$$\Delta G_{2.7}^{\circ} = -281000 + 85.23T \text{ J/mol} \ldots\ldots (2.7)^{[7]}$$

Table 2.1 Reference data about interaction coefficient.

e_i^j		j		
		P	C	O
i	P	0.054[8]	0.126[9]	0.13[10]
	C	0.051[9]	0.243[6]	-0.32[6]
	O	0.07[10]	-0.421[6]	-0.17[11]

Table 2.2 Oxygen partial pressure and corresponding rate of flow.

T/K	CO/CO_2	P_{O_2}/atm	Flow (mL/min)
1823	110/1	5.22×10^{-12}	366
1873	110/1	1.41×10^{-11}	366
1873	20/1	4.25×10^{-10}	347

For the experiments with the large $3CaO{\cdot}P_2O_5$ content in the $2CaO{\cdot}SiO_2$-$3CaO{\cdot}P_2O_5$ solid solution at 1873 K, the ratio CO/CO_2 was 20/1 in order to obtain a suitable concentration of P in Fe after reaction and for the other experiments, the ratio CO/CO_2 was 110/1.

As iron phase exists, the metal crucible like platinum crucible and molybdenum crucible could not be used. Although Al_2O_3 crucible is commonly adopted in the metallurgical experiments, Al_2O_3 could react with $2CaO \cdot SiO_2$ to form slag. From the phase diagram of the $CaO\text{-}SiO_2\text{-}MgO$ system as shown in **Figure 2.1**, MgO does not react with $2CaO \cdot SiO_2$ to form slag in the present condition. Therefore the MgO crucible was used in the present research.

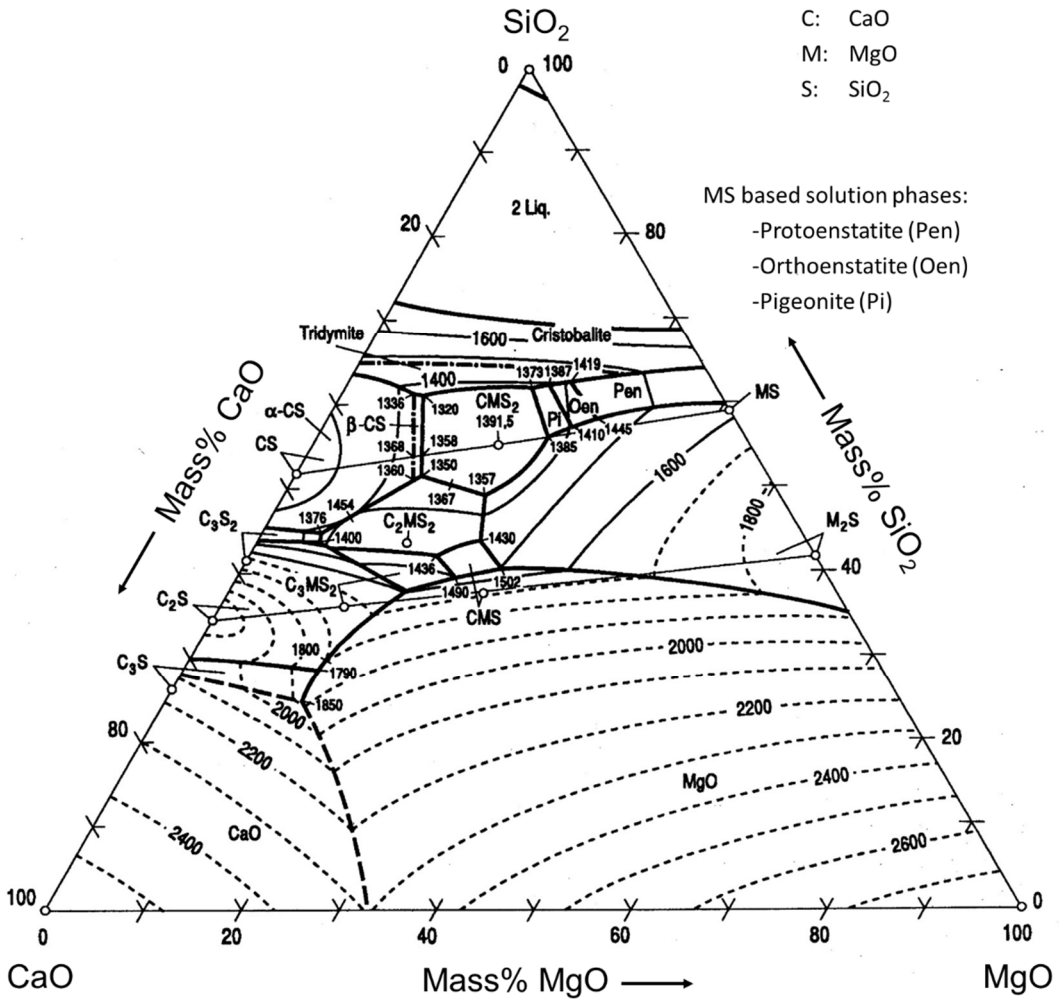

Fig. 2.1 Phase diagram of $CaO\text{-}SiO_2\text{-}MgO$.[12]

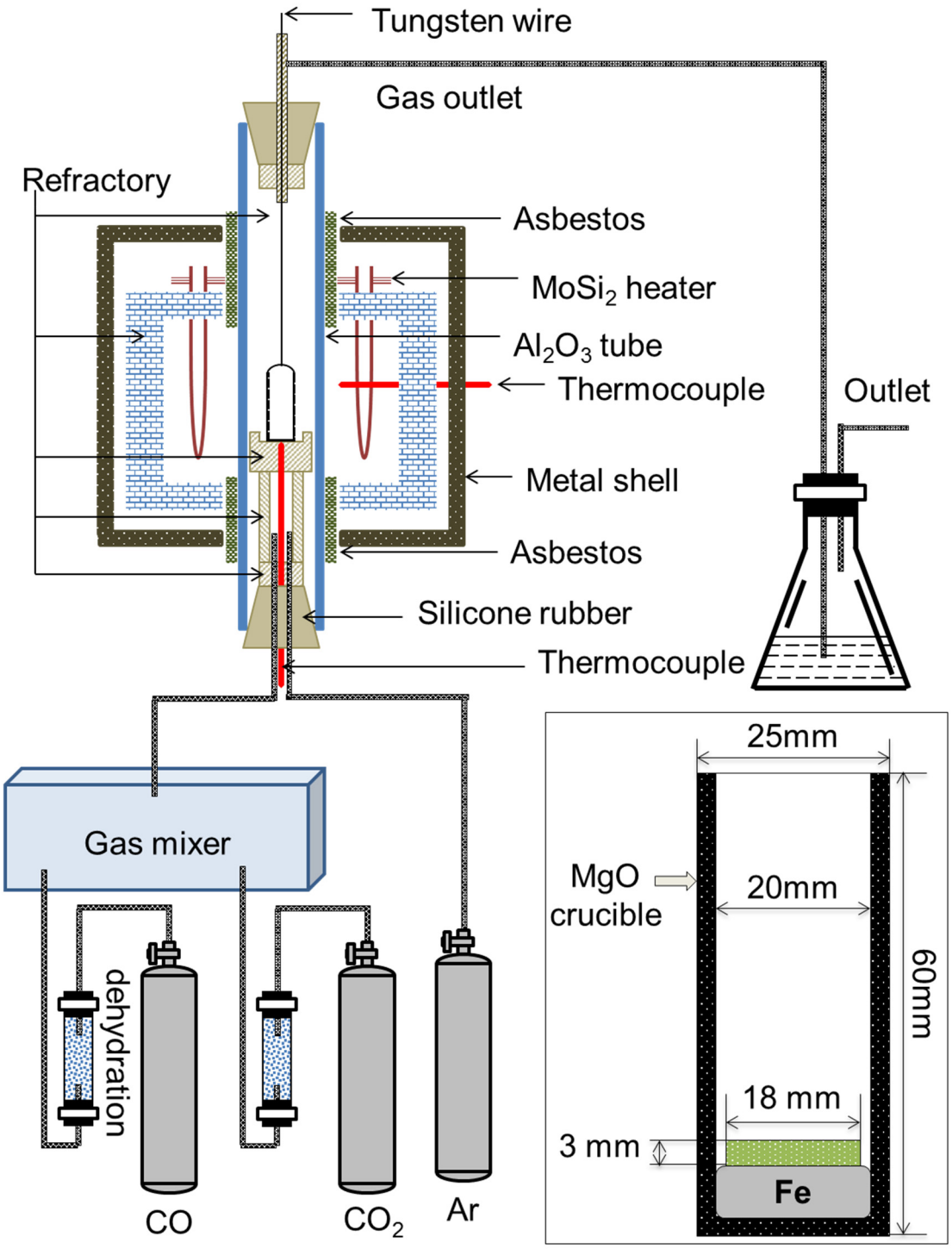

Fig. 2.2 Schematic of experimental apparatus.

Figure 2.2 shows the schematic of experimental equipment. The detail of experimental procedure is expressed as following.

The resistance furnace with $MoSi_2$ heater was applied. The experimental temperatures were 1823 and 1873 K. The B-type platinum rhodium thermocouple placed at the side of reaction

tube was used to control the temperature. And the bottom B-type platinum rhodium thermocouple was used to measure the temperature just under the crucible. Before each experiment the true temperature inside the tube was measured with a B-type platinum rhodium thermocouple from the top of the tube.

In order to achieve equilibrium as quickly as possible, only 10 g electrolytic iron was used as the metal phase and for some experiments the Fe_3P and graphite were added in advance to avoid the composition change of tablet after reaction and achieve equilibrium quickly. **Table 2.3** shows the impurity constituents of electrolytic iron and Fe_3P. The impurity contents of electrolytic iron were obtained by chemical analysis and those of Fe_3P were obtained from the supplier.

Table 2.3 Content of impurity constituent of iron and Fe_3P.

Name	mass%							
	P	Si	Ca	Mg	Al	Na	Ni	Ti
Iron	0.0003	ND	0.0006	ND	-	-	-	-
Fe_3P	-	-	-	0.0300	0.0080	0.0200	0.0030	ND

ND: negative detection

About 10 g electrolytic iron was put into the MgO crucible (high 60 mm, outer diameter 25 mm, inner diameter 20 mm). The synthesized tablet was put on the surface of the electrolytic iron. The procedure of making tablet is introduced in Section 2.3. At first the crucible was located at the upper end of the furnace tube and the air in tube was replaced by Ar gas with the flow rate of 2 L/min for 2 minutes. Then the atmosphere was changed to the mixture of CO and CO_2 gases. After five minutes the sample was put into the hot zone of the furnace.

After the equilibrium was established, the crucible was taken out from the furnace and quenched in Ar stream. After cooling down to room temperature, the tablet was separated from the surface of solidified iron and the solidified iron was separated from crucible. The tablet was ground to fine powder for chemical analysis and XRD. The solidified iron was cleaned, polished

and cut into piece with the weight around 1 g. Phosphorus concentration in Fe was analyzed by the molybdenum-blue spectrophotometric solvent extraction method or the phosphomolybdate blue spectrophotometric method depending on the concentration. P_2O_5 content in tablet was analyzed by the phosphomolybdate blue spectrophotometric method. ICP-OES was adopted for the analysis of CaO, MgO and FeO contents in tablet. Gravimetry was used for SiO_2 content in tablet.

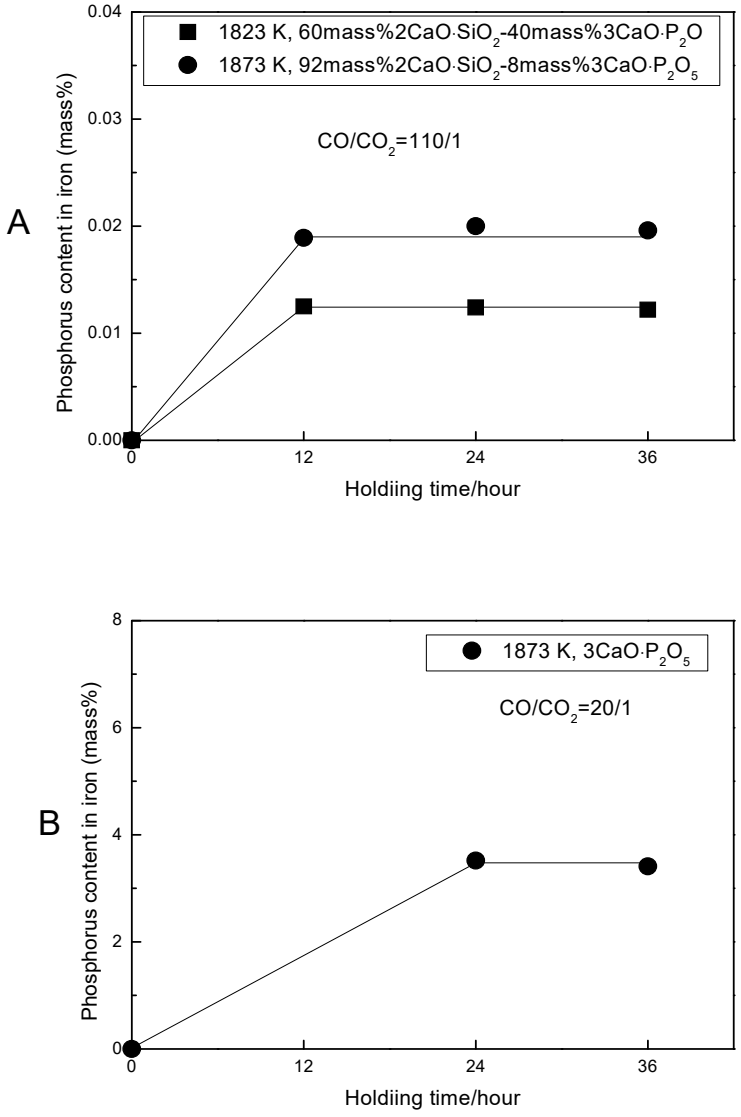

Fig. 2.3 Time for attainment of equilibrium.

Figure 2.3 A shows the concentration of P in Fe reacted with the $2CaO{\cdot}SiO_2$-$3CaO{\cdot}P_2O_5$ solid solution tablet for different reaction times at 1823 and 1873 K. For these two compositions

of solid solutions, the equilibrium was attained within 12 hours. Finally 24 hours was adopted for the subsequent experiments in order to ensure equilibrium for various compositions of solid solutions which was confirmed by the experiment with high P concentration in Fe after reaction as shown in **Figure 2.3 B**. **Figure 2.4** shows the composition changes of the tablets after reaction for different reaction times. The initially composition of the 92mass%2CaO·SiO_2-8mass%3CaO·P_2O_5 solid solution barely changed for different reaction times. Therefore, 24 hours was enough for equilibrium.

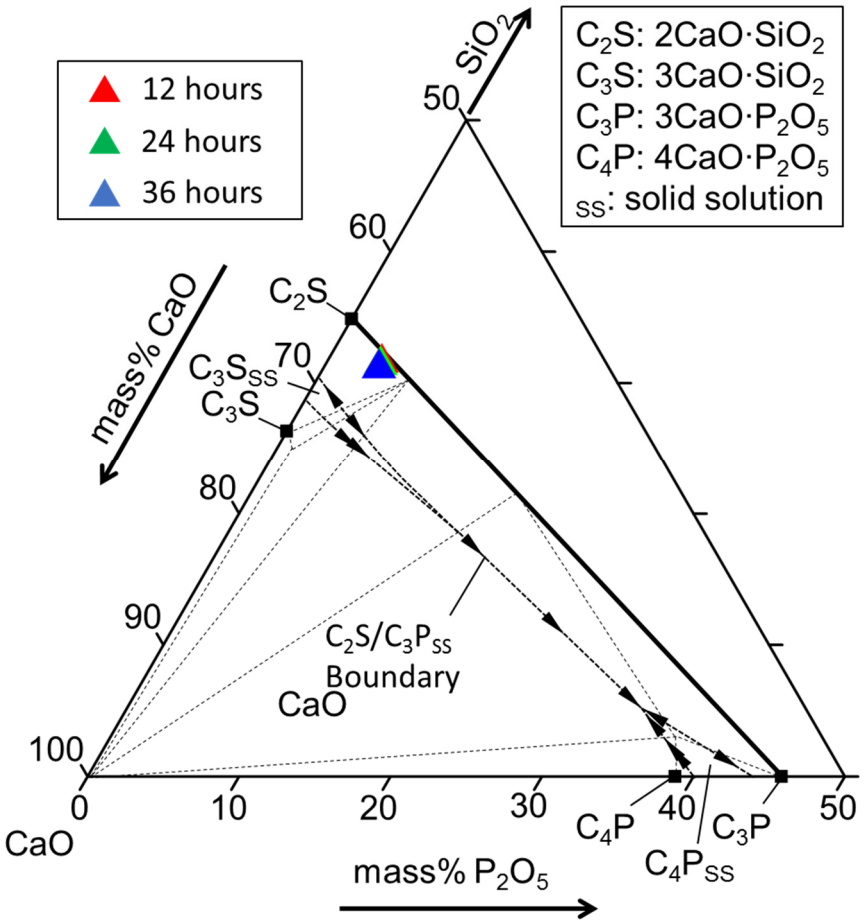

Fig. 2.4 Change of the composition which initially was the 92mass%2CaO·SiO_2-8mass%3CaO·P_2O_5 solid solution after reaction with Fe at 1873 K with different reaction times. The boundary and tie lines in the phase diagram were determined at 1773 K by Gutt.[13]

2.3 Process of making tablet of the calcium phosphate-based solid solution

The tablet was made by sintering the mixture of various ratios of reagent grade MgO, SiO_2, $CaHPO_4{\cdot}2H_2O$ and CaO. The CaO was obtained by the calcination by $CaCO_3$ according to the Eq. (2.8).

$$CaCO_3(s) = CaO(s) + CO_2(g)$$

$$\Delta G^{\circ}_{2.8} = 161000 - 137.17T \text{ J/mol} \ldots\ldots (2.8)^{[14]}$$

As the $CaCO_3$ was decomposed into CaO and CO_2 at 1173 K, 1473 K was chosen to make the $CaCO_3$ decomposing completely. The CaO crucible was used for calcination. The 70 g of reagent grade of $CaCO_3$ was charged into a crucible and it was kept at 1473 K for 12 hours in air. The CaO with the crucible was cooling down in air and then the CaO was ground into fine powder. The formation was confirmed by XRD as shown in **Figure 2.5**.

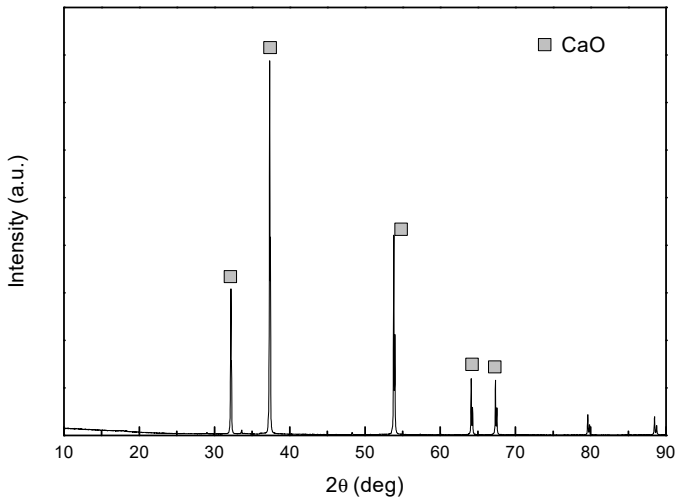

Fig. 2.5 XRD pattern of CaO sintered from calcium oxide.

For preparing the tablet, the raw materials were mixture and ground for 20 minutes. The weight of $CaHPO_4{\cdot}2H_2O$ was calculated by the mass balance of P, and the weight of CaO was calculated by the mass balance of Ca. The mixture was heated in air at 1873 K in a Pt crucible for 24 hours, quenched by Ar stream and then ground into fine powder. **Figures 2.6**, **2.7** and

2.8 show the XRD patterns of the 60mass%2CaO·SiO_2-40mass%3CaO·P_2O_5 solid solution for different sintering times. The XRD patterns of the 60mass%2CaO·SiO_2-40mass%3CaO·P_2O_5 solid solution sintered for 24 hours, 48 hours and 72 hours at 1873K were almost the same. Therefore, 24 hours was enough to form target phase. Sintering process was repeated twice totally for 48 hours.

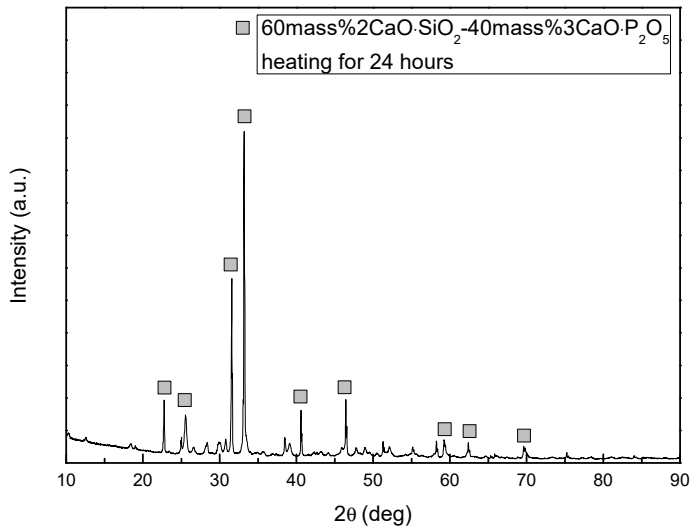

Fig. 2.6 XRD pattern of the 60mass%2CaO·SiO_2-40mass%3CaO·P_2O_5 solid solution sintered for 24 hours at 1873 K.

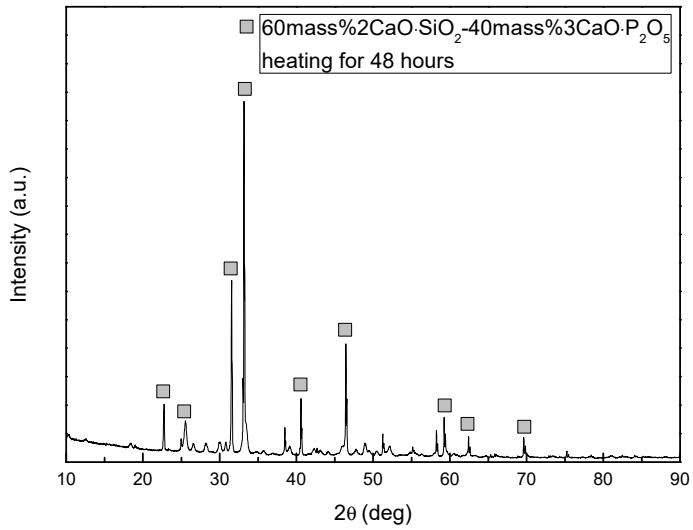

Fig. 2.7 XRD pattern of the 60mass%2CaO·SiO_2-40mass%3CaO·P_2O_5 solid solution sintered for 48 hours at 1873 K.

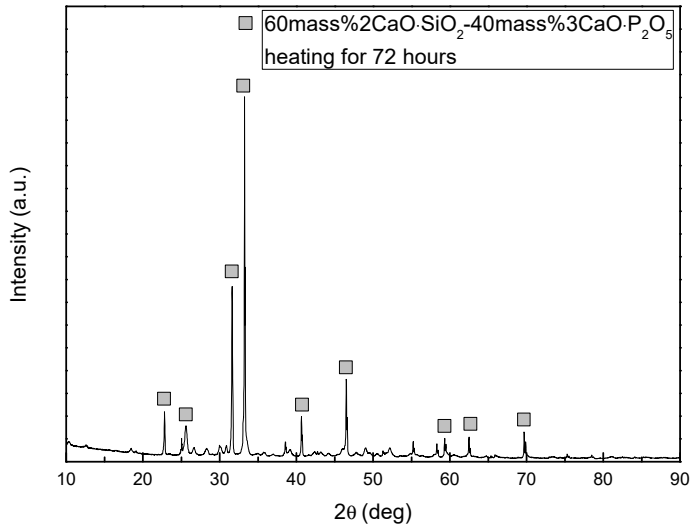

Fig. 2.8 XRD pattern of the 60mass%2CaO·SiO_2-40mass%3CaO·P_2O_5 solid solution sintered for 72 hours at 1873 K.

The XRD pattern of the 60mass%2CaO·SiO_2-40mass%3CaO·P_2O_5 solid solution are close to the XRD pattern of 7CaO·2SiO_2·P_2O_5 extremely. According to the pseudo binary phase diagram of 2CaO·SiO_2-3CaO·P_2O_5 as shown in **Figure 2.9**, for the 60mass%2CaO·SiO_2-

40mass%3CaO·P_2O_5 solid solution, the 7CaO·2SiO_2·P_2O_5 phase appears at the temperature lower than 900 °C and the 60mass%2CaO·SiO_2-40mass%3CaO·P_2O_5 solid solution may include a little amount of 7CaO·2SiO_2·P_2O_5 at room temperature. Since the lack of reference XRD pattern about the 2CaO·SiO_2-3CaO·P_2O_5 solid solution system, it is difficult to know the accurate XRD pattern of a certain composition of solid solution. In current research, the formation of each composition was confirmed by XRD and found that when the compositions changed in some range, the XRD patterns were almost the same and similar like the XRD pattern of the phase at a low temperature. In Figure 2.9, the compositions marked by the solid triangles presented the compositions of solid solution which could preserve shape after sintering and the open triangles presented the compositions of solid solution which were easily broken by external force or by itself after sintering. After preparing the powder, about 1.5 g powder was charged into a steel dies and pressed into a cylindrical tablet (diameter: 18 mm, thickness: 3 mm) at 50 MPa.

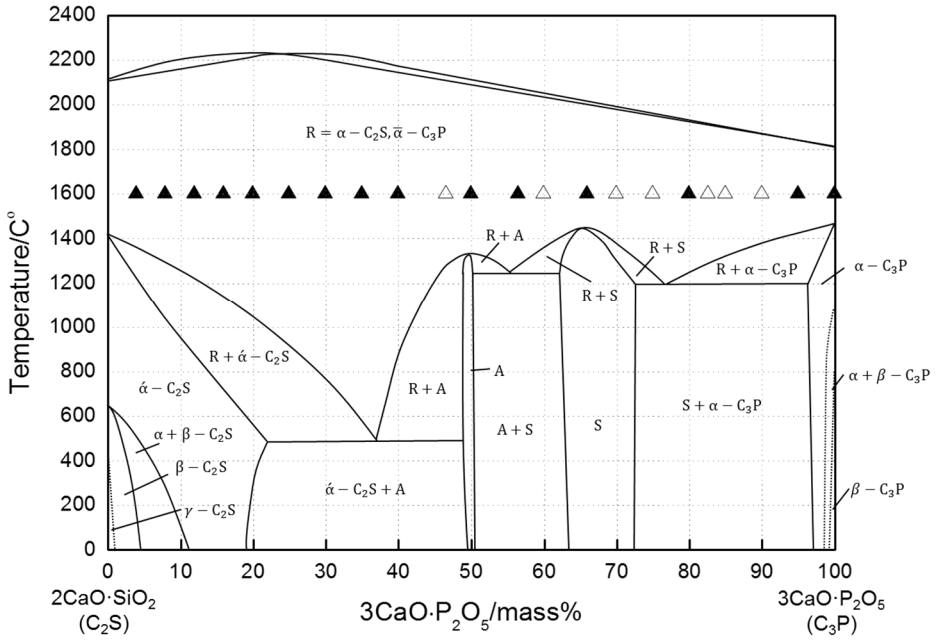

Fig. 2.9 Pseudo binary phase diagram between 2CaO·SiO_2 and 3CaO·P_2O_5.[15]

"R": 2CaO·SiO_2-3CaO·P_2O_5 solid solution, "A": 7CaO·2SiO_2·P_2O_5, "S": 5CaO·SiO_2·P_2O_5.

2.4 Methods of chemical analysis

For each sample, the concentration of P in Fe after reaction was analyzed and in order to get the accurate composition of tablet after experiment, all the possible compositions in tablet were analyzed.

2.4.1 Concentration of P in Fe and content of P_2O_5 in tablet

Depending the concentration of P in Fe two different methods were applied. When the concentration of P in Fe was greater than 0.005 mass%, the phosphomolybdate blue spectrophotometric method was adopted and when the concentration of P in Fe was smaller than 0.005 mass%, the molybdenum-blue spectrophotometric solvent extraction was adopted. For the analysis of P_2O_5 in tablet, the phosphomolybdate blue spectrophotometric method was applied.

For these two methods, the necessary chemical reagents were as following: concentrated HCl, concentrated HNO_3, concentrated $HClO_4$, $NaHSO_3$ (100 g/L), $(NH_4)_6Mo_7O_{24}\cdot 4H_2O$ (20 g/L in 35 vol% H_2SO_4), $N_2H_4\cdot H_2SO_4$ (1.5 g/L), $KH_2PO_4\cdot 2H_2O$, $SnCl_2\cdot 2H_2O$ (30 g/L in 10 vol% HCl) and $CH_3COCH_2CH(CH_3)_2$.

The calibration line of P with different concentrations was prepared with the following procedure.

0.8787 g KH_2PO_4 which had been heated at 383 K to remove the crystal water previously was dissolved into a 1L of water and the concentration of P was 0.2 g/L. Then this solution was diluted to 0.004 g/L and 0.01 g/L for standard solution, respectively.

To eliminate the influence of Fe background two calibration lines were prepared. For measuring the concentration of P in Fe, 0 mL, 1 mL, 2 mL, 4 mL, 6 mL, 8 mL, 10 mL, 15 mL, 20 mL and 25 mL standard solutions (0.004 g/L) and 1 g pure Fe powder were used to prepare the standard solutions. For measuring the P_2O_5 content in tablet, 0 mL, 2 mL, 4 mL, 6 mL, 8 mL and 10 mL standard solutions (0.01 g/L) were used.

After samples were dissolved in the mixture of 20 mL HCl and 10 mL HNO_3, about 15 mL $HClO_4$ was added to oxidize phosphorus in the solution.

After evaporating $HClO_4$, the solution was filtrated with filter paper (retain particle size: 7 μm) to separate the solid SiO_2 precipitated in the solution.

10 mL $NaHSO_3$ solution was added to the solution and heated to eliminate the effect of Fe in solution on the P analysis.

Then $(NH_4)_6Mo_7O_{24}$ solution and $N_2H_4 \cdot H_2SO_4$ solution were added to the solution and heated for 20 minutes. The solution was diluted to 100 mL and cooling down to room temperature.

The absorbance of each sample was measure by the spectrophotometer (U-2001 HITACHI), with the 10 mm, 20 mm and 40 mm cell respectively at 825 nm wavelength. **Table 2.4** shows the absorbance and **Figures 2.10** and **2.11** show the calibration lines of P. After using a period of time, the calibration line should be demarcated again.

Table 2.4 Absorbance of standard solutions with the phosphomolybdate blue spectrophotometric method.

C_P/ppm	ABS			C_P/ppm	ABS		
With Fe	10 mm	20 mm	40 mm	Without Fe	10 mm	20 mm	40 mm
0.00	0.009	0.018	0.031	0.00	0.003	0.007	0.004
0.04	0.029	0.060	0.107	0.20	0.089	0.183	0.352
0.08	0.043	0.090	0.167	0.40	0.176	0.354	0.688
0.16	0.079	0.162	0.308	0.60	0.238	0.475	0.923
0.24	0.113	0.226	0.444	0.80	0.349	0.698	1.271
0.32	0.148	0.298	0.580	1.00	0.433	0.855	1.401
0.40	0.183	0.369	0.718	-	-	-	-
0.60	0.267	0.538	1.032	-	-	-	-
0.80	0.354	0.707	1.281	-	-	-	-
1.00	0.439	0.866	1.401	-	-	-	-

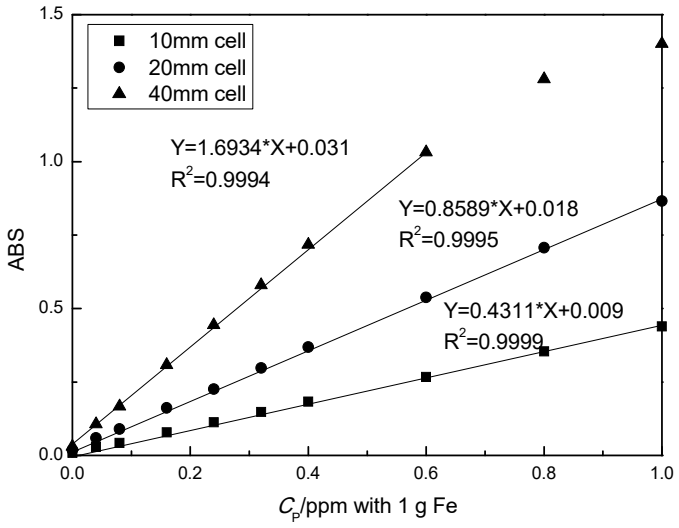

Fig. 2.10 Calibration line of P with Fe background with the phosphomolybdate blue spectrophotometric method.

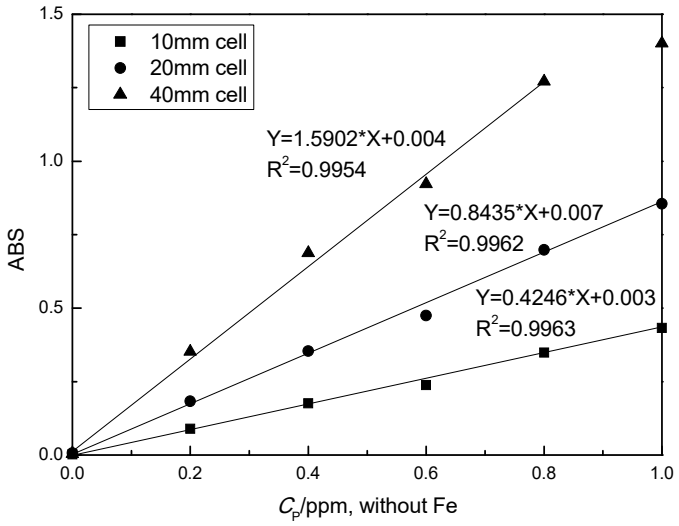

Fig. 2.11 Calibration line of P without Fe background with the phosphomolybdate blue spectrophotometric method.

The liner relationship between the absorbance and the concentration of P was obtained in the range of current concentration. The analysis method for steel and tablet were similar with the method of preparing standard solution. For analyzing the concentration of P in Fe, about 1 g

sample was added and the 20 mm cell was adopted. For analyzing the content of P_2O_5 in tablet, about 0.1g tablet powder was added and also the 20 mm cell was adopted. In the case of P_2O_5 analysis in tablet, the solid SiO_2 could be separated from solution and the solid SiO_2 gathered by filter paper (retain particle size: 4 μm) was supplied for analyzing the SiO_2 content in tablet.

Table 2.5 Absorbance of standard solutions with the molybdenum-blue spectrophotometric solvent extraction method.

C_P/ppm	ABS
With Fe	10 mm
0.00	0.009
0.08	0.029
0.16	0.043
0.32	0.079
0.48	0.113
0.64	0.148
0.80	0.183
1.20	0.267
1.60	0.354
2.00	0.439

When the concentration of P in Fe is less than 0.005 mass%, the molybdenum-blue spectrophotometric solvent extraction method was adopted. Sample solution, 8 mL $HClO_4$ and water were put in a separating funnel. After shaking well adding 10 mL $(NH_4)_6Mo_7O_{24}$ solution and shaking well again. And then 10 mL $CH_3COCH_2CH(CH_3)_2$ solution was added and the solution was shaken 1 minute. Then the aqueous phase was removed and 10 mL $HClO_4$ (25 vol%) was added, after shaking and standing the aqueous phase was removed. Then adding 10 mL $SnCl_2$ solution and shaking for 30 seconds, the absorbance of aqueous phase was measured by spectrophotometer with 10 mm cell at 700 nm wavelength. **Table 2.5** shows the absorbance

and **Figure 2.12** shows the calibration line of P for the molybdenum-blue spectrophotometric solvent extraction method.

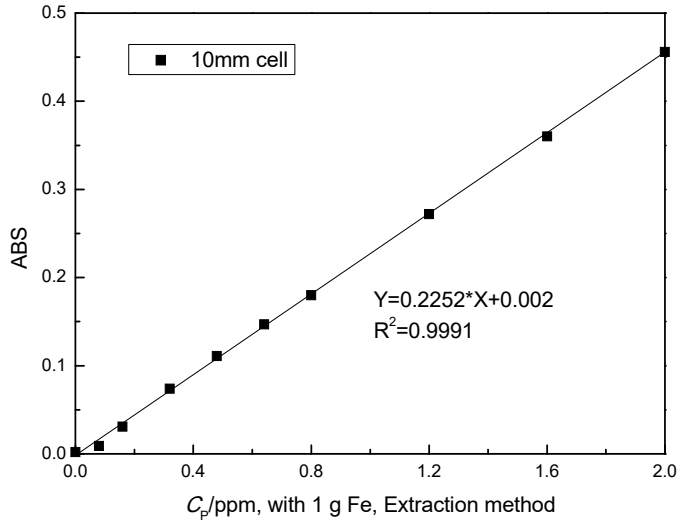

Fig. 2.12 Calibration line of P with the molybdenum-blue spectrophotometric solvent extraction method.

2.4.2 Content of SiO_2 in tablet

The chemical reagents for SiO_2 analysis were as follows: H_2SO_4 (50 vol%), concentrated HF and $K_2S_2O_3$. Filtrated SiO_2 during the P_2O_5 analysis in tablet was adopted for SiO_2 analysis.

The filter paper with tiny SiO_2 particles was put into Pt crucible and heated till all the filter paper burned out. The Pt crucible including SiO_2 particles was weighted. Then 2 mL H_2SO_4 (50 vol%) and 2 mL HF were added into the Pt crucible and the crucible was heated to evaporate SiO_2. After cooling down to room temperature, the Pt crucible was weighted. The SiO_2 content can be obtained from the difference of weight.

2.4.3 Contents of CaO, MgO and FeO in tablet

For the analysis of CaO, MgO and FeO contents in tablet, the inductively coupled plasma optical emission spectrometry (ICP-OES, SPS 7800, Seiko Instruments Inc.) was adopted. For making calibration lines of Ca, Mg and Fe, the 0 g/L, 0.002 g/L, 0.004 g/L, 0.006 g/L and 0.008 g/L standard solutions were prepared and the examples of calibration lines were shown in **Figures 2.13**, **2.14** and **2.15**. About 0.1 g powder of tablet was dissolved in HCl and the solution was diluted and supplied for the ICP-OES analysis. According to the analyzed results, there was little Fe_2O_3 in tablet after reaction, and the iron oxide was considered as FeO in the following chapters.

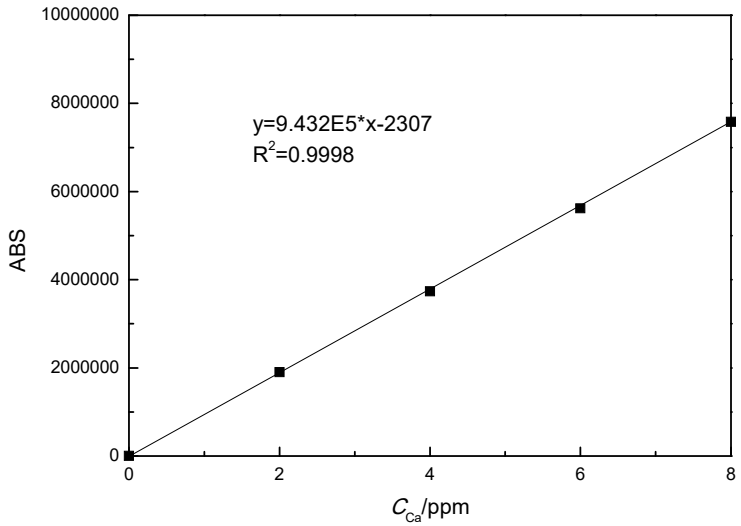

Fig. 2.13 Calibration line of Ca.

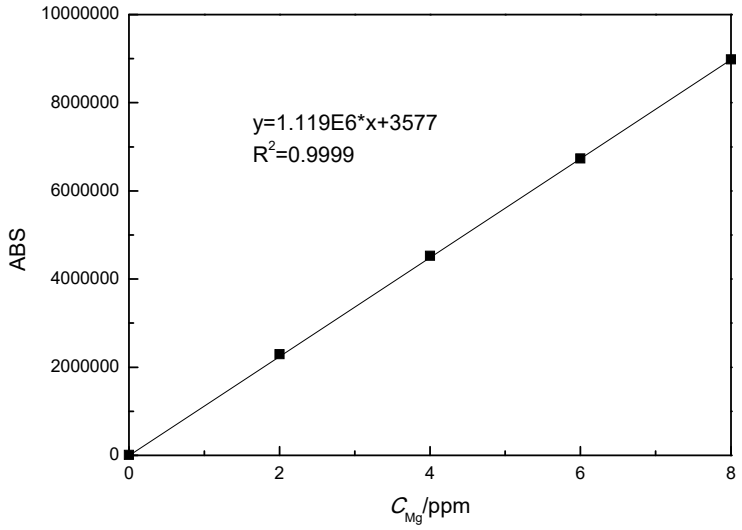

Fig. 2.14 Calibration line of Mg.

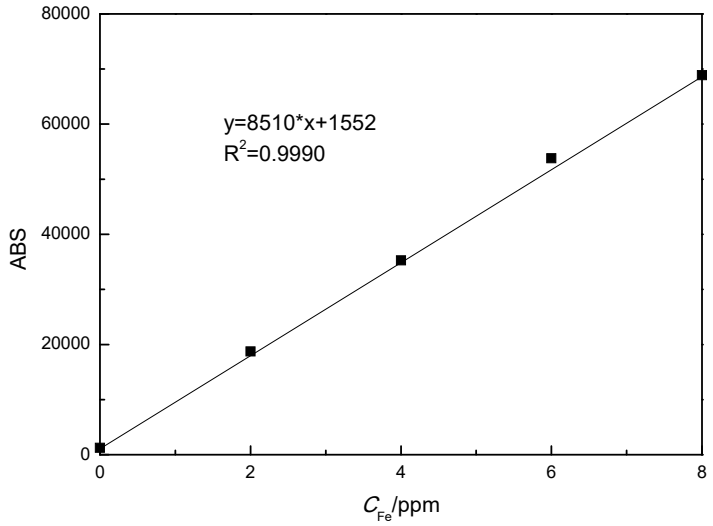

Fig. 2.15 Calibration line of Fe.

2.5 Summary

In this chapter, the experimental principle, method and parameter were introduced. The process of making tablet of the calcium phosphate-based solid solution was explained in detail. The chemical analysis methods for different components were represented, respectively.

References

1. G. Li, T. Hamano and F. Tsukihashi: *ISIJ Int.*, **45** (2005), 12-18.
2. A. Sobandi, H. G. Katayama and T. Momono: *ISIJ Int.*, **37** (1997), 1043-1049.
3. X. Gao, H. Matsuura, I. Sohn, W. Wang, D. Min and F. Tsukihashi: *Metall. Trans. B*, **43B** (2012), 694-702.
4. Y. Zhao, K. Morita, and N. Sano: *Metall. Trans. B*, **26B** (1995), 1013-1017.
5. E. T. Turkdogan: *ISIJ Int.*, **40** (2000), 964-970.
6. S. Ban-ya and S. Matoba: *Tetsu-to-Hagané*, **48** (1962), 925-932.
7. E.T. Turkdogan: Physical Chemistry of High Temperature Technology, Academic Press, New York, (1980), 7.
8. K. Yamada and E. Kato: *Tetsu-to-Hagané*, **65** (1979), 264-272.
9. H. G. Hadrys, M. G. Frohberg and J. F. Elliott: *Metall. Trans.*, **1** (1970), 1867-1874.
10. D. Dutilloy and J. Chipman: *Teans. Metall. Soc. AIME*, **218** (1960), 428.
11. H. Sakao and K. Sano: *Japan Inst. Metals*, **23** (1959), 671-674.
12. M. Allibert *et al.*: SLAG ATLAS 2nd Edition, Verein Deutscher Eisenhüttenleute, Germany, (1995), 134.
13. W. Gutt: *Nature*, **197** (1963), 142-143.
14. E.T. Turkdogan: Physical Chemistry of High Temperature Technology, Academic Press, New York, NY, (1980), 8.
15. Fit, W., H. Heymann, R. Heinke: *J. Am. Ceram. Soc.*, **52** (1969), 346-351.

Chapter 3 Thermodynamic Properties of the $2CaO{\cdot}SiO_2$-$3CaO{\cdot}P_2O_5$ Solid Solution at 1823 and 1873K

3.1 Introduction

In this chapter, the thermodynamic properties of the $2CaO{\cdot}SiO_2$-$3CaO{\cdot}P_2O_5$ solid solution at 1823 and 1873 K were measured and discussed.

3.2 Experimental conditions

The initial compositions of tablets after sintering are shown in **Table 3.1** and projected onto the ternary phase diagram of the CaO-SiO_2-P_2O_5 system as shown in **Figure 3.1**. The initial conditions of experiments are shown in **Table 3.2**. For the experiments at 1873 K, a certain amount of extra Fe_3P and graphite were added in advance in order to achieve equilibration quickly.

Table 3.1 Initial compositions of tablets.

No.	CaO /mass%	SiO_2 /mass%	P_2O_5 /mass%	$2CaO{\cdot}SiO_2$ /mass%	$3CaO{\cdot}P_2O_5$ /mass%
A01	64.7	33.5	1.8	96.0	4.0
A02	64.2	32.1	3.7	92.0	8.0
A03	63.8	30.7	5.5	88.0	12.0
A04	62.9	27.9	9.2	79.9	20.1
A05	61.9	24.4	13.7	70.0	30.0
A06	60.8	20.9	18.3	60.0	40.0
A07	60.0	18.6	21.4	53.3	46.7
A08	58.9	15.2	25.9	43.5	56.5
A09	57.9	11.9	30.2	34.0	66.0
A10	56.9	8.7	34.4	25.0	75.0

A11	55.8	5.2	39.0	15.0	85.0
A12	54.8	1.7	43.5	5.0	95.0
A13	54.2	0.0	45.8	0.0	100.0
B01	64.2	32.1	3.7	92.0	8.0
B02	62.9	27.9	9.2	80.0	20.0
B03	61.9	24.4	13.7	70.0	30.0
B04	60.8	20.9	18.3	60.0	40.0
B05	59.7	17.4	22.9	50.0	50.0
B06	58.6	13.9	27.5	40.0	60.0
B07	57.5	10.4	32.1	30.0	70.0
B08	56.4	7.0	36.6	20.0	80.0
B09	55.3	3.5	41.2	10.0	90.0
B10	54.2	0.0	45.8	0.0	100.0

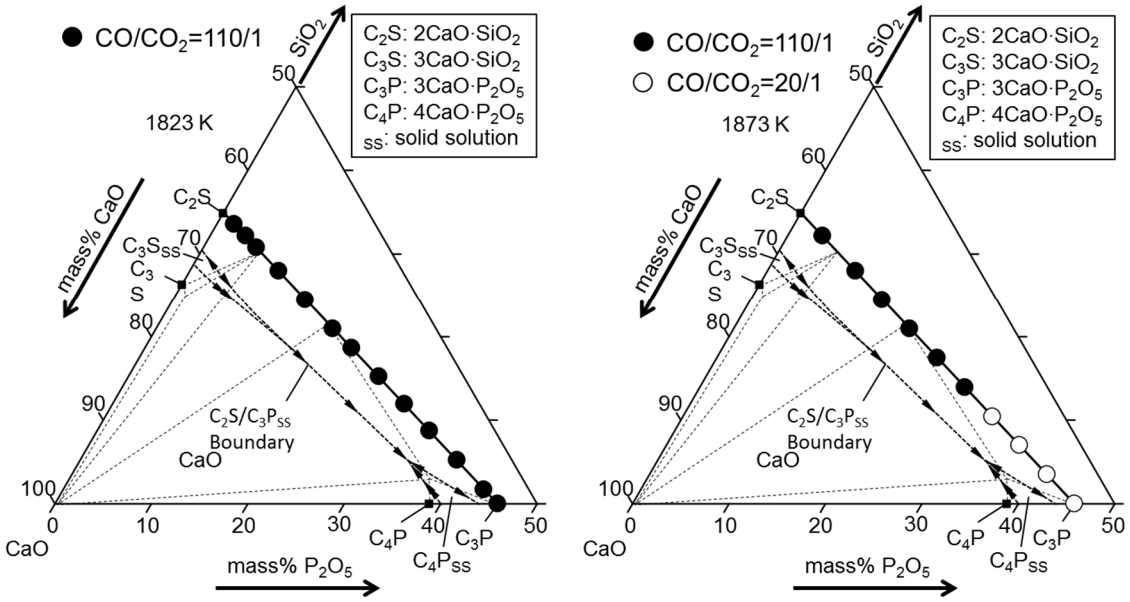

Fig. 3.1 Initial compositions of tablets on the CaO-SiO_2-P_2O_5 system. The boundary and tie lines in the phase diagram were determined at 1773 K by Gutt.[1]

Table 3.2 Initial conditions of experiments.

No.	Temp./K	CO/CO_2	Fe/g	Tablet/g	Graphite/g	Fe_3P/g
A01	1823	110/1	12.2836	2.4374	-	-
A02	1823	110/1	12.5552	1.9562	-	-
A03	1823	110/1	12.3017	2.0486	-	-
A04	1823	110/1	12.4715	1.6639	-	-
A05	1823	110/1	12.5124	1.9128	-	-
A06	1823	110/1	12.3383	1.8027	-	-
A07	1823	110/1	12.2874	1.7594	-	-
A08	1823	110/1	12.4077	1.7399	-	-
A09	1823	110/1	12.3856	1.8787	-	-
A10	1823	110/1	12.4528	1.7791	-	-
A11	1823	110/1	12.2444	1.8229	-	-
A12	1823	110/1	12.3040	1.8574	-	-
A13	1823	110/1	12.5713	1.9685	-	-
B01	1873	110/1	9.9630	1.4345	0.1848	0.0050
B02	1873	110/1	9.7859	1.4597	0.1855	0.0172
B03	1873	110/1	9.8078	1.4825	0.1866	0.0253
B04	1873	110/1	9.7786	1.4849	0.1866	0.0354
B05	1873	110/1	9.4885	1.4359	0.1854	0.3410
B06	1873	110/1	9.1414	1.5038	0.1851	0.6904
B07	1873	20/1	9.9741	1.5125	0.0310	0.1160
B08	1873	20/1	9.5852	1.5226	0.0102	0.4361
B09	1873	20/1	9.0478	1.5082	0.0163	1.0591
B10	1873	20/1	7.5935	1.4970	0.0203	2.4391

3.3 Experimental results

3.3.1 Chemical compositions of Fe and tablet

The concentration of P in Fe and the contents of P_2O_5, SiO_2, CaO, MgO and FeO in tablet after reaction are shown from **Table 3.3** to **Table 3.8**. The dilution ratio was based on that the weighted sample dissolved into a 100 mL volumetric flask was defined as 1. In Tables 3.6, 3.7 and 3.8, the values of Test/ppm were the concentrations of Ca, Mg and Fe in the solution measured by ICP-OES. **Table 3.9** summarized the analyzed the concentration of P in Fe and the compositions of tablets. Since the inevitable analytical error, the total mass% is not 100 but near to 100.

Table 3.3 Concentration of P in Fe.

No.	Weight /mg	Dilution ratio	Cell /mm	ABS	P in Fe /mass%	Ave P /mass%
A01	985.7	0.5	10	0.140	0.00274	0.00276
	995.4	0.5	10	0.143	0.00278	
A02	1140.7	0.5	10	0.164	0.00281	0.00282
	1186.0	0.5	10	0.170	0.00282	
A03	998.7	0.5	10	0.250	0.00506	0.00501
	949.1	0.5	10	0.235	0.00496	
A04	1205.5	10	20	0.096	0.0078	0.0081
	1133.6	10	20	0.097	0.0084	
A05	1160.6	10	20	0.074	0.0059	0.0059
A06	1092.5	10	20	0.130	0.0123	0.0124
	1092.5	10	20	0.128	0.0121	
	1138.6	10	20	0.139	0.0126	
	1138.6	10	20	0.139	0.0126	
A07	1007.4	10	20	0.163	0.0172	0.0175

	1003.6	10	20	0.168	0.0177	
A08	1124.7	10	20	0.241	0.0235	0.0238
	1126.5	10	20	0.247	0.0241	
A09	1010.2	10	20	0.166	0.0174	0.0178
	893.5	10	20	0.154	0.0181	
A10	993.2	50	20	0.202	0.110	0.111
	995.8	50	20	0.206	0.112	
A11	804.0	50	20	0.189	0.126	0.128
	996.5	50	20	0.236	0.129	
A12	1065.7	50	20	0.267	0.138	0.15
	1063.8	50	20	0.309	0.162	
A13	998.2	50	20	0.420	0.237	0.221
	996.5	50	20	0.362	0.204	
B01	1017.6	10	20	0.188	0.0199	0.0201
	1021.3	10	20	0.192	0.0203	
B02	1002.3	20	20	0.228	0.0497	0.0498
	1038.3	20	20	0.237	0.0499	
B03	993.5	50	20	0.199	0.108	0.109
	1010.0	50	20	0.204	0.109	
B04	1017.3	100	20	0.247	0.266	0.261
	993.6	100	20	0.232	0.256	
B05	521.9	200	20	0.166	0.674	0.661
	502.7	200	20	0.155	0.648	
B06	609.8	400	20	0.177	1.24	1.26
	694.3	400	20	0.203	1.27	
B07	678.5	50	20	0.169	0.133	0.127
	626.6	50	20	0.144	0.120	

B08	934.0	200	20	0.246	0.578	0.557
	878.0	200	20	0.216	0.535	
B09	472.6	500	20	0.136	1.49	1.49
	610.2	500	20	0.170	1.48	
B10	571.6	1000	20	0.188	3.53	3.52
	496.2	1000	20	0.164	3.51	

Annotation: the analysis data was based on the calibration curve: ABS=0.8517×C_P(ppm)+0.016 for the phosphomolybdate blue spectrophotometric method, ABS=0.2367×C_P(ppm)+0.012 for the molybdenum-blue spectrophotometric solvent extraction method. The samples tested with the 20 mm cell was analyzed by the phosphomolybdate blue spectrophotometric method. The samples tested with the 10 mm cell was analyzed by the molybdenum-blue spectrophotometric solvent extraction method.

Table 3.4 Content of P_2O_5 in tablet after reaction.

No.	Weight /mg	Dilution ratio	Cell /mm	ABS	P_2O_5 /mass%	Ave P_2O_5 /mass%
A01	101.3	50	20	0.142	1.83	1.83
	102.0	50	20	0.143	1.83	
A02	105.6	50	20	0.288	3.58	3.59
	102.7	50	20	0.282	3.60	
A03	105.9	50	20	0.440	5.46	5.44
	102.2	50	20	0.422	5.42	
A04	103.3	100	20	0.357	9.09	9.18
	101.4	100	20	0.357	9.26	
A05	101.9	100	20	0.522	13.5	13.6
	101.1	100	20	0.524	13.6	
A06	102.4	100	20	0.705	18.1	18.2
	102.7	100	20	0.709	18.2	

A07	104.5	250	20	0.344	21.6	21.8
	101.8	250	20	0.340	21.9	
A08	104.0	200	20	0.506	25.6	25.5
	105.6	200	20	0.510	25.4	
A09	103.3	250	20	0.475	30.2	30.2
	103.0	250	20	0.473	30.2	
A10	106.3	250	20	0.515	31.8	31.9
	102.8	250	20	0.500	32.0	
A11	100.4	250	20	0.568	37.2	37.2
	101.4	250	20	0.574	37.2	
A12	103.0	500	20	0.337	43.0	43.4
	103.1	500	20	0.343	43.7	
A13	105.2	500	20	0.366	45.7	45.8
	103.7	500	20	0.362	45.8	
B01	100.3	50	20	0.263	3.44	3.47
	99.9	50	20	0.266	3.50	
B02	100.9	100	20	0.328	8.53	8.6
	102.6	100	20	0.338	8.66	
B03	102.8	100	20	0.469	12.0	12.1
	101.0	100	20	0.463	12.1	
B04	101.9	250	20	0.259	16.7	16.8
	100.4	250	20	0.259	16.9	
B05	99.3	200	20	0.406	21.5	21.6
	100.2	200	20	0.411	21.6	
B06	100.9	200	20	0.485	25.3	25.3
	99.8	200	20	0.479	25.2	
B07	100.1	200	20	0.607	31.9	31.8
	99.8	200	20	0.602	31.7	

B08	99.8	200	20	0.688	36.3	36.3
	99.6	200	20	0.688	36.3	
B09	102.9	250	20	0.650	41.6	41.9
	98.4	250	20	0.630	42.1	
B10	99.5	250	20	0.704	46.6	46.5
	100.6	250	20	0.709	46.4	

Annotation: the analysis data was based on the calibration curve: ABS=0.8692×C_P(ppm)+0.001.

Table 3.5 Content of SiO_2 in tablet after reaction.

No.	Weight (1) /mg	Crucible /g	Weight (2) /g	Weight (3) /g	SiO_2 /mass%	Ave SiO_2 /mass%
A01	101.3	23.88375	23.91909	23.88600	32.67	32.78
	102.0	23.94926	23.98384	23.95030	32.88	
A02	105.6	23.88691	23.91986	23.88678	31.33	31.26
	102.7	23.95081	23.98330	23.95127	31.19	
A03	105.9	23.88436	23.91620	23.88471	29.74	29.61
	102.2	23.94974	23.98012	23.95000	29.47	
A04	103.3	23.88476	23.91555	23.88762	27.04	27.32
	101.4	23.95050	23.97960	23.95162	27.59	
A05	101.9	23.88527	23.91188	23.88710	24.32	23.85
	101.1	23.95095	23.97526	23.95162	23.38	
A06	102.4	23.88706	23.90644	23.88721	18.78	19.74
	102.7	23.94970	23.97326	23.95200	20.70	
A07	104.5	23.88572	23.90547	23.88597	18.66	18.94
	101.8	23.94969	23.96956	23.95000	19.21	
A08	104.0	23.88668	23.90323	23.88786	14.78	14.76

	105.6	23.95097	23.96736	23.95179	14.74	
A09	103.3	23.88695	23.89852	23.88678	11.36	11.47
	103.0	23.95038	23.96256	23.95063	11.58	
A10	106.3	23.88588	23.89614	23.88669	8.890	8.818
	102.8	23.94997	23.95984	23.95085	8.745	
A11	100.4	23.88407	23.89170	23.88648	5.199	5.159
	101.4	23.94950	23.95585	23.95066	5.118	
A12	103.0	23.88614	23.88885	23.88695	1.845	1.718
	103.1	23.95027	23.95239	23.95075	1.591	
B01	100.3	23.88259	23.91439	23.88541	28.89	29.5
	99.9	23.94606	23.97863	23.94858	30.1	
B02	100.9	23.88390	23.91011	23.88458	25.30	25.09
	102.6	23.94652	23.97219	23.94667	24.87	
B03	102.8	23.88398	23.90699	23.88497	21.42	21.98
	101.0	23.94465	23.96963	23.94687	22.53	
B04	101.9	23.88296	23.90427	23.88444	19.46	19.67
	100.4	23.94564	23.96581	23.94585	19.88	
B05	99.3	23.88136	23.89897	23.88195	17.1	16.7
	100.2	23.94354	23.96126	23.94503	16.20	
B06	100.9	23.88109	23.89358	23.88148	11.99	12.5
	99.8	23.94359	23.95692	23.94405	12.9	
B07	100.1	23.88044	23.89188	23.88129	10.58	10.8
	99.8	23.94339	23.95454	23.94362	10.9	
B08	99.8	23.88188	23.88857	23.88135	7.23	7.18
	99.6	23.94413	23.95108	23.94398	7.13	
B09	102.9	23.88097	23.88462	23.88101	3.508	3.49
	98.4	23.94246	23.94693	23.94353	3.46	

Annotation: the weight (1) is the weight of sample. The weight (2) is the weight of Pt crucible after the filter paper burned. The weight (3) is the weight of crucible after evaporating the SiO_2.

SiO_2/mass%=[weight (2) - weight (3)]/[weight (1)]×100000/%

Table 3.6 Content of CaO in tablet after reaction.

No.	Weight /mg	Dilution ratio	Test /ppm	CaO /mass%	Ave CaO /mass%
A01	102.6	100	4.921	67.10	67.11
	101.9	100	4.888	67.11	
A02	105.6	100	4.531	60.03	60.56
	102.7	100	4.484	61.08	
A03	103.5	100	4.750	64.21	64.5
	97.4	100	4.507	64.7	
A04	103.3	100	4.571	61.91	60.68
	101.4	100	4.309	59.45	
A05	101.9	100	4.289	58.88	59.81
	101.1	100	4.389	60.73	
A06	102.0	100	4.572	62.71	63.08
	104.8	100	4.752	63.44	
A07	101.7	100	4.412	60.69	60.8
	99.5	100	4.326	60.8	
A08	104.0	100	4.170	56.09	56.66
	105.6	100	4.320	57.23	
A09	96.2	100	4.059	59.0	59.2
	97.2	100	4.128	59.4	
A10	102.6	100	4.150	56.59	57.1

	96.2	100	3.955	57.5	
A11	102.3	100	4.167	56.99	57.3
	99.8	100	4.103	57.5	
A12	102.9	100	4.187	56.93	57.2
	99.1	100	4.075	57.5	
A13	99.5	100	3.994	56.2	56.4
	98.3	100	3.976	56.6	
B01	97.7	100	4.267	61.1	61.1
	101.9	100	4.441	60.97	
B02	97.4	100	4.023	57.8	58.0
	96.1	100	4.001	58.2	
B03	96.9	100	4.003	57.8	56.9
	96.4	100	3.857	56.0	
B04	95.7	100	3.974	58.1	57.9
	98.0	100	4.040	57.7	
B05	96.9	100	3.990	57.6	57.4
	97.2	100	3.972	57.2	
B06	96.6	100	3.934	57.0	56.6
	96.0	100	3.852	56.1	
B07	103.0	100	4.038	54.85	55.26
	102.3	100	4.070	55.66	
B08	100.4	100	3.842	53.54	53.62
	103.3	100	3.965	53.7	
B09	103.6	100	3.948	53.31	52.72
	102.6	100	3.823	52.13	
B10	100.6	100	3.726	51.82	51.54
	101.5	100	3.719	51.26	

Table 3.7 Content of MgO in tablet after reaction.

No.	Weight /mg	Dilution ratio	Test /ppm	MgO /mass%	Ave MgO /Mass%
A01	102.6	1	3.526	0.5699	0.5659
	101.9	1	3.452	0.5618	
A02	105.6	1	3.711	0.5828	0.5893
	102.7	1	3.689	0.5957	
A03	103.5	1	4.516	0.7236	0.721
	97.4	1	4.212	0.717	
A04	103.3	1	3.226	0.5179	0.5020
	101.4	1	2.972	0.4861	
A05	101.9	1	2.310	0.3760	0.3831
	101.1	1	2.379	0.3902	
A06	102.0	1	2.402	0.3905	0.3966
	104.8	1	2.544	0.4026	
A07	101.7	1	2.911	0.4747	0.476
	99.5	1	2.861	0.477	
A08	104.0	1	2.460	0.3923	0.3975
	105.6	1	2.564	0.4027	
A09	96.2	1	1.580	0.272	0.273
	97.2	1	1.599	0.273	
A10	102.6	1	4.941	0.7987	0.811
	96.2	1	4.772	0.823	
A11	102.3	1	2.178	0.3531	0.353
	99.8	1	2.122	0.353	
A12	102.9	1	1.791	0.2887	0.294
	99.1	1	1.778	0.298	

A13	99.5	1	1.581	0.264	0.266
	98.3	1	1.587	0.268	
B01	97.7	100	0.261	4.43	4.28
	101.9	100	0.254	4.134	
B02	97.4	10	2.453	4.18	4.19
	96.1	10	2.433	4.20	
B03	96.9	10	3.288	5.63	5.66
	96.4	10	3.305	5.69	
B04	95.7	10	2.143	3.71	3.67
	98.0	10	2.141	3.62	
B05	96.9	10	1.621	2.77	2.72
	97.2	10	1.560	2.66	
B06	96.6	10	1.673	2.87	2.86
	96.0	10	1.644	2.84	
B07	103.0	1	3.124	0.5030	0.5097
	102.3	1	3.185	0.5163	
B08	100.4	1	3.788	0.6257	0.6255
	103.3	1	3.894	0.6252	
B09	103.6	1	5.416	0.8670	0.8502
	102.6	1	5.156	0.8334	
B10	100.6	1	6.851	1.129	1.101
	101.5	1	6.565	1.073	

Table 3.8 Content of FeO in tablet after reaction.

No.	Weight /mg	Dilution ratio	Test /ppm	FeO /mass%	Ave FeO /Mass%
A01	102.6	1	1.747	0.2191	0.2164

	101.9	1	1.692	0.2137	
A02	105.6	1	2.253	0.2745	0.3537
	102.7	1	3.454	0.4328	
A03	103.5	1	2.890	0.3593	0.351
	97.4	1	2.589	0.342	
A04	103.3	1	2.308	0.2875	0.2988
	101.4	1	2.444	0.3101	
A05	101.9	1	3.831	0.4838	0.4893
	101.1	1	3.887	0.4947	
A06	102.0	1	2.102	0.2652	0.2676
	104.8	1	2.199	0.2700	
A07	101.7	1	1.866	0.2361	0.231
	99.5	1	1.747	0.226	
A08	104.0	1	2.556	0.3162	0.3276
	105.6	1	2.781	0.3389	
A09	96.2	1	2.246	0.300	0.286
	97.2	1	2.051	0.272	
A10	102.6	1	5.499	0.6896	0.697
	96.2	1	5.260	0.704	
A11	102.3	5	3.660	2.302	2.316
	99.8	5	3.612	2.33	
A12	102.9	1	3.501	0.4378	0.435
	99.1	1	3.331	0.433	
A13	99.5	1	3.861	0.499	0.467
	98.3	1	3.317	0.434	
B01	97.7	1	1.285	0.169	0.173
	101.9	1	1.406	0.1775	

B02	97.4	1	2.484	0.328	0.331
	96.1	1	2.498	0.334	
B03	96.9	1	4.345	0.577	0.575
	96.4	1	4.295	0.573	
B04	95.7	1	2.384	0.321	0.317
	98.0	1	2.387	0.313	
B05	96.9	1	2.005	0.266	0.261
	97.2	1	1.925	0.255	
B06	96.6	1	2.421	0.322	0.319
	96.0	1	2.347	0.315	
B07	103.0	1	1.734	0.2166	0.2087
	102.3	1	1.596	0.2007	
B08	100.4	1	2.307	0.2957	0.2759
	103.3	1	2.056	0.2561	
B09	103.6	1	5.245	0.6514	0.7038
	102.6	1	6.029	0.7561	
B10	100.6	1	2.384	0.3049	0.3192
	101.5	1	2.631	0.3335	

Table 3.9 Compositions of tablets and concentration of P in Fe after reaction.

No.	/mass%						P in Fe
	P_2O_5	SiO_2	CaO	MgO	FeO	Total	/mass%
A01	1.83	32.8	67.1	0.566	0.216	102.5	0.00276
A02	3.59	31.3	60.6	0.589	0.354	96.4	0.00282
A03	5.44	29.6	64.5	0.721	0.351	100.6	0.00501
A04	9.18	27.3	60.7	0.502	0.299	98.0	0.0081
A05	13.6	23.9	59.8	0.383	0.489	98.1	0.0059

A06	18.2	19.7	63.1	0.397	0.268	101.7	0.0124
A07	21.8	18.9	60.8	0.476	0.231	102.2	0.0175
A08	25.5	14.8	56.7	0.398	0.328	97.7	0.0238
A09	30.2	11.5	59.2	0.273	0.286	101.5	0.0178
A10	31.9	8.82	57.1	0.811	0.697	99.3	0.111
A11	37.2	5.16	57.3	0.353	2.32	102.3	0.128
A12	43.4	1.72	57.2	0.294	0.436	103.1	0.150
A13	45.8	0	56.4	0.266	0.467	102.9	0.221
B01	3.47	29.5	61.1	4.28	0.174	98.5	0.0201
B02	8.6	25.1	58	4.19	0.331	96.2	0.0498
B03	12.1	22	56.9	5.66	0.575	97.2	0.109
B04	16.8	19.7	57.9	3.67	0.317	98.4	0.261
B05	21.6	16.7	57.4	2.72	0.261	98.7	0.661
B06	25.3	12.5	56.6	2.86	0.319	97.6	1.26
B07	31.8	10.8	55.3	0.51	0.209	98.6	0.127
B08	36.3	7.18	53.6	0.626	0.276	98.0	0.557
B09	41.9	3.49	52.7	0.85	0.704	99.6	1.49
B10	46.5	0	51.5	1.1	0.319	99.4	3.52

3.3.2 XRD pattern of the $2CaO{\cdot}SiO_2$-$3CaO{\cdot}P_2O_5$ solid solution

The phases of the $2CaO{\cdot}SiO_2$-$3CaO{\cdot}P_2O_5$ solid solution were analyzed by XRD as shown from **Figure 3.2** to **3.19**. In all samples the CaO, SiO_2 and P_2O_5 phases were not detected. For some compositions the phase at low temperature was detected since the eutectoid appeared during quenching. From **Figure 3.2** to **3.19**, the detected phases were marked and the rest phase was considered as the $2CaO{\cdot}SiO_2$-$3CaO{\cdot}P_2O_5$ solid solution.

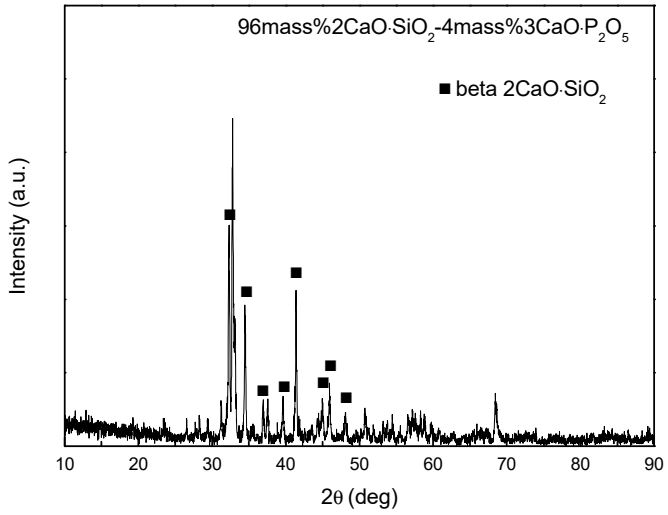

Fig. 3.2 XRD pattern of the 96mass%$2CaO{\cdot}SiO_2$-4mass%$3CaO{\cdot}P_2O_5$ solid solution.

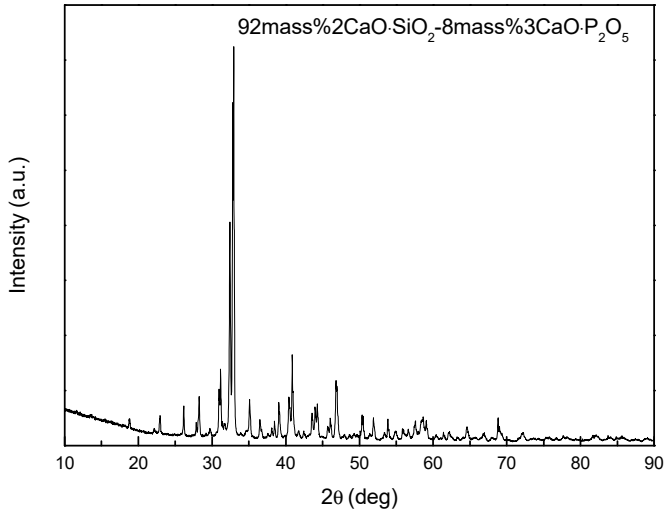

Fig. 3.3 XRD pattern of the 92mass%$2CaO{\cdot}SiO_2$-8mass%$3CaO{\cdot}P_2O_5$ solid solution.

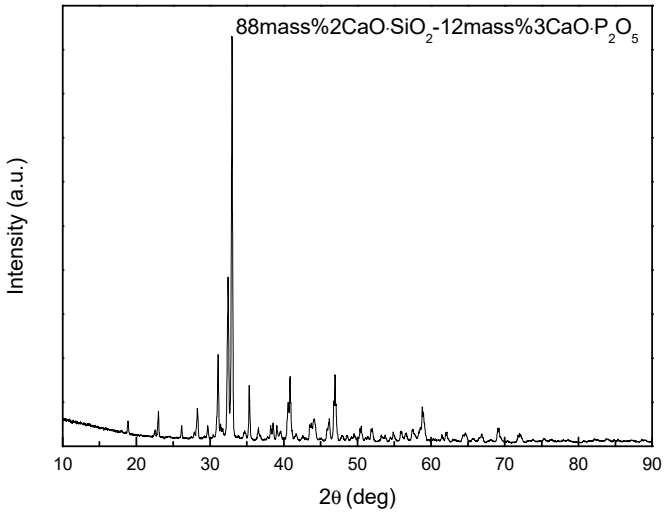

Fig. 3.4 XRD pattern of the 88mass%2CaO·SiO_2-12mass%3CaO·P_2O_5 solid solution.

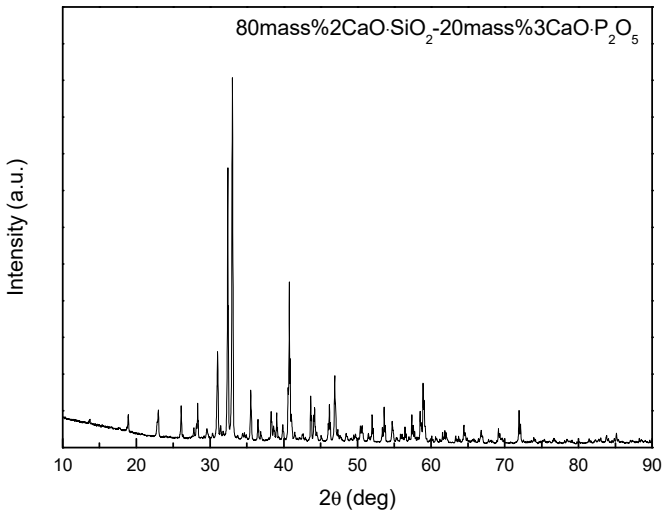

Fig. 3.5 XRD pattern of the 80mass%2CaO·SiO_2-20mass%3CaO·P_2O_5 solid solution.

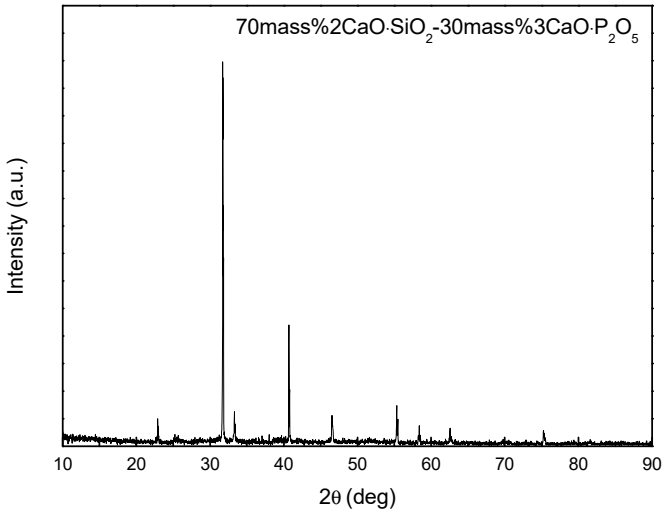

Fig. 3.6 XRD pattern of the 70mass%2CaO·SiO_2-30mass%3CaO·P_2O_5 solid solution.

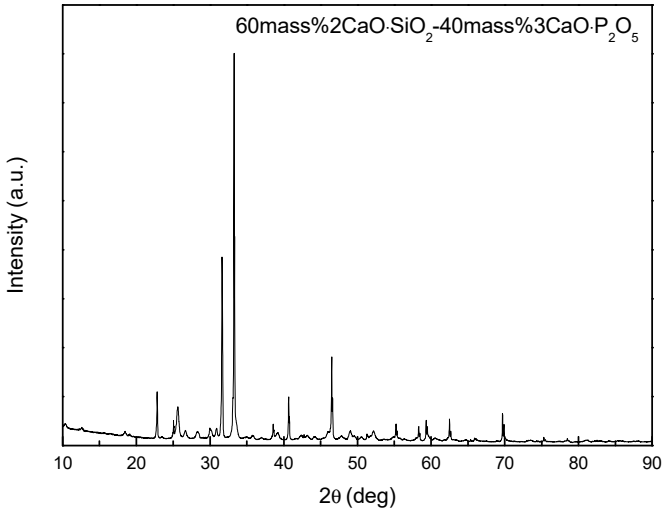

Fig. 3.7 XRD pattern of the 60mass%2CaO·SiO_2-40mass%3CaO·P_2O_5 solid solution.

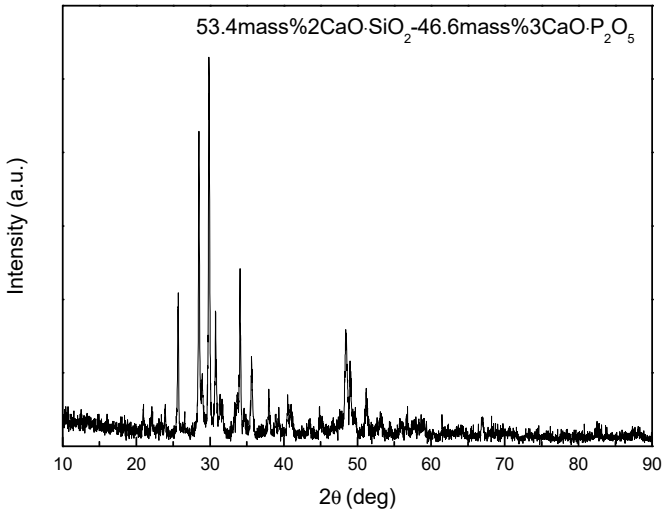

Fig. 3.8 XRD pattern of the 53.4mass%2CaO·SiO_2-46.6mass%3CaO·P_2O_5 solid solution.

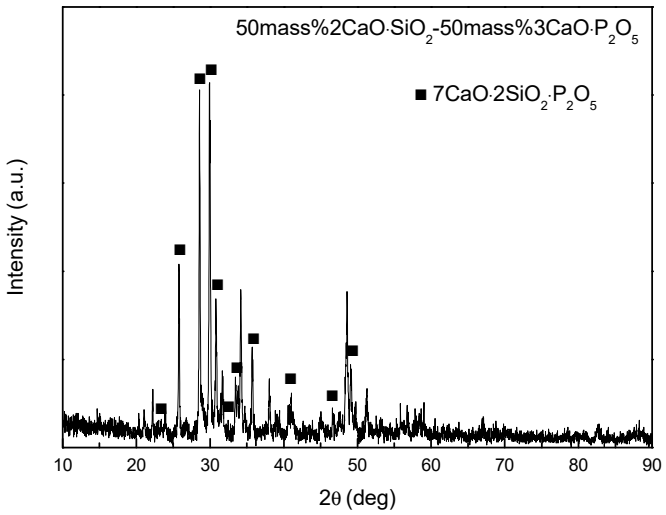

Fig. 3.9 XRD pattern of the 50mass%2CaO·SiO_2-50mass%3CaO·P_2O_5 solid solution.

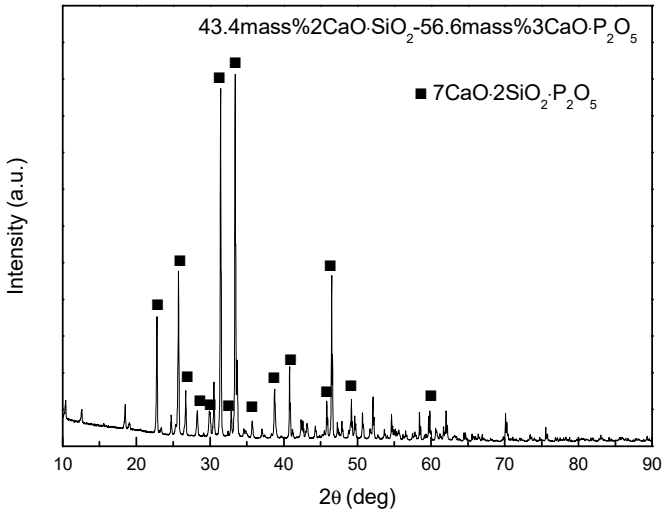

Fig. 3.10 XRD pattern of the 43.4mass%2CaO·SiO_2-56.6mass%3CaO·P_2O_5 solid solution.

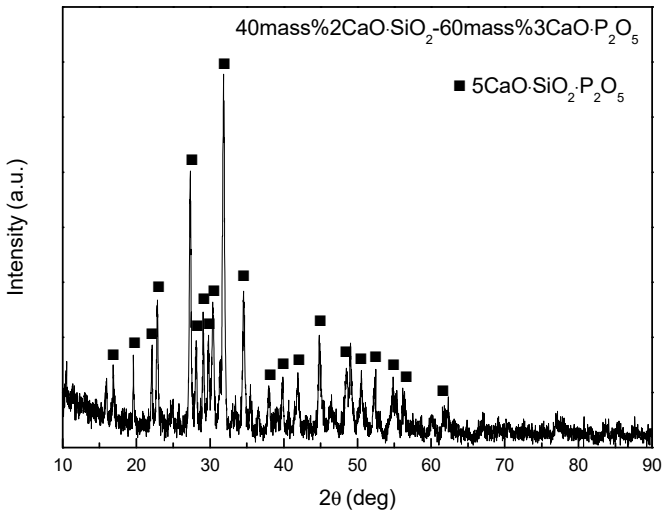

Fig. 3.11 XRD pattern of the 40mass%2CaO·SiO_2-60mass%3CaO·P_2O_5 solid solution.

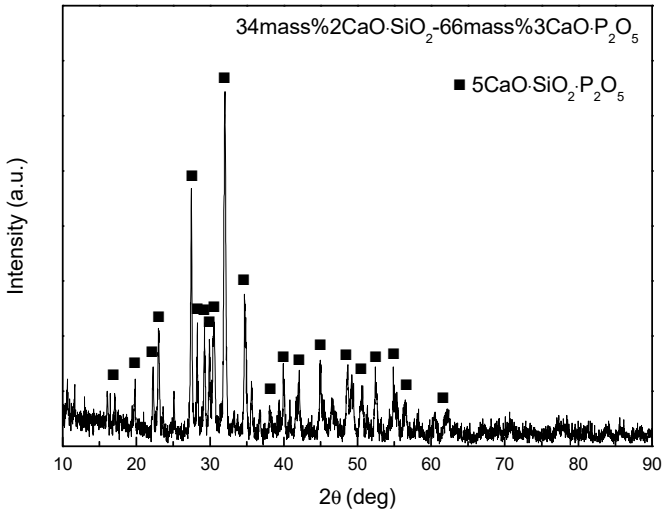

Fig. 3.12 XRD pattern of the 34mass%2CaO·SiO_2-66mass%3CaO·P_2O_5 solid solution.

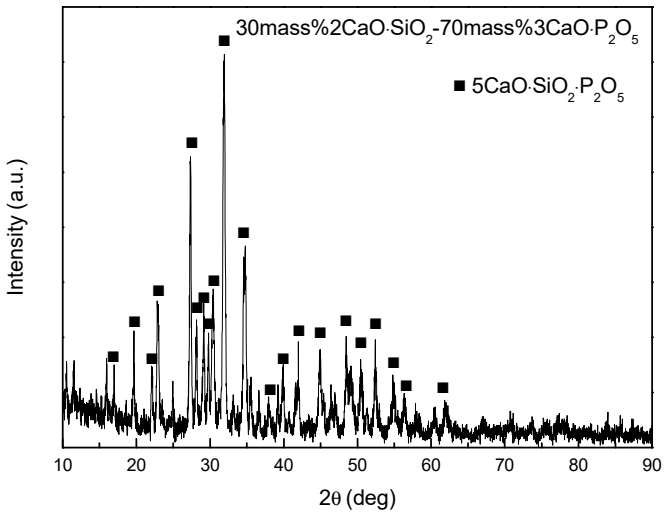

Fig. 3.13 XRD pattern of the 30mass%2CaO·SiO_2-70mass%3CaO·P_2O_5 solid solution.

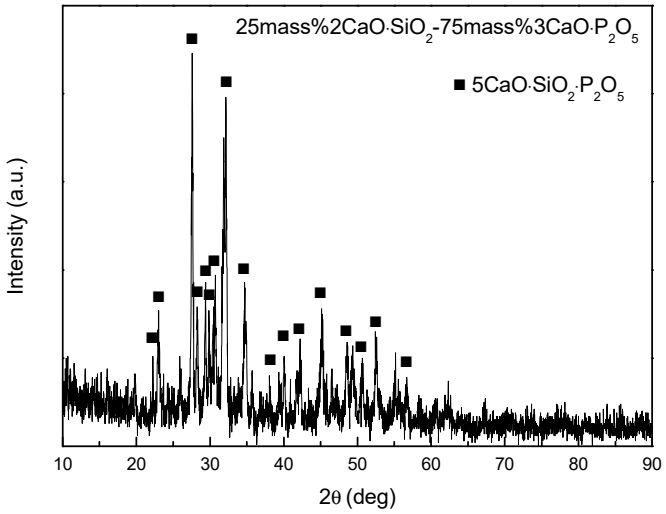

Fig. 3.14 XRD pattern of the 25mass%2CaO·SiO_2-75mass%3CaO·P_2O_5 solid solution.

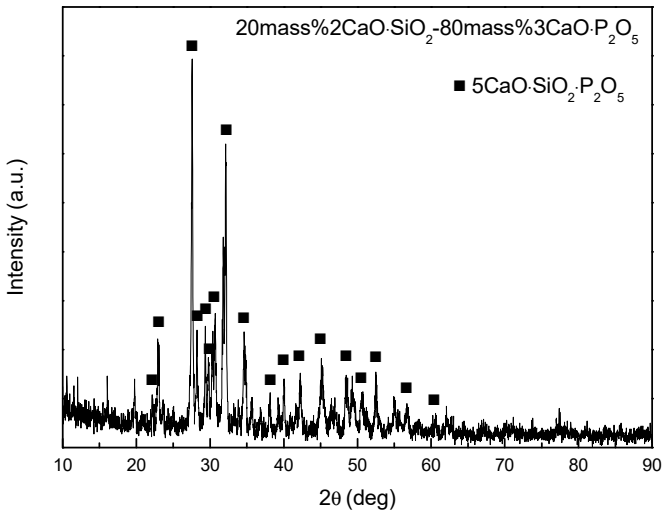

Fig. 3.15 XRD pattern of the 20mass%2CaO·SiO_2-80mass%3CaO·P_2O_5 solid solution.

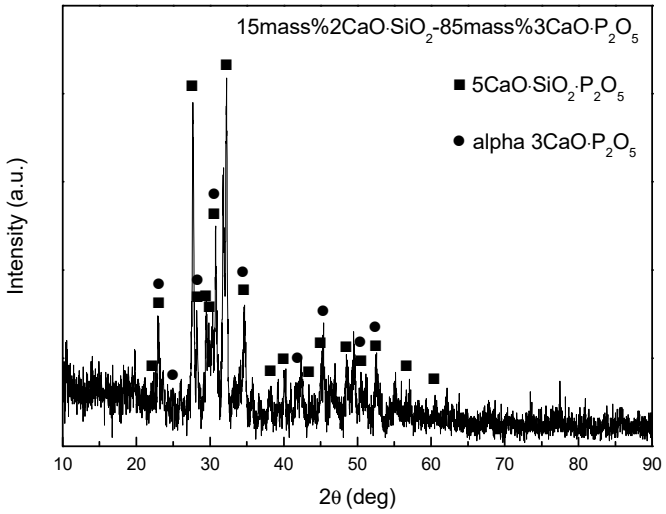

Fig. 3.16 XRD pattern of the 15mass%2CaO·SiO_2-85mass%3CaO·P_2O_5 solid solution.

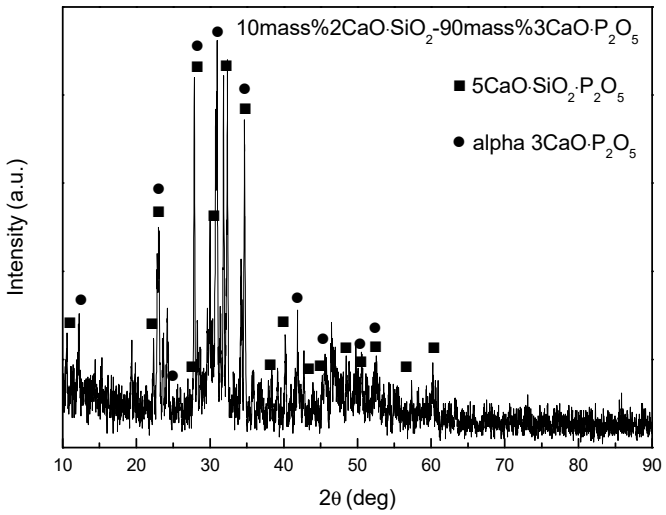

Fig. 3.17 XRD pattern of the 10mass%2CaO·SiO_2-90mass%3CaO·P_2O_5 solid solution.

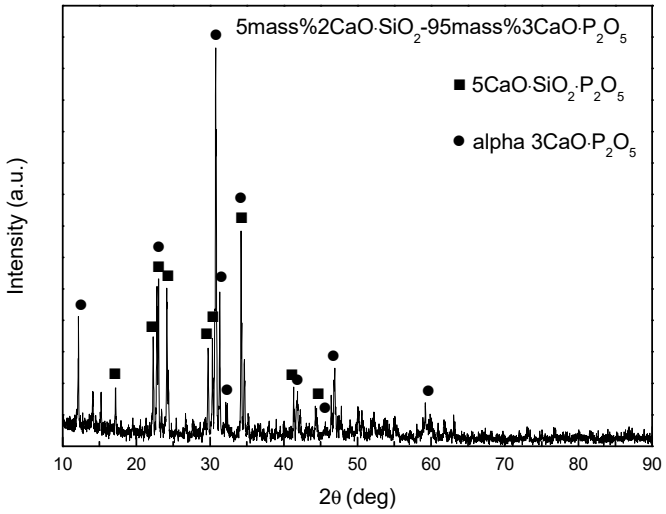

Fig. 3.18 XRD pattern of the 5mass%2CaO·SiO_2-95mass%3CaO·P_2O_5 solid solution.

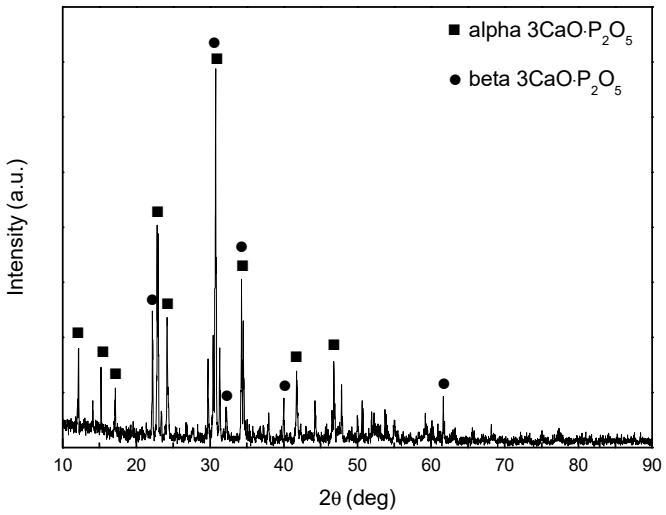

Fig. 3.19 XRD pattern of the pure 3CaO·P_2O_5.

3.3.3 XRD pattern of the $2CaO{\cdot}SiO_2$-$3CaO{\cdot}P_2O_5$ solid solution after reaction

The phases of tablet after reaction were analyzed by XRD as shown from **Figures 3.20** to **3.42**. The XRD pattern after reaction was almost the same comparing with that before reaction. For some samples, the MgO phase was detected since the tablets were contaminated with the MgO crucible particles during separate from the solidified steel in the MgO crucible.

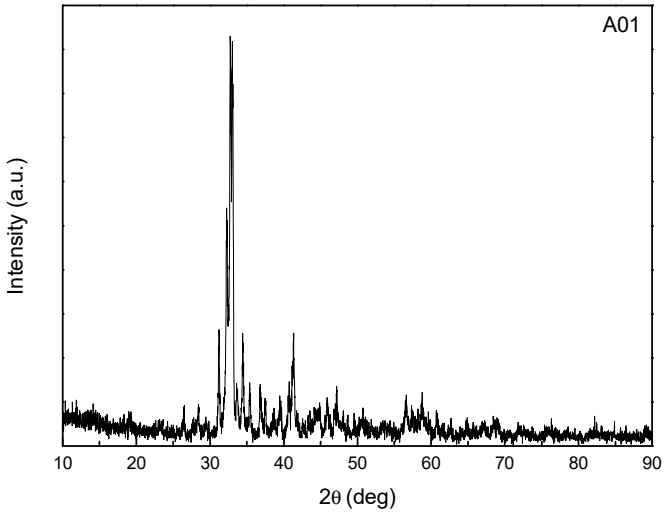

Fig. 3.20 XRD pattern of sample A01 after reaction.

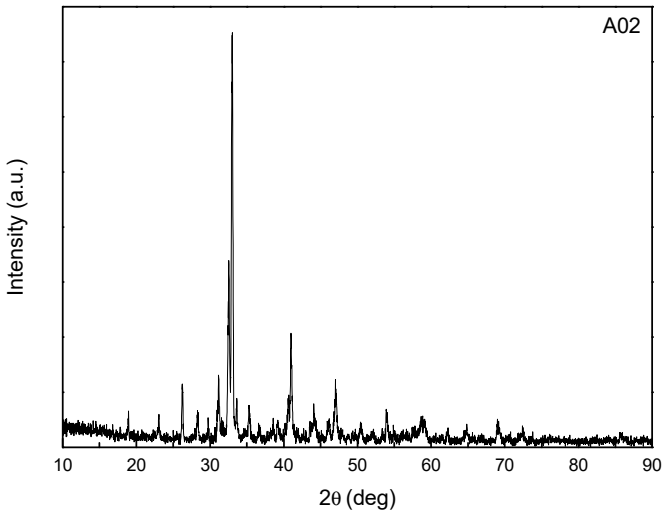

Fig. 3.21 XRD pattern of sample A02 after reaction.

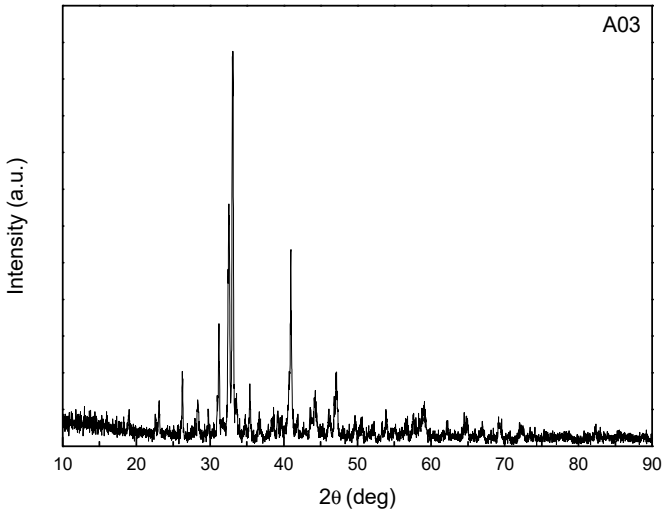

Fig. 3.22 XRD pattern of sample A03 after reaction.

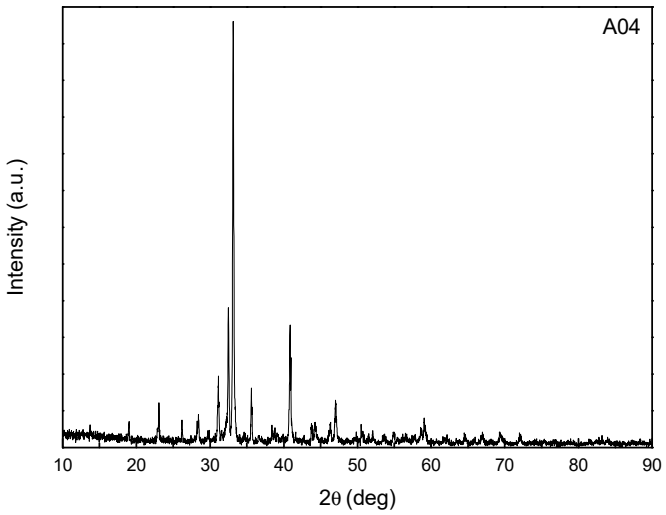

Fig. 3.23 XRD pattern of sample A04 after reaction.

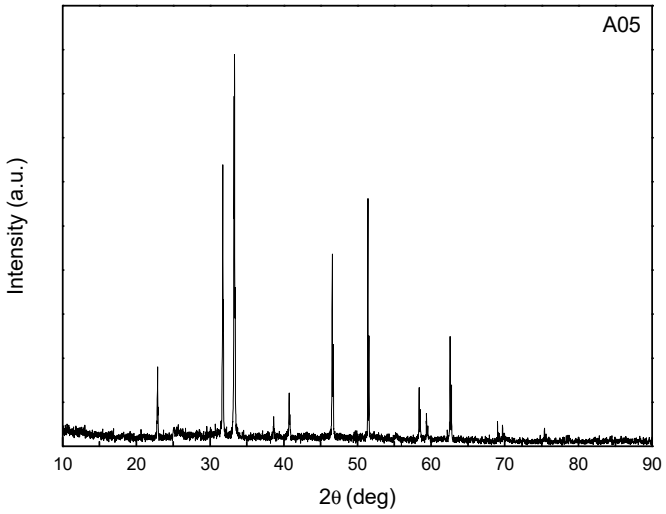

Fig. 3.24 XRD pattern of sample A05 after reaction.

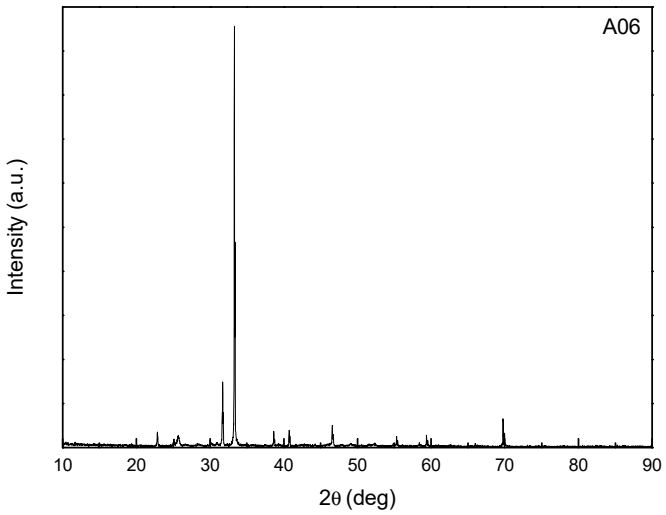

Fig. 3.25 XRD pattern of sample A06 after reaction.

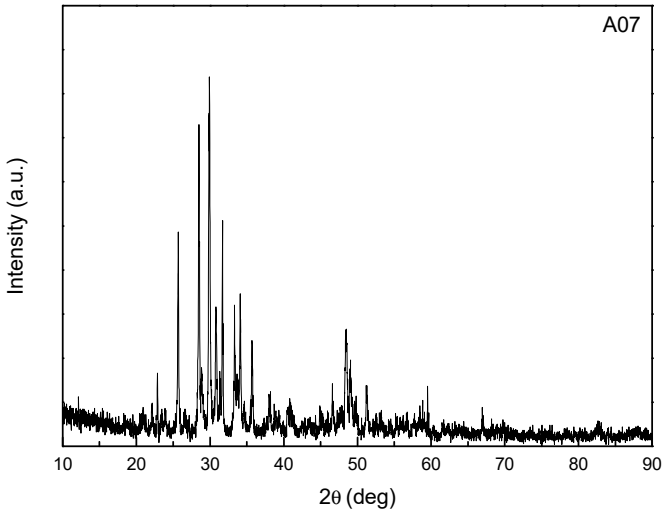

Fig. 3.26 XRD pattern of sample A07 after reaction.

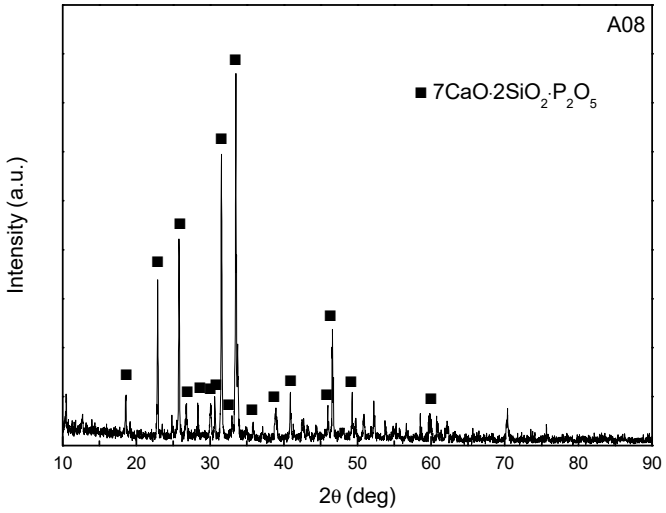

Fig. 3.27 XRD pattern of sample A08 after reaction.

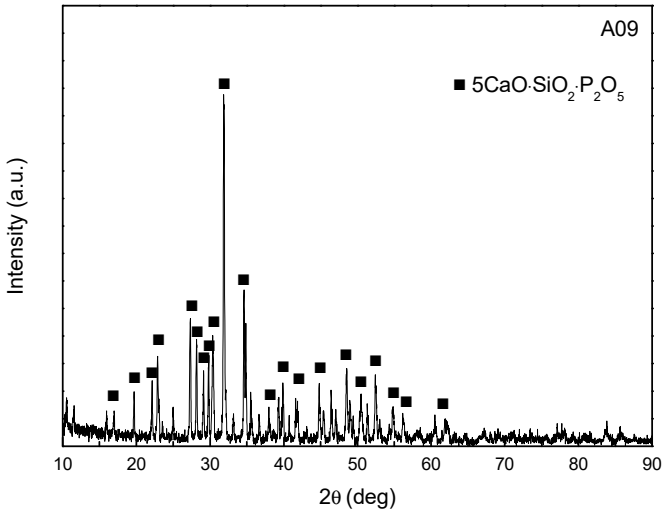

Fig. 3.28 XRD pattern of sample A09 after reaction.

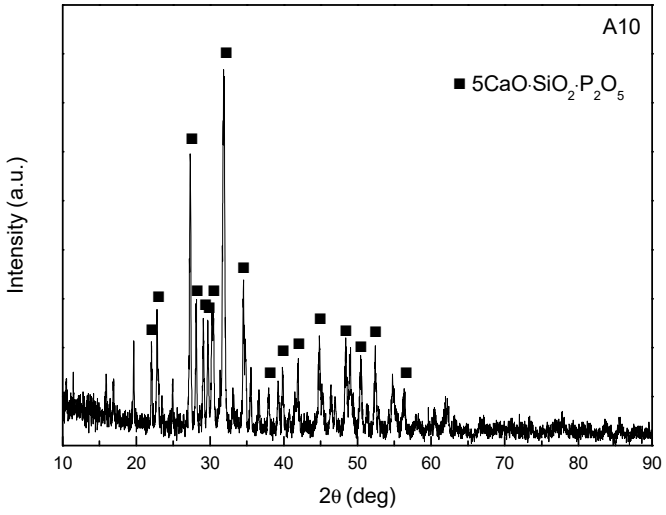

Fig. 3.29 XRD pattern of sample A10 after reaction.

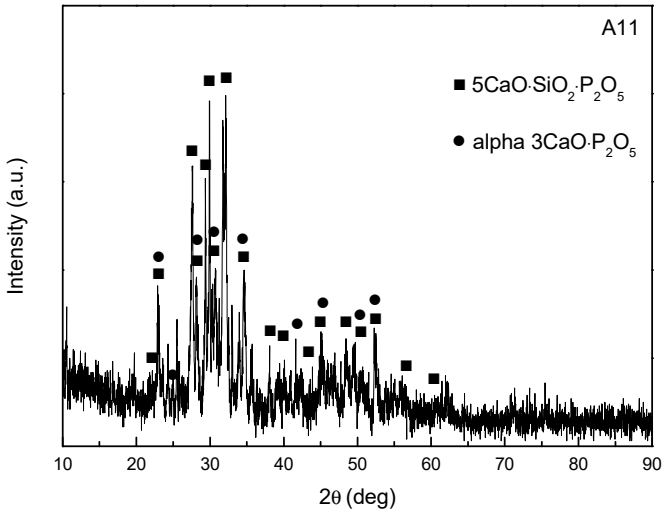

Fig. 3.30 XRD pattern of sample A11 after reaction.

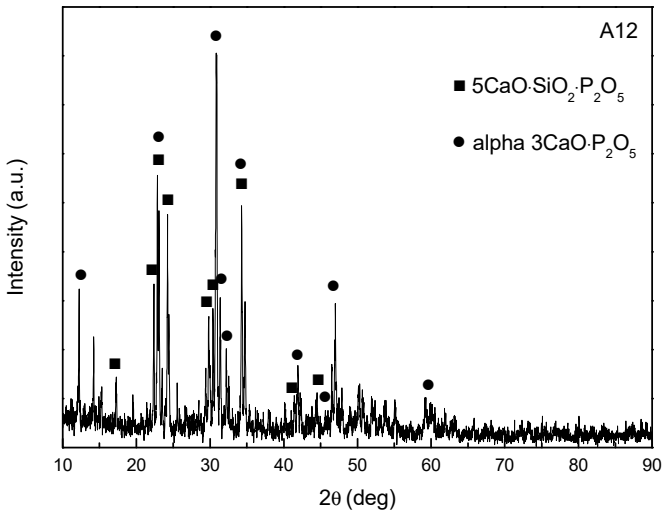

Fig. 3.31 XRD pattern of sample A12 after reaction.

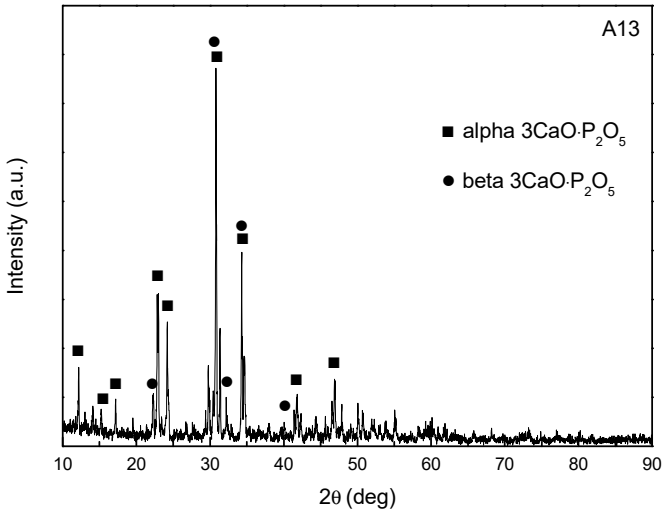

Fig. 3.32 XRD pattern of sample A13 after reaction.

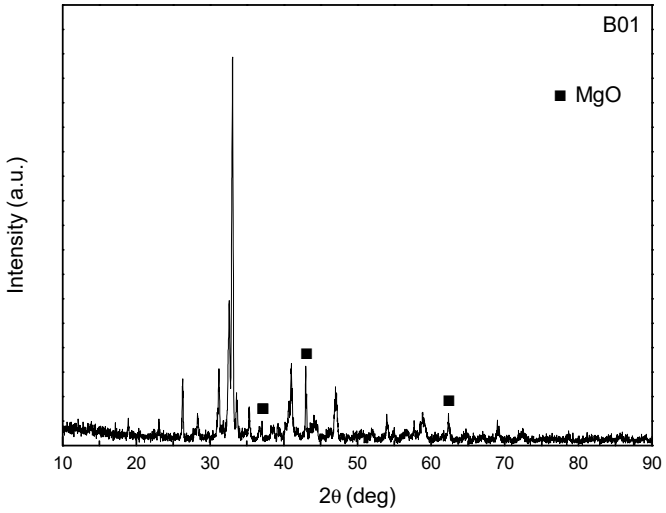

Fig. 3.33 XRD pattern of sample B01 after reaction.

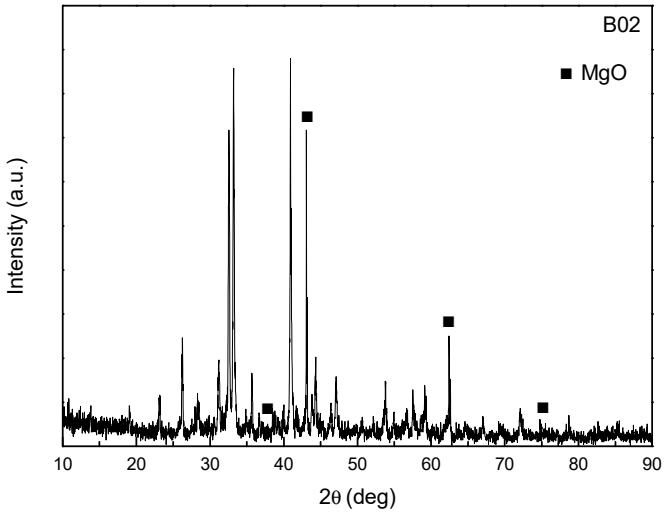

Fig. 3.34 XRD pattern of sample B02 after reaction.

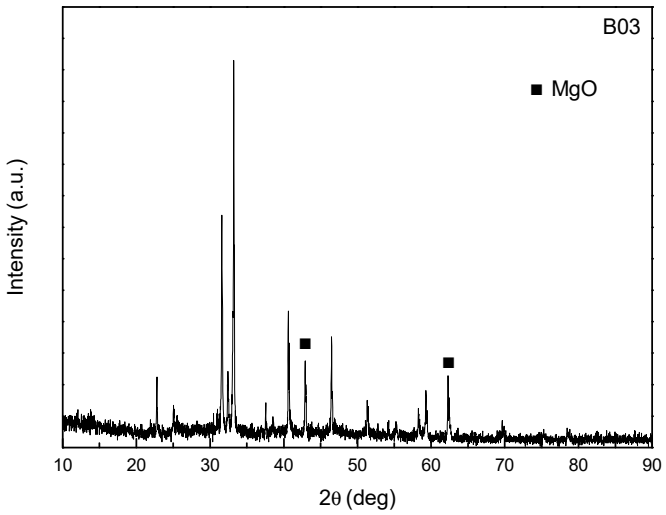

Fig. 3.35 XRD pattern of sample B03 after reaction.

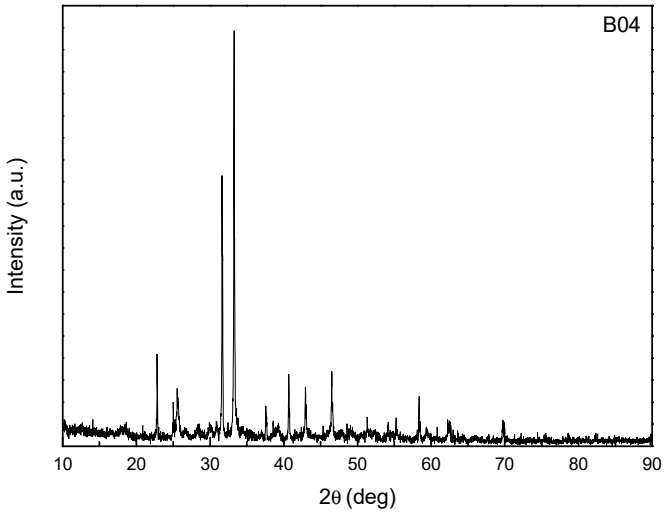

Fig. 3.36 XRD pattern of sample B04 after reaction.

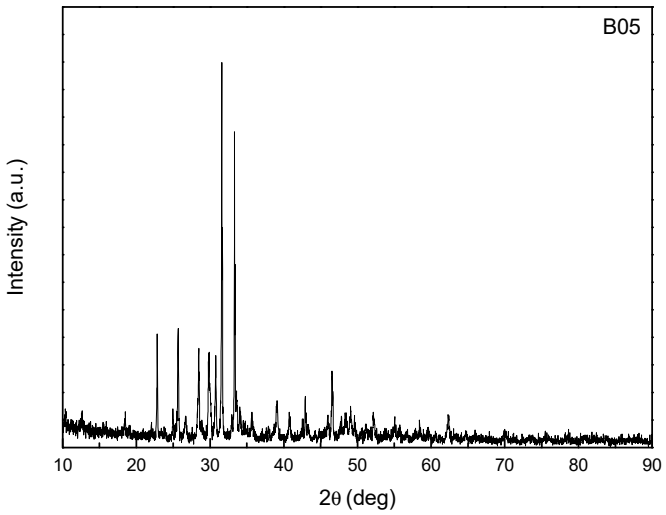

Fig. 3.37 XRD pattern of sample B05 after reaction.

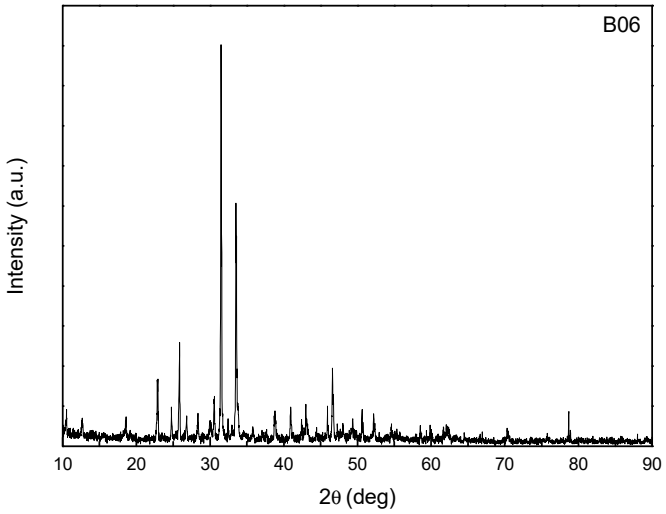

Fig. 3.38 XRD pattern of sample B06 after reaction.

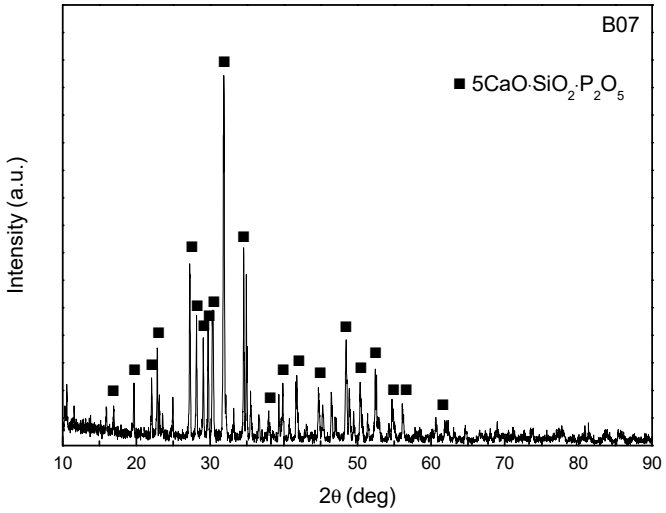

Fig. 3.39 XRD pattern of sample B07 after reaction.

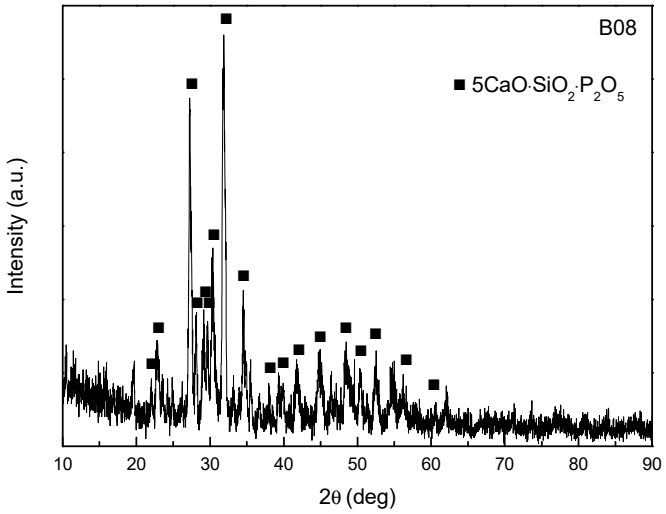

Fig. 3.40 XRD pattern of sample B08 after reaction.

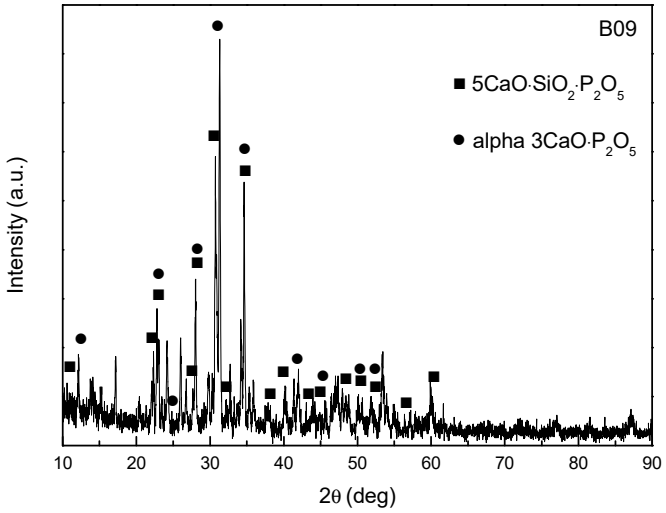

Fig. 3.41 XRD pattern of sample B09 after reaction.

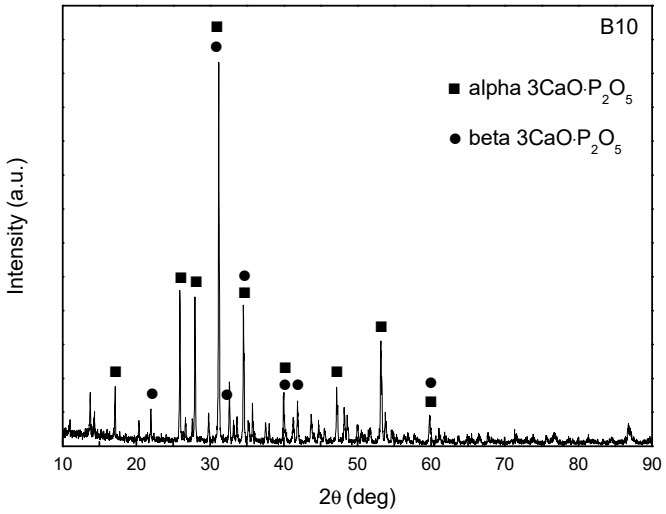

Fig. 3.42 XRD pattern of sample B10 after reaction.

3.4 Discussion

From the analyzed compositions shown in Table 3.9, the mole fraction of $3CaO \cdot P_2O_5$, P_2O_5 and FeO after reaction were shown in **Table 3.10**. The content of $3CaO \cdot P_2O_5$ in the solid solution was calculated from the analyzed P_2O_5 content.

Table 3.10 Compositions of tablets after reaction.

No.	$3CaO \cdot P_2O_5$/mol%	P_2O_5/mol%	FeO/mol%
A01	2.3	0.734	0.170
A02	4.6	1.55	0.300
A03	7.2	2.28	0.287
A04	12.5	4.04	0.257
A05	19.4	6.14	0.432
A06	28.1	8.11	0.234
A07	32.8	9.89	0.205
A08	42.2	12.5	0.315
A09	52.6	14.6	0.271
A10	60.5	16.2	0.684
A11	75.3	19.1	2.29
A12	91.4	22.6	0.444
A13	100.0	24.3	0.485
B01	4.7	1.52	0.141
B02	12.7	4.01	0.284
B03	18.9	5.81	0.496
B04	26.5	8.00	0.281
B05	35.4	10.5	0.238
B06	46.1	12.8	0.302
B07	55.5	16.1	0.207

B08	68.2	19.2	0.285
B09	83.6	22.8	0.741
B10	100.0	26.3	0.348

The compositions were projected on the CaO-SiO_2-P_2O_5 phase diagram as shown in **Figure 3.43**. The compositions after reaction changed from the initial compositions, but no liquid phase was observed for all the samples.

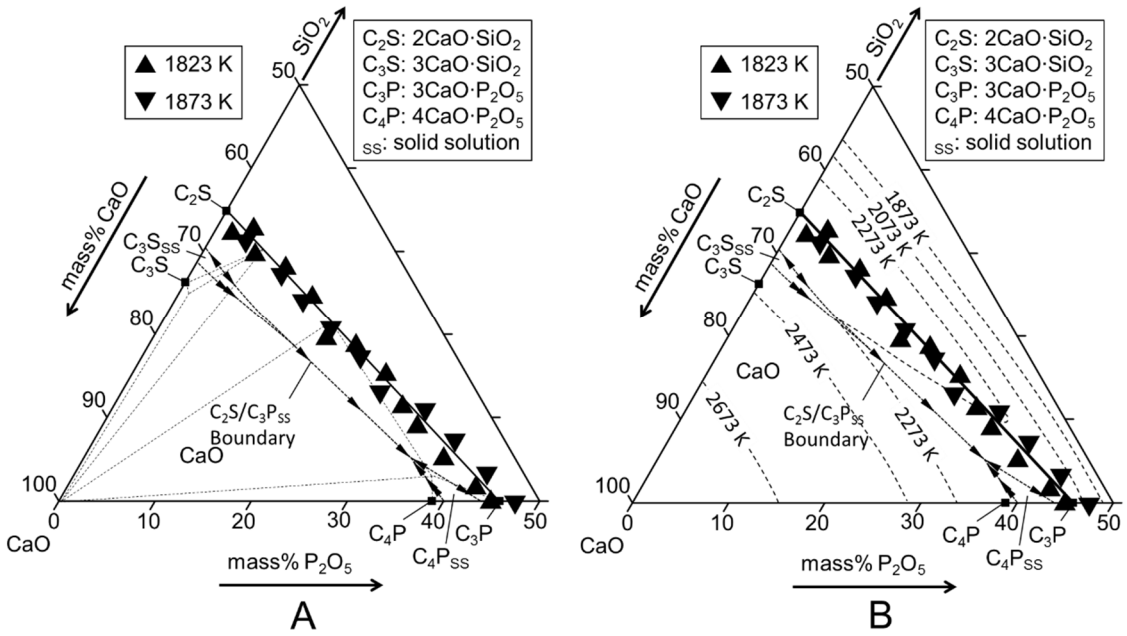

Fig. 3.43 A: Compositions of tablets after reaction on the CaO-SiO_2-P_2O_5 system.

B: Compositions of tablets after reaction on the liquidus surface of CaO-SiO_2-P_2O_5 system.[2]

3.4.1 Contents of FeO and MgO in the tablet after reaction

Figure 3.44 shows the relationship between the P_2O_5 content and the FeO and MgO contents in tablet after reaction. For most samples, the contents of FeO and MgO were smaller than 1 mass%. The contents of FeO and MgO barely changed with the increase of P_2O_5 content. Since the tablet was contaminated with more or less MgO crucible particles and metallic iron particles when the tablet was separated from the surface of solidified iron in the MgO crucible, contents of FeO and MgO were larger for some samples.

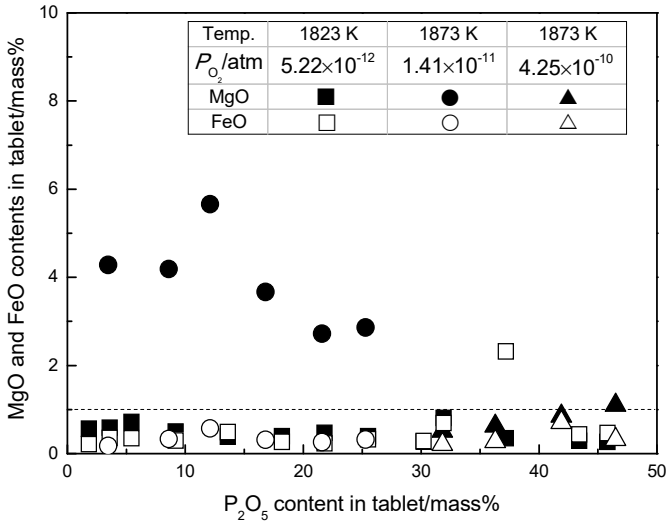

Fig. 3.44 Contents of FeO and MgO in the tablet after reaction.

3.4.2 Activity coefficient of FeO in the tablet after reaction

Since the oxygen partial pressure was controlled by the mixture of CO and CO_2 gases and the tablet was equilibrium with molten iron, the activity of FeO in the tablet was constant at a certain temperature and oxygen partial pressure. The activity of FeO was calculated by Eq. (3.1) and the oxygen partial pressure listed in Table 2.2.

$$\mathrm{FeO(l)} = \mathrm{Fe(l)} + 1/2\,\mathrm{O_2(g)}$$

$$\Delta G^{\circ}_{3.1} = 256000 - 53.68T\ \mathrm{J/mol} \ldots\ldots (3.1)^{[3]}$$

At 1823 K with the oxygen partial pressure of 5.22×10^{-12} atm, the activity of FeO relative to hypothetical pure liquid FeO is 6.72×10^{-11}. At 1873 K with the oxygen partial pressure of 1.41×10^{-11} atm, the activity of FeO is 1.74×10^{-10}. At 1873 K with the oxygen partial pressure of 4.25×10^{-10} atm, the activity of FeO is 9.51×10^{-10}. The activity coefficient of FeO was calculated and shown in **Figure 3.45** and **Table 3. 11** as a function of $3CaO{\cdot}P_2O_5$ content in the solid solution.

At a certain temperature and oxygen partial pressure, the activity coefficient of FeO was almost constant. The activity coefficient of FeO with the oxygen partial pressure of 1.41×10^{-11} atm at 1873 K was larger than that with the oxygen partial pressure of 5.22×10^{-12} atm at 1823 K and smaller than that with the oxygen partial pressure of 4.25×10^{-10} atm at 1873 K.

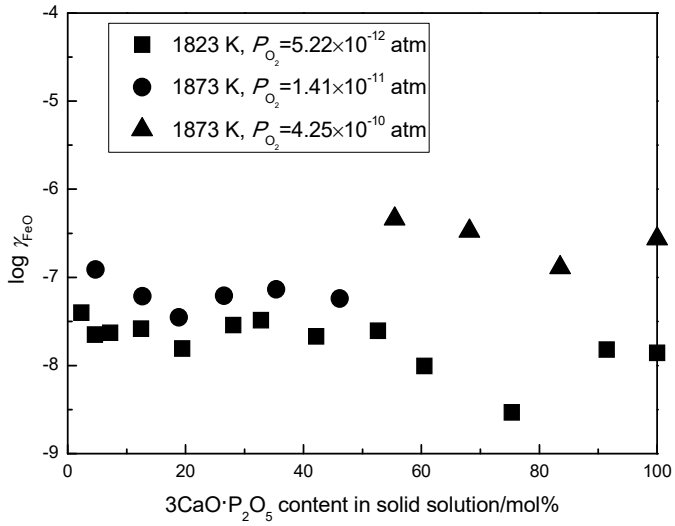

Fig. 3.45 Activity coefficient of FeO in tablet after reaction.

Table 3.11 Thermodynamic data of the $2CaO{\cdot}SiO_2$-$3CaO{\cdot}P_2O_5$ solid solution.

No.	γ_{FeO}	$\frac{(mass\%P)}{[mass\%P]}$	$a_{P_2O_5}$	$\gamma_{P_2O_5}$
A01	3.96×10^{-8}	2.84×10^{2}	2.74×10^{-25}	3.73×10^{-23}
A02	2.24×10^{-8}	5.82×10^{2}	2.86×10^{-25}	1.84×10^{-23}
A03	2.34×10^{-8}	4.76×10^{2}	9.06×10^{-25}	3.97×10^{-23}
A04	2.61×10^{-8}	5.1×10^{2}	2.4×10^{-24}	5.9×10^{-23}
A05	1.56×10^{-8}	1.0×10^{3}	1.3×10^{-24}	2.0×10^{-23}
A06	2.87×10^{-8}	6.35×10^{2}	5.59×10^{-24}	6.90×10^{-23}
A07	3.27×10^{-8}	5.36×10^{2}	1.12×10^{-23}	1.13×10^{-22}
A08	2.13×10^{-8}	4.82×10^{2}	2.09×10^{-23}	1.67×10^{-22}
A09	2.48×10^{-8}	7.34×10^{2}	1.16×10^{-23}	7.95×10^{-23}
A10	9.82×10^{-9}	1.28×10^{2}	4.97×10^{-22}	3.07×10^{-21}
A11	2.93×10^{-9}	1.27×10^{2}	6.73×10^{-22}	3.52×10^{-21}
A12	1.51×10^{-8}	1.23×10^{2}	9.46×10^{-22}	4.19×10^{-21}
A13	1.39×10^{-8}	8.85×10^{1}	2.21×10^{-21}	9.11×10^{-21}
B01	1.23×10^{-7}	8.01×10^{1}	1.45×10^{-23}	9.55×10^{-22}
B02	6.12×10^{-8}	8.22×10^{1}	9.21×10^{-23}	2.30×10^{-21}
B03	3.51×10^{-8}	5.33×10^{1}	4.70×10^{-22}	8.08×10^{-21}
B04	6.20×10^{-8}	2.99×10^{1}	3.16×10^{-21}	3.95×10^{-20}
B05	7.30×10^{-8}	1.49×10^{1}	3.09×10^{-20}	2.95×10^{-19}
B06	5.76×10^{-8}	9.29×10^{0}	2.11×10^{-19}	1.65×10^{-18}
B07	4.59×10^{-7}	1.12×10^{2}	3.10×10^{-18}	1.92×10^{-17}
B08	3.34×10^{-7}	2.93×10^{1}	9.38×10^{-17}	4.88×10^{-16}
B09	1.28×10^{-7}	1.25×10^{1}	1.79×10^{-15}	7.87×10^{-15}
B10	2.73×10^{-7}	5.89×10^{0}	8.53×10^{-14}	3.24×10^{-13}

3.4.3 Equilibrium concentration of P in molten iron

Figure 3.46 shows the relationship between the equilibrium concentration of P in molten iron and the $3CaO{\cdot}P_2O_5$ content in the solid solution. The concentration of P in Fe increased with the increase of the $3CaO{\cdot}P_2O_5$ content in the solid solution. And for a constant composition of solid solution, the equilibrium concentration of P in molten iron with the oxygen partial pressure of 1.41×10^{-11} atm at 1873 K was larger than that with the oxygen partial pressure of 5.22×10^{-12} atm at 1823 K. At 1873 K as the oxygen partial pressure changed from 1.41×10^{-11} atm to 4.25×10^{-10} atm, the equilibrium concentration of P in molten iron decreased.

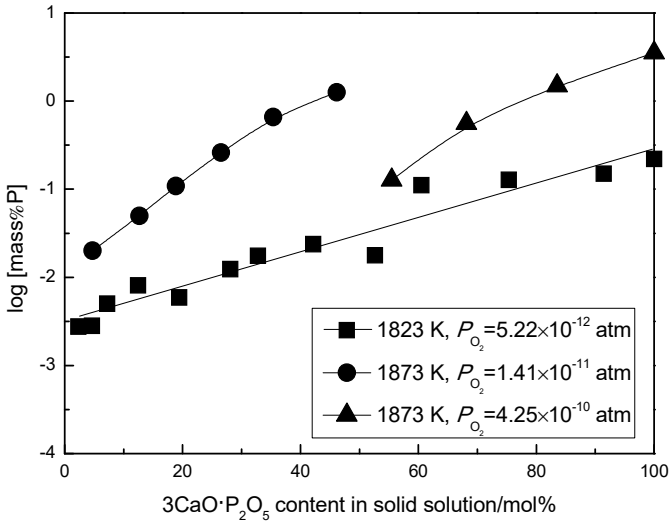

Fig. 3.46 Equilibrium concentration of P in molten iron.

3.4.4 Phosphorus partition ratio between $2CaO{\cdot}SiO_2$-$3CaO{\cdot}P_2O_5$ solid solution and molten iron

The phosphorus partition ratio between $2CaO{\cdot}SiO_2$-$3CaO{\cdot}P_2O_5$ solid solution and molten iron (mass%P)/[mass%P] was shown in Table 3.11. **Figure 3.47** shows the relationship between the phosphorus partition ratio between $2CaO{\cdot}SiO_2$-$3CaO{\cdot}P_2O_5$ solid solution and molten iron and the $3CaO{\cdot}P_2O_5$ content in the solid solution. The phosphorus partition ratios decreased with the increase of the $3CaO{\cdot}P_2O_5$ content in the solid solution at both temperatures. At 1873 K when the oxygen partial pressure changed from 1.41×10^{-11} atm to 4.25×10^{-10} atm, the phosphorus partition ratio increased.

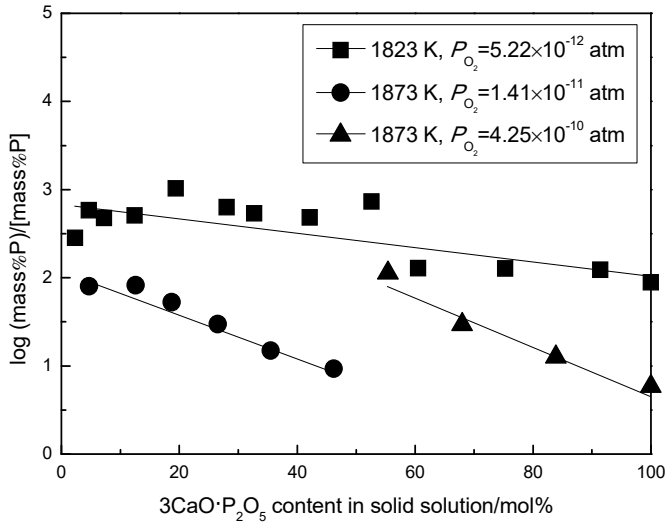

Fig. 3.47 Phosphorus partition ratio between $2CaO{\cdot}SiO_2$-$3CaO{\cdot}P_2O_5$ solid solution and molten iron.

3.4.5 Activity of P_2O_5 in the $2CaO{\cdot}SiO_2$-$3CaO{\cdot}P_2O_5$ solid solution

The activity of P_2O_5 was shown in Table 3.11. **Figure 3.48** shows the relationship between the activity of P_2O_5 relative to hypothetical pure liquid P_2O_5 in the solid solution and the $3CaO{\cdot}P_2O_5$ content. The activity of P_2O_5 increased with the increase of the $3CaO{\cdot}P_2O_5$ content in the solid solution at 1823 and 1873 K. The activity of P_2O_5 at 1873 K was larger than that at 1823 K.

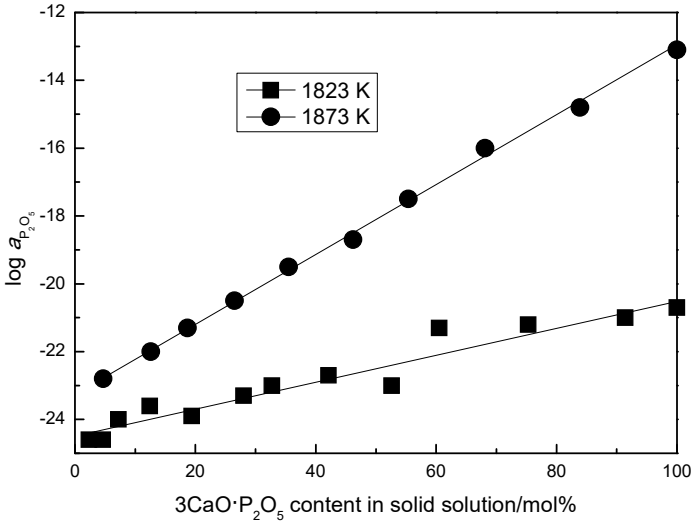

Fig. 3.48 Activity of P_2O_5 in the $2CaO{\cdot}SiO_2$-$3CaO{\cdot}P_2O_5$ solid solution.

3.4.6 Activity coefficient of P_2O_5 in the $2CaO{\cdot}SiO_2$-$3CaO{\cdot}P_2O_5$ solid solution

Figure 3.49 shows the activity coefficient of P_2O_5 in the solid solution comparing with those reported by Pahlevani *et al*.[4] and Hasegawa *et al*.[5] with the values shown in Table 3.11. In Figure 3.49, the mole fraction of P_2O_5 in Pahlevani *et al*.'s research was estimated by the analyzed contents of SiO_2, P_2O_5 and CaO. The dashed line means the pure $3CaO{\cdot}P_2O_5$ that containing 25 mol% P_2O_5. Due to the analytical error, the P_2O_5 contents for some samples were beyond 25 mol%. The activity coefficient of P_2O_5 in large $3CaO{\cdot}P_2O_5$ content region increased from about 10^{-20} to 10^{-12} when the temperature increased from 1823 K to 1873 K. At both temperatures, the activity coefficient of P_2O_5 increased with the increase of P_2O_5 content in the solid solution. On the contrary, Pahlevani *et al*. reported that the activity coefficient of P_2O_5 measured at 1673 and 1573 K showed no obvious difference. The activity coefficient of P_2O_5 in the solid solution was between 10^{-17} and 10^{-13}. Comparing with the values reported by Pahlevani *et al*., the current values were smaller. Besides, the activity coefficient of P_2O_5 calculated according to the activity of P_2O_5 measured by Hasegawa *et al*. at 1573 K increased with the increase of P_2O_5 content in the solid solution and the current values were larger than those because of the higher temperature.

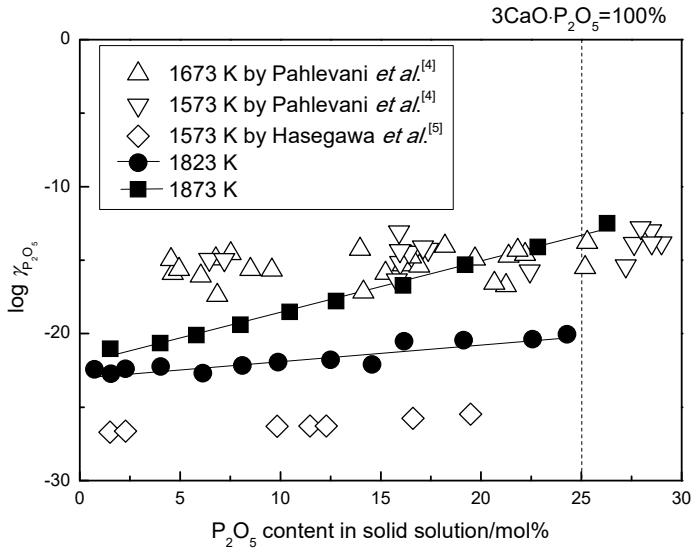

Fig. 3.49 Activity coefficient of P_2O_5 in the $2CaO{\cdot}SiO_2$-$3CaO{\cdot}P_2O_5$ solid solution.

3.5 Summary

By applying chemical equilibration method, the equilibrium of phosphorus between the $2CaO{\cdot}SiO_2$-$3CaO{\cdot}P_2O_5$ solid solution tablet and liquid iron has been measured at 1823 and 1873 K with the oxygen partial pressure of 5.22×10^{-12} atm or 1.41×10^{-11} atm or 4.25×10^{-10} atm. After reaction, the contents of MgO and FeO in tablet were less than 1 mass% for most samples. At a certain temperature and oxygen partial pressure, the activity coefficient of FeO was constant. The equilibrium concentration of P in molten iron increased with the increase of the $3CaO{\cdot}P_2O_5$ content in the solid solution. The phosphorus partition ratio between $2CaO{\cdot}SiO_2$-$3CaO{\cdot}P_2O_5$ solid solution and molten iron decreased with the increase of the $3CaO{\cdot}P_2O_5$ content in the solid solution. The activity of P_2O_5 relative to hypothetical pure liquid in the $2CaO{\cdot}SiO_2$-$3CaO{\cdot}P_2O_5$ solid solution changed from 2.74×10^{-25} to 2.21×10^{-21} at 1823 K and from 1.45×10^{-23} to 8.53×10^{-14} at 1873 K with the increase of the $3CaO{\cdot}P_2O_5$ content in the solid solution. The activity coefficient of P_2O_5 in the $2CaO{\cdot}SiO_2$-$3CaO{\cdot}P_2O_5$ solid solution changed from 1.84×10^{-23} to 9.11×10^{-21} at 1823 K and from 9.55×10^{-22} to 3.24×10^{-13} at 1873 K with the increase of the $3CaO{\cdot}P_2O_5$ content in the solid solution.

References

1. W. Gutt: *Nature*, **197** (1963), 142-143.
2. Drewes, E.-J.,M. Olette: *Arch. Eisenhüttenwes.*, **30** (1977), 163-175.
3. E.T. Turkdogan: Physical Chemistry of High Temperature Technology, Academic Press, New York, (1980), 7.
4. F. Pahlevani, S. Kitamura, H. Shibata and N. Maruoka: *ISIJ Int.*, **50** (2010), 822-829.
5. M. Hasegawa, Y. Kashiwaya and M. Iwase: *High Temp. Mater. Proc.*, **31** (2012), 421-430.

Chapter 4 Thermodynamic Properties of the $2CaO·SiO_2$-$3CaO·P_2O_5$ Solid Solution Containing 8 and 24 mass% CaO at 1823 and 1873 K

4.1 Introduction

Since the excess lime is added into slag for a better effect in practical dephosphorization process, it is necessary to study the thermodynamic properties of the $2CaO·SiO_2$-$3CaO·P_2O_5$ solid solution saturated with CaO. In this chapter, the thermodynamic properties of the $2CaO·SiO_2$-$3CaO·P_2O_5$ solid solution containing 8 and 24 mass% CaO at 1823 and 1873 K were measured and discussed.

4.2 Experimental conditions

The initial compositions of tablets were the $2CaO·SiO_2$-$3CaO·P_2O_5$ solid solution containing 8 and 24 mass% CaO as shown in **Table 4.1** and **Figure 4.1**. In Figure 4.1, the tablets with the compositions marked by open circles turned into slag after reaction at 1873 K and the compositions of slag were analyzed by SEM and EDS. The initial conditions of experiments are shown in **Table 4.2**.

Table 4.1 Initial compositions of tablets.

No.	CaO /mass%	SiO_2 /mass%	P_2O_5 /mass%	$2CaO·SiO_2$ /mass%	$3CaO·P_2O_5$ /mass%	CaO /mass%
C01	71.8	21.2	7.0	60.8	15.2	24
C02	70.2	15.9	13.9	45.6	30.4	24
C03	68.5	10.6	20.9	30.4	45.6	24
C04	66.9	5.3	27.8	15.2	60.8	24
C05	66.0	2.7	31.3	7.6	68.4	24
D01	71.8	21.2	7.0	60.8	15.2	24

D02	70.2	15.9	13.9	45.6	30.4	24
D03	68.5	10.6	20.9	30.4	45.6	24
D04	66.9	5.3	27.9	15.2	60.8	24
D05	66.0	2.7	31.3	7.6	68.4	24
E01	65.9	25.7	8.4	73.6	18.4	8
E02	63.9	19.2	16.9	55.2	36.8	8
E03	61.9	12.8	25.3	36.8	55.2	8
E04	59.9	6.4	33.7	18.4	73.6	8
E05	58.9	3.2	37.9	9.2	82.8	8
F01	65.9	25.7	8.4	73.6	18.4	8
F02	63.9	19.2	16.9	55.2	36.8	8
F03	61.9	12.8	25.3	36.8	55.2	8
F04	59.9	6.4	33.7	18.4	73.6	8
F05	58.9	3.2	37.9	9.2	82.8	8

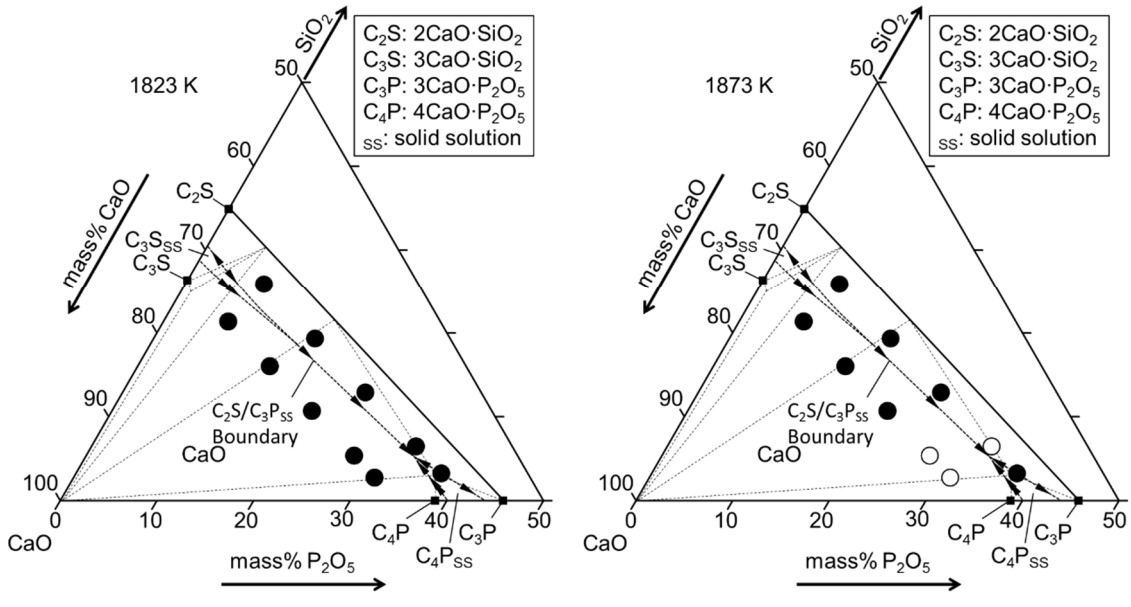

Fig. 4.1 Initial compositions of tablets on the CaO-SiO_2-P_2O_5 system. The boundary and tie lines in the phase diagram were determined at 1773 K by Gutt.[1]

Table 4.2 Initial conditions of experiments.

With the $2CaO{\cdot}SiO_2$-$3CaO{\cdot}P_2O_5$ solid solution containing 24 mass% CaO				
No.	Temp./K	CO/CO_2	Fe/g	Tablet/g
C01	1823	110/1	9.8661	1.4952
C02	1823	110/1	9.9741	1.5155
C03	1823	110/1	11.0208	1.5357
C04	1823	110/1	11.8368	1.3535
C05	1823	110/1	11.4988	1.5821
D01	1873	110/1	10.5323	1.5100
D02	1873	110/1	10.4915	1.5322
D03	1873	110/1	10.0162	1.5185
D04	1873	110/1	10.7550	1.4791
D05	1873	110/1	11.3649	1.4735
With the $2CaO{\cdot}SiO_2$-$3CaO{\cdot}P_2O_5$ solid solution containing 8 mass% CaO				
No.	Temp./K	CO/CO_2	Fe/g	Tablet/g
E01	1823	110/1	11.8083	1.4959
E02	1823	110/1	9.8845	1.5342
E03	1823	110/1	11.4012	1.4815
E04	1823	110/1	11.3510	1.5311
E05	1823	110/1	10.7208	1.4228
F01	1873	110/1	9.9975	1.5200
F02	1873	110/1	9.9044	1.5163
F03	1873	110/1	11.3925	1.5170
F04	1873	110/1	11.4632	1.4610
F05	1873	110/1	11.6995	1.5046

4.3 Experimental results

4.3.1 Chemical compositions of Fe and tablet

The concentration of P in Fe, the contents of P_2O_5, SiO_2, CaO, MgO and FeO in tablet after reaction are shown from **Table 4.3** to **4.8**. In Tables 4.6, 4.7 and 4.8, the values of Test/ppm were the concentrations of Ca, Mg and Fe in the solution measured by ICP-OES. **Table 4.9** summarized the analyzed the concentration of P in Fe and the compositions of tablets.

Table 4.3 Concentration of P in Fe.

No.	Weight /mg	Dilution ratio	Cell /mm	ABS	P in Fe /mass%	Ave P /mass%
C01	1041.5	0.5	10	0.227	0.00480	0.00479
	1080.7	0.5	10	0.233	0.00477	
C02	1077.0	1	10	0.245	0.00914	0.00917
	1087.2	1	10	0.249	0.00920	
C03	1096.7	10	20	0.166	0.0157	0.0153
	1105.4	10	20	0.160	0.0149	
C04	1168.8	20	20	0.082	0.0130	0.015
	1394.0	20	20	0.113	0.0159	
C05	1045.8	20	20	0.084	0.0150	0.016
	1470.0	20	20	0.116	0.0155	
D01	1006.6	0.5	10	0.238	0.00522	0.00553
	984.1	0.5	10	0.261	0.00584	
D02	674.8	10	20	0.073	0.0095	0.0093
	610.3	10	20	0.065	0.0090	
D03	754.4	10	20	0.118	0.0154	0.0150
	655.3	10	20	0.100	0.0146	
E01	620.4	0.5	10	0.077	0.0027	0.0028

	627.2	0.5	10	0.080	0.0028	
E02	922.5	1	10	0.073	0.0035	0.0035
	1021.9	1	10	0.084	0.0035	
E03	1272.6	10	20	0.108	0.00825	0.00836
	1323.9	10	20	0.114	0.00846	
E04	1271.1	10	20	0.250	0.0212	0.0214
	1151.6	10	20	0.232	0.0216	
E05	1042.0	10	20	0.464	0.0498	0.0491
	986.7	10	20	0.429	0.0484	
F01	1275.6	1	10	0.103	0.00351	0.0036
	1124.7	1	10	0.095	0.0036	
F02	1017.0	1	10	0.154	0.00664	0.00666
	779.6	1	10	0.119	0.00667	
F03	1119.4	10	20	0.290	0.0282	0.0267
	1054.1	10	20	0.244	0.0250	
F05	975.2	10	20	0.656	0.0761	0.0734
	1113.8	10	20	0.695	0.0707	

Annotation: the analysis data was based on the calibration curve: ABS=0.8595×C_P(ppm)+0.018 for the phosphomolybdate blue spectrophotometric method, ABS=0.2252×C_P(ppm)+0.002 for the molybdenum-blue spectrophotometric solvent extraction method except sample C02. For sample C02 the calibration curve was adopted as: ABS=0.2367×C_P(ppm)+0.012. The samples tested with the 20 mm cell was analyzed by the phosphomolybdate blue spectrophotometric method. The samples tested with the 10 mm cell was analyzed by the molybdenum-blue spectrophotometric solvent extraction method.

Table 4.4 Content of P_2O_5 in tablet after reaction.

No.	Weight /mg	Dilution ratio	Cell /mm	ABS	P_2O_5 /mass%	Ave P_2O_5 /mass%

C01	101.7	100	20	0.266	6.91	6.94
	102.9	100	20	0.271	6.97	
C02	100.9	100	20	0.529	13.8	13.8
	101.4	100	20	0.529	13.7	
C03	104.2	100	20	0.794	20.5	20.6
	102.3	100	20	0.786	20.7	
C04	102.4	200	20	0.538	28.1	28.2
	103.3	200	20	0.546	28.3	
C05	102.8	200	20	0.608	31.7	31.7
	103.8	200	20	0.610	31.6	
D01	107.4	100	20	0.284	6.99	6.98
	106.4	100	20	0.280	6.97	
D02	101.0	200	20	0.261	13.7	13.8
	105.7	200	20	0.275	13.8	
D03	102.2	200	20	0.393	20.5	20.6
	102.2	200	20	0.394	20.6	
E01	107.7	100	20	0.352	8.70	8.73
	107.0	100	20	0.352	8.75	
E02	104.8	100	20	0.673	17.2	17.2
	105.3	100	20	0.671	17.1	
E03	106.5	200	20	0.527	26.5	26.5
	103.7	200	20	0.512	26.5	
E04	104.9	200	20	0.680	34.8	34.7
	103.8	200	20	0.668	34.6	
E05	104.0	250	20	0.590	38.0	38.0
	102.5	250	20	0.581	38.0	
F01	104.3	100	20	0.337	8.59	8.58
	106.1	100	20	0.342	8.57	

F02	108.3	100	20	0.691	17.2	17.2
	103.0	100	20	0.660	17.2	
F03	102.5	200	20	0.506	26.5	26.5
	103.6	200	20	0.510	26.4	
F05	104.4	250	20	0.594	38.2	38.6
	105.3	250	20	0.612	39.0	

Annotation: the results based on the calibration curve: ABS=0.8436×C_P(ppm)+0.007 except sample C02 with the calibration curve: ABS=0.8692×C_P(ppm)+0.001.

Table 4.5 Content of SiO_2 in tablet after reaction.

No.	Weight (1) /mg	Crucible /g	Weight (2) /g	Weight (3) /g	SiO_2 /mass%	Ave SiO_2 /mass%
C01	101.7	23.87524	23.89837	23.87666	21.35	21.23
	102.9	23.93771	23.95958	23.93787	21.10	
C02	100.9	23.87912	23.89431	23.87880	15.37	15.47
	101.4	23.94025	23.95547	23.93968	15.57	
C03	104.2	23.87344	23.88728	23.87635	10.49	10.68
	102.3	23.93652	23.94868	23.93757	10.86	
C04	102.4	23.87509	23.88096	23.87567	5.166	5.187
	103.3	23.93645	23.94252	23.93714	5.208	
C05	102.8	23.87444	23.87730	23.87483	2.403	2.469
	103.8	23.93582	23.93910	23.93647	2.534	
D01	107.4	23.87405	23.89688	23.87468	20.67	20.64
	106.4	23.93585	23.95829	23.93637	20.60	
D02	101.0	23.87240	23.88951	23.87254	16.80	16.49
	105.7	23.93390	23.95160	23.93450	16.18	
D03	102.2	23.87281	23.88301	23.87302	9.775	9.878

	102.2	23.93458	23.94495	23.93475	9.980	
E01	107.7	23.87136	23.89951	23.87258	25.00	25.05
	107.0	23.93406	23.96118	23.93432	25.10	
E02	104.8	23.87047	23.89158	23.87180	18.87	18.74
	105.3	23.93259	23.95305	23.93346	18.60	
E03	106.5	23.86812	23.88286	23.86840	13.58	13.63
	103.7	23.93072	23.94500	23.93082	13.67	
E04	104.9	23.86871	23.87555	23.86872	6.511	6.517
	103.8	23.93048	23.93743	23.93066	6.522	
E05	104.0	23.87168	23.87210	23.86871	3.260	3.357
	102.5	23.93367	23.93367	23.93013	3.454	
F01	104.3	23.87128	23.89862	23.87199	25.53	25.60
	106.1	23.93318	23.96101	23.93377	25.67	
F02	108.3	23.87123	23.89037	23.87163	17.30	17.41
	103.0	23.93272	23.95157	23.93353	17.51	
F03	102.5	23.86849	23.88217	23.86920	12.65	12.78
	103.6	23.92984	23.94440	23.93103	12.91	
F05	104.4	23.87128	23.87128	23.86791	3.228	3.262
	105.3	23.93292	23.93336	23.92989	3.295	

Annotation: the weight (1) is the weight of sample. The weight (2) is the weight of Pt crucible after the filter paper burned. The weight (3) is the weight of crucible after evaporating the SiO_2.

SiO_2/mass%=[weight (2) - weight (3)]/[weight (1)]×100000/%

Table 4.6 Content of CaO in tablet after reaction.

No.	Weight /mg	Dilution ratio	Test /ppm	CaO /mass%	Ave CaO /mass%

C01	101.1	100	4.953	68.54	67.98
	104.4	100	5.031	67.42	
C02	97.6	100	4.630	66.4	66.3
	98.2	100	4.642	66.1	
C03	102.0	100	4.766	65.37	65.37
	102.1	100	4.771	65.37	
C04	101.2	100	4.549	62.89	63.69
	100.8	100	4.646	64.48	
C05	102.0	100	4.589	62.94	63.45
	101.6	100	4.644	63.95	
D01	104.0	100	5.098	68.58	68.63
	101.4	100	4.977	68.67	
D02	103.5	100	5.104	68.99	67.95
	105.7	100	5.055	66.91	
D03	103.5	100	4.932	66.67	65.87
	103.1	100	4.795	65.07	
E01	106.3	100	4.734	62.30	62.17
	108.3	100	4.802	62.03	
E02	104.7	100	4.349	58.11	58.44
	106.0	100	4.452	58.76	
E03	108.2	100	4.496	58.13	58.27
	105.9	100	4.421	58.40	
E04	106.7	100	4.282	56.14	56.53
	103.0	100	4.191	56.92	
E05	103.9	100	4.304	57.95	57.80
	102.6	100	4.228	57.65	
F01	107.2	100	4.663	60.85	60.19

	105.2	100	4.476	59.52	
F02	104.7	100	4.372	58.42	57.71
	103.2	100	4.204	56.99	
F03	106.8	100	4.518	59.18	59.13
	102.7	100	4.336	59.07	
F05	103.8	100	4.190	56.47	56.85
	106.4	100	4.352	57.22	

Table 4.7 Content of MgO in tablet after reaction.

No.	Weight /mg	Dilution ratio	Test /ppm	MgO /mass%	Ave MgO /mass%
C01	101.1	1	2.972	0.4875	0.4880
	104.4	1	3.075	0.4885	
C02	97.6	1	4.565	0.776	0.771
	98.2	1	4.537	0.766	
C03	102.0	1	2.248	0.3655	0.3650
	102.1	1	2.244	0.3645	
C04	101.2	1	1.988	0.3258	0.3305
	100.8	1	2.037	0.3351	
C05	102.0	1	1.528	0.2484	0.2534
	101.6	1	1.583	0.2584	
D01	104.0	1	4.120	0.6570	0.6465
	101.4	1	3.888	0.6359	
D02	103.5	1	3.323	0.5325	0.5335
	105.7	1	3.406	0.5344	
D03	103.5	1	4.612	0.7390	0.7404
	103.1	1	4.611	0.7417	

E01	106.3	1	1.791	0.2794	0.2785
	108.3	1	1.812	0.2775	
E02	104.7	1	1.461	0.2314	0.2320
	106.0	1	1.486	0.2325	
E03	108.2	1	2.537	0.3889	0.3947
	105.9	1	2.557	0.4004	
E04	106.7	1	1.708	0.2655	0.2673
	103.0	1	1.671	0.2691	
E05	103.9	1	1.842	0.2940	0.2962
	102.6	1	1.846	0.2984	
F01	107.2	1	2.502	0.3871	0.3914
	105.2	1	2.510	0.3957	
F02	104.7	1	2.270	0.3596	0.3565
	103.2	1	2.199	0.3534	
F03	106.8	1	4.200	0.6522	0.6688
	102.7	1	4.244	0.6853	
F05	103.8	1	2.637	0.4213	0.4283
	106.4	1	2.793	0.4353	

Table 4.8 Content of FeO in tablet after reaction.

No.	Weight /mg	Dilution ratio	Test /ppm	FeO /mass%	Ave FeO /mass%
C01	101.1	1	3.042	0.3872	0.3833
	104.4	1	3.078	0.3794	
C02	97.6	1	3.329	0.439	0.416
	98.2	1	2.994	0.392	
C03	102.0	1	2.933	0.3700	0.3919

	102.1	1	3.283	0.4137	
C04	101.2	1	3.663	0.4657	0.4689
	100.8	1	3.698	0.4721	
C05	102.0	1	2.857	0.3604	0.3625
	101.6	1	2.878	0.3645	
D01	104.0	1	6.130	0.7584	0.7491
	101.4	1	5.830	0.7398	
D02	103.5	1	6.848	0.8514	0.8550
	105.7	1	7.053	0.8586	
D03	103.5	1	7.603	0.9452	0.9411
	103.1	1	7.507	0.9369	
E01	106.3	1	6.921	0.8378	0.8411
	108.3	1	7.107	0.8444	
E02	104.7	1	7.324	0.9001	0.9057
	106.0	1	7.506	0.9112	
E03	108.2	1	5.559	0.6611	0.6339
	105.9	1	4.993	0.6067	
E04	106.7	1	2.719	0.3279	0.3366
	103.0	1	2.763	0.3452	
E05	103.9	10	1.130	1.399	1.379
	102.6	10	1.084	1.359	
F01	107.2	10	1.074	1.289	1.275
	105.2	10	1.031	1.261	
F02	104.7	10	1.723	2.118	2.137
	103.2	10	1.729	2.156	
F03	106.8	1	2.019	0.2433	0.2470
	102.7	1	2.001	0.2507	

F05	103.8	1	2.487	0.3083	0.2899
	106.4	1	2.244	0.2714	

Table 4.9 Compositions of tablets and concentration of P in Fe after reaction.

No.	Solid solution/mass%						P in Fe
	P_2O_5	SiO_2	CaO	MgO	FeO	Total	/mass%
C01	6.94	21.23	67.98	0.4880	0.3833	97.0	0.00479
C02	13.8	15.47	66.3	0.771	0.416	96.8	0.00917
C03	20.6	10.68	65.37	0.3650	0.3919	97.4	0.0153
C04	28.2	5.187	63.69	0.3305	0.4689	97.9	0.015
C05	31.7	2.469	63.45	0.2534	0.3625	98.2	0.016
D01	6.98	20.64	68.63	0.6465	0.7491	97.6	0.00553
D02	13.8	16.49	67.95	0.5335	0.8550	99.6	0.0093
D03	20.6	9.878	65.87	0.7404	0.9411	98.0	0.0150
E01	8.73	25.05	62.17	0.2785	0.8411	97.1	0.0028
E02	17.2	18.74	58.44	0.2320	0.9057	95.5	0.0035
E03	26.5	13.63	58.27	0.3947	0.6339	99.4	0.00836
E04	34.7	6.517	56.53	0.2673	0.3366	98.4	0.0214
E05	38.0	3.357	57.80	0.2962	1.379	100.8	0.0491
F01	8.58	25.60	60.19	0.3914	1.275	96.0	0.0036
F02	17.2	17.41	57.71	0.3565	2.137	94.8	0.00666
F03	26.5	12.78	59.13	0.6688	0.2470	99.3	0.0267
F05	38.6	3.262	56.85	0.4283	0.2899	99.4	0.0734

4.3.2 Slag compositions for the samples with the tablet turned into slag after reaction.

The slag compositions for the samples with the tablet turned into slag after reaction as shown in Figure 4.1 marked by the open circles were measured by SEM and EDS. No obvious boundary was observed because of the resolution limit. The slag compositions analyzed by SEM and EDS were shown in **Table 4.10** and projected onto the liquidus surface of the CaO-SiO_2-P_2O_5 system as shown in **Figure 4.2**. There was no dependency between the content of P_2O_5 and the contents of MgO and FeO as shown in **Figure 4.3**. Both solid phase and liquid phase were detected and meanwhile the saturated amount of CaO was detected. Since the lack phase relationship for these three compositions, the further discussion was not conducted in the following content.

Table 4.10 Slag compositions of the samples D04, D05 and F04.

No.	P_2O_5/mass%	SiO_2/mass%	CaO/mass%	MgO/mass%	FeO/mass%
D04-01	19.1	4.8	76.1	0.0	0.0
D04-02	20.7	13.2	61.5	0.0	4.6
D04-03	28.4	5.4	58.7	1.6	5.9
D04-04	36.1	4.8	58.3	0.0	0.8
D04-05	31.9	7.7	58.7	0.5	1.2
D04-06	18.5	7.5	67.2	0.1	6.7
D04-07	38.8	0.0	61.0	0.2	0.0
D04-08	32.2	16.2	51.3	0.3	0.0
D04-09	34.4	0.1	64.2	0.0	1.3
D04-10	24.3	10.2	54.8	2.1	8.6
D04-11	32.0	4.7	58.7	1.2	3.4
D04-12	37.8	6.7	52.8	0.2	2.5
D05-01	32.2	0.0	65.1	0.9	1.8
D05-02	36.0	10.5	53.0	0.0	0.5

D05-03	31.4	11.8	52.1	2.1	2.6
D05-04	21.4	2.7	73.5	1.8	0.6
D05-05	26.4	0.5	71.9	1.2	0.0
D05-06	0.0	0.1	87.9	2.1	9.9
D05-07	33.4	1.1	63.4	2.1	0.0
D05-08	31.8	8.6	58.8	0.5	0.3
D05-09	4.4	0.2	88.2	2.6	4.6
D05-10	33.2	8.2	57.3	0.0	1.3
D05-11	0.0	1.9	90.6	0.3	7.2
D05-12	22.4	6.4	68.2	0.9	2.1
F04-01	31.1	13.0	53.4	0.6	1.9
F04-02	33.1	12.1	53.6	0.0	1.2
F04-03	33.4	12.7	53.0	0.1	0.8
F04-04	31.8	9.6	57.3	1.3	0.0
F04-05	29.2	11.7	58.5	0.6	0.0
F04-06	8.2	2.7	81.3	5.9	1.9
F04-07	0.0	1.8	88.2	1.2	8.8
F04-08	25.3	8.0	65.1	0.1	1.5
F04-09	43.5	2.8	53.7	0.0	0.0
F04-10	37.6	0.6	61.1	0.7	0.0
F04-11	40.3	1.3	56.7	1.1	0.6
F04-12	32.3	12.3	54.5	0.0	0.9

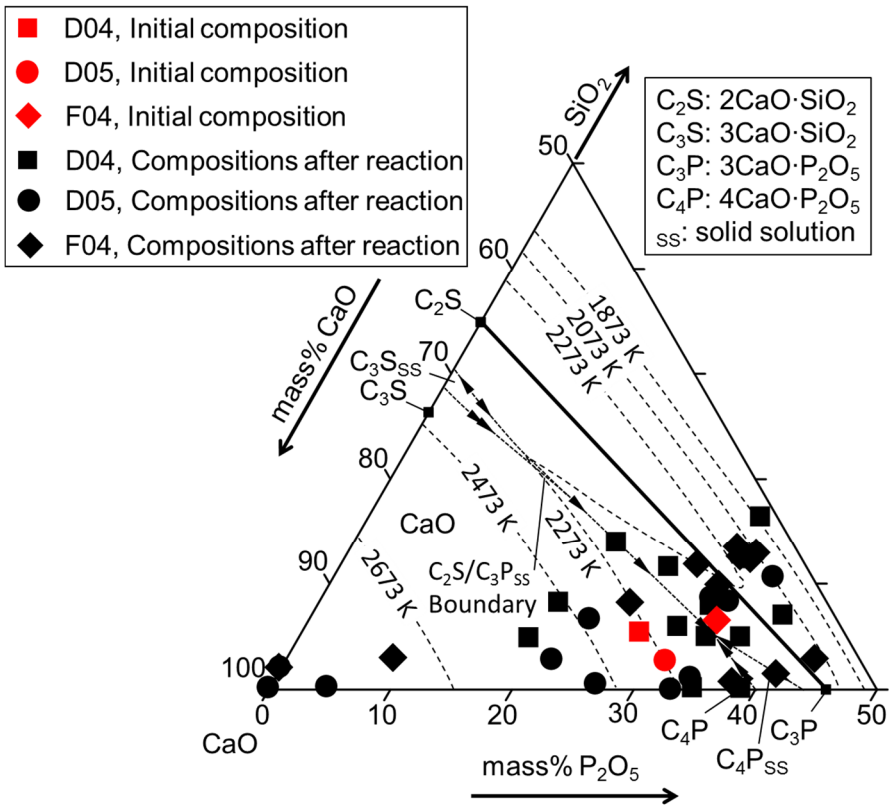

Fig. 4.2 Slag compositions of the samples D04, D05 and F04 on the liquidus surface of the CaO-SiO_2-P_2O_5 system.[2]

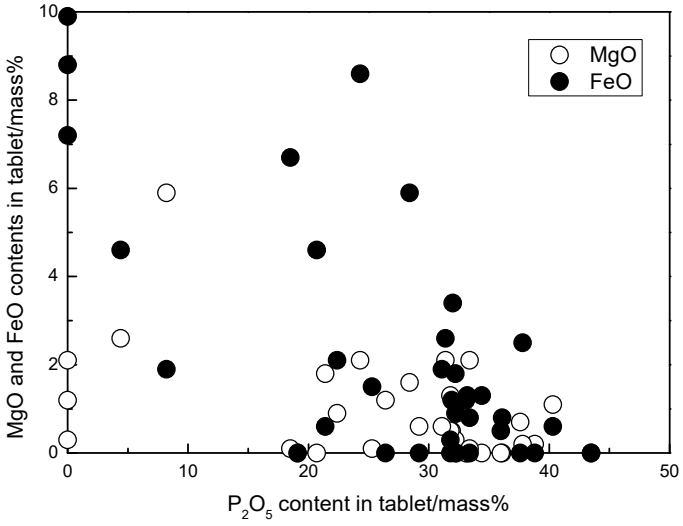

Fig. 4.3 Relationship between the content of P_2O_5 and the contents of MgO and FeO.

4.3.3 XRD pattern of the $2CaO{\cdot}SiO_2$-$3CaO{\cdot}P_2O_5$ solid solution containing 8 and 24 mass% CaO

The phases of the $2CaO{\cdot}SiO_2$-$3CaO{\cdot}P_2O_5$ solid solution containing 8 and 24 mass% CaO were analyzed by XRD as shown from **Figure 4.4** to **4.13**. In all samples, the SiO_2 and P_2O_5 phases were undetected, but the CaO phase was detected. The eutectoid appeared during quenching.

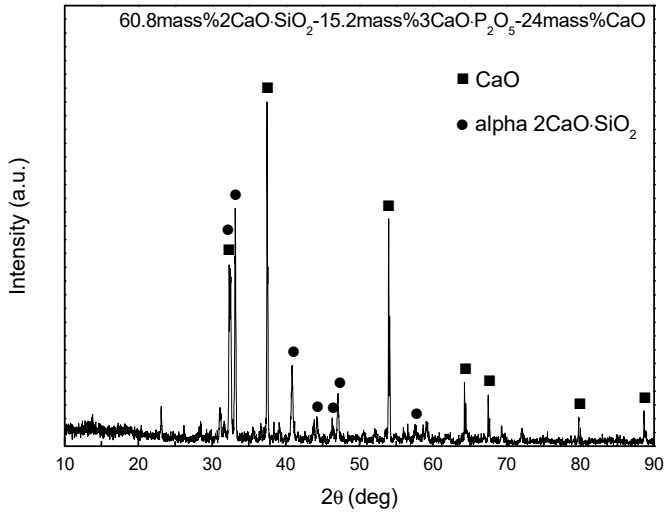

Fig. 4.4 XRD pattern of the 60.8mass%$2CaO{\cdot}SiO_2$-15.2mass%$3CaO{\cdot}P_2O_5$ solid solution-24mass%CaO.

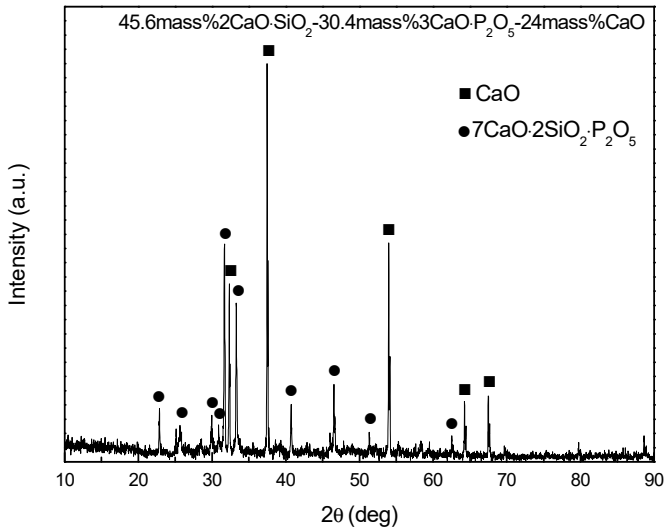

Fig. 4.5 XRD pattern of the 45.6mass%2CaO·SiO_2-30.4mass%3CaO·P_2O_5 solid solution-24mass%CaO.

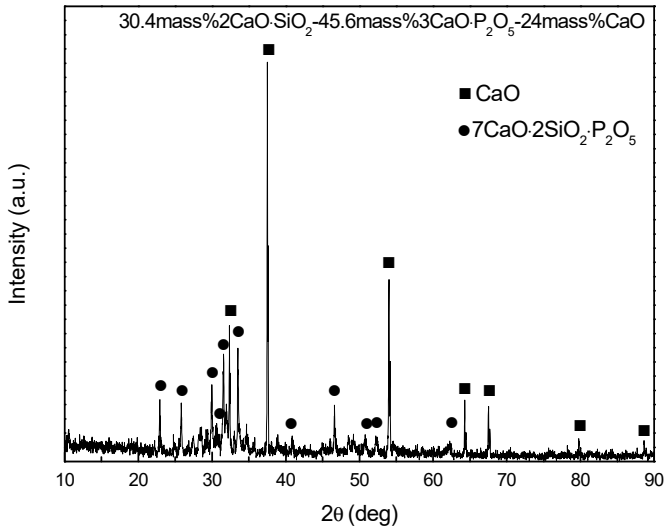

Fig. 4.6 XRD pattern of the 30.4mass%2CaO·SiO_2-45.6mass%3CaO·P_2O_5 solid solution-24mass%CaO.

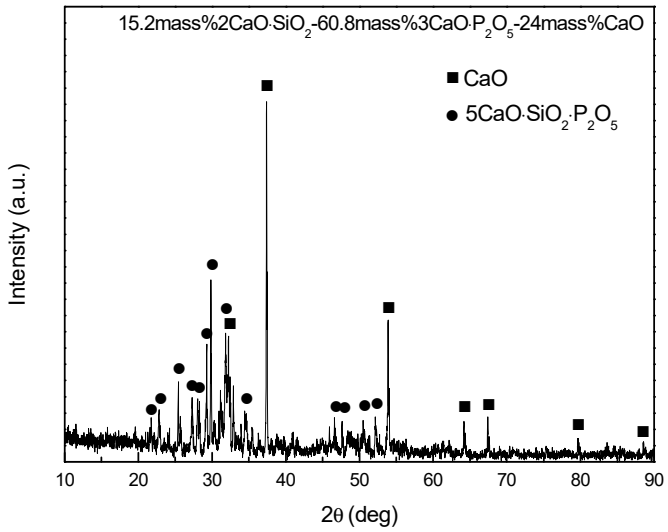

Fig. 4.7 XRD pattern of the 15.2mass%2CaO·SiO_2-60.8mass%3CaO·P_2O_5 solid solution-24mass%CaO.

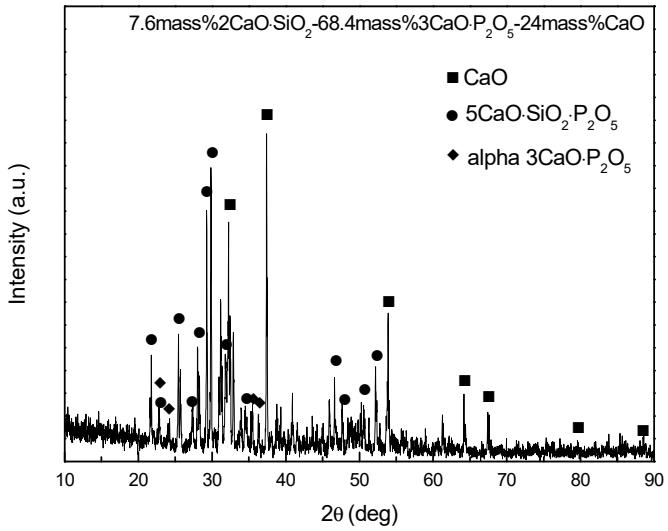

Fig. 4.8 XRD pattern of the 7.6mass%2CaO·SiO_2-68.4mass%3CaO·P_2O_5 solid solution-24mass%CaO.

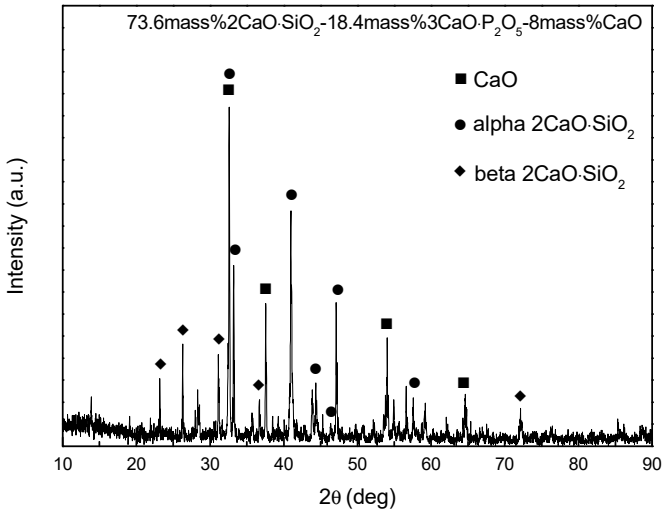

Fig. 4.9 XRD pattern of the 73.6mass%2CaO·SiO_2-18.4mass%3CaO·P_2O_5 solid solution-8mass%CaO.

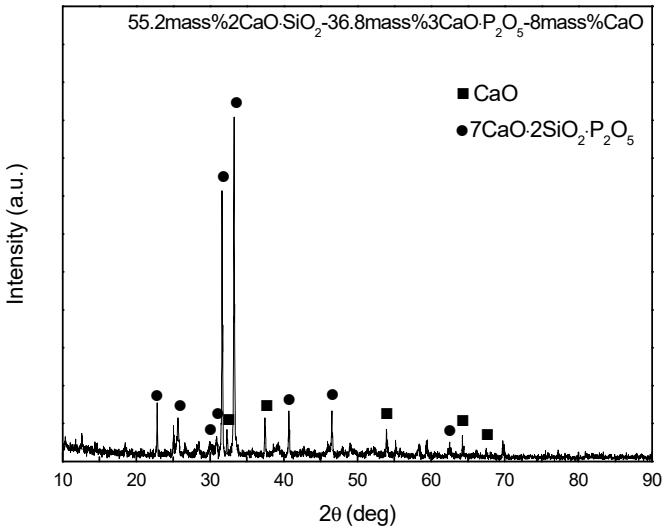

Fig. 4.10 XRD pattern of the 55.2mass%2CaO·SiO_2-36.8mass%3CaO·P_2O_5 solid solution-8mass%CaO.

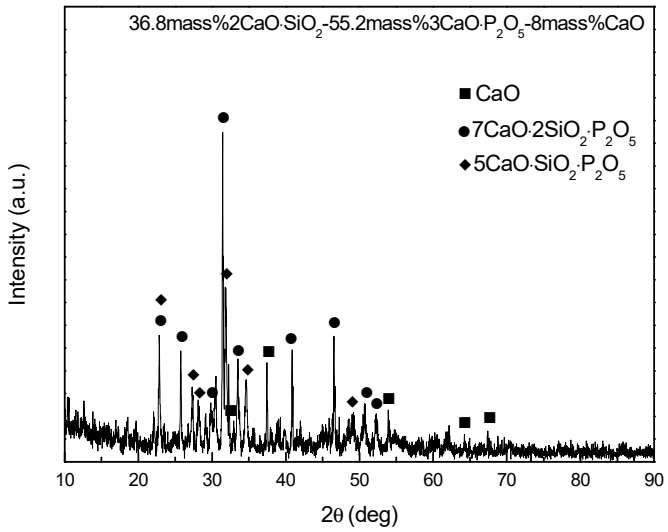

Fig. 4.11 XRD pattern of the 36.8mass%2CaO·SiO_2-55.2mass%3CaO·P_2O_5 solid solution-8mass%CaO.

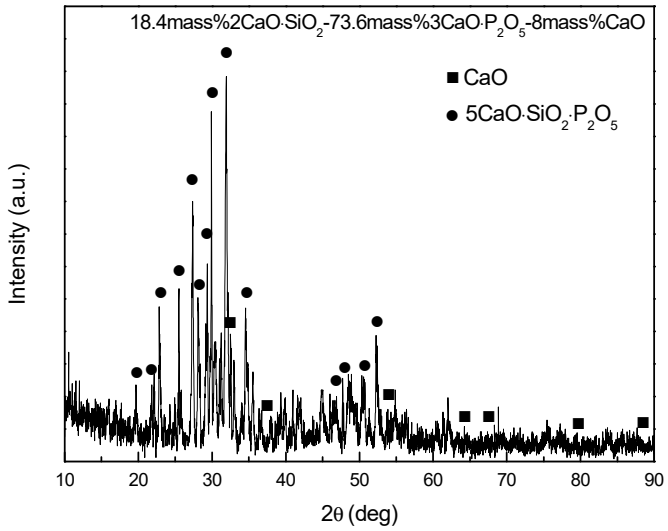

Fig. 4.12 XRD pattern of the 18.4mass%2CaO·SiO_2-73.6mass%3CaO·P_2O_5 solid solution-8mass%CaO.

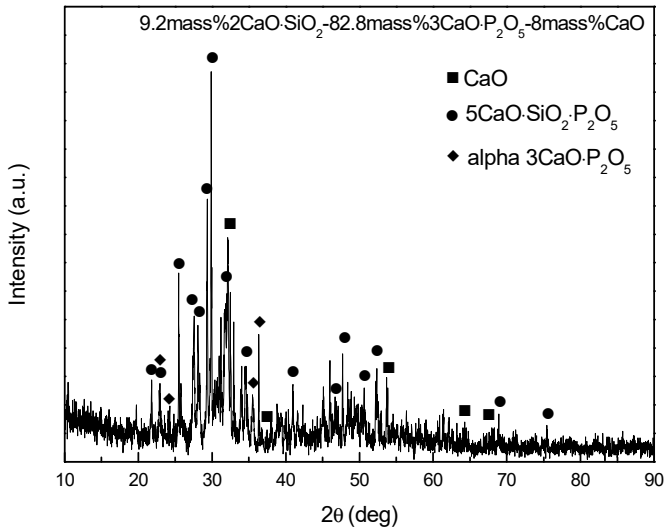

Fig. 4.13 XRD pattern of the 9.2mass%2CaO·SiO_2-82.8mass%3CaO·P_2O_5 solid solution-8mass%CaO.

4.3.4 XRD pattern of the $2CaO{\cdot}SiO_2$-$3CaO{\cdot}P_2O_5$ solid solution containing 8 and 24 mass% CaO after reaction

The phases of the tablet after reaction were analyzed by XRD as shown from **Figure 4.14** to **4.30**. The CaO phase was detected in the whole samples except the sample F05. The eutectoid appeared during quenching.

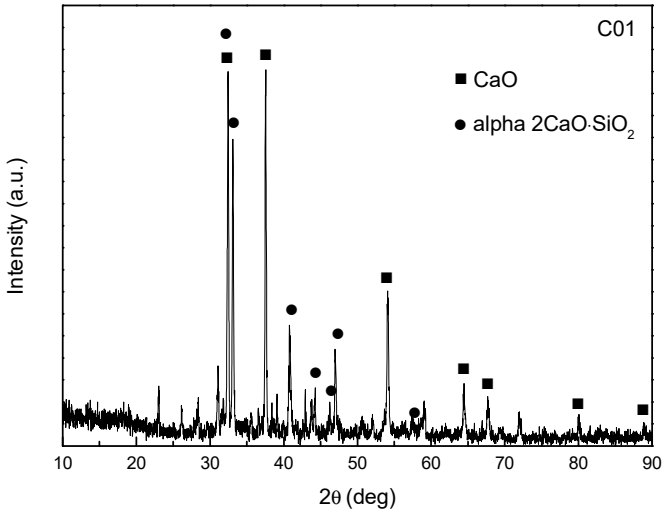

Fig. 4.14 XRD pattern of sample C01 after reaction.

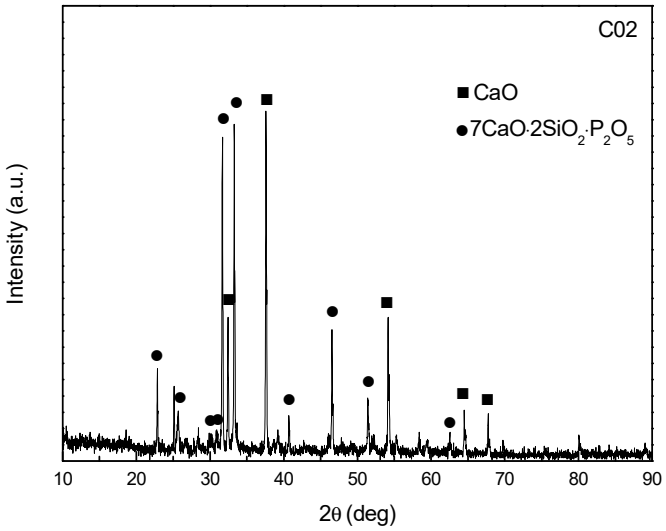

Fig. 4.15 XRD pattern of sample C02 after reaction.

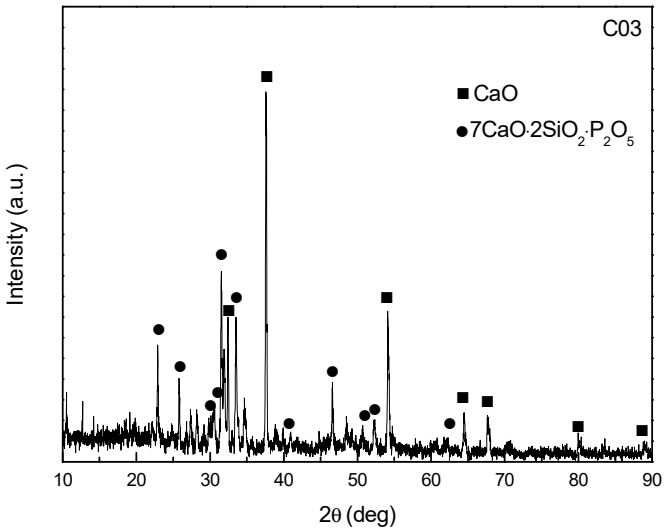

Fig. 4.16 XRD pattern of sample C03 after reaction.

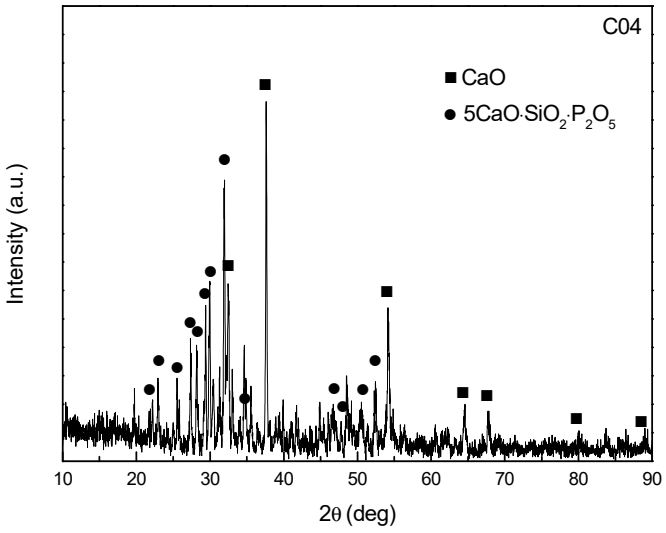

Fig. 4.17 XRD pattern of sample C04 after reaction.

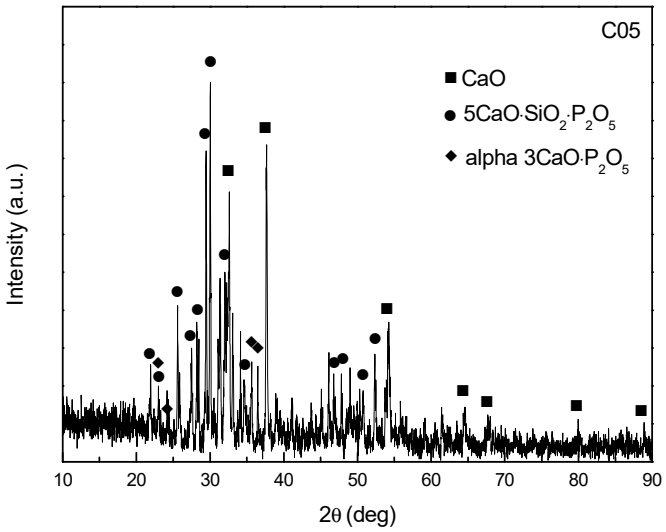

Fig. 4.18 XRD pattern of sample C05 after reaction.

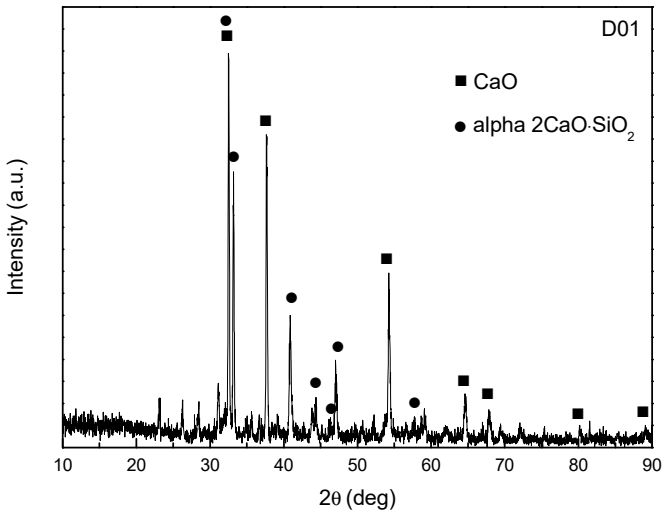

Fig. 4.19 XRD pattern of sample D01 after reaction.

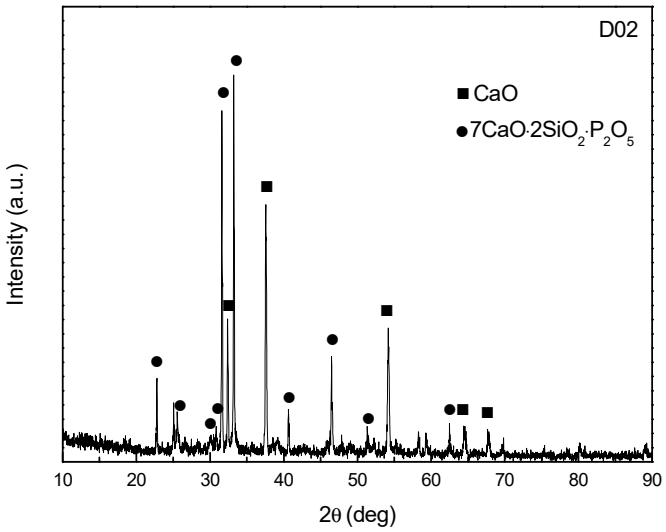

Fig. 4.20 XRD pattern of sample D02 after reaction.

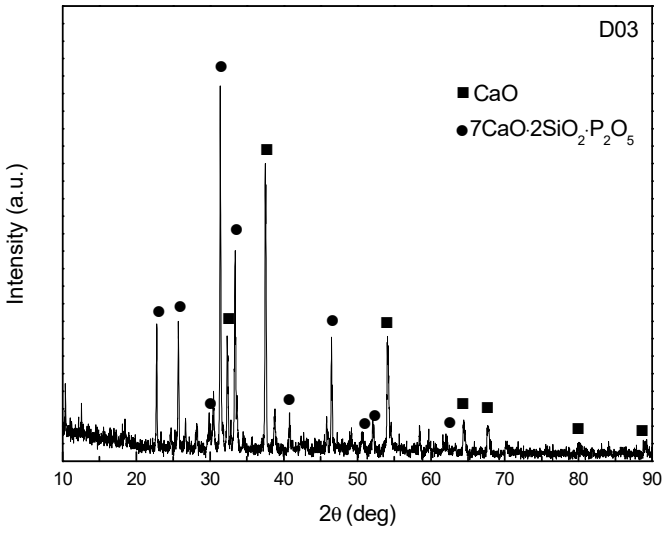

Fig. 4.21 XRD pattern of sample D03 after reaction.

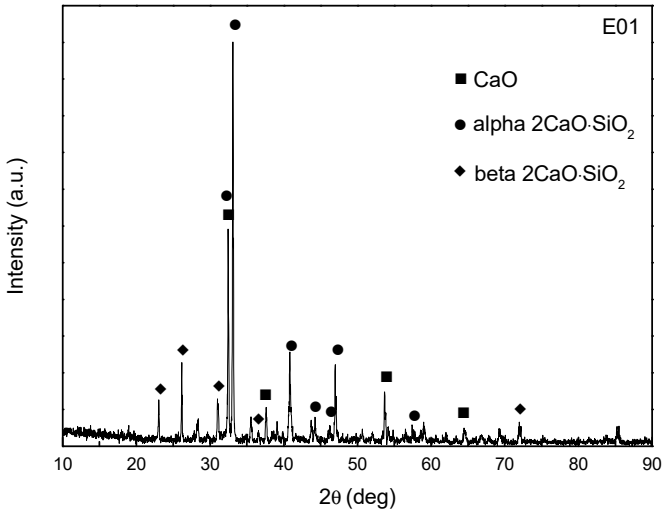

Fig. 4.22 XRD pattern of sample E01 after reaction.

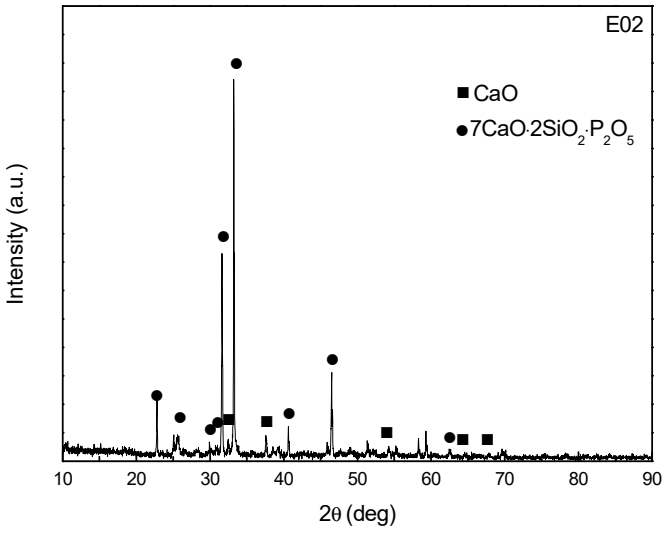

Fig. 4.23 XRD pattern of sample E02 after reaction.

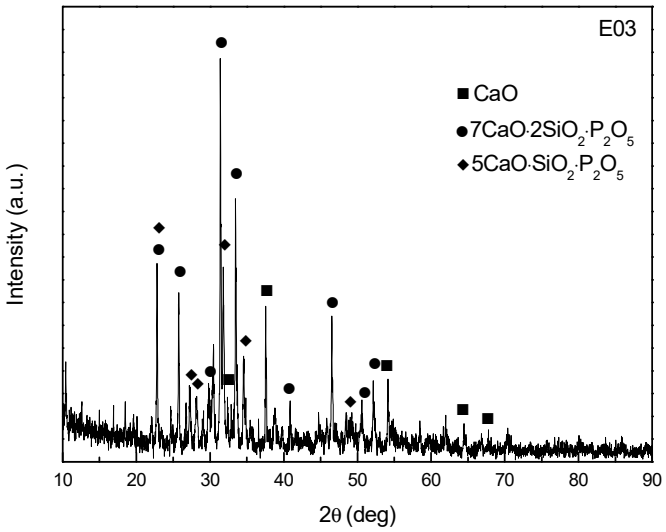

Fig. 4.24 XRD pattern of sample E03 after reaction.

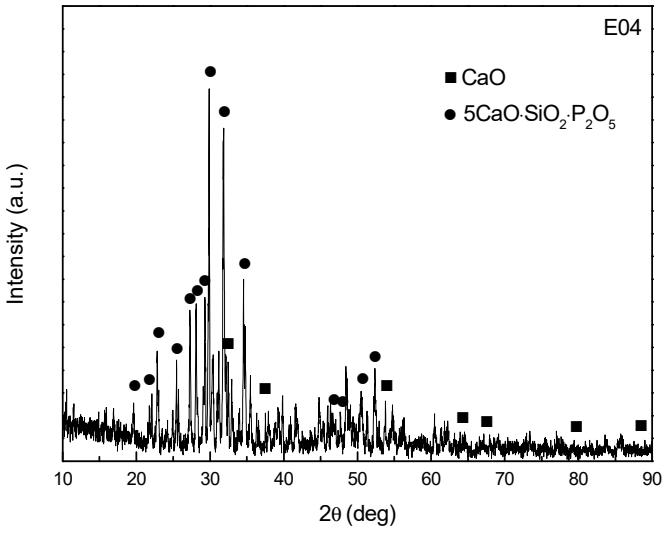

Fig. 4.25 XRD pattern of sample E04 after reaction.

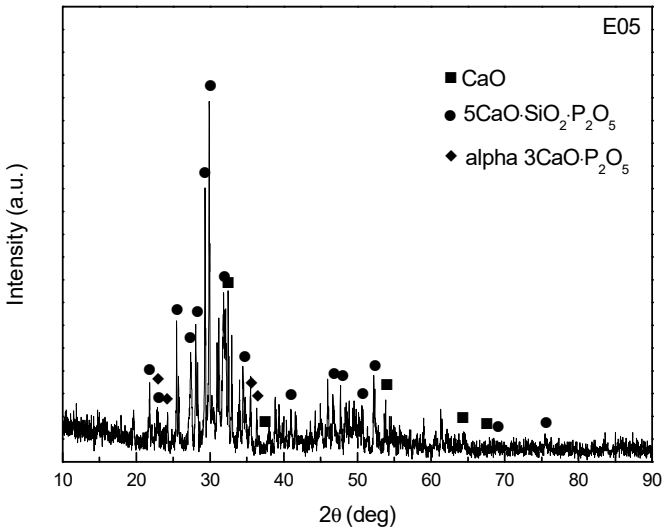

Fig. 4.26 XRD pattern of sample E05 after reaction.

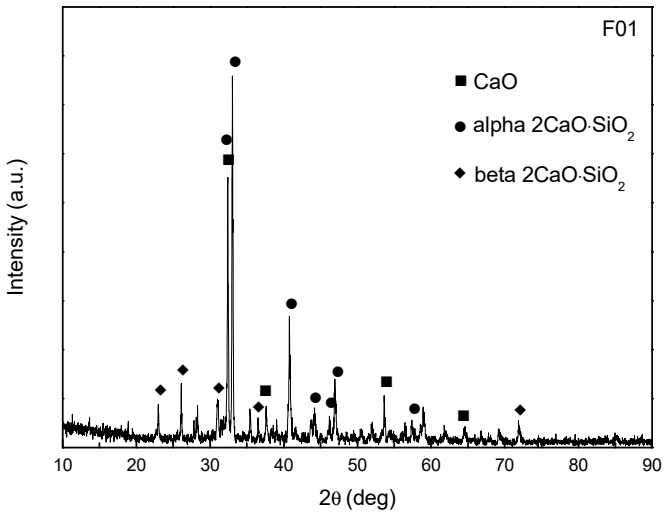

Fig. 4.27 XRD pattern of sample F01 after reaction.

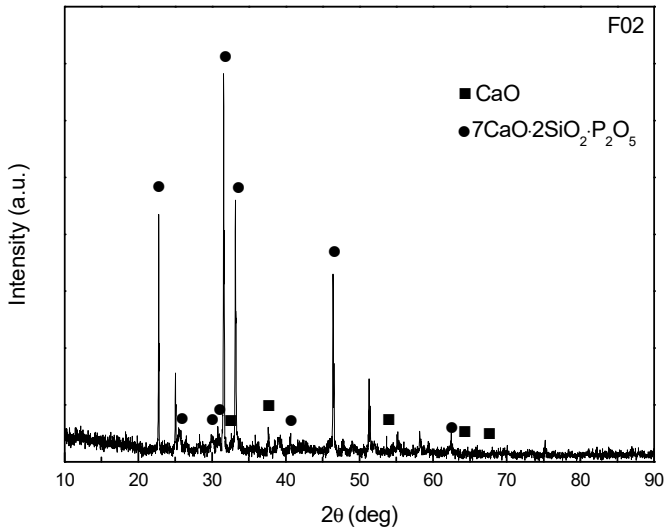

Fig. 4.28 XRD pattern of sample F02 after reaction.

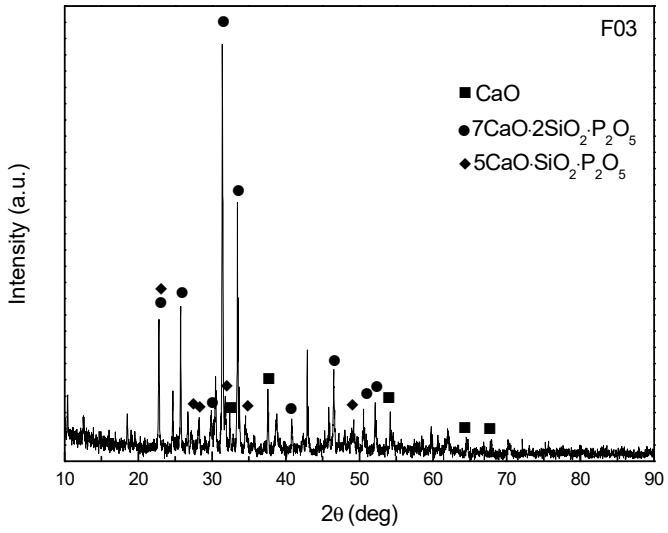

Fig. 4.29 XRD pattern of sample F03 after reaction.

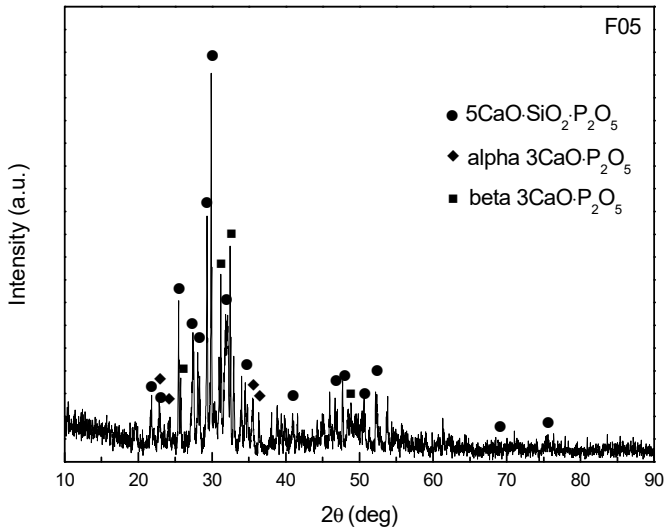

Fig. 4.30 XRD pattern of sample F05 after reaction.

4.4 Discussion

From the compositions as shown in Table 4.9, the mole fraction of $3CaO·P_2O_5$ and P_2O_5 in the $2CaO·SiO_2$-$3CaO·P_2O_5$ solid solution, the mole fraction of FeO and the mass fraction of extra CaO in tablets after reaction were shown in **Table 4.11**. The content of $3CaO·P_2O_5$ in the $2CaO·SiO_2$-$3CaO·P_2O_5$ solid solution was calculated from the analyzed P_2O_5 content. The extra content of CaO was calculated by the total content of CaO minus the parts consumed by $2CaO·SiO_2$ and $3CaO·P_2O_5$. The mole fraction of P_2O_5 in the solid solution was calculated from the content of $3CaO·P_2O_5$.

Table 4.11 Compositions of tablets after reaction.

No.	$3CaO·P_2O_5$/mol%	P_2O_5/mol%	FeO/mol%	Extra CaO/mass%
C01	12.2	3.89	0.327	20.9
C02	27.4	8.37	0.371	22.0
C03	44.9	13.0	0.363	21.7
C04	69.7	18.9	0.455	21.2
C05	84.5	22.0	0.359	21.8
D01	12.5	4.01	0.635	22.7
D02	26.2	8.02	0.741	21.2
D03	46.9	13.5	0.865	23.9
E01	12.9	4.11	0.730	5.3
E02	28.0	8.53	0.845	3.3
E03	45.1	13.1	0.600	1.4
E04	69.3	18.8	0.342	3.3
E05	82.7	21.6	1.39	6.6
F01	12.4	3.98	1.12	2.4
F02	29.5	8.95	2.01	5.2
F03	46.7	13.5	0.233	3.9

F05	83.4	21.7	0.298	5.1

The compositions were projected on the CaO-SiO_2-P_2O_5 system as shown in **Figure 4.31**. The compositions in which the CaO phase was detected were marked as solid circles.

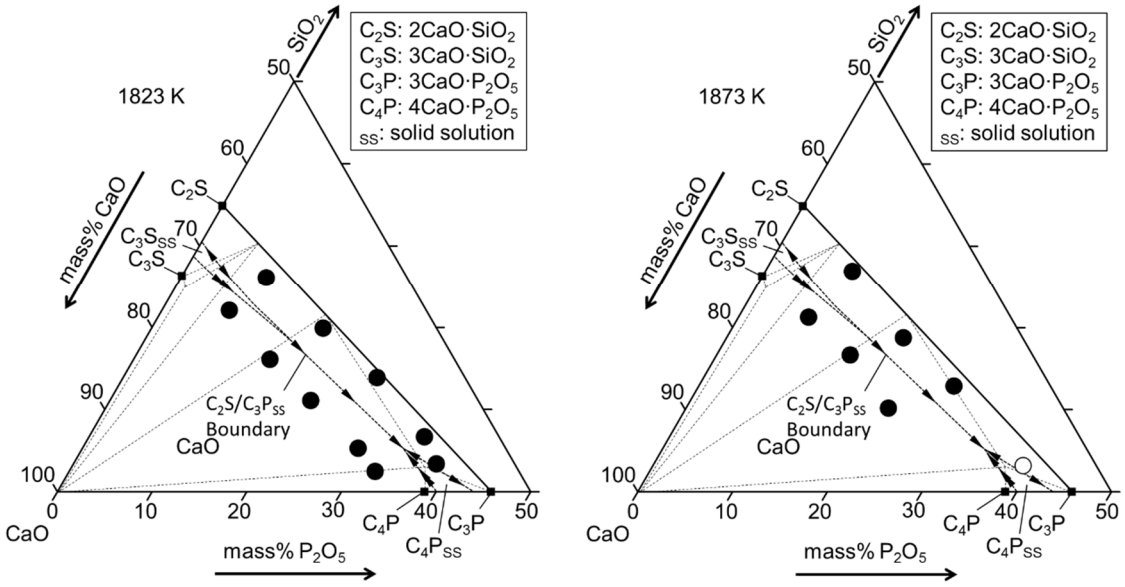

Fig. 4.31 Compositions of tablets after reaction on the CaO-SiO_2-P_2O_5 system. In the compositions marked by the solid circles CaO phase was detected by XRD. In the composition marked by the open circles CaO phase was undetected by XRD.

4.4.1 Contents of FeO and MgO in the tablet after reaction

Figure 4.32 shows the relationship between the P_2O_5 content and the FeO and MgO contents in tablets after reaction. The contents of MgO and FeO barely changed with the change of P_2O_5 content. Since the tablet was contaminated with more or less metallic iron particles when the tablet was separated from the surface of solidified iron, the content of FeO was larger for some samples. For most samples, the contents of FeO and MgO were smaller than 1 mass%.

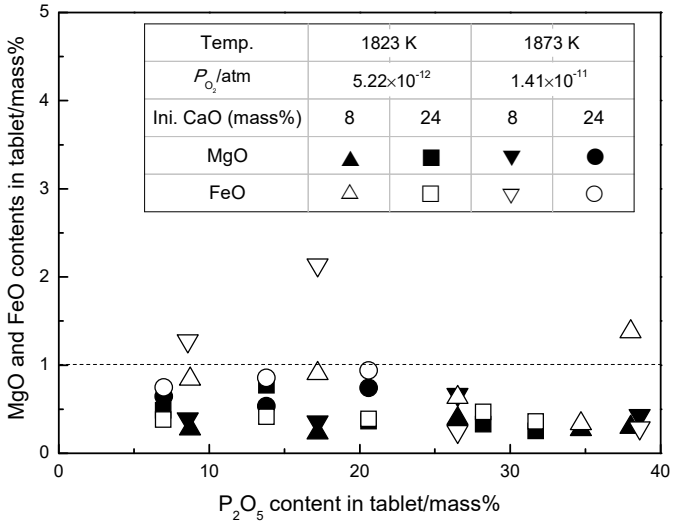

Fig. 4.32 Contents of FeO and MgO in the tablet after reaction.

4.4.2 Activity coefficient of FeO in the tablet after reaction

According to the activity of FeO introduced in Chapter 3, the activity coefficient of FeO relative to hypothetical pure liquid FeO was calculated and shown in **Table 4.12** and **Figure 4.33** as a function of $3CaO{\cdot}P_2O_5$ content in the solid solution. At a certain temperature and oxygen partial pressure, the activity coefficient of FeO was almost constant. The activity coefficient of FeO was in the range from 4.83×10^{-9} to 7.45×10^{-8}.

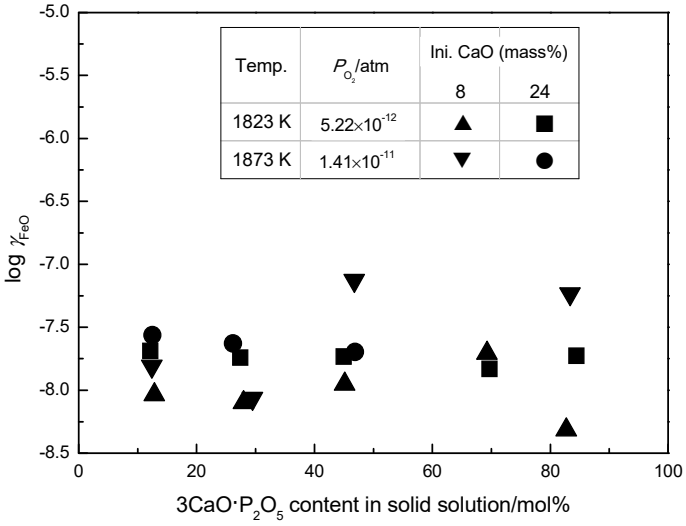

Fig. 4.33 Activity coefficient of FeO in the tablet after reaction.

Table 4.12 Thermodynamic data of the $2CaO{\cdot}SiO_2$-$3CaO{\cdot}P_2O_5$ solid solution containing 8 and 24 mass% CaO.

No.	γ_{FeO}	$\frac{(mass\%P)}{[mass\%P]}$	$a_{P_2O_5}$	$\gamma_{P_2O_5}$	$a_{3CaO\cdot P_2O_5}$	$\gamma_{3CaO\cdot P_2O_5}$
C01	2.05×10^{-8}	6.58×10^{2}	8.28×10^{-25}	2.13×10^{-23}	9.49×10^{-6}	7.80×10^{-5}
C02	1.81×10^{-8}	6.88×10^{2}	3.05×10^{-24}	3.64×10^{-23}	3.49×10^{-5}	1.27×10^{-4}
C03	1.85×10^{-8}	6.08×10^{2}	8.54×10^{-24}	6.56×10^{-23}	9.79×10^{-5}	2.18×10^{-4}
C04	1.48×10^{-8}	8.5×10^{2}	8.2×10^{-24}	4.4×10^{-23}	9.4×10^{-5}	1.3×10^{-4}
C05	1.87×10^{-8}	8.9×10^{2}	9.3×10^{-24}	4.3×10^{-23}	1.1×10^{-4}	1.3×10^{-4}
D01	2.74×10^{-8}	5.73×10^{2}	1.08×10^{-24}	2.71×10^{-23}	4.77×10^{-6}	3.81×10^{-5}
D02	2.35×10^{-8}	6.6×10^{2}	3.1×10^{-24}	3.8×10^{-23}	1.4×10^{-5}	5.2×10^{-5}
D03	2.01×10^{-8}	6.22×10^{2}	8.06×10^{-24}	5.96×10^{-23}	3.55×10^{-5}	7.57×10^{-5}
E01	9.21×10^{-9}	1.4×10^{3}	2.8×10^{-25}	6.9×10^{-24}	3.2×10^{-6}	2.5×10^{-5}
E02	7.95×10^{-9}	2.3×10^{3}	4.4×10^{-25}	5.18×10^{-24}	5.1×10^{-6}	1.8×10^{-5}
E03	1.12×10^{-8}	1.41×10^{3}	2.53×10^{-24}	1.94×10^{-23}	2.90×10^{-5}	6.42×10^{-5}
E04	1.97×10^{-8}	7.24×10^{2}	1.68×10^{-23}	8.97×10^{-23}	1.93×10^{-4}	2.78×10^{-4}
E05	4.83×10^{-9}	3.41×10^{2}	9.12×10^{-23}	4.22×10^{-22}	1.04×10^{-3}	1.26×10^{-3}
F01	1.55×10^{-8}	1.1×10^{3}	4.6×10^{-25}	1.15×10^{-23}	2.0×10^{-6}	1.6×10^{-5}
F02	8.64×10^{-9}	1.22×10^{3}	1.57×10^{-24}	1.76×10^{-23}	6.93×10^{-6}	2.35×10^{-5}
F03	7.45×10^{-8}	4.40×10^{2}	2.58×10^{-23}	1.92×10^{-22}	1.14×10^{-4}	2.43×10^{-4}
F05	5.84×10^{-8}	2.32×10^{2}	2.05×10^{-22}	9.44×10^{-22}	-	-

4.4.3 Equilibrium concentration of P in molten iron and phosphorus partition ratio between the mixture of $2CaO{\cdot}SiO_2$-$3CaO{\cdot}P_2O_5$ solid solution and CaO and molten iron

Figure 4.34 shows the relationship between the equilibrium concentration of P in molten iron and the $3CaO{\cdot}P_2O_5$ content in the solid solution. The concentration of P in molten iron increased with the increase of the $3CaO{\cdot}P_2O_5$ content in the solid solution. The phosphorus partition ratio between the mixture of $2CaO{\cdot}SiO_2$-$3CaO{\cdot}P_2O_5$ solid solution and CaO and molten iron was shown in **Figure 4.35** and Table 4.12. The phosphorus partition ratio decreased with the increase of the $3CaO{\cdot}P_2O_5$ content in the solid solution.

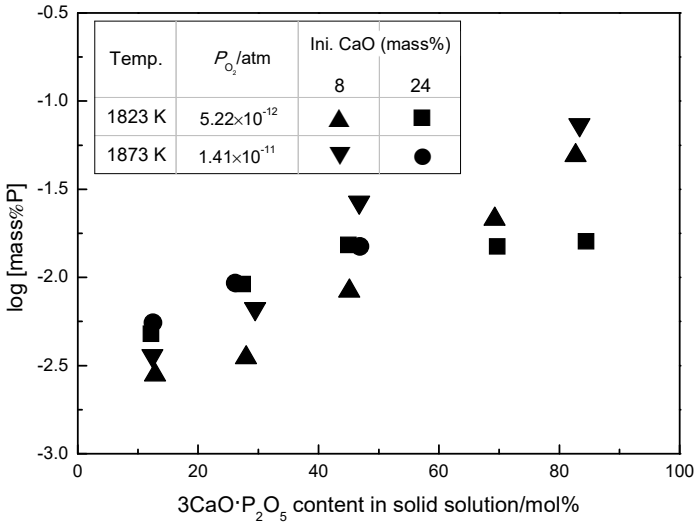

Fig. 4.34. Equilibrium concentration of P in molten iron after reaction.

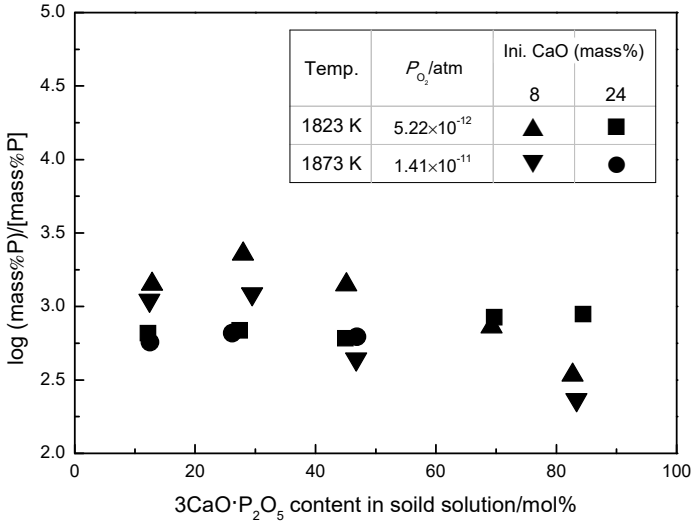

Fig. 4.35 Phosphorus partition ratio between the mixture of $2CaO \cdot SiO_2$-$3CaO \cdot P_2O_5$ solid solution and CaO and molten iron.

4.4.4 Activity and activity coefficient of P_2O_5 in the $2CaO{\cdot}SiO_2$-$3CaO{\cdot}P_2O_5$ solid solution containing 8 and 24 mass% CaO

Figures 4.36 and **4.37** show the activity and activity coefficient of P_2O_5 as a function of $3CaO{\cdot}P_2O_5$ content in the solid solution with the values shown in Table 4.12. The activity and activity coefficient of P_2O_5 increased with the increase of the $3CaO{\cdot}P_2O_5$ content in the solid solution. For a constant composition of solid solution, the activity and activity coefficient of P_2O_5 barely changed with the change of the temperature. Comparing with the P_2O_5 activity estimated by Hasegawa *et al.*[3] at 1573 K, the current values measured at higher temperature were larger. The activity of P_2O_5 changed from 2.8×10^{-25} to 2.05×10^{-22} and the activity coefficient of P_2O_5 changed from 5.2×10^{-24} to 9.44×10^{-22}.

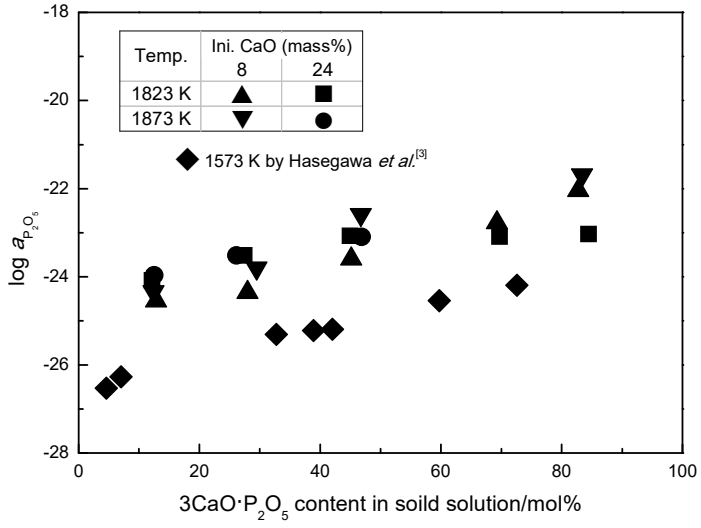

Fig. 4.36 Activity of P_2O_5 in the $2CaO{\cdot}SiO_2$-$3CaO{\cdot}P_2O_5$ solid solution containing 8 and 24 mass% CaO.

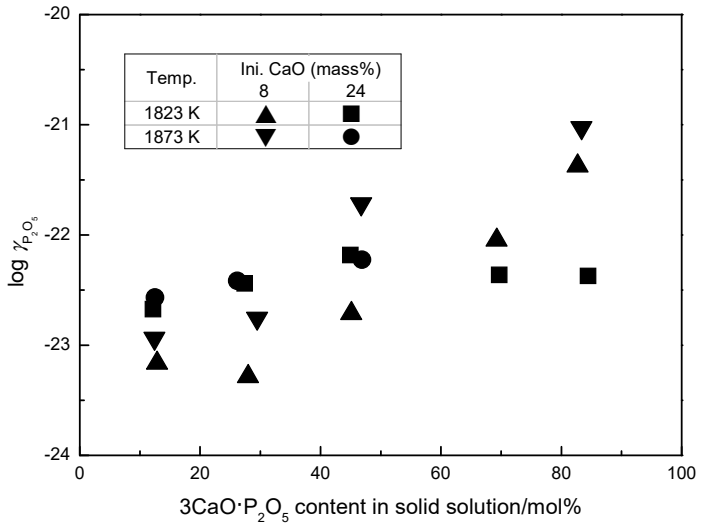

Fig. 4.37 Activity coefficient of P_2O_5 in the $2CaO{\cdot}SiO_2$-$3CaO{\cdot}P_2O_5$ solid solution containing 8 and 24 mass% CaO.

4.4.5 Activity and activity coefficient of $3CaO·P_2O_5$ in the $2CaO·SiO_2$-$3CaO·P_2O_5$ solid solution saturated with CaO

For the compositions in which the CaO phase was detected after reaction as shown in Figure 4.31 marked by solid circles, the activity and activity coefficient of $3CaO·P_2O_5$ were calculated from the activity of P_2O_5 by Eqs. (4.1) and (4.2). The activity and activity coefficient of $3CaO·P_2O_5$ in the $2CaO·SiO_2$-$3CaO·P_2O_5$ solid solution saturated with CaO were shown in Table 4.12. **Figures 4.38** and **4.39** show the activity and activity coefficient of $3CaO·P_2O_5$ in the $2CaO·SiO_2$-$3CaO·P_2O_5$ solid solution saturated with CaO as a function of $3CaO·P_2O_5$ content. The activity and activity coefficient of $3CaO·P_2O_5$ increased with the increase of the $3CaO·P_2O_5$ content in the solid solution. For a constant composition of solid solution, the activity and activity coefficient of $3CaO·P_2O_5$ barely changed with the change of the temperature. The activity of $3CaO·P_2O_5$ changed from 2.0×10^{-6} to 1.04×10^{-3} and the activity coefficient of $3CaO·P_2O_5$ changed from 1.6×10^{-5} to 1.26×10^{-3}.

$$3CaO(s) + P_2(g) + 5/2\ O_2(g) = 3CaO \cdot P_2O_5(s)$$

$$\Delta G^{\circ}_{4.1} = -2198000 + 504T\ \text{J/mol} \ldots\ldots (4.1)^{[4]}$$

$$P_2(g) + 5/2\ O_2(g) = P_2O_5(l)$$

$$\Delta G^{\circ}_{4.2} = -1655480 + 571.0T\ \text{J/mol} \ldots\ldots (4.2)^{[5]}$$

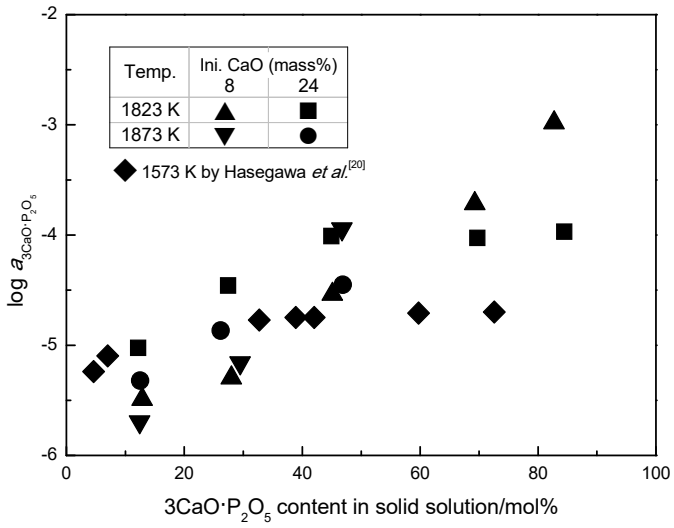

Fig. 4.38 Activity of $3CaO\cdot P_2O_5$ in the $2CaO\cdot SiO_2$-$3CaO\cdot P_2O_5$ solid solution containing 8 and 24 mass% CaO.

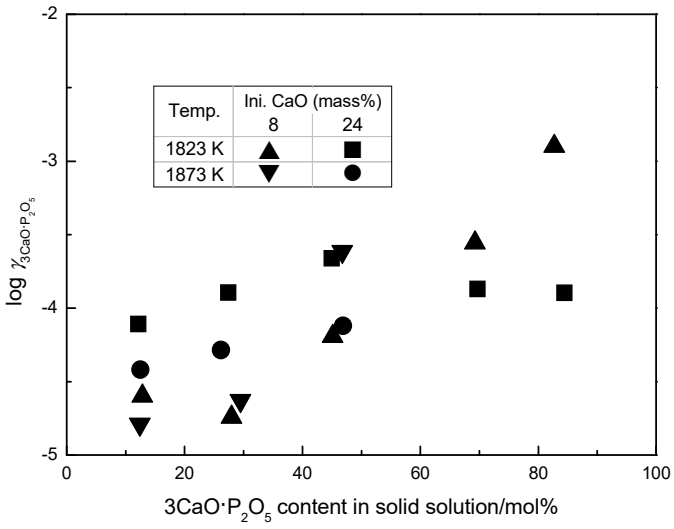

Fig. 4.39 Activity coefficient of $3CaO\cdot P_2O_5$ in the $2CaO\cdot SiO_2$-$3CaO\cdot P_2O_5$ solid solution containing 8 and 24 mass% CaO.

4.4.6 Activity and activity coefficient of $2CaO{\cdot}SiO_2$ and SiO_2 in the $2CaO{\cdot}SiO_2$-$3CaO{\cdot}P_2O_5$ solid solution saturated with CaO

By the Gibbs-Duhem equation as Eq. (4.3) for the $2CaO{\cdot}SiO_2$-$3CaO{\cdot}P_2O_5$ pseudo-binary system, the activity of $2CaO{\cdot}SiO_2$ in the solid solution was calculated from the activity of $3CaO{\cdot}P_2O_5$.

$$x_{3CaO{\cdot}P_2O_5}\,\mathrm{d}\ln a_{3CaO{\cdot}P_2O_5} + x_{2CaO{\cdot}SiO_2}\,\mathrm{d}\ln a_{2CaO{\cdot}SiO_2} = 0 \ldots\ldots (4.3)$$

The relationship between the activity coefficient of $3CaO{\cdot}P_2O_5$ and the mole fraction of $3CaO{\cdot}P_2O_5$ in the solid solution was expressed with a linear function by the least square method at the mole fraction of $3CaO{\cdot}P_2O_5$ from 0.122 to 0.845 at 1823 K and from 0.124 to 0.469 at 1873 K as shown by Eqs. (4.4) and (4.5), respectively.

$$\ln \gamma_{3CaO{\cdot}P_2O_5} = 3.0962 x_{3CaO{\cdot}P_2O_5} - 10.551 \text{ at } 1823\text{ K} \ldots\ldots (4.4)$$

$$\ln \gamma_{3CaO{\cdot}P_2O_5} = 4.8787 x_{3CaO{\cdot}P_2O_5} - 11.346 \text{ at } 1873\text{ K} \ldots\ldots (4.5)$$

The activity coefficient of $2CaO{\cdot}SiO_2$ was shown in **Figure 4.40** and the activity of $2CaO{\cdot}SiO_2$ was shown in **Figure 4.41**.

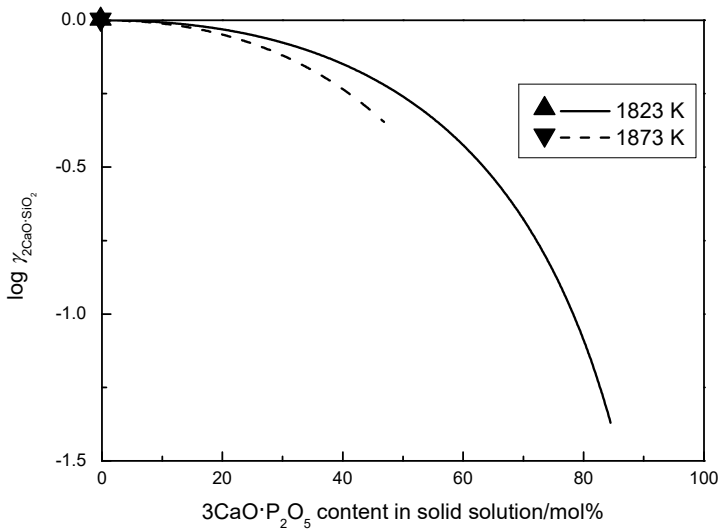

Fig. 4.40 Estimated activity coefficient of $2CaO{\cdot}SiO_2$ in the $2CaO{\cdot}SiO_2$-$3CaO{\cdot}P_2O_5$ solid solution saturated with CaO.

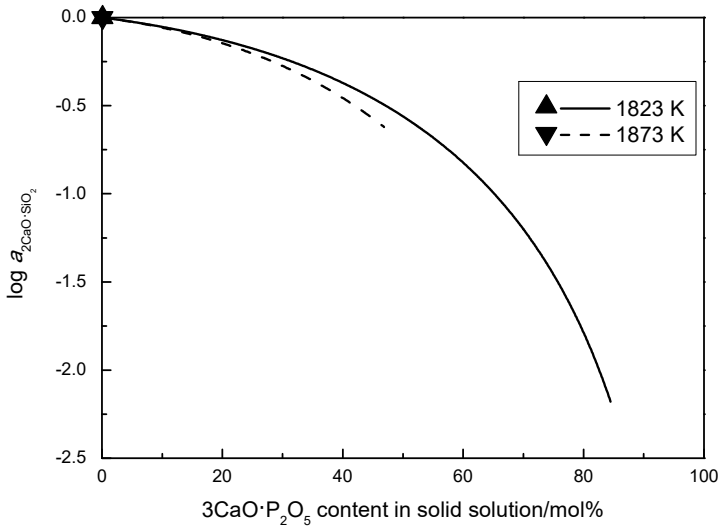

Fig. 4.41 Estimated activity of $2CaO\cdot SiO_2$ in the $2CaO\cdot SiO_2$-$3CaO\cdot P_2O_5$ solid solution saturated with CaO.

The activity and activity coefficient of $2CaO\cdot SiO_2$ in the $2CaO\cdot SiO_2$-$3CaO\cdot P_2O_5$ solid solution saturated with CaO decreased with the increase of the $3CaO\cdot P_2O_5$ content in the solid solution. The temperature dependency of the activity and activity coefficient of $2CaO\cdot SiO_2$ was small within the experimental error. Moreover, the activity of SiO_2 relative to solid SiO_2 in the $2CaO\cdot SiO_2$-$3CaO\cdot P_2O_5$ solid solution saturated with CaO was calculated from the activity of $2CaO\cdot SiO_2$ by Eq. (4.6) as shown in **Figure 4.42** and the activity coefficient of SiO_2 was shown in **Figure 4.43.** Temperature dependency of the activity and activity coefficient of SiO_2 was small. The activity of SiO_2 in the solid solution saturated with CaO decreased monotonically from 1.0×10^{-4} to 6.9×10^{-7} with the increase of the $3CaO\cdot P_2O_5$ content up to 84.5 mol% at 1823 K.

$$2\mathrm{CaO(s)} + \mathrm{SiO_2(s)} = 2\mathrm{CaO\cdot SiO_2(s)}$$

$$\Delta G^{\circ}_{4.6} = -119000 - 11T \text{ J/mol} \ldots\ldots (4.6)^{[6]}$$

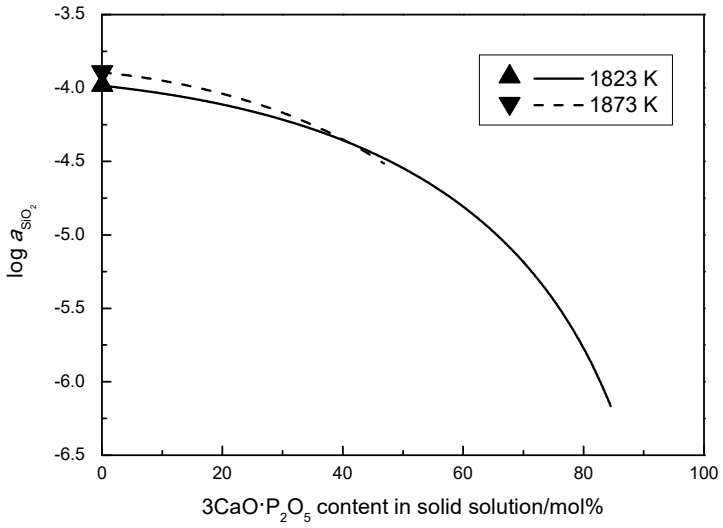

Fig. 4.42 Estimated activity of SiO_2 in the $2CaO{\cdot}SiO_2$-$3CaO{\cdot}P_2O_5$ solid solution saturated with CaO.

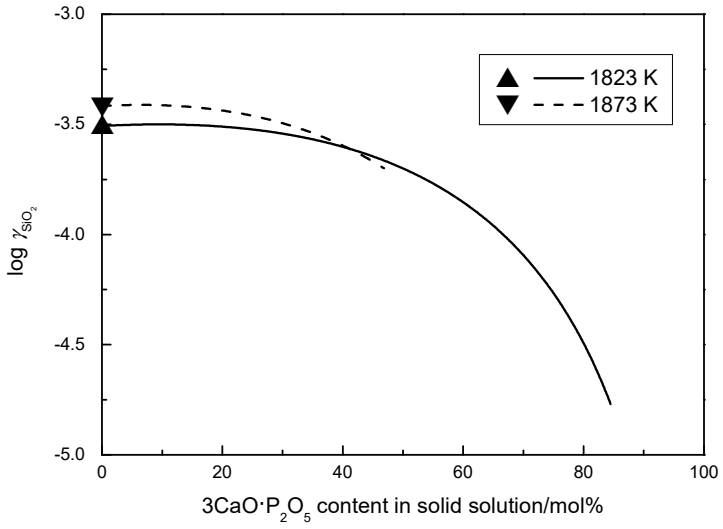

Fig. 4.43 Estimated activity coefficient of SiO_2 in the $2CaO{\cdot}SiO_2$-$3CaO{\cdot}P_2O_5$ solid solution saturated with CaO.

4.5 Summary

By applying the chemical equilibrium method, the equilibrium of phosphorus between the mixture of $2CaO{\cdot}SiO_2$-$3CaO{\cdot}P_2O_5$ solid solution and CaO and molten iron was measured at 1823 K with the oxygen partial pressure of 5.22×10^{-12} atm and 1873 K with the oxygen partial pressure of 1.41×10^{-11} atm. The activity of P_2O_5 relative to hypothetical pure liquid P_2O_5 in the $2CaO{\cdot}SiO_2$-$3CaO{\cdot}P_2O_5$ solid solution containing 8 and 24 mass% CaO increased from 2.8×10^{-25} to 2.05×10^{-22} and the activity coefficient of P_2O_5 increased from 5.2×10^{-24} to 9.44×10^{-22} with the increase of the $3CaO{\cdot}P_2O_5$ content in the solid solution from 12.2 to 84.5 mol%. Since the CaO phase was detected for some samples after reaction, the activity of $3CaO{\cdot}P_2O_5$ in the $2CaO{\cdot}SiO_2$-$3CaO{\cdot}P_2O_5$ solid solution saturated with CaO was estimated from 2.0×10^{-6} to 1.04×10^{-3} and the activity coefficient of $3CaO{\cdot}P_2O_5$ was estimated from 1.6×10^{-5} to 1.26×10^{-3}. The activity of $2CaO{\cdot}SiO_2$ estimated by the Gibbs-Duhem equation and the activity of SiO_2 in the solid solution saturated with CaO decreased with the increase of the $3CaO{\cdot}P_2O_5$ content in the solid solution.

References

1. W. Gutt: *Nature*, **197** (1963), 142-143.
2. Drewes, E.-J.,M. Olette: *Arch. Eisenhüttenwes.*, **30** (1977), 163-175.
3. M. Hasegawa, Y. Kashiwaya and M. Iwase: *High Temp. Mater. Proc.*, **31** (2012), 421-430.
4. A. Tagaya, F. Tsukihashi, and N. Sano: *Trans. ISS*, **11** (1991), 63-69.
5. E. T. Turkdogan: *ISIJ Int.*, **40** (2000), 964-970.
6. E.T. Turkdogan: Physical Chemistry of High Temperature Technology, Academic Press, New York, (1980), 8.

Chapter 5 Thermodynamic Properties of the $2CaO·SiO_2$-$3CaO·P_2O_5$ Solid Solution Containing 8 and 24 mass% MgO at 1823 and 1873 K

5.1 Introduction

Since there is more or less MgO in the metallurgical slag, it is necessary to study the thermodynamic properties of the $2CaO·SiO_2$-$3CaO·P_2O_5$ solid solution containing a certain amount of MgO to investigate the effect caused by MgO.

5.2 Experimental conditions

The initial compositions of tablets were the $2CaO·SiO_2$-$3CaO·P_2O_5$ solid solution containing 8 and 24 mass% MgO as shown in **Table 5.1** and **Figure 5.1**. The tablets with the compositions marked by open circles in Figure 5.1 turned into slag after reaction at 1873 K. The initial conditions of experiments are shown in **Table 5.2**.

Table 5.1 Initial compositions of tablets.

No.	CaO /mass%	SiO_2 /mass%	P_2O_5 /mass%	MgO /mass%	$2CaO·SiO_2$ /mass%	$3CaO·P_2O_5$ /mass%	MgO /mass%
G01	47.8	21.2	7.0	24.0	60.8	15.2	24.0
G02	46.2	15.9	13.9	24.0	45.6	30.4	24.0
G03	44.5	10.6	20.9	24.0	30.4	45.6	24.0
G04	42.9	5.3	27.8	24.0	15.2	60.8	24.0
H01	47.8	21.2	7.0	24.0	60.8	15.2	24.0
H02	46.2	15.9	13.9	24.0	45.6	30.4	24.0
H03	44.5	10.6	20.9	24.0	30.4	45.6	24.0
H04	42.9	5.3	27.8	24.0	15.2	60.8	24.0

I01	57.9	25.7	8.4	8.0	73.6	18.4	8.0
I02	55.9	19.2	16.9	8.0	55.2	36.8	8.0
I03	53.9	12.8	25.3	8.0	36.8	55.2	8.0
I04	51.9	6.4	33.7	8.0	18.4	73.6	8.0
J01	57.9	25.7	8.4	8.0	73.6	18.4	8.0
J02	55.9	19.2	16.9	8.0	55.2	36.8	8.0
J03	53.9	12.8	25.3	8.0	36.8	55.2	8.0
J04	51.9	6.4	33.7	8.0	18.4	73.6	8.0

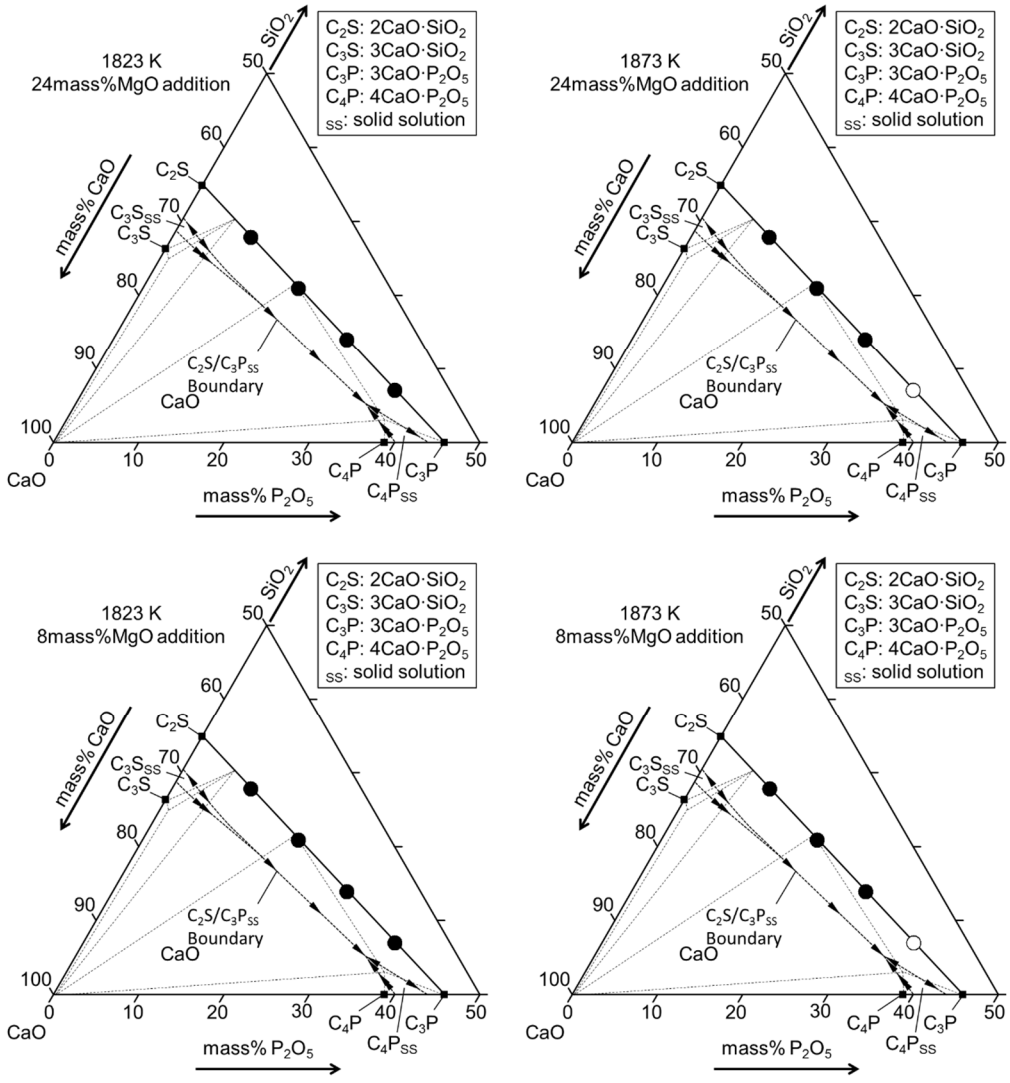

Fig. 5.1 Initial compositions of tablets on the CaO-SiO_2-P_2O_5 system. The boundary and tie lines in the phase diagram were determined at 1773 K by Gutt.[1]

Table 5.2 Initial conditions of experiments.

With the $2CaO \cdot SiO_2$-$3CaO \cdot P_2O_5$ solid solution containing 24 mass% MgO				
No.	Temp./K	CO/CO_2	Fe/g	Tablet/g
G01	1823	110/1	12.4883	1.5053
G02	1823	110/1	10.6410	1.4873
G03	1823	110/1	12.8895	1.4812
G04	1823	110/1	12.9600	1.5198
H01	1873	110/1	14.6774	1.4730
H02	1873	110/1	10.6351	1.4910
H03	1873	110/1	12.4712	1.5014
H04	1873	110/1	9.8099	1.4786
With the $2CaO \cdot SiO_2$-$3CaO \cdot P_2O_5$ solid solution containing 8 mass% MgO				
No.	Temp./K	CO/CO_2	Fe/g	Tablet/g
I01	1823	110/1	11.9418	1.5043
I02	1823	110/1	9.9766	1.4720
I03	1823	110/1	11.0544	1.4987
I04	1823	110/1	10.7003	1.4990
J01	1873	110/1	13.9198	1.4777
J02	1873	110/1	11.2496	1.5003
J03	1873	110/1	11.5870	1.4917
J04	1873	110/1	10.2708	1.4805

5.3 Experimental results

5.3.1 Chemical compositions of Fe and tablet

The concentration of P in Fe, the contents of P_2O_5, SiO_2, CaO, MgO and FeO in tablet after reaction are shown from **Tables 5.3** to **5.8**. In Tables 5.6, 5.7 and 5.8, the values of Test/ppm were the concentrations of Ca, Mg and Fe in the solution measured by ICP-OES. **Table 5.9** summarized the analyzed the concentration of P in Fe and the compositions of tablets.

Table 5.3 Concentration of P in Fe.

No.	Weight /mg	Dilution ratio	Cell /mm	ABS	P in Fe /mass%	Ave P /mass%
G01	1543.8	1	10	0.173	0.00492	0.00506
	1275.4	1	10	0.151	0.00519	
G02	1243.4	10	20	0.144	0.0118	0.0124
	1181.4	10	20	0.149	0.0129	
G03	1232.7	10	20	0.213	0.0184	0.0179
	1698.6	10	20	0.271	0.0173	
G04	1362.2	10	20	0.373	0.0303	0.0292
	1574.2	10	20	0.397	0.0280	
H01	1095.9	1	10	0.197	0.00790	0.00798
	981.0	1	10	0.180	0.00805	
H02	741.4	10	20	0.126	0.0170	0.0171
	636.9	10	20	0.112	0.0171	
H03	870.6	10	20	0.185	0.0223	0.0220
	852.9	10	20	0.177	0.0217	
I01	1338.2	1	10	0.185	0.00608	0.00635
	1115.3	1	10	0.168	0.00661	
I02	1236.5	1	10	0.221	0.00786	0.00903

	1141.9	1	10	0.264	0.0102	
I03	1290.3	2	10	0.342	0.0234	0.0206
	1099.5	1	10	0.443	0.0178	
I04	1100.7	10	20	0.371	0.0373	0.0372
	980.5	10	20	0.330	0.0370	
J01	1511.8	1	10	0.335	0.00979	0.00995
	1598.9	1	10	0.367	0.0101	
J02	1122.3	2	10	0.256	0.0219	0.0213
	1350.3	2	10	0.316	0.0206	
J03	1336.1	5	10	0.228	0.0374	0.0369
	1254.9	5	10	0.207	0.0363	

Annotation: the analysis data was based on the calibration curve: ABS=0.8595×C_P(ppm)+0.018 for the phosphomolybdate blue spectrophotometric method, ABS=0.2252×C_P(ppm)+0.002 for the molybdenum-blue spectrophotometric solvent extraction method. The samples tested with the 20 mm cell was analyzed by the phosphomolybdate blue spectrophotometric method. The samples tested with the 10 mm cell was analyzed by the molybdenum-blue spectrophotometric solvent extraction method.

Table 5.4 Content of P_2O_5 in tablet after reaction.

No.	Weight /mg	Dilution ratio	Cell /mm	ABS	P_2O_5 /mass%	Ave P_2O_5 /mass%
G01	104.1	100	20	0.274	6.97	6.97
	102.7	100	20	0.270	6.96	
G02	106.0	250	20	0.222	13.8	13.8
	104.2	250	20	0.220	13.8	
G03	103.1	500	20	0.169	21.3	21.1
	101.6	500	20	0.163	20.9	
G04	112.2	250	20	0.469	28.0	27.9

	109.8	250	20	0.456	27.7	
H01	103.6	100	20	0.270	6.90	6.91
	101.0	100	20	0.264	6.92	
H02	106.4	250	20	0.222	13.7	13.8
	103.1	250	20	0.218	13.9	
H03	104.7	500	20	0.167	20.8	21.0
	102.8	500	20	0.167	21.2	
I01	104.6	100	20	0.333	8.45	8.47
	107.6	100	20	0.344	8.49	
I02	106.1	100	20	0.662	16.8	16.8
	104.4	100	20	0.654	16.8	
I03	107.3	500	20	0.198	24.1	24.3
	109.2	500	20	0.204	24.5	
I04	109.7	250	20	0.551	33.7	33.7
	108.6	250	20	0.545	33.6	
J01	108.2	100	20	0.335	8.23	8.28
	106.2	100	20	0.333	8.32	
J02	103.2	100	20	0.634	16.5	16.5
	106.2	100	20	0.653	16.5	
J03	108.0	500	20	0.199	24.2	24.0
	102.2	500	20	0.186	23.8	
Annotation: the results based on the calibration curve: ABS=0.8436×C_P(ppm)+0.007.						

Table 5.5 Content of SiO_2 in tablet after reaction.

No.	Weight (1) /mg	Crucible /g	Weight (2) /g	Weight (3) /g	SiO_2 /mass%	Ave SiO_2 /mass%
G01	104.1	23.85968	23.88078	23.86069	19.30	19.73

	102.7	23.92143	23.94515	23.92445	20.16	
G02	106.0	23.85904	23.87763	23.86098	15.71	16.00
	104.2	23.92281	23.94094	23.92398	16.28	
G03	103.1	23.85875	23.87103	23.85989	10.81	10.69
	101.6	23.92284	23.93443	23.92369	10.57	
G04	112.2	23.8539	23.86095	23.85505	5.258	5.275
	109.8	23.91869	23.92466	23.91885	5.291	
H01	103.6	23.85705	23.88118	23.85899	21.42	20.99
	101.0	23.92163	23.94446	23.92369	20.56	
H02	106.4	23.85740	23.87610	23.85835	16.68	16.30
	103.1	23.92213	23.93944	23.92303	15.92	
H03	104.7	23.85740	23.86851	23.85740	10.61	10.62
	102.8	23.92141	23.93310	23.92217	10.63	
I01	104.6	23.86589	23.89214	23.86546	25.51	24.83
	107.6	23.92820	23.95397	23.92798	24.15	
I02	106.1	23.86378	23.88561	23.86570	18.77	18.63
	104.4	23.92708	23.94716	23.92786	18.49	
I03	107.3	23.86346	23.87847	23.86526	12.31	12.36
	109.2	23.92623	23.94140	23.92785	12.41	
I04	109.7	23.85503	23.86296	23.85603	6.317	6.317
	108.6	23.91919	23.92657	23.91971	6.317	
J01	108.2	23.86446	23.89086	23.86486	24.03	24.10
	106.2	23.92681	23.95253	23.92687	24.16	
J02	103.2	23.86327	23.88240	23.86408	17.75	18.17
	106.2	23.92583	23.94645	23.92672	18.58	
J03	108.0	23.86304	23.87708	23.86338	12.69	12.60
	102.2	23.92569	23.93895	23.92618	12.50	

Annotation: the weight (1) is the weight of sample. The weight (2) is the weight of Pt crucible after the filter paper burned. The weight (3) is the weight of crucible after evaporating the SiO_2.

SiO_2/mass%=[weight (2) - weight (3)]/[weight (1)]×100000/%

Table 5.6 Content of CaO in tablet after reaction.

No.	Weight /mg	Dilution ratio	Test /ppm	CaO /mass%	Ave CaO /mass%
G01	102.2	100	3.363	46.04	45.96
	101.8	100	3.338	45.87	
G02	109.2	100	3.454	44.25	44.36
	102.9	100	3.270	44.46	
G03	102.8	100	3.148	42.84	42.71
	102.8	100	3.129	42.58	
G04	110.6	100	3.273	41.40	41.48
	101.5	100	3.015	41.56	
H01	106.5	100	3.492	45.87	45.55
	109.1	100	3.527	45.23	
H02	103.8	100	3.277	44.17	44.24
	102.6	100	3.249	44.30	
H03	104.2	100	3.178	42.67	42.65
	104.9	100	3.196	42.62	
I01	100.6	100	3.981	55.36	55.89
	102.0	100	4.113	56.41	
I02	106.2	100	4.108	54.12	53.97
	105.8	100	4.070	53.82	
I03	102.3	100	3.855	52.72	52.51

	105.8	100	3.955	52.30	
I04	107.8	100	3.860	50.09	50.85
	102.4	100	3.777	51.60	
J01	103.6	100	4.118	55.61	55.65
	107.1	100	4.263	55.69	
J02	105.4	100	3.976	52.77	52.80
	102.9	100	3.885	52.82	
J03	107.4	100	3.982	51.87	52.36
	105.1	100	3.970	52.85	

Table 5.7 Content of MgO in tablet after reaction.

No.	Weight /mg	Dilution ratio	Test /ppm	MgO /mass%	Ave MgO /mass%
G01	102.2	100	1.448	23.50	23.42
	101.8	100	1.432	23.33	
G02	109.2	100	1.501	22.80	23.12
	102.9	100	1.454	23.43	
G03	102.8	100	1.468	23.68	23.66
	102.8	100	1.465	23.64	
G04	110.6	100	1.537	23.05	22.99
	101.5	100	1.403	22.92	
H01	106.5	100	1.498	23.33	23.16
	109.1	100	1.512	22.98	
H02	103.8	100	1.465	23.41	23.52
	102.6	100	1.462	23.63	
H03	104.2	100	1.481	23.57	23.73
	104.9	100	1.511	23.89	

I01	100.6	10	4.534	7.475	7.531
	102.0	10	4.666	7.587	
I02	106.2	10	5.075	7.925	7.801
	105.8	10	4.897	7.676	
I03	102.3	10	4.815	7.806	7.864
	105.8	10	5.053	7.921	
I04	107.8	10	4.982	7.664	7.841
	102.4	10	4.951	8.018	
J01	103.6	10	5.220	8.358	8.383
	107.1	10	5.429	8.407	
J02	105.4	10	5.500	8.654	8.668
	102.9	10	5.387	8.682	
J03	107.4	10	5.515	8.516	8.520
	105.1	10	5.401	8.523	

Table 5.8 Analysis data for the content of FeO in tablet after reaction.

No.	Weight /mg	Dilution ratio	Test /ppm	FeO /mass%	Ave FeO /mass%
G01	102.2	1	4.707	0.5926	0.6069
	101.8	1	4.914	0.6211	
G02	109.2	1	5.357	0.6312	0.6431
	102.9	1	5.238	0.6550	
G03	102.8	1	5.215	0.6528	0.6446
	102.8	1	5.084	0.6364	
G04	110.6	1	3.395	0.3950	0.4514
	101.5	1	4.006	0.5078	
H01	106.5	1	6.984	0.8438	0.8568

	109.1	1	7.374	0.8697	
H02	103.8	10	1.081	1.340	1.323
	102.6	10	1.041	1.306	
H03	104.2	10	1.048	1.294	1.289
	104.9	10	1.047	1.284	
I01	100.6	1	3.659	0.4680	0.4822
	102.0	1	3.934	0.4963	
I02	106.2	1	4.146	0.5023	0.4986
	105.8	1	4.069	0.4949	
I03	102.3	1	3.720	0.4679	0.4775
	105.8	1	4.004	0.4870	
I04	107.8	1	2.661	0.3176	0.3387
	102.4	1	2.863	0.3598	
J01	103.6	1	6.189	0.7687	0.7680
	107.1	1	6.386	0.7672	
J02	105.4	1	4.373	0.5339	0.5379
	102.9	1	4.333	0.5418	
J03	107.4	1	3.615	0.4331	0.4272
	105.1	1	3.440	0.4212	

Table 5.9 Compositions of tablets and concentration of P in Fe after reaction.

No.	Solid solution/mass%						P in Fe
	P_2O_5	SiO_2	CaO	MgO	FeO	Total	/mass%
G01	6.97	19.73	45.96	23.42	0.6069	96.7	0.00506
G02	13.8	16.00	44.36	23.12	0.6431	97.9	0.0124
G03	21.1	10.69	42.71	23.66	0.6446	98.8	0.0179
G04	27.9	5.275	41.48	22.99	0.4514	98.1	0.0292

H01	6.91	20.99	45.55	23.16	0.8568	97.5	0.00798
H02	13.8	16.30	44.24	23.52	1.323	99.2	0.0171
H03	21.0	10.62	42.65	23.73	1.289	99.3	0.0220
I01	8.47	24.83	55.89	7.531	0.4822	97.2	0.00635
I02	16.8	18.63	53.97	7.801	0.4986	97.7	0.00903
I03	24.3	12.36	52.51	7.864	0.4775	97.5	0.0206
I04	33.7	6.317	50.85	7.841	0.3387	99.0	0.0372
J01	8.28	24.10	55.65	8.383	0.7680	97.2	0.00995
J02	16.5	18.17	52.80	8.668	0.5379	96.7	0.0213
J03	24.0	12.60	52.36	8.520	0.4272	97.9	0.0369

5.3.2 XRD pattern of the $2CaO{\cdot}SiO_2$-$3CaO{\cdot}P_2O_5$ solid solution containing 8 and 24 mass% MgO

The phases of the $2CaO{\cdot}SiO_2$-$3CaO{\cdot}P_2O_5$ solid solution containing 8 and 24 mass% MgO were analyzed by XRD as shown from **Figure 5.2** to **5.9**. In all samples, the CaO, SiO_2 and P_2O_5 phases were undetected but the MgO phase was detected. The eutectoid appeared during quenching.

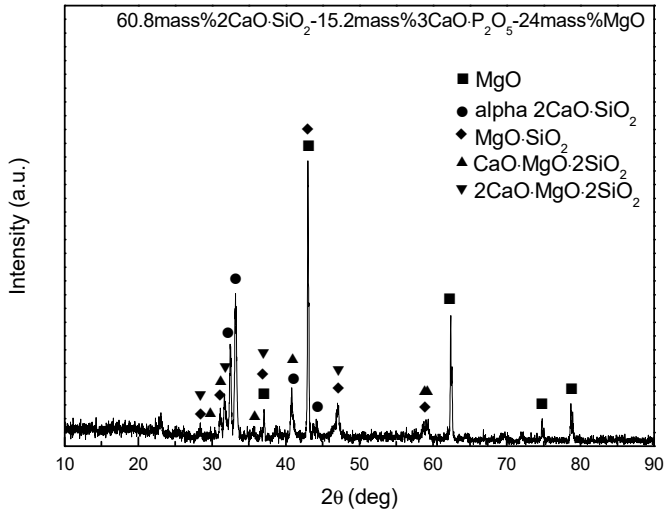

Fig. 5.2 XRD pattern of the 60.8mass%$2CaO{\cdot}SiO_2$-15.2mass%$3CaO{\cdot}P_2O_5$ solid solution-24mass%MgO.

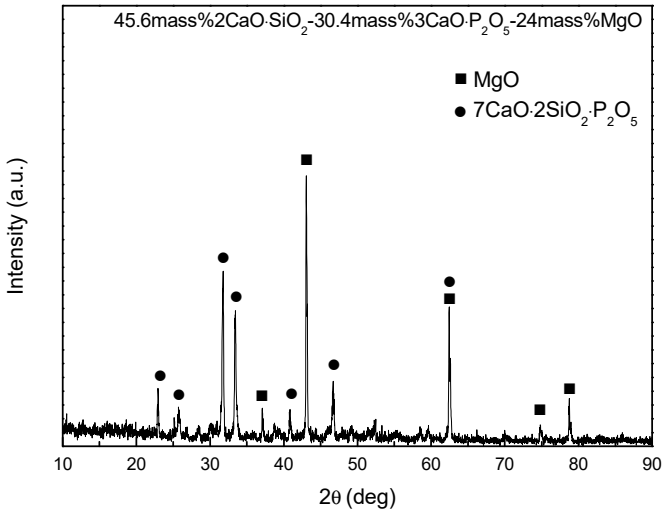

Fig. 5.3 XRD pattern of the 45.6mass%2CaO·SiO_2-30.4mass%3CaO·P_2O_5 solid solution-24mass%MgO.

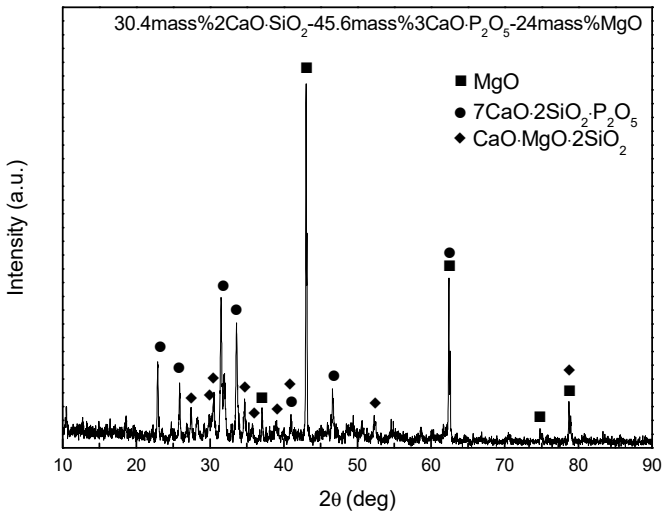

Fig. 5.4 XRD pattern of the 30.4mass%2CaO·SiO_2-45.6mass%3CaO·P_2O_5 solid solution-24mass%MgO.

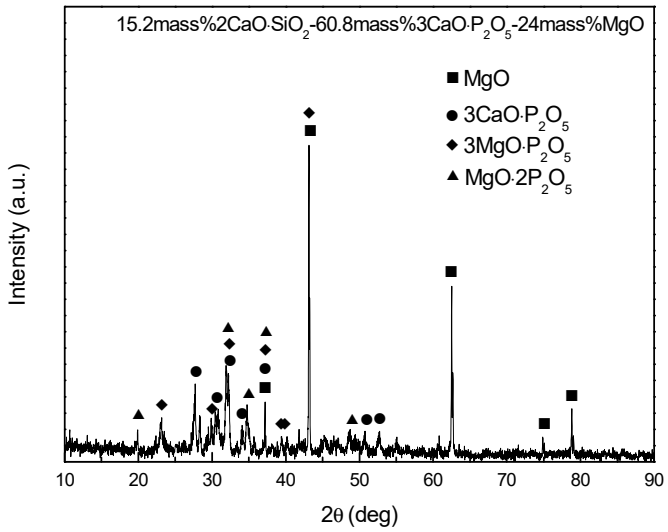

Fig. 5.5 XRD pattern of the 15.2mass%2CaO·SiO_2-60.8mass%3CaO·P_2O_5 solid solution-24mass%MgO.

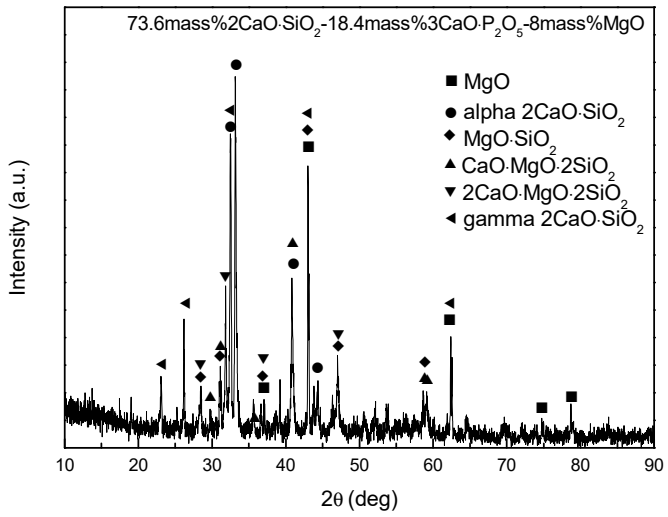

Fig. 5.6 XRD pattern of the 73.6mass%2CaO·SiO_2-18.4mass%3CaO·P_2O_5 solid solution-8mass%MgO.

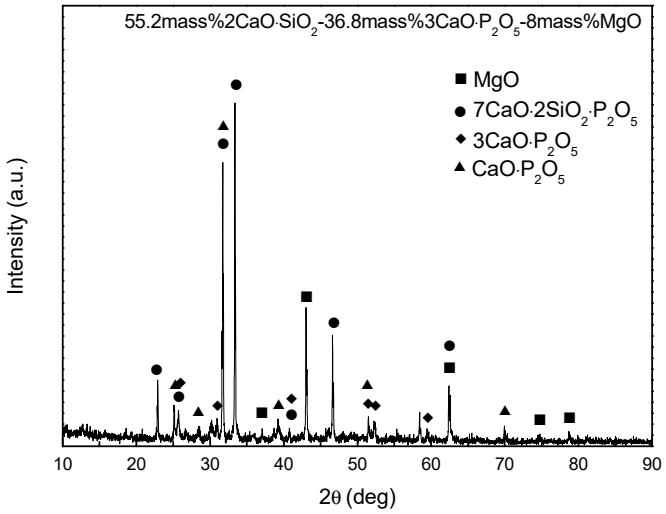

Fig. 5.7 XRD pattern of the 55.2mass%2CaO·SiO_2-36.8mass%3CaO·P_2O_5 solid solution-8mass%MgO.

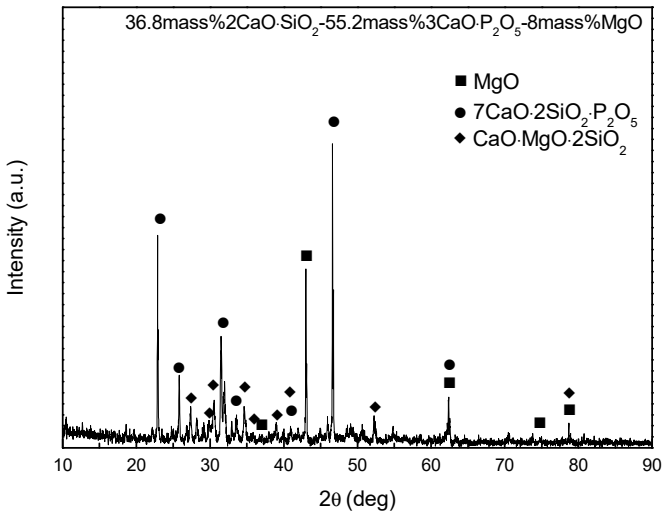

Fig. 5.8 XRD pattern of the 36.8mass%2CaO·SiO_2-55.2mass%3CaO·P_2O_5 solid solution-8mass%MgO.

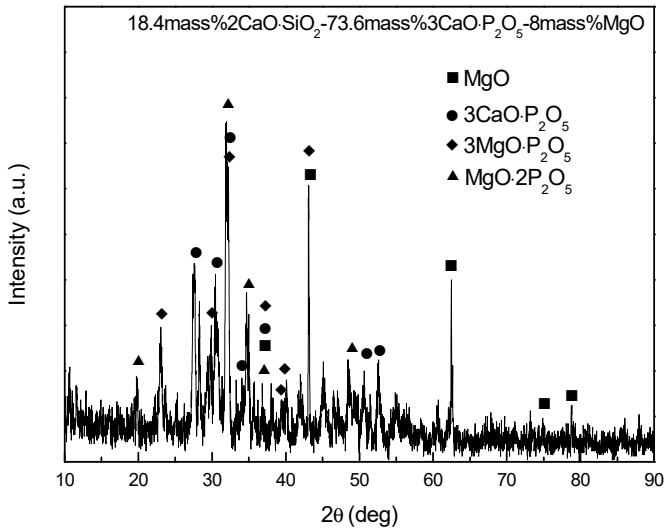

Fig. 5.9 XRD pattern of the 18.4mass%2CaO·SiO_2-73.6mass%3CaO·P_2O_5 solid solution-8mass%MgO.

5.3.3 XRD pattern of the $2CaO{\cdot}SiO_2$-$3CaO{\cdot}P_2O_5$ solid solution containing 8 and 24 mass% MgO after reaction

The phases of the tablet after reaction were analyzed by XRD as shown from **Figure 5.10** to **5.23**. The MgO phase was detected in the whole samples. The eutectoid appeared during quenching.

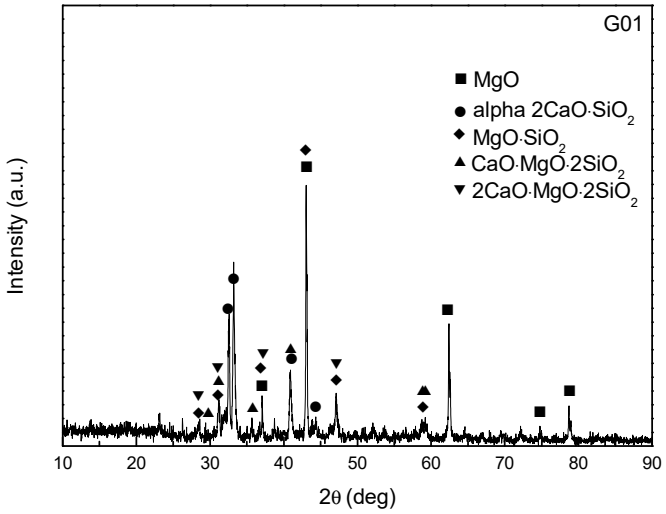

Fig. 5.10 XRD pattern of sample G01 after reaction.

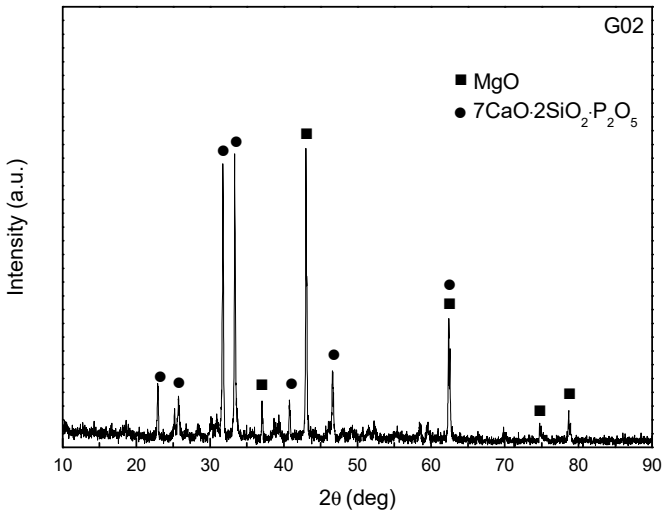

Fig. 5.11 XRD pattern of sample G02 after reaction.

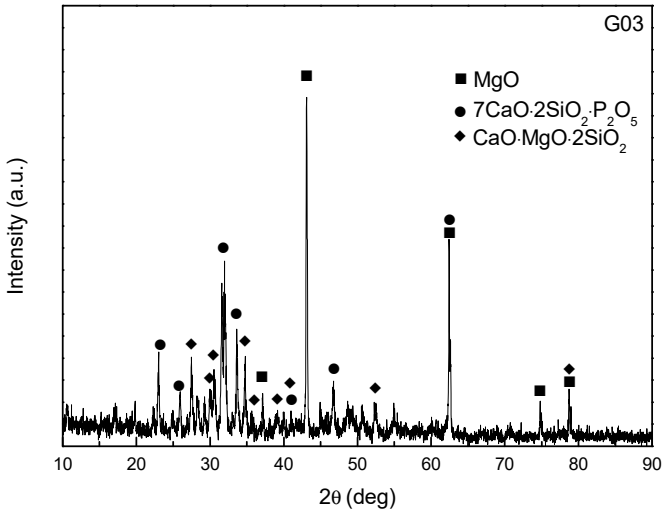

Fig. 5.12 XRD pattern of sample G03 after reaction.

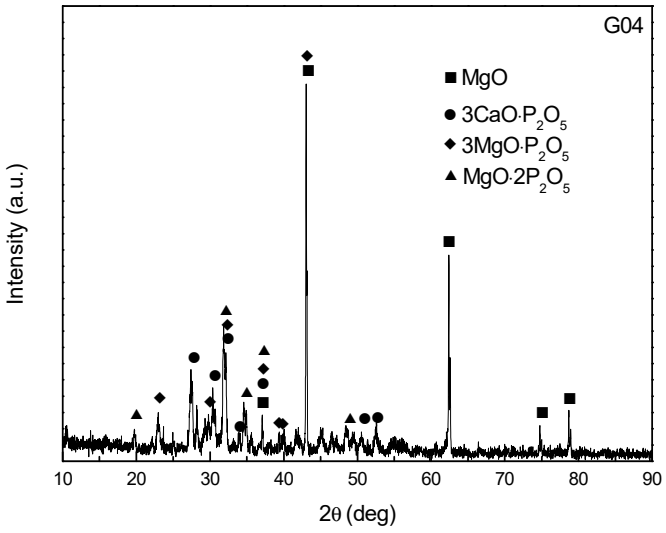

Fig. 5.13 XRD pattern of sample G04 after reaction.

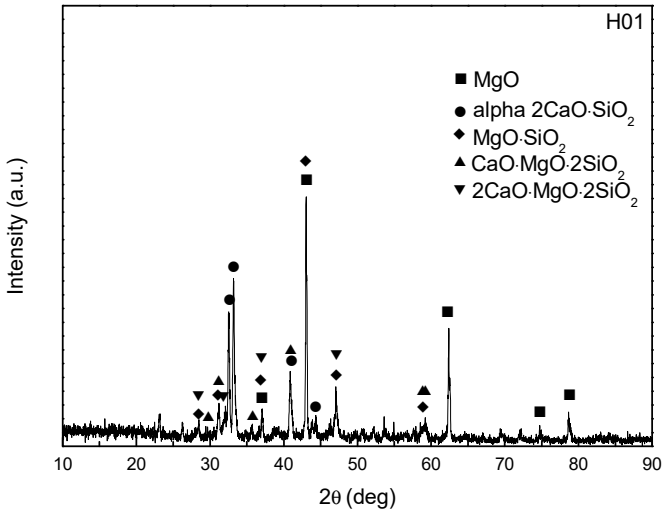

Fig. 5.14 XRD pattern of sample H01 after reaction.

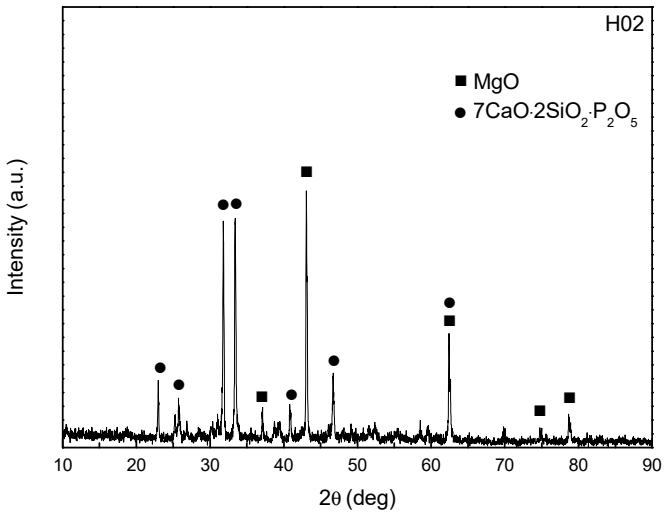

Fig. 5.15 XRD pattern of sample H02 after reaction.

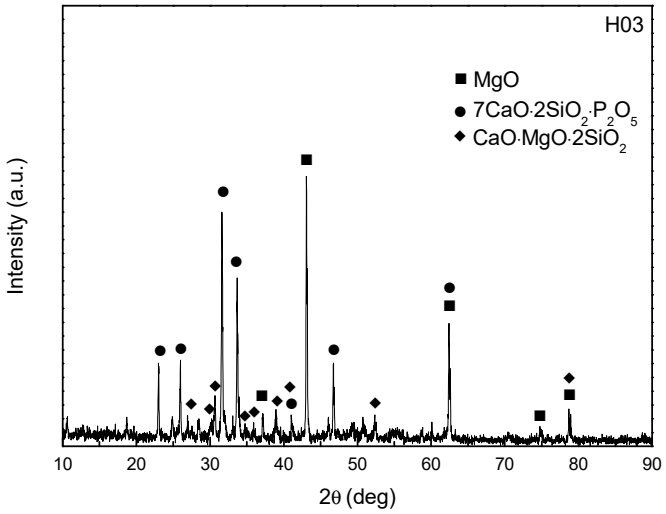

Fig. 5.16 XRD pattern of sample H03 after reaction.

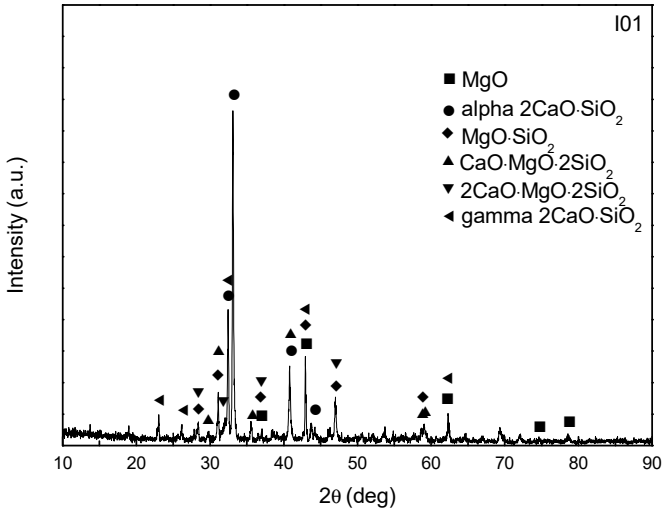

Fig. 5.17 XRD pattern of sample I01 after reaction.

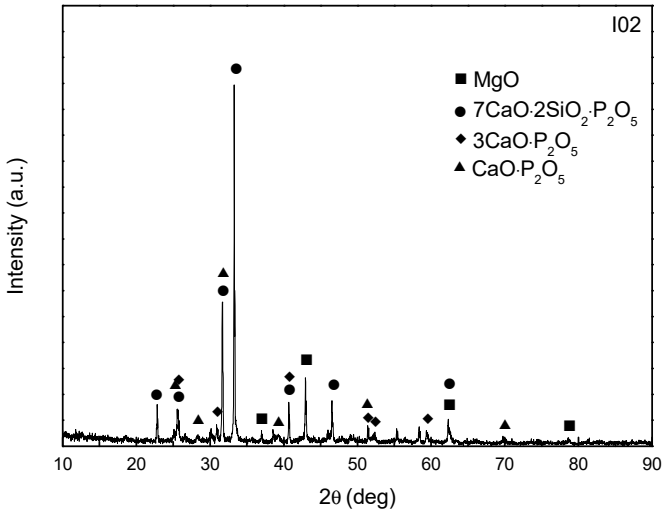

Fig. 5.18 XRD pattern of sample I02 after reaction.

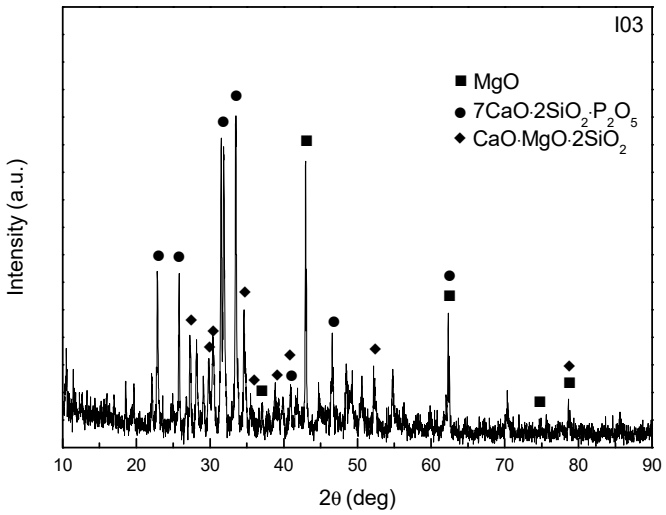

Fig. 5.19 XRD pattern of sample I03 after reaction.

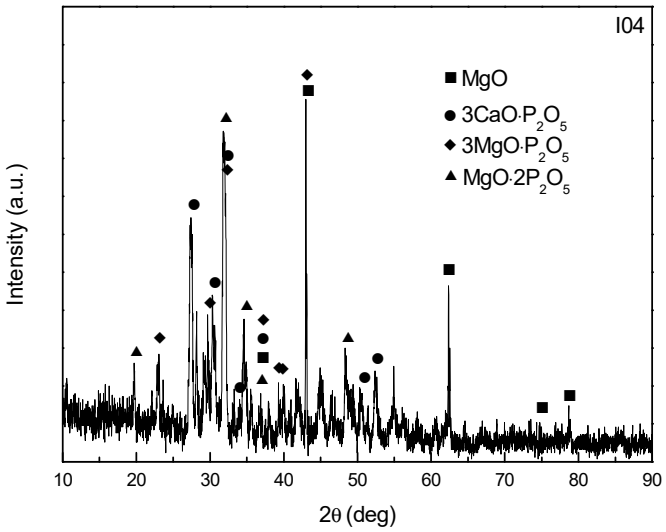

Fig. 5.20 XRD pattern of sample I04 after reaction.

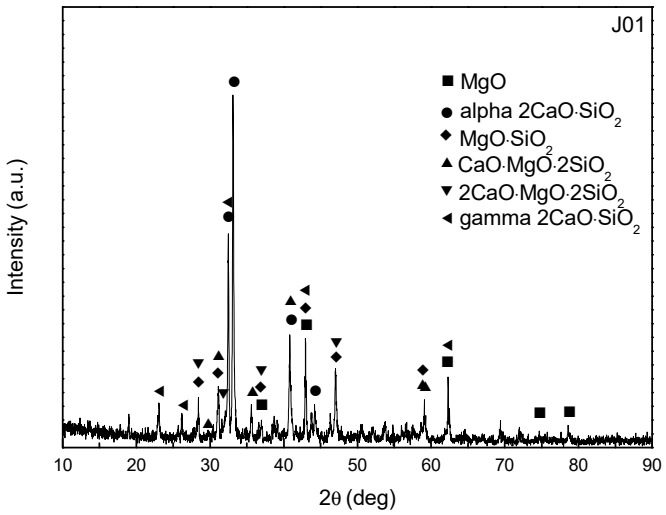

Fig. 5.21 XRD pattern of sample J01 after reaction.

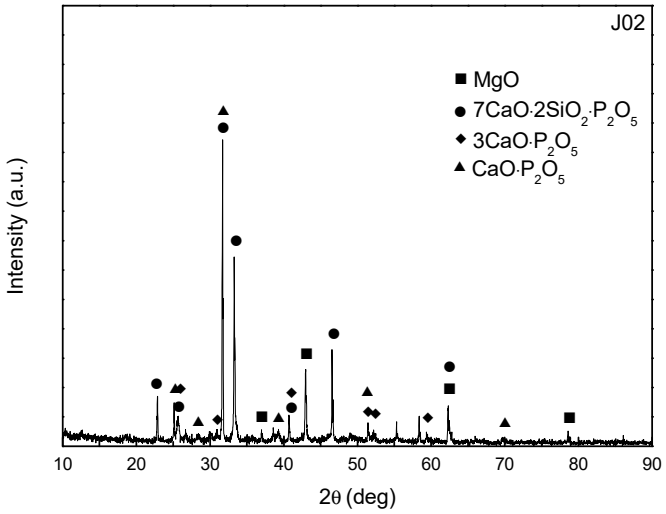

Fig. 5.22 XRD pattern of sample J02 after reaction.

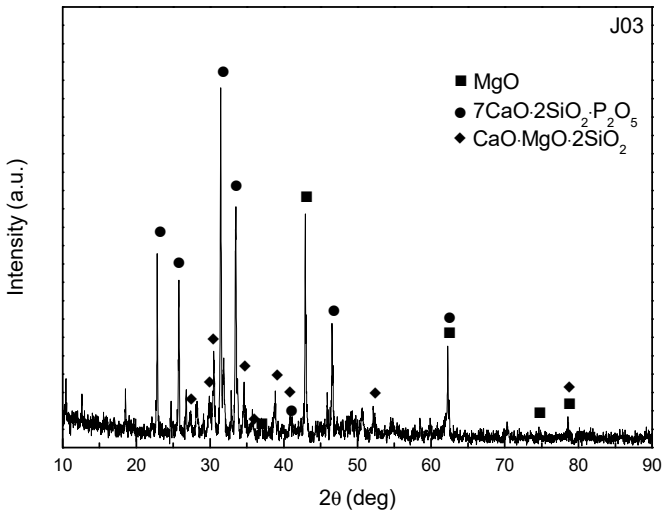

Fig. 5.23 XRD pattern of sample J03 after reaction.

5.4 Discussion

From the compositions as shown in Table 5.9, the mole fraction of $3CaO·P_2O_5$ and P_2O_5 in the $2CaO·SiO_2$-$3CaO·P_2O_5$ solid solution, the mole fraction of FeO in tablets after reaction were shown in **Table 5.10**. The content of $3CaO·P_2O_5$ in the $2CaO·SiO_2$-$3CaO·P_2O_5$ solid solution was calculated from the analyzed content P_2O_5. The mole fraction of P_2O_5 in the solid solution was calculated from the content of $3CaO·P_2O_5$. The compositions were projected onto the CaO-SiO_2-P_2O_5 system as shown in **Figure 5.24**.

Table 5.10 Compositions of tablets after reaction.

No.	$3CaO·P_2O_5$/mol%	P_2O_5/mol%	FeO/mol%
G01	13.0	4.10	0.473
G02	26.7	8.42	0.516
G03	45.5	13.7	0.533
G04	69.1	19.2	0.393
H01	12.2	4.02	0.664
H02	26.4	8.40	1.05
H03	45.6	13.6	1.06
I01	12.6	4.06	0.404
I02	27.6	8.51	0.437
I03	45.4	13.0	0.439
I04	69.3	19.0	0.326
J01	12.7	4.02	0.641
J02	27.8	8.55	0.473
J03	44.6	12.9	0.389

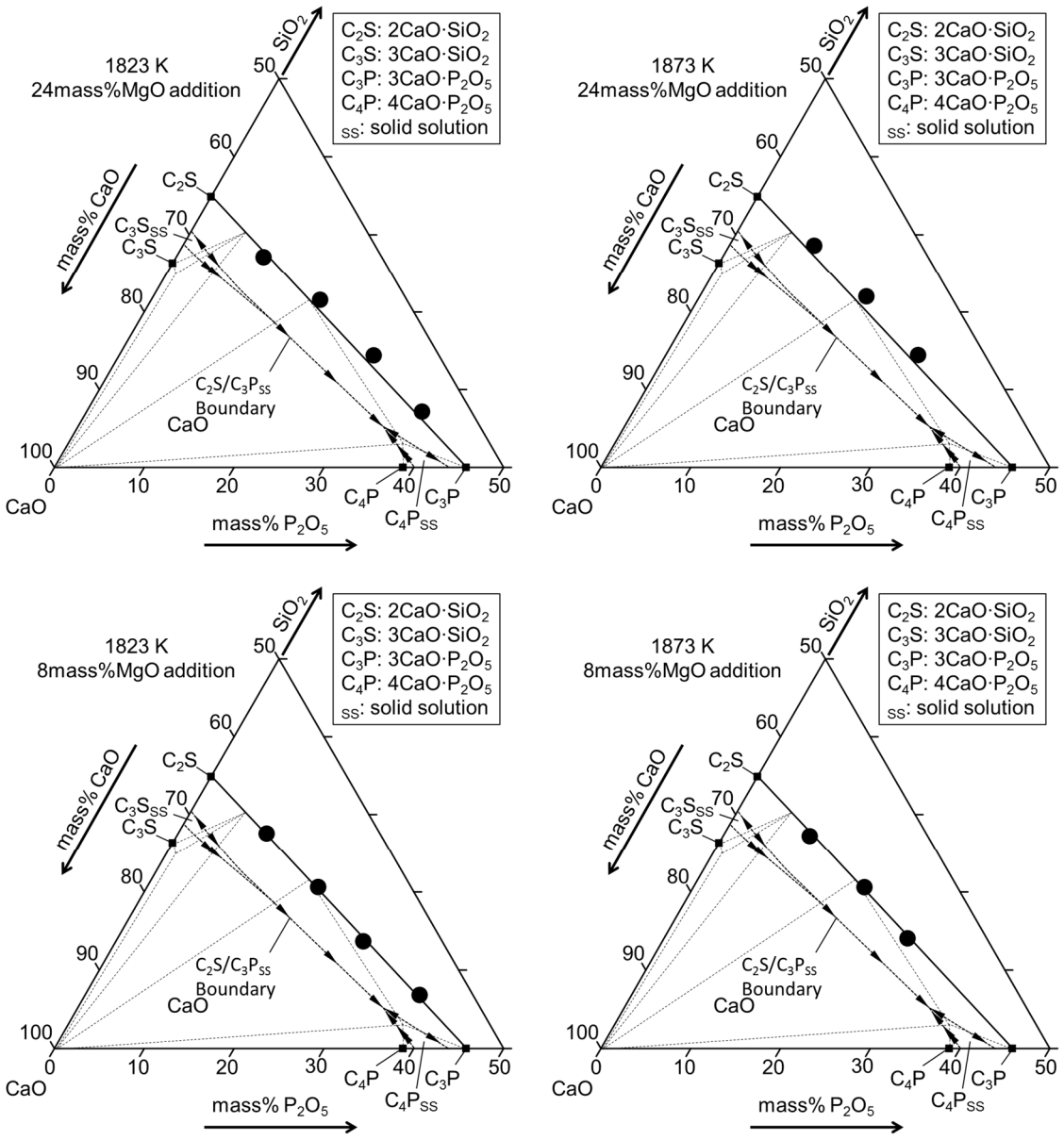

Fig. 5.24 Compositions of tablets after reaction on the CaO-SiO_2-P_2O_5 system.

5.4.1 Contents of FeO and MgO and activity coefficient of FeO in the tablet after reaction

Figure 5.25 shows the relationship between the P_2O_5 content and the FeO and MgO contents in tablets after reaction. The content of FeO was smaller than 1 mass% for most samples. The content of MgO after reaction was almost the same from the initial content.

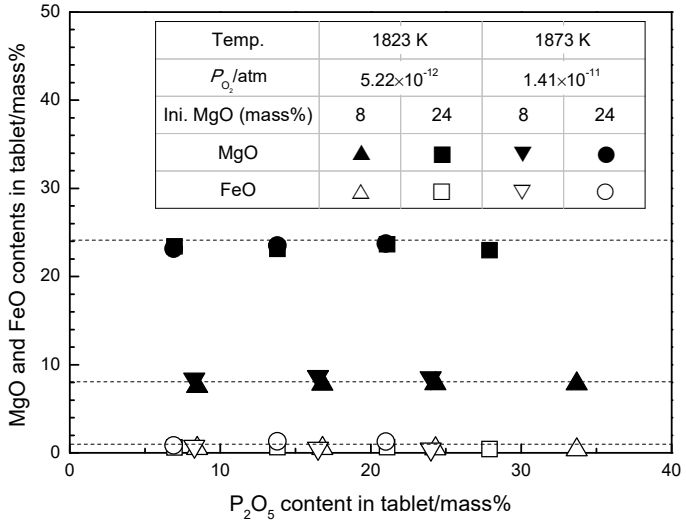

Fig. 5.25 Contents of FeO and MgO in the tablet after reaction.

According to the activity of FeO introduced in Chapter 3, the activity coefficient of FeO relative to hypothetical pure liquid FeO was calculated and shown in **Table 5.11** and **Figure 5.26**. At a certain temperature and oxygen partial pressure, the activity coefficient of FeO was almost constant. The activity coefficient of FeO was in the range from 1.30×10^{-8} to 4.47×10^{-8}.

Table 5.11 Thermodynamic data of the $2CaO{\cdot}SiO_2$-$3CaO{\cdot}P_2O_5$ solid solution containing 8 and 24 mass% MgO.

No.	γ_{FeO}	$\frac{(mass\%P)}{[mass\%P]}$	$a_{P_2O_5}$	$\gamma_{P_2O_5}$	$a_{3MgO\cdot P_2O_5}$
G01	1.42×10^{-8}	8.28×10^{2}	9.24×10^{-25}	2.22×10^{-23}	6.65×10^{-12}
G02	1.30×10^{-8}	6.55×10^{2}	5.59×10^{-24}	6.83×10^{-23}	4.03×10^{-11}
G03	1.26×10^{-8}	6.91×10^{2}	1.17×10^{-23}	8.90×10^{-23}	8.44×10^{-11}

G04	1.71×10^{-8}	5.59×10^{2}	3.16×10^{-23}	1.69×10^{-22}	2.27×10^{-10}
H01	2.62×10^{-8}	5.15×10^{2}	2.26×10^{-24}	5.78×10^{-23}	8.99×10^{-12}
H02	1.66×10^{-8}	4.74×10^{2}	1.05×10^{-23}	1.30×10^{-22}	4.17×10^{-11}
H03	1.64×10^{-8}	5.11×10^{2}	1.75×10^{-23}	1.32×10^{-22}	6.94×10^{-11}
I01	1.66×10^{-8}	6.53×10^{2}	1.46×10^{-24}	3.61×10^{-23}	1.05×10^{-11}
I02	1.54×10^{-8}	9.09×10^{2}	2.96×10^{-24}	3.51×10^{-23}	2.13×10^{-11}
I03	1.53×10^{-8}	5.78×10^{2}	1.56×10^{-23}	1.18×10^{-22}	1.12×10^{-10}
I04	2.06×10^{-8}	4.35×10^{2}	5.17×10^{-23}	2.75×10^{-22}	3.72×10^{-10}
J01	2.72×10^{-8}	4.13×10^{2}	3.53×10^{-24}	8.69×10^{-23}	1.40×10^{-11}
J02	3.67×10^{-8}	3.87×10^{2}	1.64×10^{-23}	1.93×10^{-22}	6.50×10^{-11}
J03	4.47×10^{-8}	3.19×10^{2}	4.99×10^{-23}	3.85×10^{-22}	1.98×10^{-10}

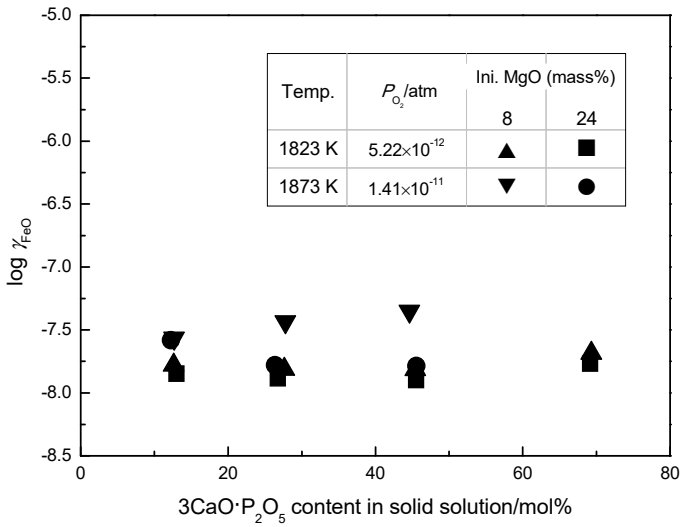

Fig. 5.26 Activity coefficient of FeO in the tablet after reaction.

5.4.2 Equilibrium concentration of P in molten iron and phosphorus partition ratio between the mixture of $2CaO{\cdot}SiO_2$-$3CaO{\cdot}P_2O_5$ solid solution and MgO and molten iron

Figure 5.27 shows the relationship between the equilibrium concentration of P in molten iron and the $3CaO{\cdot}P_2O_5$ content in the solid solution. The concentration of P in molten iron increased with the increase of the $3CaO{\cdot}P_2O_5$ content in the solid solution. The phosphorus partition ratio between the mixture of $2CaO{\cdot}SiO_2$-$3CaO{\cdot}P_2O_5$ solid solution and MgO and molten iron was shown in **Figure 5.28** and Table 5.11. The phosphorus partition ratio decreased with the increase of the $3CaO{\cdot}P_2O_5$ content in the solid solution.

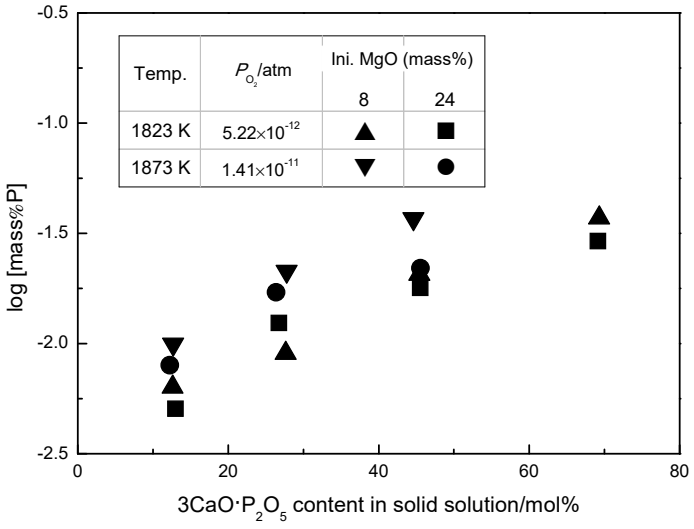

Fig. 5.27 Equilibrium concentration of P in molten iron.

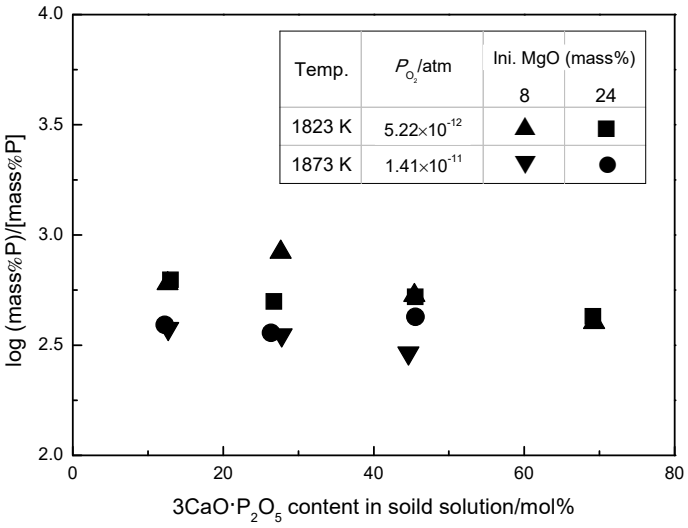

Fig. 5.28 Phosphorus partition ratio between the mixture of $2CaO{\cdot}SiO_2$-$3CaO{\cdot}P_2O_5$ solid solution and MgO and molten iron.

5.4.3 Activity and activity coefficient of P_2O_5 in the $2CaO{\cdot}SiO_2$-$3CaO{\cdot}P_2O_5$ solid solution containing 8 and 24 mass% MgO

Figures 5.29 and **5.30** show activity and activity coefficient of P_2O_5 as a function of $3CaO{\cdot}P_2O_5$ content in the solid solution with the values shown in Table 5.11. For a constant composition of solid solution, the activity and activity coefficient of P_2O_5 barely changed with the change of the temperature and the extra MgO content. The activity of P_2O_5 changed from 9.24×10^{-25} to 5.17×10^{-23} and the activity coefficient of P_2O_5 changed from 2.22×10^{-23} to 3.85×10^{-22}.

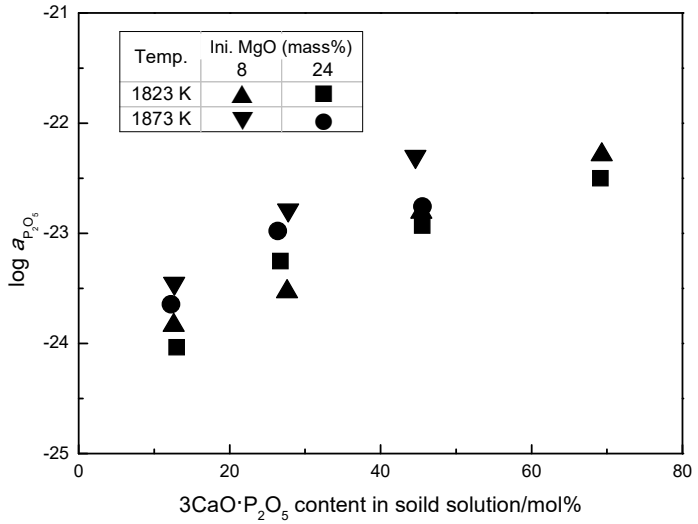

Fig. 5.29 Activity of P_2O_5 in the $2CaO{\cdot}SiO_2$-$3CaO{\cdot}P_2O_5$ solid solution containing 8 and 24 mass% MgO.

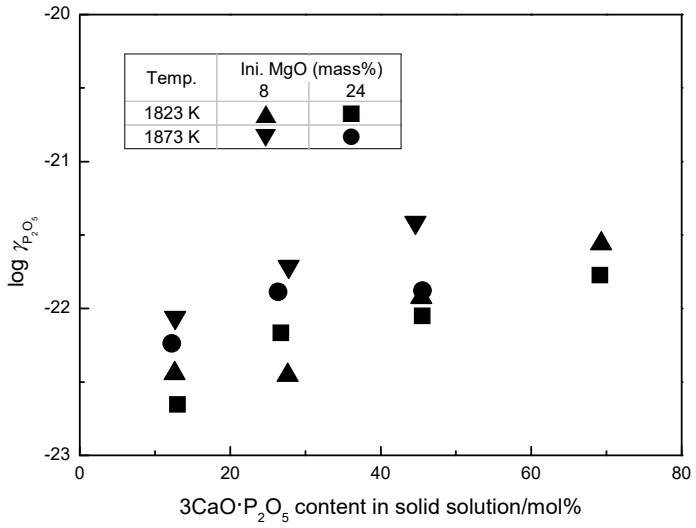

Fig. 5.30 Activity coefficient of P_2O_5 in the $2CaO{\cdot}SiO_2$-$3CaO{\cdot}P_2O_5$ solid solution containing 8 and 24 mass% MgO.

5.4.4 Activity of $3MgO{\cdot}P_2O_5$ in the $2CaO{\cdot}SiO_2$-$3CaO{\cdot}P_2O_5$ solid solution saturated with MgO

Since the MgO phase was detected after reaction, the activity of $3MgO{\cdot}P_2O_5$ was calculated from the activity of P_2O_5 by Eqs. (5.1) and (5.2). The activity of $3MgO{\cdot}P_2O_5$ in the $2CaO{\cdot}SiO_2$-$3CaO{\cdot}P_2O_5$ solid solution saturated with MgO were shown in **Figure 5.31** with the values in Table 5.11. The activity of $3MgO{\cdot}P_2O_5$ increased with the increase of the $3CaO{\cdot}P_2O_5$ content in the solid solution. For a constant composition of solid solution, the activity of $3MgO{\cdot}P_2O_5$ barely changed with the change of the temperature and the MgO content. The activity of $3MgO{\cdot}P_2O_5$ changed from 6.65×10^{-12} to 3.72×10^{-10}.

$$3\mathrm{MgO(s)} + \mathrm{P_2(g)} + 5/2\,\mathrm{O_2(g)} = 3\mathrm{MgO}\cdot\mathrm{P_2O_5(s)}$$

$$\Delta G^{\circ}_{5.1} = -1993000 + 510.0T\ \mathrm{J/mol} \ldots\ldots (5.1)^{[2]}$$

$$\mathrm{P_2(g)} + 5/2\,\mathrm{O_2(g)} = \mathrm{P_2O_5(l)}$$

$$\Delta G^{\circ}_{5.2} = -1655480 + 571.0T\ \mathrm{J/mol} \ldots\ldots (5.2)^{[3]}$$

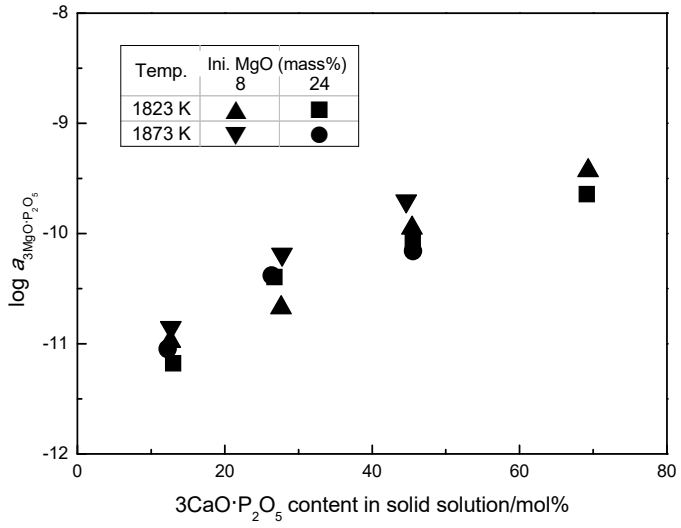

Fig. 5.31 Activity of $3MgO{\cdot}P_2O_5$ in the $2CaO{\cdot}SiO_2$-$3CaO{\cdot}P_2O_5$ solid solution containing 8 and 24 mass% MgO.

5.5 Summary

By applying the chemical equilibrium method, the equilibrium of phosphorus between the mixture of $2CaO{\cdot}SiO_2$-$3CaO{\cdot}P_2O_5$ solid solution and MgO and molten iron was measured at 1823 K with the oxygen partial pressure of 5.22×10^{-12} atm and 1873 K with the oxygen partial pressure of 1.41×10^{-11} atm. The activity of P_2O_5 relative to hypothetical pure liquid P_2O_5 in the $2CaO{\cdot}SiO_2$-$3CaO{\cdot}P_2O_5$ solid solution containing 8 and 24 mass% MgO increased from 9.24×10^{-25} to 5.17×10^{-23} and the activity coefficient of P_2O_5 increased from 2.22×10^{-23} to 3.85×10^{-22} with the increase of the $3CaO{\cdot}P_2O_5$ content in the solid solution from 12.2 to 69.3 mol%. The activity of $3MgO{\cdot}P_2O_5$ in the $2CaO{\cdot}SiO_2$-$3CaO{\cdot}P_2O_5$ solid solution saturated with MgO was estimated from 6.65×10^{-12} to 3.72×10^{-10} with the increase of the $3CaO{\cdot}P_2O_5$ content in the solid solution.

References

1. W. Gutt: *Nature*, **197** (1963), 142-143.
2. E.T. Turkdogan: Physical Chemistry of High Temperature Technology, Academic Press, New York, (1980), 14.
3. E. T. Turkdogan: *ISIJ Int.*, **40** (2000), 964-970.

Chapter 6 Summary of the Thermodynamic Properties of the Calcium Phosphate-based Solid Solution and Prospect of Utilizing the Multi-phase Flux

6.1 Introduction

In this chapter the thermodynamic properties about the calcium phosphate-based solid solution measured in the Chapters 3, 4 and 5 were summarized. Moreover the prospect of application of multi-phase flux on the dephosphorization process was primitively introduced.

6.2 Content of FeO and activity coefficient of FeO in the tablet after reaction under various conditions

Figure 6.1 shows the content of FeO in the tablet after reaction under various conditions. The content of FeO barely changed with the increase of P_2O_5 content in the tablet. For most samples, the content of FeO was smaller than 1 mass%.

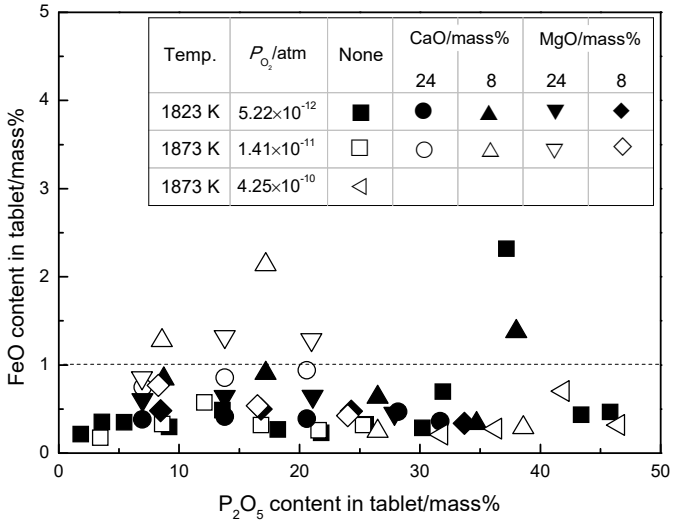

Fig. 6.1 Content of FeO in the tablet after reaction.

Figure 6.2 summarized the activity coefficient of FeO in the tablet after reaction under various conditions. The activity coefficient of FeO was maintained at a stable value at a constant temperature and oxygen partial pressure and the activity coefficient of FeO with the oxygen partial pressure of 4.25×10^{-10} atm at 1873 K was larger than the others.

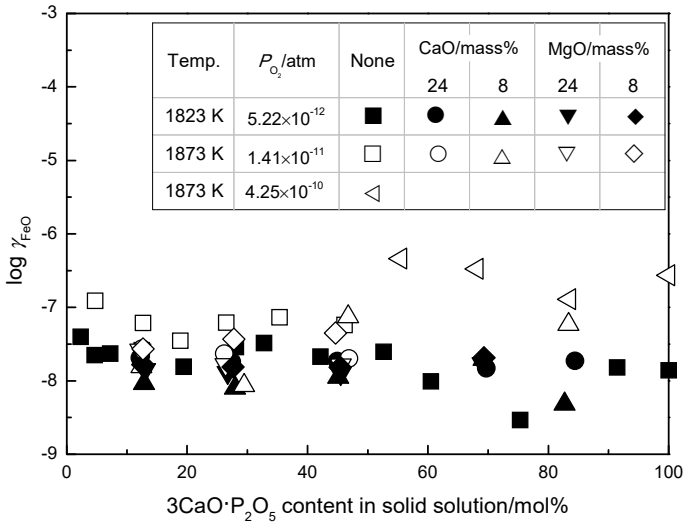

Fig. 6.2 Activity coefficient of FeO in the tablet after reaction.

6.3 Activity and activity coefficient of P_2O_5 in the $2CaO{\cdot}SiO_2$-$3CaO{\cdot}P_2O_5$ solid solution under various conditions

The activity and activity coefficient of P_2O_5 in the $2CaO{\cdot}SiO_2$-$3CaO{\cdot}P_2O_5$ solid solution under various conditions in current research were summarized in **Figures 6.3** and **6.4** comparing with the values conducted by Hasegawa *et al*.[1] and Pahlevani *et al*.[2] All the activity and activity coefficient of P_2O_5 were very small, because of this the method of multi-phase flux could be applied for dephosphorization. The current values and the values conducted by Hasegawa *et al*. increased with the increase of the $3CaO{\cdot}P_2O_5$ content in the solid solution. The values conducted by Pahlevani *et al*. barely changed with the increase of the $3CaO{\cdot}P_2O_5$ content in the solid solution. The temperature dependency for the values conducted by Pahlevani *et al*. was not clear.

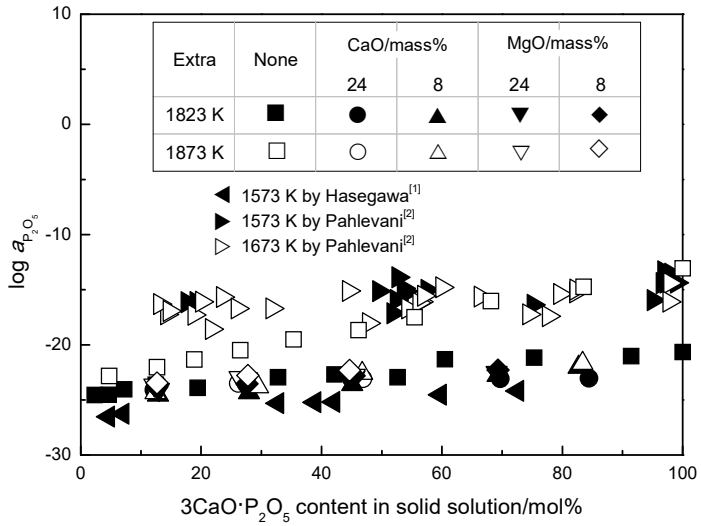

Fig. 6.3 Activity of P_2O_5 in the $2CaO{\cdot}SiO_2$-$3CaO{\cdot}P_2O_5$ solid solution under various conditions.

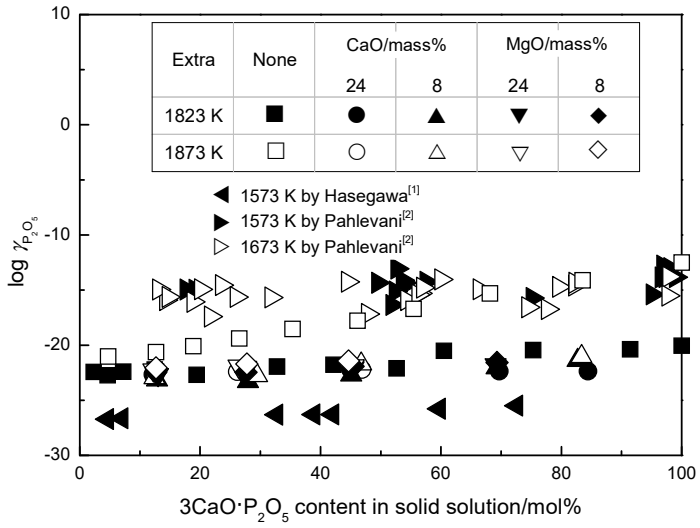

Fig. 6.4 Activity coefficient of P_2O_5 in the $2CaO{\cdot}SiO_2$-$3CaO{\cdot}P_2O_5$ solid solution under various conditions.

6.4 Effect of MgO on the activity of P_2O_5 in the $2CaO{\cdot}SiO_2$-$3CaO{\cdot}P_2O_5$ solid solution

At a certain temperature for a certain composition of the $2CaO{\cdot}SiO_2$-$3CaO{\cdot}P_2O_5$ solid solution, the product of $a_{CaO}{}^3$ and $a_{P_2O_5}$ is constant from Eq. (6.1). The activity of P_2O_5 in the $2CaO{\cdot}SiO_2$-$3CaO{\cdot}P_2O_5$ solid solution saturated with CaO was smaller than that in the $2CaO{\cdot}SiO_2$-$3CaO{\cdot}P_2O_5$ solid solution unsaturated with CaO as described in Chapters 3 and 4.

$$3CaO(s) + P_2O_5(l) = 3CaO \cdot P_2O_5(s)$$

$$K = \frac{a_{3CaO\cdot P_2O_5}}{a_{CaO}{}^3 a_{P_2O_5}} \ldots\ldots (6.1)$$

For the effect of MgO on the activity of P_2O_5 in the $2CaO{\cdot}SiO_2$-$3CaO{\cdot}P_2O_5$ solid solution, the comparison of P_2O_5 activity was shown in **Figure 6.5**. Obviously, the activity of P_2O_5 in the $2CaO{\cdot}SiO_2$-$3CaO{\cdot}P_2O_5$ solid solution saturated with MgO marked by solid circles and squares was larger than the activity of P_2O_5 in the $2CaO{\cdot}SiO_2$-$3CaO{\cdot}P_2O_5$ solid solution saturated with CaO marked by open circles and squares.

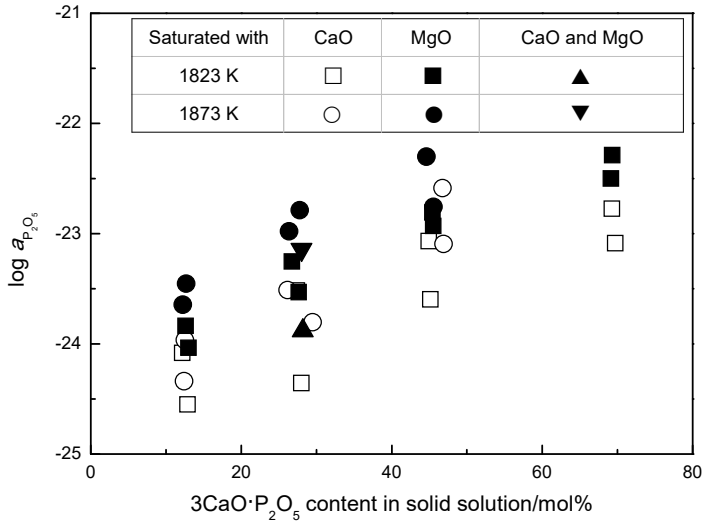

Fig. 6.5 Comparison of P_2O_5 activity.

In Figure 6.5 the solid triangles presented the activity of P_2O_5 in the $2CaO{\cdot}SiO_2$-$3CaO{\cdot}P_2O_5$

solid solution saturated with CaO and MgO with the experimental conditions and results as shown in **Tables 6.1**, **6.2** and **6.3**. The phases of CaO and MgO in tablets were detected by XRD before and after reaction as shown in **Figures 6.6**, **6.7** and **6.8**. The activity of P_2O_5 in the $2CaO{\cdot}SiO_2$-$3CaO{\cdot}P_2O_5$ solid solution saturated with CaO and MgO was larger than that saturated with CaO and smaller than that saturated with MgO.

Table 6.1 Initial compositions of tablets.

No.	Compositions of tablets/mass%							
	CaO	SiO_2	P_2O_5	MgO	$2CaO{\cdot}SiO_2$	$3CaO{\cdot}P_2O_5$	MgO	CaO
K01	55.6	10.9	9.5	24.0	31.2	20.8	24.0	24.0
K02	55.6	10.9	9.5	24.0	31.2	20.8	24.0	24.0

Table 6.2 Initial conditions of experiments.

No.	Temp./K	CO/CO_2	Fe/g	Tablet/g
K01	1823	110/1	9.8366	1.4975
K02	1823	110/1	9.9548	1.4937

Table 6.3 Chemical analyzed results and activity of P_2O_5.

No.	Compositions of tablets/mass%						P in iron /mass%	$3CaO{\cdot}P_2O_5$ /mol%	$a_{P_2O_5}$
	P_2O_5	SiO_2	CaO	MgO	FeO	Total			
K01	9.3	10.0	52.9	23.0	0.760	96.0	0.00603	28.2	1.31×10^{-24}
K02	9.2	10.0	51.7	23.5	1.25	95.7	0.0142	28.0	7.22×10^{-24}

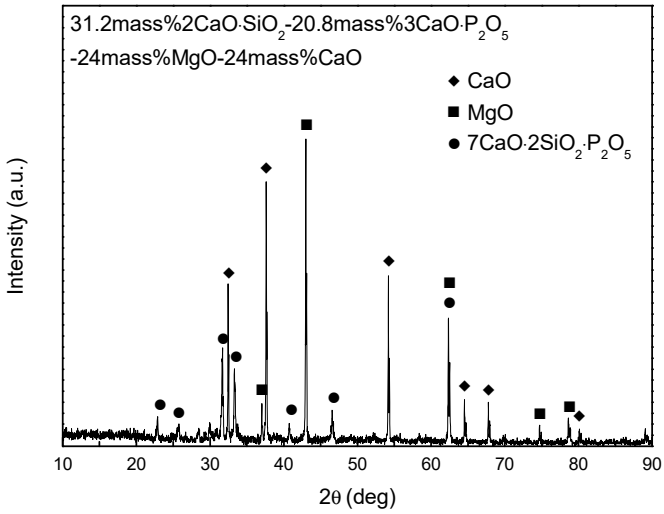

Fig. 6.6 XRD pattern of 31.2mass%2CaO·SiO_2-20.8mass%3CaO·P_2O_5 solid solution-24mass%MgO-24mass%CaO.

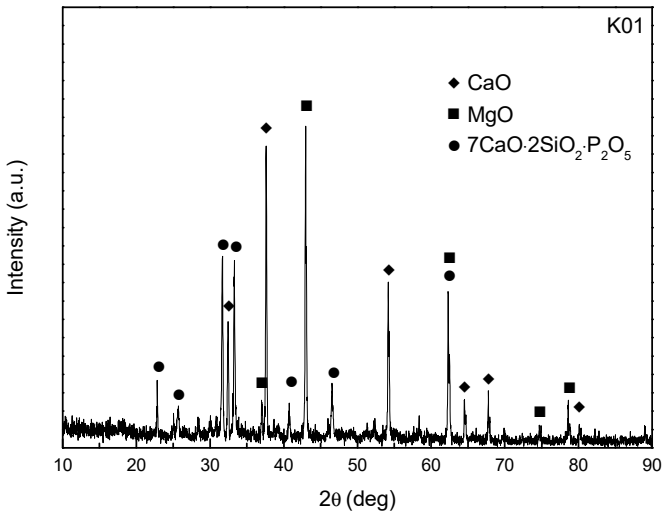

Fig. 6.7 XRD pattern of sample K01 after reaction.

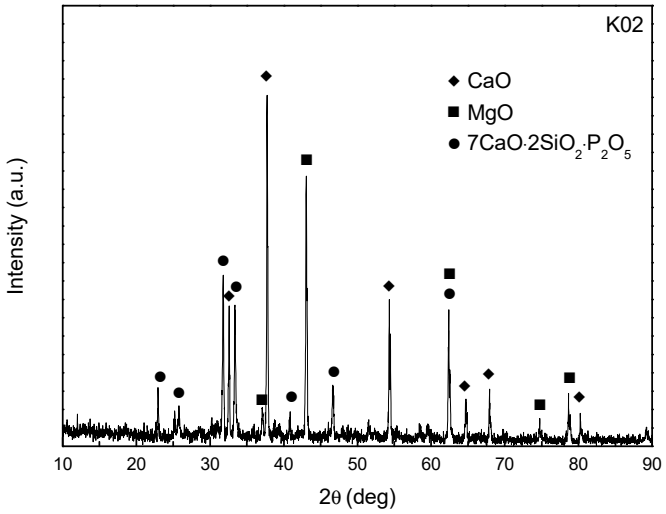

Fig. 6.8 XRD pattern of sample K02 after reaction.

The compositions of the $2CaO{\cdot}SiO_2$-$3CaO{\cdot}P_2O_5$ solid solution saturated with MgO after reaction were projected onto the CaO-MgO-SiO_2 system and the CaO-MgO-P_2O_5 system as shown in **Figures 6.9** and **6.10**. In both systems, the compositions were located in the three-phase equilibrium region at 1645 or 1273 K, but it was not the case at 1823 or 1873 K since the activity of P_2O_5 increased with the increase of the $3CaO{\cdot}P_2O_5$ in the solid solution. In addition, not only $2CaO{\cdot}SiO_2$ and $3CaO{\cdot}P_2O_5$ could form solid solution but also $2CaO{\cdot}SiO_2$ and $2MgO{\cdot}SiO_2$, and also $3CaO{\cdot}P_2O_5$ and $3MgO{\cdot}P_2O_5$ could form solid solution in a certain composition range as shown in Figures 6.9 and 6.10. For the $2CaO{\cdot}SiO_2$-$3CaO{\cdot}P_2O_5$ solid solution, the composition range of solid solution enlarges with the increase of the temperature,[5] and it is assumed that the composition range of solid solution also enlarges with the increase of the temperature for the $2CaO{\cdot}SiO_2$-$2MgO{\cdot}SiO_2$ and the $3CaO{\cdot}P_2O_5$-$3MgO{\cdot}P_2O_5$ solid solutions since the phase relationships at 1823 and 1873 K are unavailable for these two systems. Based on this assumption, the initial composition was simply considered as the mixture of $2CaO{\cdot}SiO_2$-$3CaO{\cdot}P_2O_5$ solid solution and MgO and after reaction once one of these two kinds of solid solutions formed, the extra CaO is generated as explained by **Figure 6.11**. According to the similarity between Ca^{2+} and Mg^{2+} ions, the various solid solutions were probable to from the

complex 2CaO(MgO)·SiO_2-3CaO(MgO)·P_2O_5 solid solution. Since the activity of P_2O_5 in the 2CaO·SiO_2-3CaO·P_2O_5 solid solution saturated with CaO and MgO was smaller than that saturated with MgO, the extra generated CaO was unsaturated. The final component of the mixture of 2CaO·SiO_2-3CaO·P_2O_5 solid solution and MgO was the 2CaO(MgO)·SiO_2-3CaO(MgO)·P_2O_5 solid solution-MgO with a certain amount of dissolved CaO.

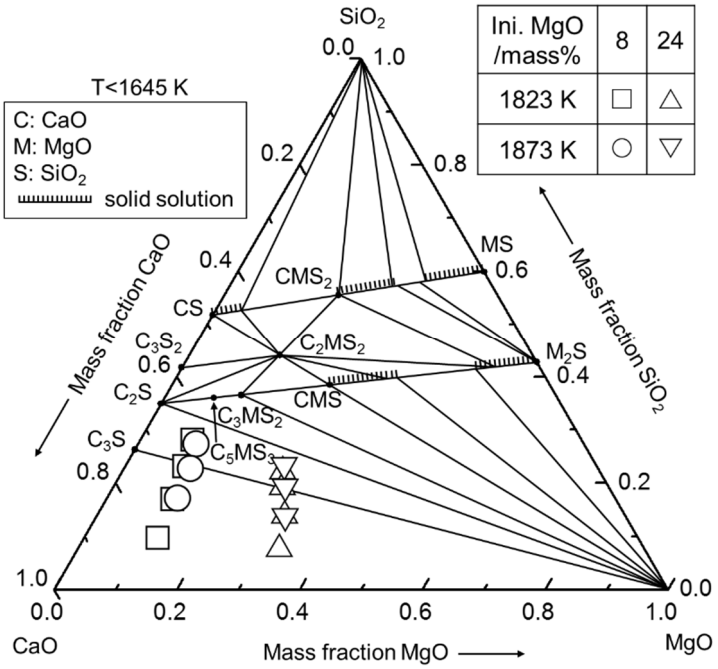

Fig. 6.9 Projection of the 2CaO·SiO_2-3CaO·P_2O_5 solid solution initially containing 8 and 24 mass% MgO after reaction on the CaO-MgO-SiO_2 system. The phase relationship was measured at less than 1645 K.[3]

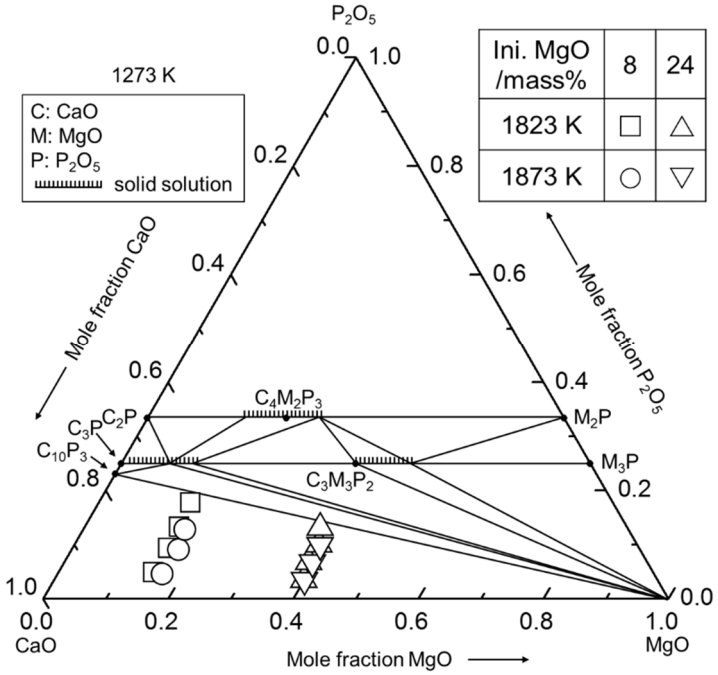

Fig. 6.10 Projection of the $2CaO{\cdot}SiO_2$-$3CaO{\cdot}P_2O_5$ solid solution initially containing 8 and 24 mass% MgO after reaction on the CaO-MgO-P_2O_5 system. The phase relationship was measured at 1273 K.[4]

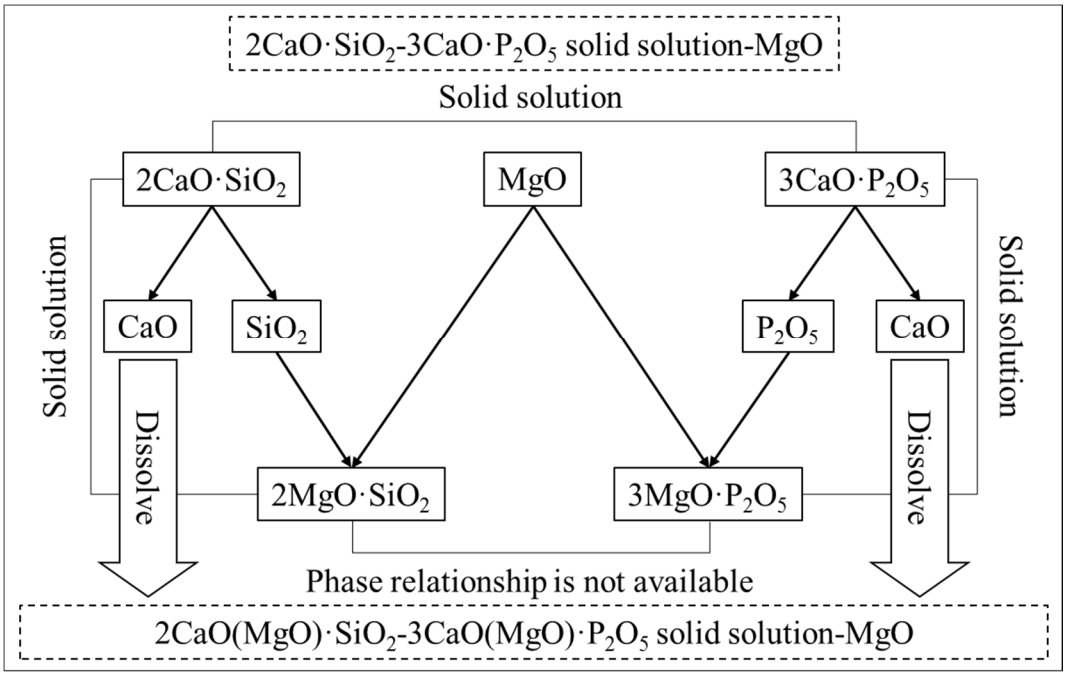

Fig. 6.11 Demonstration for the composition change of the $2CaO{\cdot}SiO_2$-$3CaO{\cdot}P_2O_5$ solid solution saturated with MgO.

For the CaO-MgO-SiO_2-P_2O_5 quaternary system the several feasible compositions were shown in **Figure 6.12**. The mixture of $2CaO{\cdot}SiO_2$-$3CaO{\cdot}P_2O_5$ solid solution and MgO is located on the triangle plane shown in Figure 6.12 A. If only the $3CaO{\cdot}P_2O_5$-$3MgO{\cdot}P_2O_5$ solid solution could form, the composition was located on the plane as shown in Figure 6.12 B. If only the $2CaO{\cdot}SiO_2$-$2MgO{\cdot}SiO_2$ solid solution could form, the composition was located on the plane as shown in Figure 6.12 C and if both of $2CaO{\cdot}SiO_2$-$2MgO{\cdot}SiO_2$ and the $3CaO{\cdot}P_2O_5$-$3MgO{\cdot}P_2O_5$ solid solutions could form the composition was located on the plane shown in Figure 6.12 D.

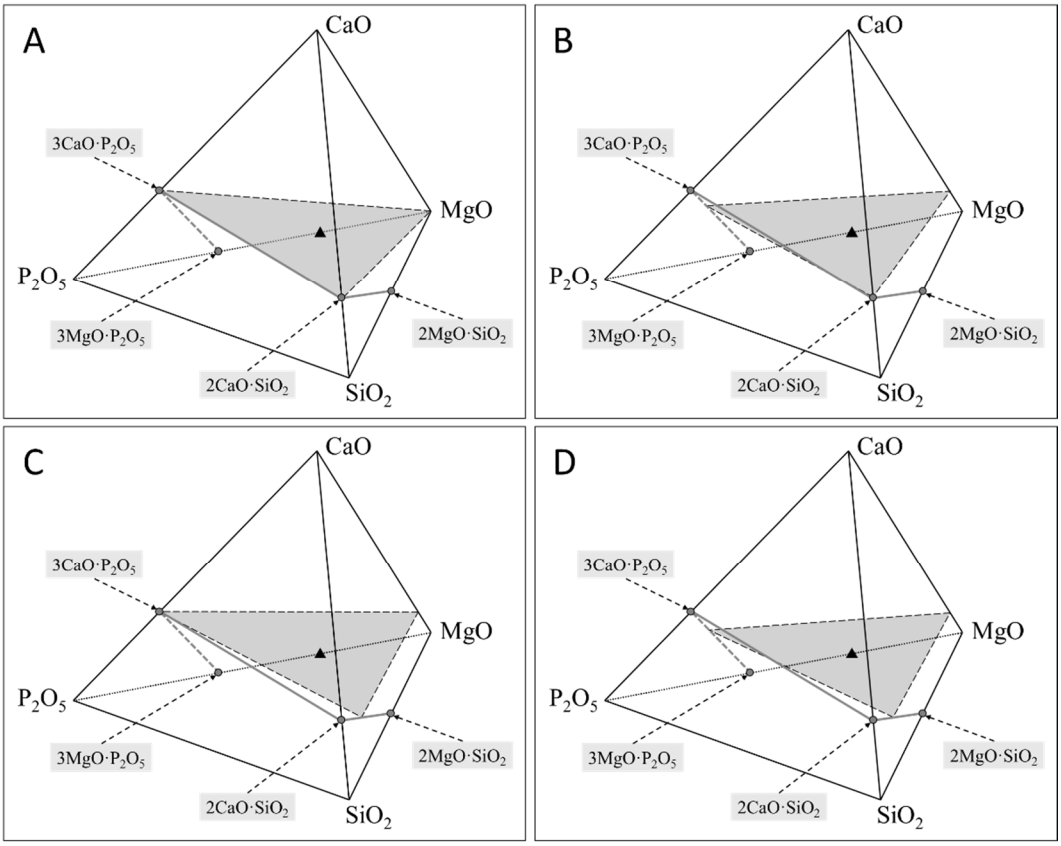

Fig. 6.12 A: Composition as the $2CaO{\cdot}SiO_2$-$3CaO{\cdot}P_2O_5$ solid solution-MgO.

B: Composition as the $2CaO{\cdot}SiO_2$-$3CaO(MgO){\cdot}P_2O_5$ solid solution-MgO-CaO.

C: Composition as the $2CaO(MgO){\cdot}SiO_2$-$3CaO{\cdot}P_2O_5$ solid solution-MgO-CaO.

D: Composition as the $2CaO(MgO){\cdot}SiO_2$-$3CaO(MgO){\cdot}P_2O_5$ solid solution-MgO-CaO.

6.5 Prospect of application of multi-phase flux

According to the activity of P_2O_5 in the $2CaO{\cdot}SiO_2$-$3CaO{\cdot}P_2O_5$ solid solution at 1823 K, the relationship between the logarithm P_2O_5 activity and the mole fraction of $3CaO{\cdot}P_2O_5$ in the solid solution was fitted with a liner relationship by least square method as Eq. (6.2). The equilibrium concentration of P in molten iron under various oxygen partial pressures was calculated by Eq. (6.3) as shown in **Figure 6.13**. When the oxygen partial pressure was 10^{-12} atm, the $2CaO{\cdot}SiO_2$-$3CaO{\cdot}P_2O_5$ solid solution barely has ability of dephosphorization. On the contrary, when the oxygen partial pressure was 10^{-10} atm, the whole composition of the $2CaO{\cdot}SiO_2$-$3CaO{\cdot}P_2O_5$ solid solution has huge ability of dephosphorization.

$$\log a_{P_2O_5} = 3.9987 x_{3CaO{\cdot}P_2O_5} - 24.446 \ (R^2 = 0.9385) \ldots\ldots (6.2)$$

$$P_2O_5(l) = 2\underline{P}(mass\%) + 5/2O_2(g)$$

$$\Delta G^{\circ}_{6.5} = 1400000 + 603T \ J/mol \ \ldots\ldots (6.3)^{[6,\ 7,\ 8]}$$

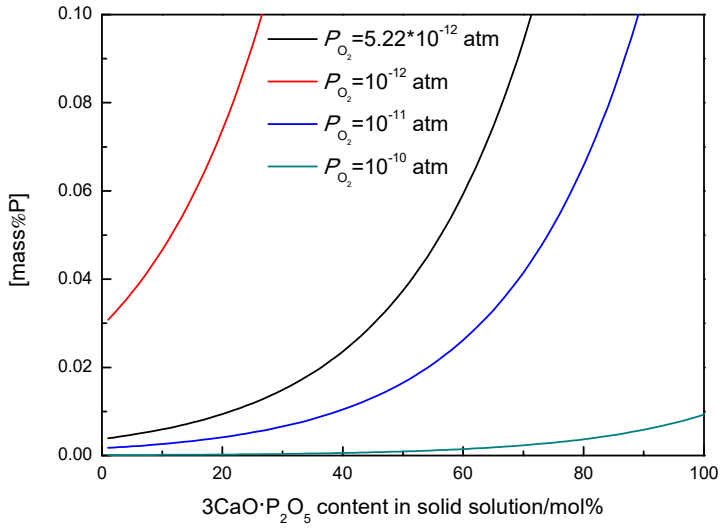

Fig. 6.13 Equilibrium concentration of P in molten iron with various oxygen partial pressures.

Base on above calculation, if the oxygen partial pressure could be controlled at a reasonable value, $2CaO{\cdot}SiO_2$ could be applied as a dephosphorization agent. But if only $2CaO{\cdot}SiO_2$ is adopted after forming $2CaO{\cdot}SiO_2$-$3CaO{\cdot}P_2O_5$ solid solution, the consumption of CaO is larger than P_2O_5 to decrease the basicity of slag. From this view, $2CaO{\cdot}SiO_2$ is not the first choice for

dephosphorization although the slag could be well recycled. At present, CaO is still recommended as the dephosphorization agent and how to utilize the unreacted CaO is deserved to develop.

The concept is as following. At first the CaO is added into BOF slag for the first time dephosphorization and after dephosphorization the solid phase is separated from the heterogeneous slag. At this time, the solid phase is the CaO wrapped with the $2CaO{\cdot}SiO_2$-$3CaO{\cdot}P_2O_5$ solid solution. In order to utilize the unreacted CaO, the solid phase should be crushed and agglomeration again. At this time, the solid phase considered as the mixture of $2CaO{\cdot}SiO_2$-$3CaO{\cdot}P_2O_5$ solid solution and CaO still has the huge ability of dephosphorization which could be applied for another time of dephosphorization. With the increase of reusing times, the contents of $3CaO{\cdot}P_2O_5$ and MgO increase in the solid solution which decrease the effect of dephosphorization. As shown in **Figure 6.14** at first CaO is adopted and with the increase of reusing times, composition of solid phase shifts along the arrow. When the CaO is saturated or the CaO is unsaturated but the composition is near the $2CaO{\cdot}SiO_2$-$3CaO{\cdot}P_2O_5$ solid solution with low content of $CaO{\cdot}P_2O_5$ as shown in the green region, the solid phase has the ability of dephosphorization. But when the composition is located in the red region, it is recommended to replace the solid phase to new CaO.

For the solid phase which has been applied several times for dephosphorization in BOF slag, even if it drastically loses the ability of dephosphorization, it still could be applied in the process of pretreatment since the low temperature and high concentration of P in pig iron as shown in **Figure 6.15**. In the process of dephosphorization at BOF furnace, the slag is continuously used only the solid phase is replaced. The advantage is it could decrease the volume of slag and the consumption of CaO. In addition, the BOF slag is easily to be reused. Finally the solid phase could be utilized as phosphate fertilizer.

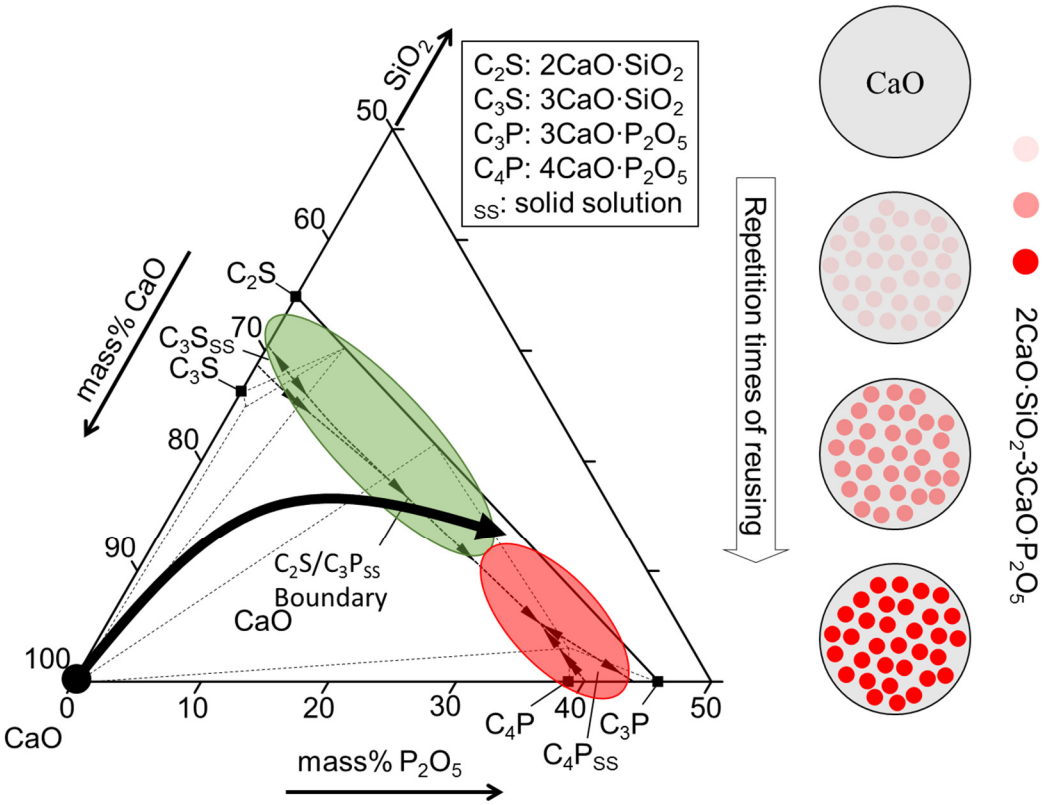

Fig. 6.14 Composition change for the solid phase in the multi-phase flux.

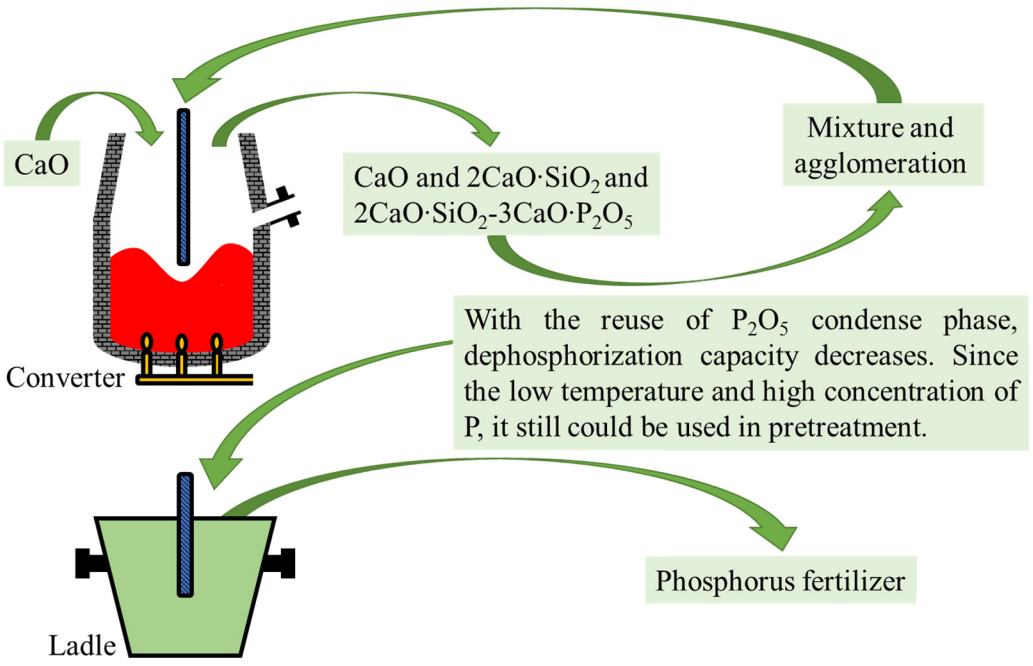

Fig. 6.15 Flow chart for applying multi-phase flux with CaO as the initial dephosphorization agent.

6.6 Summary

In this chapter, the activity coefficient of FeO in the tablet after reaction under various conditions was summarized. In addition, the activity of P_2O_5 in the calcium phosphate-based solid solution was summarized comparing with the values reported by Hasegawa *et al*. and Pahlevani *et al*. Moreover, the effect of MgO on the thermodynamics of the calcium phosphate-based solid solution was discussed. The activity of P_2O_5 in the $2CaO{\cdot}SiO_2$-$3CaO{\cdot}P_2O_5$ solid solution saturated with MgO was larger than that saturated with CaO. The CaO was unsaturated in the $2CaO{\cdot}SiO_2$-$3CaO{\cdot}P_2O_5$ solid solution including 8 or 24mass% MgO and the component of the $2CaO{\cdot}SiO_2$-$3CaO{\cdot}P_2O_5$ solid solution saturated with MgO was considered as the mixture of the $2CaO(MgO){\cdot}SiO_2$-$3CaO(MgO){\cdot}P_2O_5$ solid solution and MgO with a certain amount of dissolved CaO. Finally the innovative dephosphorization process was proposed according to the current and previous researches.

References

1. M. Hasegawa, Y. Kashiwaya and M. Iwase: *High Temp. Mater. Proc.*, **31** (2012), 421-430.
2. F. Pahlevani, S. Kitamura, H. Shibata and N. Maruoka: *ISIJ Int.*, **50** (2010), 822-829.
3. M. Allibert *et al.*: SLAG ATLAS 2nd Edition, Verein Deutscher Eisenhüttenleute, Germany, (1995), 134.
4. M. Allibert *et al.*: SLAG ATLAS 2nd Edition, Verein Deutscher Eisenhüttenleute, Germany, (1995), 133.
5. W. Fix, H. Heymann and R. S. Heinke: *J. Am. Ceram. Soc.*, **52** (1969), 346-351.
6. E. T. Turkdogan: *ISIJ Int.*, **40** (2000), 964-970.
7. S. Ban-ya and S. Matoba: *Tetsu-to-Hagané*, **48** (1962), 925-932.
8. E.T. Turkdogan: Physical Chemistry of High Temperature Technology, Academic Press, New York, (1980), 7.

Chapter 7 Conclusions

Generally speaking phosphorus is a harmful element for steel. It causes cold brittlement and temper brittlement to decrease the plasticity and the toughness. In order to meet the requirement of high quality steel, phosphorus should be removed as much as possible. As a cheap and efficient dephosphorization agent, CaO is commonly adopted. The excess CaO is added into slag in order to achieve better dephosphorization efficiency and thus the amount of slag and the consumption of CaO increase. Meanwhile due to CaO which remains unreacted or precipitates during solidification of dephosphorization slag, the slag is difficult to be reused. In consequence of the harm for environment and human, fluorite is strictly used although it can enhance the dissolution of CaO into slag. Under this condition, the concept of multi-phase flux was considered. In order to deeper understand and better apply this method, it is eagerly to obtain the thermodynamic data of the $2CaO{\cdot}SiO_2$-$3CaO{\cdot}P_2O_5$ solid solution which is considered as the main solid phase in the multi-phase flux. For this reason, the thermodynamics of the calcium phosphate-based solid solution for steelmaking were studied in current research.

Chapter 1 mainly introduced the research background and the previous researches. CaO could react with SiO_2 to form $2CaO{\cdot}SiO_2$ on the surface of the block CaO and prevent dissolution of CaO into slag. Even so, the $2CaO{\cdot}SiO_2$ could react with P_2O_5 to form a kind of P_2O_5 condensed phase which was considered as the solid phase in the multi-phase flux. According to previous researches, the P_2O_5 condensed phase was confirmed as a binary solid solution between $2CaO{\cdot}SiO_2$ and $3CaO{\cdot}P_2O_5$ and in order to utilize the solid solution the current research was proposed. About this topic, the reaction mechanism between solid CaO or $2CaO{\cdot}SiO_2$ and slag, the distribution of P_2O_5 between solid solution and liquid slag and the activity of P_2O_5 in the P_2O_5 condensed phase estimated by applying the regular solution model have been studied. The phase relationship of CaO-SiO_2-FeO-5mass%P_2O_5(-5mass%Al_2O_3) system has been well studied. The current research focuses on the thermodynamics about the calcium phosphate-based solid solution for steelmaking and the activity of P_2O_5 was measured directly by chemical equilibration method.

The chemical equilibration method was adopted for experiments as introduced in **Chapter 2**. The experimental principle and parameters were introduced. The oxygen partial pressure was controlled by the mixture of CO and CO_2 gases. The vertical-resistance furnace with an Al_2O_3 tube (outer diameter: 60 mm, inner diameter: 50 mm, length: 1000 mm) was applied for the experiments. Before each experiment, temperature was measured by a B-type thermocouple from the top of the tube and the suitable hot zone with temperature of 1823 K ± 1 K or 1873 K ± 1 K was determined. Temperature during the experiment was monitored by a B-type thermocouple placed at the bottom of an MgO crucible. The electrolytic iron was equilibrium with the artificial tablet in an MgO crucible for 24 hours which was confirmed long enough to reach equilibrium by preliminary experiments. After the equilibrium was established, the sample was quenched by Ar stream. The molybdenum-blue spectrophotometric solvent extraction method or the phosphomolybdate blue spectrophotometric method was adopted for analyzing the concentration of P in iron. The content of P_2O_5 in the tablet was analyzed by the phosphomolybdate blue spectrophotometric method. The content of SiO_2 in the tablet was analyzed by the gravimetry. The contents of CaO, FeO and MgO in the tablet were analyzed by ICP-OES. The formation of phases in the tablet was confirmed by XRD. The tablet was made by sintering the mixture with various ratios of reagent grade SiO_2, MgO, $CaHPO_4{\cdot}2H_2O$ and CaO obtained by the calcination of reagent grade $CaCO_3$. The mixture was heated in air at 1873 K in a Pt crucible for 24 hours, quenched by Ar stream and then ground into fine powder. These steps were repeated twice to obtain the powder for making tablet. About 1.5 g of powder was charged into a steel dies to be pressed into a cylindrical tablet (diameter: 18 mm, thickness: 3 mm) at 50 MPa.

The thermodynamic properties of the $2CaO{\cdot}SiO_2$-$3CaO{\cdot}P_2O_5$ solid solution at 1823 and 1873 K were studied in **Chapter 3**. Since the tablet was contaminated with more or less MgO crucible particles and metallic iron particles when the tablet was separated from the surface of solidified iron in the MgO crucible after reaction, contents of FeO and MgO were larger for some samples. Except the irregular points, both of the contents of FeO and MgO were smaller than 1 mass%. In addition, the activity coefficient of FeO in the tablet after reaction was estimated. At a certain

temperature and oxygen partial pressure, the change of activity coefficient of FeO was not clear. For a constant temperature and oxygen partial pressure, the concentration of P in molten iron increased with the increase of the $3CaO·P_2O_5$ content in the solid solution. The activity and activity coefficient of P_2O_5 in the $2CaO·SiO_2$-$3CaO·P_2O_5$ solid solution increased with the increase of the $3CaO·P_2O_5$ content in the solid solution at a certain temperature and the values at 1873 K was larger than those at 1823 K.

In practical dephosphorization process, the excess lime is added into slag for a better effect of dephosphorization. In **Chapter 4**, the compositions of tablets were the $2CaO·SiO_2$-$3CaO·P_2O_5$ solid solution containing 8 and 24 mass% CaO. The contents of FeO and MgO in tablet after reaction and the activity coefficient of FeO in the tablet were discussed at first. Later the concentration of P in molten iron and phosphorus partition ratio between the mixture of $2CaO·SiO_2$-$3CaO·P_2O_5$ solid solution and CaO and molten iron were discussed. The activity and activity coefficient of P_2O_5 in the $2CaO·SiO_2$-$3CaO·P_2O_5$ solid solution containing 8 and 24 mass% CaO at 1823 and 1873 K increased with the increase of the $3CaO·P_2O_5$ content in the solid solution. For a constant composition of solid solution, the activity and activity coefficient of P_2O_5 barely changed with the change of the temperature. For the compositions in which the CaO phase was detected after reaction, the activity and activity coefficient of $3CaO·P_2O_5$ were calculated by the estimated activity of P_2O_5 and the activity of CaO which was unit. The activity and activity coefficient of $3CaO·P_2O_5$ increased with the increase of the $3CaO·P_2O_5$ content in the solid solution. For a constant composition of solid solution, the activity and activity coefficient of $3CaO·P_2O_5$ barely changed with the change of the temperature. Furthermore, the activity of $2CaO·SiO_2$ in the solid solution was calculated with the estimated activity of $3CaO·P_2O_5$ by using the Gibbs-Duhem equation. The activity of $2CaO·SiO_2$ in the $2CaO·SiO_2$-$3CaO·P_2O_5$ solid solution decreased with the increase of the $3CaO·P_2O_5$ content in the solid solution and the temperature dependency of the activity of $2CaO·SiO_2$ was not clear within the experimental error range.

Since there is more or less MgO in metallurgical slag and the MgO is also adopted as the refractory it is necessary to study the thermodynamic properties of the $2CaO·SiO_2$-$3CaO·P_2O_5$

solid solution containing 8 and 24 mass% MgO at 1823 and 1873 K. In **Chapter 5** the content of FeO in tablet after reaction and the activity coefficient of FeO were discussed at first. Later the concentration of P in Fe and phosphorus partition ratio between the mixture of $2CaO{\cdot}SiO_2$-$3CaO{\cdot}P_2O_5$ solid solution and MgO and molten iron were discussed. The activity and activity coefficient of P_2O_5 in the $2CaO{\cdot}SiO_2$-$3CaO{\cdot}P_2O_5$ solid solution containing 8 and 24 mass% MgO at 1823 and 1873 K increased with the increase of the $3CaO{\cdot}P_2O_5$ content in the solid solution. For a constant composition of solid solution, the activity and activity coefficient of P_2O_5 barely changed with the change of the temperature. The MgO phase was detected in each composition after reaction and the activity of $3MgO{\cdot}P_2O_5$ was calculated by the estimated activity of P_2O_5 and the activity of MgO which was unit.

Chapter 6 summarized the thermodynamic properties of the calcium phosphate-based solid solution determined in Chapters 3, 4 and 5 and proposed the application of multi-phase flux. The activity of P_2O_5 in the $2CaO{\cdot}SiO_2$-$3CaO{\cdot}P_2O_5$ solid solution saturated with MgO was larger than that saturated with CaO. From the phase relationship of CaO-MgO-SiO_2 system and CaO-MgO-P_2O_5 system, it was inferred the extra CaO was generated with an unsaturated amount in the $2CaO{\cdot}SiO_2$-$3CaO{\cdot}P_2O_5$ solid solution saturated with MgO. Finally the prospect of application of multi-phase flux was proposed. In the process of dephosphorization at BOF, the liquid slag is continuously used only the solid phase is replaced. After losing the ability of dephosphorization at BOF the solid phase is used for dephosphorization at the process of pretreatment and finally the solid phase is utilized as the phosphate fertilizer.

In current research, the thermodynamics of the calcium phosphate-based solid solution were measured directly. It provided the necessary urgent basic thermodynamic data for dephosphorization. Combining with present and previous researches, the method of multi-phase flux is realizable.

Acknowledgement

As time goes by, whilom strange streets, buildings, customs and the whilom freshness are leaving. When I could know the food names in cafeteria only through smelling and I could expertly open the laboratory doors at midnight even without any light, I realize that I am also leaving from this devoted indelible place. Three years is not very long, but it is long enough to imprint every tree and bush of here on my heart. Whenever think back to the days when I tried my best to enter this world-renowned university, I feel a bit speechless mood. At this moment I cannot accurately express my emotion, because I love here and you more than I can say.

Dear Professor Fumitaka Tsukihashi, at first I'd like to express my heartfelt thanks and great respect to you. Up to now, I could remember the day of the first interview on Jan. 9th, 2012. From that moment, it is no exaggeration to say you altered the course of my life and made me closer to my dream. During these three years, I gain so much suggestions and care from you and the more important, you teach me not only how to be an eligible scholar but also how to develop the personality charm.

Meanwhile, I wish to express my sincere gratitude to dear Associate Professor Hiroyuki Matsuura. It's hard to forget that on the night of Sept. 28th, 2012, we met for the first time and the scene you were working with your whole heart hit me very deep. I know you are my role model and I must work hard to be a respectable scholar like you in the future. Thank you very much for suggestions from you and since the precious suggestions I was short on a few detours.

I am also grateful to the members of the thesis evaluation committee: Professor Kazuki Morita (Graduate School of Engineering, The University of Tokyo), Professor Kazuo Terashima (Graduate School of Frontier Sciences, The University of Tokyo) and Associate Professor Toshihiro Okamoto (Graduate School of Frontier Sciences, The University of Tokyo). Thank you very much for your very valuable constructive opinions and suggestions about my thesis and future work.

I am appreciated to the members from Tsukihashi · Matsuura group: Professor Volodymyr Shatokha, Professor Guangqang Li, Professor Baokuan Li, Professor Zhangfu Yuan, Professor

Xiaojun Hu, Professor Deyong Wang, Associate Professor Likun Zang, Associate Professor Guohua Zhang, Lecturer Canguo Wang, Dr. Yang Cui, Dr. Xiao Yang, Dr. Xu Gao, Dr. Xiaorui Zhang, Dr. Wonjin Choi, Dr. Sokur Yuliia and so on. Thank you very much for your kind concern.

For the students once or now together with me in the lab: Mr. Shota Amano, Mr. Masato Kurehashi, Mr. Gouji Kaneda, Mr. Katsuki Goto, Mr. Kyohei Kenmotsu, Mr. Hiroshi Yamaguchi, Ms. Yusheng Lang, Mr. Masayuki Sato, Mr. Hiroaki Nishi, Mr. Fuminori Katabe, Mr. Yoshifumi Inose, Mr. Akihiro Sanada, Mr. Koki Yano, Mr. Hiroki Kitao, Mr. Toshiki Nonaka, Mr. Songjie Tang, Mr. Hiroyuki Tate, Mr. Kanta Iwaya, Mr. Kohei Kondo, Mr. Hitoshi Mukai, Ms. Yan Wu, Mr. Guodong Sun, Mr. Minggang Li, Ms. Qian Zhou, Mr. Kiyotaka Saito, Mr. Ryosuke Shimakura, Mr. Stsunori Suzuki and Mr. Kazuaki Hirakawa, because of you the exotic life is no longer alone and because of you, I could gain the happiness not only from research.

My appreciation is also given to Ms. Yuko Shoji. Thank you very much for helping me on the daily life.

The last gratitude is for my parents. You gave me the life. I am loving you better than words can tell with saying nothing at all.

June 2015